ABB Inc.
FINAL TECHNICAL REPORT

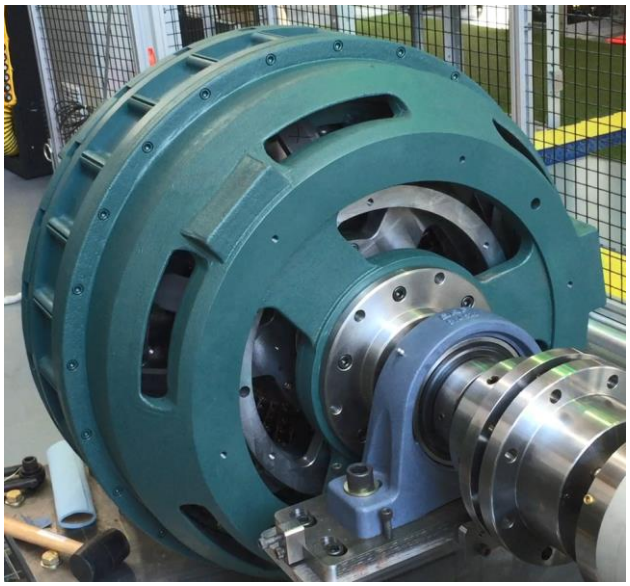

Advanced Direct-Drive Generator for Improved Availability of Oscillating Wave Surge Converter Power Generation Systems
DE-FOA-0000848

Award:	DE-EE0006400
Lead Recipient:	ABB Inc.
Project Title:	Advanced Direct-Drive Generator for Improved Availability of Oscillating Wave Surge Converter (OWSC) Power Generation Systems
Principal Investigator:	V. R. Ramanan
Team Member Organizations	Resolute Marine Energy, Inc (RME) Texas A&M Engineering Experiment Station (TEES)
Date of Report:	March 3, 2017
Reporting Period:	December 1, 2013 – December 30, 2016

Notice:

Acknowledgment:

This material is based upon work supported by the Department of Energy under Award Number DE-EE0006400.

Disclaimer:

EXECUTIVE SUMMARY

This report summarizes the activities conducted under the DOE-EERE funded project DE-EE0006400, where ABB Inc. (ABB), in collaboration with Texas A&M's Advanced Electric Machines & Power Electronics (EMPE) Lab and Resolute Marine Energy (RME) designed, derisked, developed, and demonstrated a novel magnetically geared electrical generator for direct-drive, low-speed, high torque MHK applications

The project objective was to investigate a novel and compact direct-drive electric generator and its system aspects that would enable elimination of hydraulic components in the Power Take-Off (PTO) of a Marine and Hydrokinetic (MHK) system with an oscillating wave surge converter (OWSC), thereby improving the availability of the MHK system. The scope of this project was limited to the development and dry lab demonstration of a low speed generator to enable future direct drive MHK systems.

The project was organized into two phases with the first phase work including the design, manufacture, and testing of two alternative 1 kilowatt, 300 revolution-per-minute proof of concept machines. The main objective of the second phase, building on the results from the first phase, was to design, build, and test a larger 10 kilowatt, 30 revolution-per-minute prototype, as well as use the test results from the phase two prototype to design a full-scale, direct-drive electrical generator for integration with a wave energy converter.

The original project goals were to (1) validate the reduction in size and weight of the direct-drive generator by more than 50% relative to an equivalent commercial, off-the-shelf (COTS) direct drive permanent magnet (PM) electrical machine, and (2) establish that the availability of the MHK system compared to the baseline Oscillating Wave Surge Converter full-system with hydraulic PTO is improved by reducing the downtime by at least 50% and that the levelized cost of electricity (LCOE) is reduced by at least 10%. Prototype test results from three variations of electrical generator during phase 1 led to the selection and design of the phase 2 prototype with a hundredfold increase in rated torque. Specifically, a tooth-wound inner stator outperformed a pole-modulated inner stator machine due to an extremely low 0.50 power factor. An axial flux offered the highest theoretical power and torque density but faces increasing manufacturing difficulty and expensive as the size increases. Additionally, a large diameter, axial-flux machine does not integrate as well with the RME oscillating surge wave energy converter targeted in this project.

Based on the phase 1 results and aggressive torque density targets, the phase 2 prototype design was a radial-flux, integrated magnetic gear and generator with tooth-wound inner stator. The test results from the roughly m in diameter phase 2 prototype further validated the overall design and modeling process. For example the measured peak torque of 3870 Nm and 92% efficiency under rated 10kW, 30 rpm operation were compared to calculated predictions of 3905 Nm and 92%. The final, full-scale design for an ocean wave application used the same design process to scale-up a modified version of the of phase 2 prototype.

Including this full-scale machine design, as of the conclusion of this project, we have validated the potential for a close to 3 times potential reduction in weight and 6 times reduction in mass compared to the closest commercial, off-the-shelf (COTS) direct drive permanent magnet electrical machines. A 50% reduction in downtime is expected through a combination reduced scheduled maintenance and unscheduled downtime, however, this benefit was difficult to validate for the prototype demonstration project. Details on initial availability calculations are

included in Appendix 7. However, even assuming equivalent system availability, a near-shore ocean wave energy conversion can be shown to offer a more than 18% reduction in LCOE using the proposed low-speed generator and electrical power take-off system instead of the hydraulic alternative. This reduced electricity cost is enabled by increased energy conversion efficiency. The improvement can be further increased to more than 35% if the thermal limits of the inherently “over-loadable” electrical generator and system are used to increase the peak power output compared to an equivalent cost hydraulic system.

ACCOMPLISHMENTS AND COMPARISON TO OBJECTIVES

Objectives	Accomplishments
Design and prototype a 1 kW, 300 rpm, outer rotor, pole modulated permanent magnet electrical generator	Prototype designed, built and tested showing low power factor resulting in inferior overall performance compared to a demonstrated tooth-wound stator alternative.
Design and prototype a 1 kW, 300 rpm axial flux integrated magnetically geared generator	Prototype designed, built, and tested, verifying the design procedure and performance predictions. Axial flux geometry found to be difficult to scale mechanically. Full load testing prevented by a dislodged magnet.
Design and prototype a 10 kW, 30 rpm low speed, high torque generator for wave, MHK, and similar applications	A radial flux, integrated magnetically geared generator was designed, built, and tested, verifying the design procedure and performance predictions. Generator was successfully tested under constant, sinus oscillation, and simulated ocean wave speeds.
Design a full scale, 40 kW, 1.7 rpm electrical generator to meet the target torque density and cost requirements	Paper design of a full scale, radial flux magnetically geared generator completed with 93 kNm/m^3 and 33 Nm/kg using active material or 88 kNm/m^3 and 21 Nm/kg using total materials
Complete LCOE calculations for the OWSC system with baseline hydraulic PTO and proposed direct drive electrical PTO	LCOE calculations completed in and independently evaluated by NREL scientists show a potential reduction of 18% from increased energy conversion efficiency and more than 35% if the momentary thermal limits of the electrical system are used to increase the maximum power output for the PTO system

DETAILS OF PROJECT ACTIVITIES

This project was organized into the seven main tasks listed below.

- Task 1. Initial Generator Specifications from System Aspects Including Wave Profiles, Wave Energy Converter (WEC) Characteristics, and Electrical PTO Requirements
- Task 2. Modeling, Design, and Testing of Initial Prototype
- Task 3. Modeling, Design, and Testing of Alternative Prototype
- Task 4.0: Test Bed and Models Development
- Task 5.0: Design and Testing of Robust Budget Period 2 Prototype
- Task 6.0: Full Scale MHK System and Integration Studies
- Task 7.0: System Performance Impact Analysis

The highlights from each of the tasks are included and summarized below. Additional details are also presented in the Appendices where the Milestone Delivery reports are attached.

Task 1. Initial Generator Specifications

The state of the art power take-off system from RME for flap-type oscillating wave surge converters use hydraulic power take-off (PTO) components. A direct-drive electrical generator and PTO system could offer significant advantages in terms of system simplicity and availability. However, the large generator size and cost for this extremely low and variable speed application is not currently available or competitive using conventional technology. The main challenge addressed by this project is the design of an electrical generator of a sufficiently reduced size and cost to be competitive with the hydraulic alternatives. One of the project goals addressed by the generator and system specifications is to determine roughly what is required from the generator and direct drive electrical PTO system in order to substitute for the hydraulic system.
Figure 1 illustrates the scale of the flap and generators, showing one possible configuration with the outer rotors of two separate generators joined to the base of the flap on either end of the common axis. Another alternative, depending on the generator length and final system bearing solution, could also use a single generator in the middle along the flap axis.

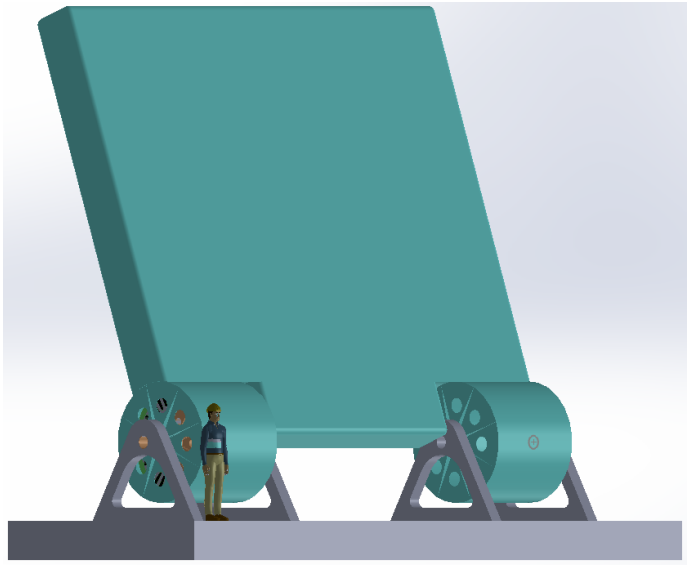

Figure 1. Concept illustration of flap integrated with two outer-rotor generators

A baseline flap and hydraulic PTO system have been defined for reference, target setting, and comparison to the proposed electrical PTO system. The reference system is rated for 30 kW electrical power output to the grid using a single 8 m wide by 7 m tall flap at rated sea conditions of 2.5 m wave height and 12 sec wave period. Both rated wave conditions as well as an annual distribution of wave conditions have been defined as input. Additionally, representative half-hour, data sets of simulated flap torque and speed for both rated sea conditions and a few reduced wave heights have been provided for partial load calculation and comparison.

The motion of the flap and directly coupled generator are unique for this application. Instead of the constant speed, continuous rotation typical for most electric motors and generators, the direct drive generator in this case will oscillate, rotating back and forth with the flap, stopping and changing direction twice every cycle. The average speed is low but the oscillations contribute highly variable peak values of speed and torque at irregular intervals. For the project Phase I and Phase II prototype development at reduced scale, the generators are designed and tested with an increased constant speed in order to make the prototypes more manageable. However, for the target application of the generator directly coupled with the FLAP in the sea bed, the actual motion is oscillating back and forth, as shown in Figure 2. The slow motion averages around 0.18 rad/sec and the rotation angle varies within ±70 degrees, usually much less. The peak to average speed ratio for this data set is nearly 4:1.

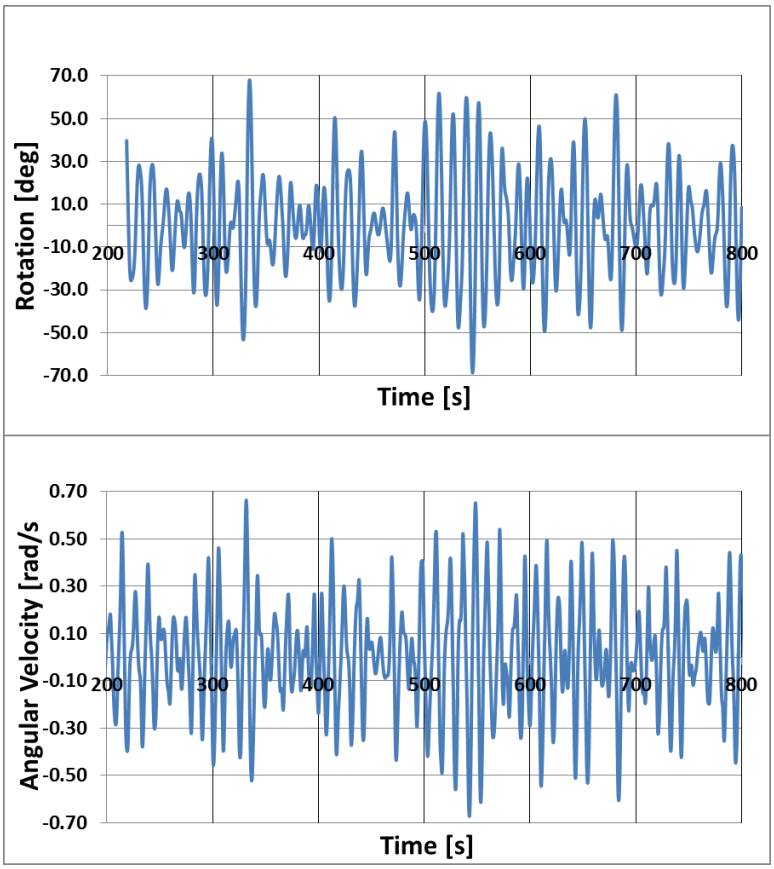

Figure 2. Example flap angle and velocity for 10 min interval with load torque limited to

Additional details of the system components and estimated costs for the baseline hydraulic-electric and proposed direct-drive electrical PTO systems are compared in the Task 1 report

attached as Appendix 1. These values suggest a reasonable, direct-drive electrical PTO system can be cost competitive with the baseline hydraulic PTO system described in the same report. It is important to highlight at this point some of the potential benefits from the direct drive electrical PTO system, including increased power conversion system efficiency and simplified and more flexible control including the ability to limit the generator torque. Furthermore, the "over loading" ability of the electrical PTO system can take advantage of thermal limits and the transient, long cycle times of ocean waves to momentarily process a large amount of power followed by recovery intervals of reduced power generation. As a result, the electrical PTO system can better match the application requirements and variable conditions, with increased overall power output and reduced installation requirements compared to hydraulic equipment sized and capable of operating up to a fixed maximum rating. These advantages are typical and expected for an electrical system compared to a hydraulic alternative, independent of the generator design. However, conventional electrical generators would be large, heavy, and expensive for an application with the low average speeds of ocean waves. The solution adopted in this project to enable power generation at the low speed is to integrate a magnetic gear into the design of the electrical generator to increase the generator speed while maintaining a (pseudo) direct-drive, all-electric solution. The initial design values and cost estimations of Task 1 shown in Appendix 1 from early in the project are also revisited and updated as part of the final Task 7 LCOE calculations.

Tasks 2 & 3: Modeling, Design, and Testing of Phase I Prototypes

The goal of the first stage of the project was to derisk, develop, and validate design and performance calculation tools for novel generators for MHK-type low-speed, high torque, applications starting from a smaller and more manageable 1 kW, 300 rpm generator design. In fact, three different Phase I prototypes were actually designed, built and tested. Two versions of outer rotor, radial flux, surface permanent magnet machine were created using the same rotor first combined with a novel, pole modulated stator and second with a 5 phase tooth-wound stator. In addition to these two prototypes, a magnetically-geared axial flux, permanent magnet electrical generator was also developed and tested. Details of these Phase I Prototypes are included in the following sections and shown for comparison below in Figure 3.

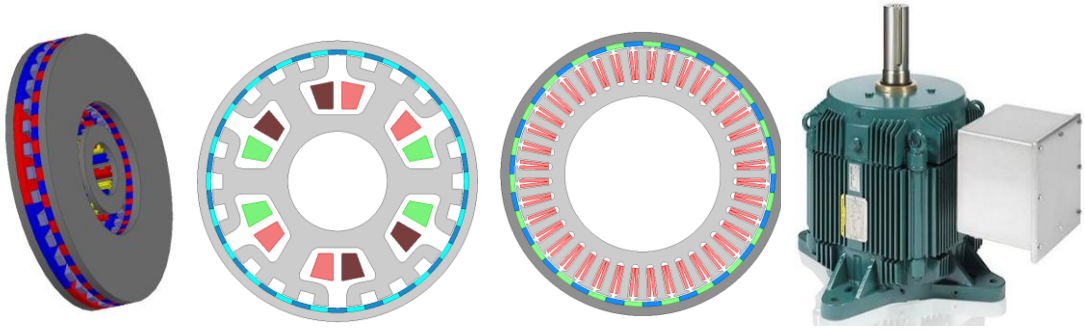

Axial Flux Pole Modulator Tooth-Wound Commercial Baseline

Figure 3. Comparison of Phase I motor topologies

A summary of the Phase I prototypes is included in Table 1. Similar values calculated for full scale, 40 kW, 1.7 rpm generator versions from Phase I are shown in Table 2. The material costs in both tables are calculated assuming $50/kg for the magnets, $10/kg for the copper, and $2/kg for the lamination electrical steel.

The Task 2.2 Milestone Deliverable report "1 kW Generator Prototype Test Results," included as Appendix 2, describes the results of the experimental performance evaluation of the pole-modulated, 300 rpm generator prototype as well as a tooth wound stator using the same surface permanent magnet outer rotor. Similarly, the Task 3.2 report (Appendix 3) describes equivalent results for the alternative, axial flux magnetically geared machine, shown in Figure 4.

The primary goals of these tests were to

- Demonstrate the feasibility of the novel machine designs
- Compare the mass and volumetric torque density of the prototypes against the baseline targets
- Measure test data for calibration and validation of performance calculations
- Identify potential risks and opportunities to improve the electromagnetic, mechanical, structural, or thermal performance of the larger second prototype

Following an initial description of the test-set-up and generator configurations, the rest of the reports compares mechanical, electromagnetic, and thermal measured test data to finite element calculated predictions. Finally, a comparison is made between the different configurations of the

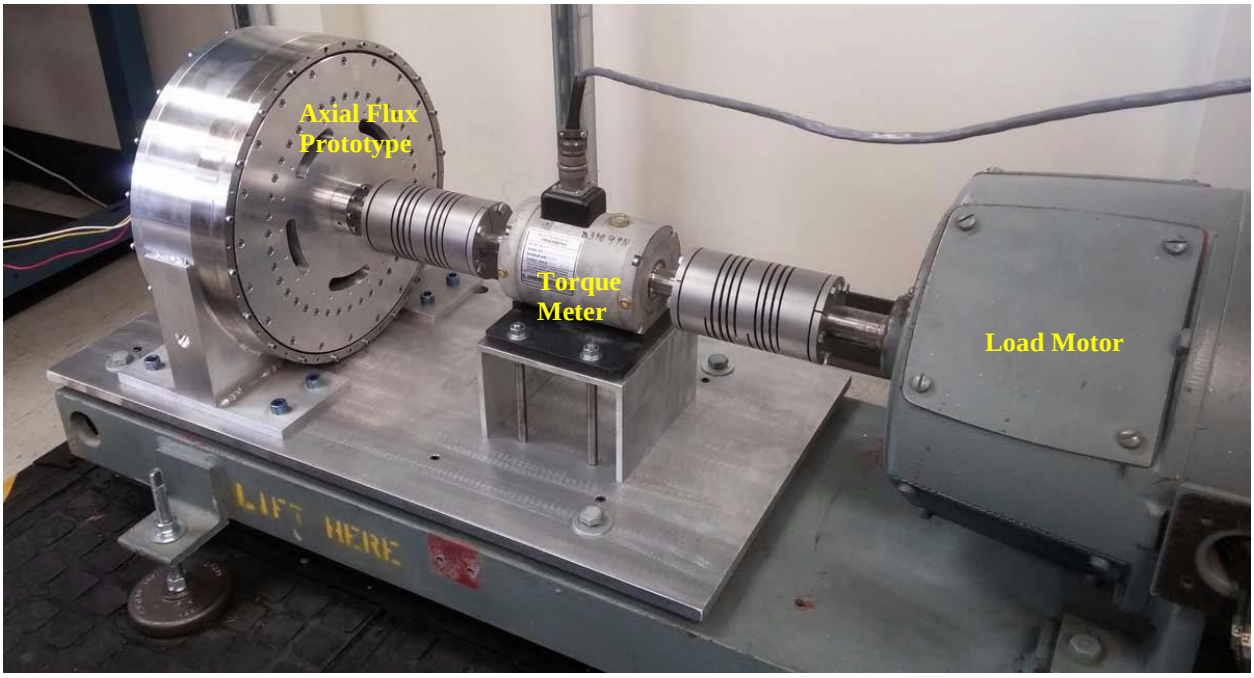

Figure 4. Test bed for Phase I Alternative, Axial Flux Prototype

Phase I prototypes and the baseline reference values. Some of the key observations are summarized below.

1) All three prototypes have been designed and tested and the results are consistent with the design predictions.
2) An inline torque transducer was necessary for accurate torque and efficiency measurements.
3) The pole modulated design uses the iron pole harmonics in the air gap region. The stator structure is simple and easy to manufacture. It can achieve high power and torque only under

low, leading power factor operation, which introduces extra loss and cost from the system side for power factor conditioning and higher current requirements.

4) The tooth wound design features a high winding factor which contributes to the target power generation density with the power factor close to unity. This design can provide low winding losses and high overall efficiency. While the stator winding coils will be more effort to manufacture than with the pole modulated design, a modular design and machine winding process can be applied to significantly reduce the manufacturing cost.

5) The magnet loss is not a major loss component as observed in these prototype tests. Large thermal margin and low rotor temperature were observed during testing with both pole-modulated and tooth wound stators. The iron and magnet losses are not concerns for the targeted low speed application. The stator winding loss is the most significant source of generator loss.

6) Only no load testing was completed on alternative Phase I prototype integrated, axial flux magnetically geared generator. Unfortunately, this prototype was damaged by a dislodged magnet during initial load testing. Not only the magnet but the bearings and structural assembly were damaged from the severe shock of the sudden stop caused by the loose magnet lodging between the modulator and rotor. Nevertheless, the static torque and no load losses of the machine were fully characterized, providing a good indication of the prototype mechanical, core, and magnet losses.

7) Based on the no load loss measurements, the full load efficiency of the Phase I prototype integrated, axial flux magnetically geared generator is expected to be about 60%, with electrical efficiency values of about 80% for the magnetic gear components and about 75% for the off the shelf generator. Higher efficiencies are achievable with reduced bearing loss, minimizing eddy current losses in structural material, dedicated design of the generator components (reduced winding resistance, higher quality laminations, and design for low harmonics for example) as well as additional focus on efficiency of the magnetic gear from steps like magnet segmentation, pole-combination selection, and laminating the modulator segments.

Table 1. Phase I 300 rpm, 1 kW* generator prototype summary

Design Parameters	Axial Flux Gear+Generator	Pole Modulated	Tooth Wound	Commercial Reference 7 hp (5.2 kW), 300 rpm
Gear Ratio	9	-	-	-
Outer Diameter (mm)	260	310	310	-
Inner Diameter (mm)	60	95.25	95.25	-
Stack Length (mm)	55	60	60	-
Est. Coil Head Length [mm]	0	37.5	20	-
Magnet Material (kg)	1.7	1.8	1.8	-
Electrical Steel Core Material (kg)	9.1	17.2	15.1	-
Copper Material (kg)	0.45	2.4	2.1	-
Total Active Weight (kg)	11	21	19	-
Continuous Power Output (kW)	1	3.8	4.1	-
Efficiency	~0.60	0.90	0.92	-
Power Factor	1.00	0.40	1.00	-
PM per kW (kg/kW)	1.7	0.5	0.4	-
Iron per kW (kg/kW)	9.1	4.5	3.7	-
Copper per kW (kg/kW)	0.5	0.6	0.5	-
Total Active Weight per kW (kg/kW)	11	6	5	-
Torque Density (kNm/m^3) Target ≥ 16 kNm/m^3	12	13	19	8.2
Torque Density (Nm/kg) Target ≥ 4 Nm/kg	2.8	5.7	6.9	1.8
Active Material Cost (USD)	108	148	141	505
Active Material Cost per kW (USD/kW) Target ≤ $50 USD/kW	108	39	34	97

*The initial target for the Phase 1 Prototypes was 1 kW at 300 rpm. In fact, the single air gap machines were scaled up to around 4 kW to better match the outer diameter and more easily compare to the conventional, off-the-shelf reference motor.

Table 2. Full Scale, 40 kW, 1.7 rpm design projections

Design Parameter	Integrated Axial Flux Gear+Generator	Pole Modulated Generator	Tooth Wound Generator	Integrated Radial Flux Gear+Pole Modulated	Integrated Radial Flux Gear+Tooth Wound Generator	Commercial Reference 250 hp (186.5 kW) 125 rpm
Gear Ratio	9	-	-	11	11	-
Outer Diameter (m)	2.5	2	2	2	2	-
Inner Diameter (m)	0.9	1.24	1.28	0.2	0.23	-
Stack Length (m)	0.38	3.2	3	0.9	0.9	-
Est. Coil Head Length (m)	0	0.4	0.25	0	0	-
Magnet Material (kg)	2,160	1,750	1,650	2,420	2,370	-
Electrical Steel Core Material (kg)	4,700	14,300	15,400	9,350	9,050	-
Copper Material (kg)	160	9,100	6,600	180	130	-
Total Active Weight (kg)	7,020	25,150	23,650	11,950	11,550	-
Active Torque Density (kNm/m^3) Target ≥ 84 kNm/m^3	139	29	35	80	81	33
Active Torque Density (Nm/kg) Target ≥ 14 Nm/kg	32	9	10	19	19	5.5
Active Material Cost (kUSD) Target ≤ $200 kUSD	119	207	179	142	138	12

In summary, these are the key points from the generator topology comparison:

- The pole-modulated generator prototype did not provide an advantage in terms of torque density, but the measured low power factor (~0.5 leading for maximum power output) would be a significant PTO system disadvantage.
- The single air gap machines are not expected to be able to meet the target full scale torque density targets.
- The axial flux integrated magnetic gear generator requires a larger diameter for high flux density, which will be more difficult to integrate with the flap-type oscillating wave surge converter in the full scale design. (The generator diameter must be less than 1.6 m to avoid impacting the hydrodynamic performance of the baseline flap.)
- The air gaps will be challenging to maintain with the full scale axial flux topology. The mechanical assembly and supporting structure will be more complicated and expensive than with a radial flux topology.

The radial flux topology simplifies the mechanical challenges of the axial flux prototype. This mechanical disadvantage would be an increasingly serious drawback at larger scale. Initial examinations based on our Phase I effort predict a radial flux integrated magnetically geared generator topology has potential to meet the torque density targets and meet the project goals by enabling an all-electric PTO system. Based on these points and our progress over Phase I, the project decided on an integrated radial flux magnetic gear with an inner, radial flux tooth-wound generator for the Phase II prototype. The development of the Phase II prototype is described in the next sections of the report.

Task 4.0: Test Bed and Models Development

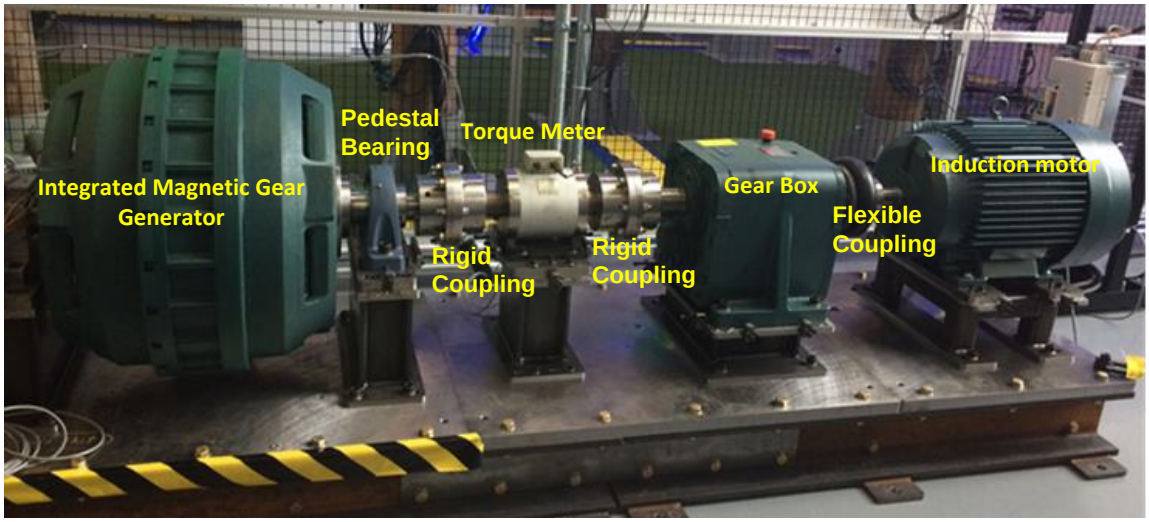

Figure 5. Phase II test bed

The assembled test bench is shown in Figure 5. Due to the low speed and high torque requirements of this machine it was necessary to design a purpose-built test stand. The stand uses a Baldor/ABB 60 hp (44.7 kW), 1,800 rpm induction motor as a prime mover, a Dodge/ABB Maxum XT 21.52:1 gear reducer, a Himmelstein torque transducer rated at 50,000 in·lbs (5,649 Nm) and a 45 kW ABB ACS850 drive to control the induction motor. The drive may be

programmed independently but it may also be controlled via an Agilent 33500B waveform generator permitting specification of custom torque wave-forms, like sinewaves or more random ocean waveforms. The torque transducer is coupled to the generator and gearbox with Dodge rigid-rigid couplings which were chosen to provide accurate torque measurements during oscillating tests. (Torsionally compliant couplings would create a phase shift between the measured and applied torque). The drive machine is coupled to the gearbox via a Dodge Paraflex coupling which adds compliance to the drivetrain and reduces peak-torques imposed on the gearbox.

The use of rigid couplings requires precision alignment of the drivetrain, and it should be noted, is not the typical method for mounting a torque transducer in a drive-train where precision measurements are desired. Due to inherent manufacturing inaccuracies, "perfect" alignment is not possible: shaft run out, mis-alignment of the machine shaft extension with the machine axis, etc. contribute to the error. The final error in the torque measurement is assumed to be ±75in·lbs (8.5N·m) and was determined by rotating the machine and measuring the static torque at the 12, 3, 6, and 9 o'clock positions.

With only the single prototype to work with, testing was structured to move generally from the safest, lowest risk tests first to the more difficult and higher risk tests. This would maximize the available data in case of any difficulties with the generator. Tests started by measuring the machine's static torque curve to identify the systems maximum slip torque, in order to remain below that value for the remainder of the tests. The slip torque of the machine affects the testing in two ways: (1) it limits the constant speed torque achievable by the machine and (2) it places a limit on the permissible waveforms for oscillating testing. Although slipping a pole is an inherent safety feature of the machine, we would rather minimize the potential risk to the prototype until later in testing. Although both points can be addressed by limiting the torque from the drive, it is worth considering what constraint this places on the wave-forms. Without considering the drive train, the effective inertia of the machine relative to the input is

$$I_{eff} = \ I_{LS} + g^2 I_{HS} = 1{,}680\ kg \cdot m^2$$

If the machine is not loaded, the imposed acceleration which will exceed the peak torque is

$$\frac{d\omega_{LS}}{dt} = \frac{\tau_{LS}}{I_{eff}} = \frac{3{,}870N \cdot m}{1{,}680\ kg \cdot m^2} = 2.3rad \cdot s^{-2}.$$

Which indicates, for example that if the machine is accelerated to rated speed (30rpm) the ramp must be of at least 1.4 second duration or the machine will slip. If the machine is loaded, the peak angular acceleration at the input which will cause slip can be found via an energy balance to be

$$P_{shaft} = P_{loss} + P_{inertia} + P_{gen}$$

$$\frac{d\omega_{LS}}{dt} = \frac{\tau_{LS}\omega_{LS} - P_{loss} - P_{gen}}{I_{eff}}$$

$$\frac{d\omega_{LS}}{dt} = \frac{\tau_{LS}}{I_{eff}} - \left(\frac{P_{loss} + P_{gen}}{I_{eff}\omega_{LS}}\right).$$

Since the quantity in brackets is positive this indicates that peak accelerations must be reduced under load, as would be expected.

This type of analysis may be useful in application, where the machine will be more massive and the generator will be tied to a converter. If the machine's inertia is known and the generator's speed can be monitored (e.g. via the back emf) the electrical load can be reduced if the machine approaches its slip torque. Finally, as a generalization we can note that the ocean wave- forms of interest for this study tend to have low peak accelerations and do not therefore impose a significant constraint on testing.

After the static torque measurement, the machine was characterized over the full speed range under no load, with the stator windings left unconnected as an open circuit. Next, for constant speed testing, the machine was loaded with a resistive load and torque and speed data measured for a range of fixed resistive loads over the full speed range. Later, the generator was tested under the more challenging oscillating speed waveforms after proving out the fixed speed operation. The oscillations initially used simple sinusoidal curves and then applied example ocean wave speed profiles defined by RME in Task 1 (during Phase 1) based on hydrodynamic simulations of the WEC performance, still with a range of fixed resistive loads. Finally, select fixed speed and oscillating speed waveforms were repeated using an active converter to control the generator output instead of a passive resistive load. To prevent slipping the machine during testing, the machine was driven to within 95% of the slip torque. Resonance was observed near 20 and 28 rpm as an increase in the noise level of the generator during load testing, but this did not impact the generator testing. The source of this resonance appears to be the modulator, however, the root cause has not been determined. The temperature rise was not expected to be a limiting factor because of the low loss and high mass of the machine. Still, the generator winding temperature was monitored during testing to avoid overheating coils or magnets, and the low, only 13 degree stator winding temperature rise under full load verified the good thermal performance of the machine.

Tasks 5.0 Phase II Prototype Design, Manufacture, and Test

Table 3 includes key details of the Phase II Prototype, shown in cross-section in Figure 6, for the active, electromagnetic components. The Appendix 4 Phase II Prototype Test Report covers additional Phase II Prototype details. The design criteria targeted a peak torque of around 4000 Nm to enable the 10 kW output at 30 rpm, assuming a worst case 80% efficiency, as well as torque density values of 84 kNm/m^3 and 14 Nm/kg of active material volume and mass. The magnetic gear is first sized to achieve these targets. The generator development is constrained by the dimension of the magnetic gear design. With increased speed due to the magnetic gear ratio, the power of generator can be achieved with a smaller footprint, enabling a compact, integrated active structure.

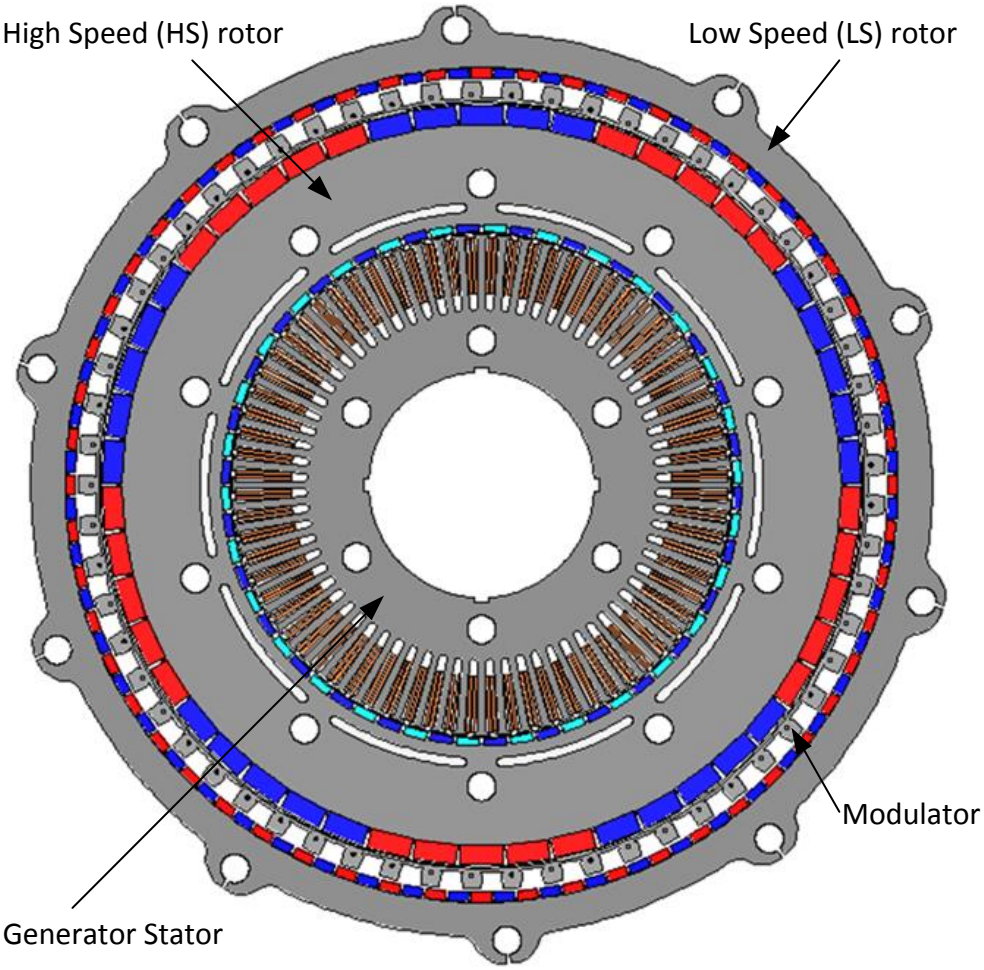

Figure 6. Magnetically geared generator cross-section

The components were designed to handle a static peak torque of at least 5,000 Nm and a temperature rise of 50 deg. C. All components were designed to satisfy this criteria. The machine was designed to be readily machined using processes that were available and typical for machines of the diameter of the Phase II machine. The rotors and modulator were designed to be modular so that each could be separated from its end bells and machined independently. Each component was designed to be similar to the others to limit engineering time, e.g. the end bells are mostly scaled.

The prototype consists of five basic assemblies: (1) shaft, (2) stator, (3) high speed (HS) rotor, (4) modulator, and the (5) low speed (LS) rotor. The central shaft and stator are both fixed at the innermost location within the machine. The magnetic gear modulator section is the other stationary component, fixed between the inner, high speed and outer, low speed rotors. The two rotors rotate in opposite directions. The speed of the high speed rotor is increase by 11.33 times for this design, with the magnetic gear ratio determined by the number of low speed rotor pole pairs, 68, divided by the number of high speed rotor pole pairs, 6. The number of modulator poles, 74, is the sum of the number of low and high speed rotor pole pairs.

Table 3. Prototype machine properties

Property	**Value**
Rated Power	10 kW
Rated Speed	30 rpm
Rated Torque	3,183 N·m
Stator diameter	239.9 mm
Stator airgap	2.5 mm
Stator magnet size	7.6 x 29.2 mm
HS rotor OD (magnet seat)	648.67 mm
HS rotor/modulator airgap	3 mm
HS magnet size	15 x 32.3 mm
LS rotor ID (magnet seat)	710.5 mm
LS rotor/modulator airgap	3 mm
LS magnet size	7.5 x 15.2 mm
LS rotor poles	136
HS rotor poles	12
Modulator pole-pieces	74
Gear stack length	93 mm
Stator stack length	53 mm
Magnetic gear ratio	11.33:1
Overall length (brng-brng)	613 mm
Overall diameter	838 mm
Overall mechanical volume (bounding cylinder)	0.338 m^3
Machine mass	1008 kg
Inertia of LS rotor ($I_{zz)}$	36.7 kg·m^2
Inertia of HS rotor ($I_{zz)}$	12.8 kg·m^2

Shaft

The machine has an outer rotor and an inner stator thus the machine shaft is stationary. The mechanical arrangement has the two rotors mounted on four bearings on the fixed shaft as shown in Figure 7. The bearings used on this machine were standard deep groove roller bearings where the high speed rotor was supported on 6028ZZ bearings and the low speed rotor was supported on 6024 bearings. Despite supporting less mass, the high speed rotor used larger bearings to accommodate necessary steps in the shaft design. This bearing arrangement was not designed for

submersion in sea-water: the necessary housing and seals would be required of future work. Two possible drivetrains were considered: (1) A full shaft with a gear or chain drive, and (2) A partial shaft with a shaft extension to accommodate an axial drivetrain configuration. The first option was discarded due to the perceived additional cost and complexity that would be required of the test stand and the machine was designed to be driven via a shaft extension. Note that this shaft configuration supports a moment and force reaction at the non-drive end (NDE) but only supports a force reaction at the drive-end (DE). Finally, it was decided to drive the machine on axis for testing purposes. This necessitated the addition of an external pillow-block bearing, SKF SY100TF. The primary goal of this machine was to demonstrate the operation of the magnetic gear in a dry laboratory environment, validating the design procedure and predicted performance. Bearings were designed to accommodate prototype and test-stand requirements accordingly.

The shaft has a central bore for extracting the power-leads and two instrumentation slots are also provided at the 6 and 9o'clock positions for pulling instrumentation leads from the interior of the machine. The slots run underneath the inner races of the machine bearings and were added to isolate the instruments from potential noise.

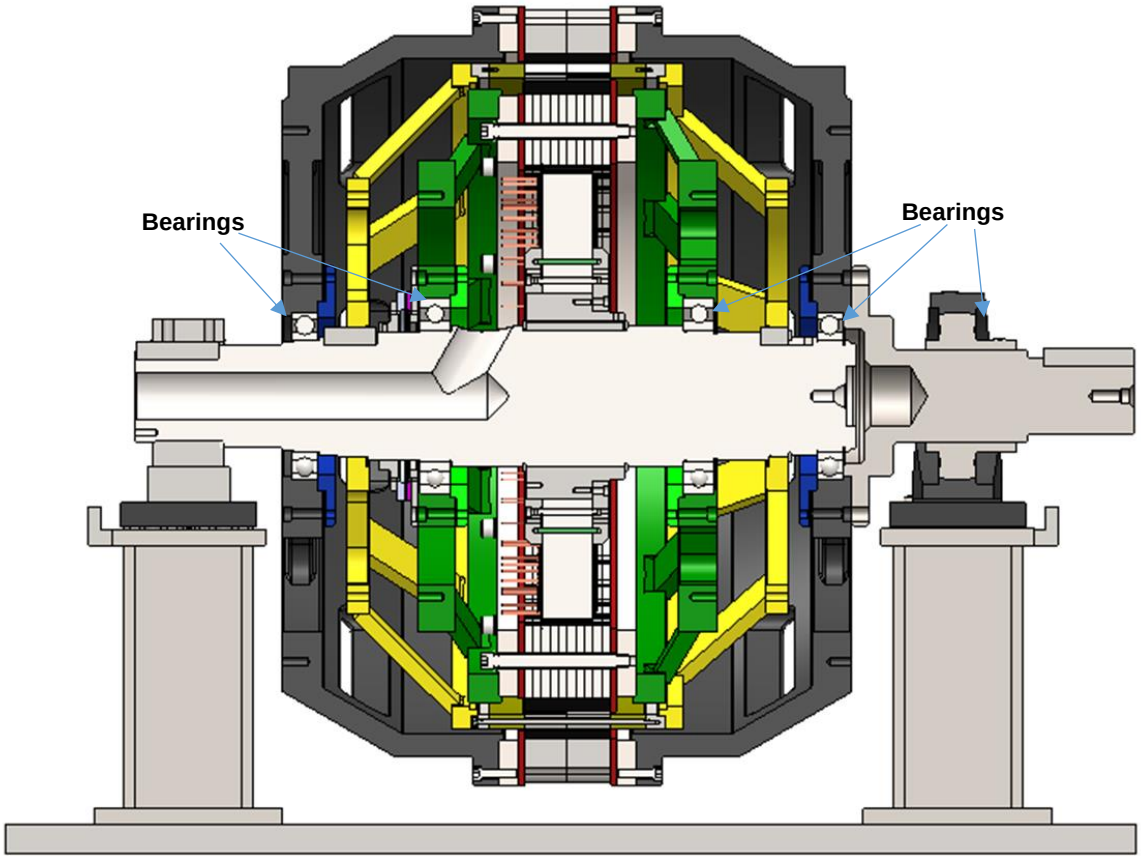

Figure 7. Phase II generator cross-section showing rotor bearing positions on fixed central shaft

Stator

The six phase, 48 slot stator is tooth-wound and was assembled and mounted to a hub which was then keyed to the machine shaft. The stator is subject to the machine torque divided by the gear ratio. The measured stator phase resistance was about 0.235 Ohms, The stator is shown mounted to the machine shaft in Figure 8.

Figure 8. Stator mounted on shaft

HS Rotor

The HS rotor has 12 poles that cover 30º of arc. Since arc magnets of the size required would be expensive, difficult to fabricate and difficult to install, the poles were segmented into five pieces. Although this reduces the cost of the pieces, this creates some difficulty during assembly since the magnets will be not be installed alternating poles and some care must be taken to ensure that the magnets "stay on the iron." The back iron was sized based for both rotors based on electromagnetic requirements. The back iron width of the high speed and low speed rotors were not scrutinized in great detail. Based on prior experience with traditional motors, the already significant widths were expected to be sufficiently rigid to accommodate the loads, and the much thinner modulator section was of more concern as a potential point of failure.

With respect to design for maximum shear stress, for the low speed and high speed rotor we verified that the interlaminar pressures (from a 1D analysis) were sufficient to prevent slip of the laminations under an assumed peak torque condition of 4500 Nm. Although it was not quantified, it should be noted that the magnets are bonded to the laminations and provide significant additional strength to the machine. These are not designed to be structural members, but they nevertheless do improve the stiffness of the machine.

The HS rotor, LS rotor and modulator share a basic strategy wherein we assemble an active core composed of the laminations, stand-offs, and end-rings. This method permits easy handling of the individual components for installing magnets and for the final machining operations (facing and turning rabbets), and these structures are then fit to their end-bells. The stand-offs were fabricated from NEMA grade G11 glass reinforced epoxy laminate and are used to separate the

mechanical structure from the laminations in an effort to reduce losses. The principal disadvantage of this approach is the additional stack-up tolerances that are incurred by adding an additional joint. The laminations for the HS rotor are single piece (non-segmented) 29 gauge electrical steel. The assembled HS rotor is shown in during manufacture in Figure 9 and during assembly in Figure 10.

Figure 9. High speed rotor with wood clamp on last magnet until affixing epoxy set

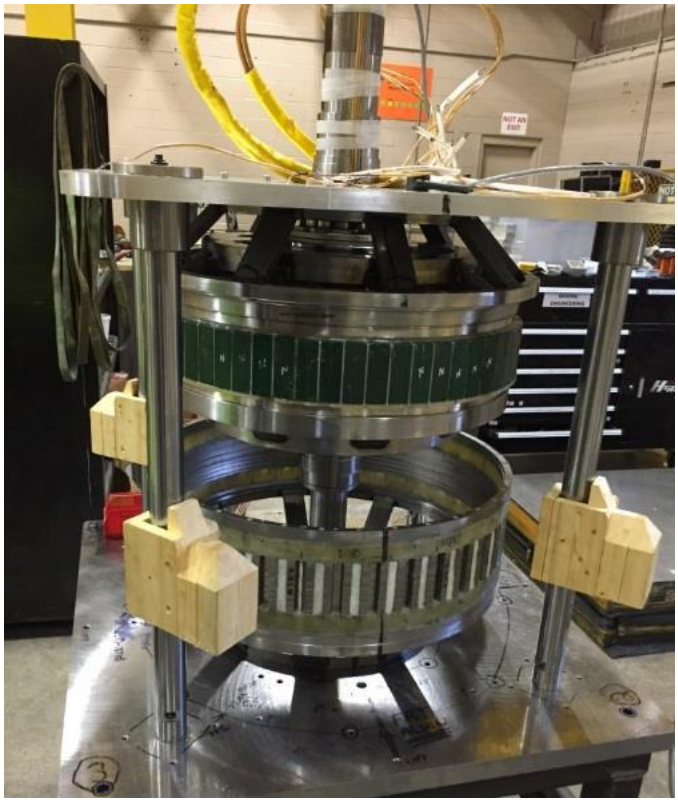

Figure 10. High speed rotor being inserted into modulator

Modulator:
The modulator is subject to the full machine torque but is also the most delicate structure in the machine. In the early design stages the target rating of the machine was 4,000 Nm of torque with a design margin of 500 Nm so that the modulator was designed to handle 4,500 Nm. The modulator was investigated thoroughly before the prototype was constructed using conservative assumptions about material properties and boundary conditions to determine deflections. Deflection under load was determined to be 0.006 in (5% of the air gap) under load as shown in Figure 11. We chose a bridge style modulator with consideration of the following factors:

1. Electromagnetic performance.
   The bridges create a flux leakage path which reduces the machine torque. Despite the flux leakage, bridges can also filter some higher order harmonics which reduces the losses on the HS magnets
2. Structural strength.
   The bridges add significant stiffness to the structure and the increase in area is beneficial for bonding segments.
3. Handling requirements.
   It is desirable to minimize the bridge thickness to mitigate the flux leakage between the pole-pieces. Based on experience it was decided that a 3mm bridge was as small as was practical for cutting and handling purposes with the 29 gauge lamination material.

Due to the small size of the annulus of the modulator with respect to the imposed loads, it was decided to follow a "belt and suspenders" approach to its design. The laminations are bonded together using an adhesive coated lamination material, and the structural components are bonded to the core using an epoxy. The manufacturer specified shear capability of the adhesives were verified to provide the necessary shear capability for this application. In addition to the adhesive, the laminations and structural components are joined together using glass-laminated, G11, 0.1875in diameter through rods which provide alignment for assembly and the requisite shear capability.

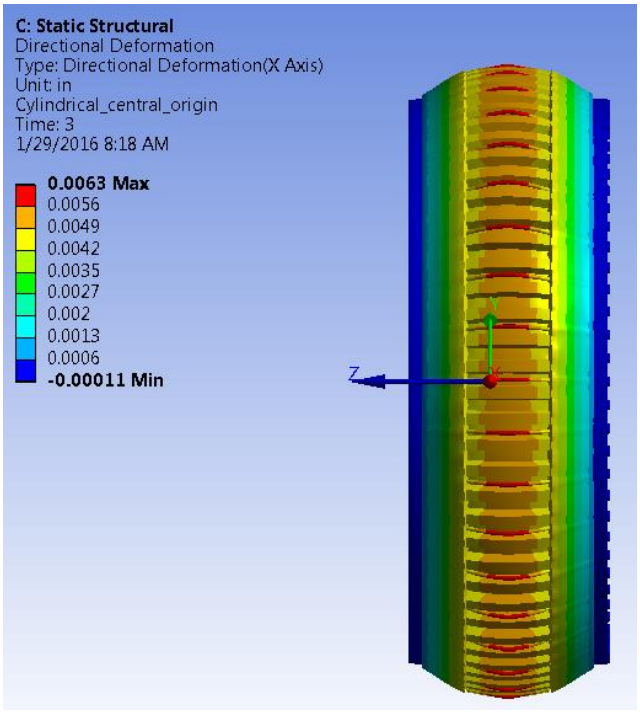

Figure 11. Modulator deformation calculation

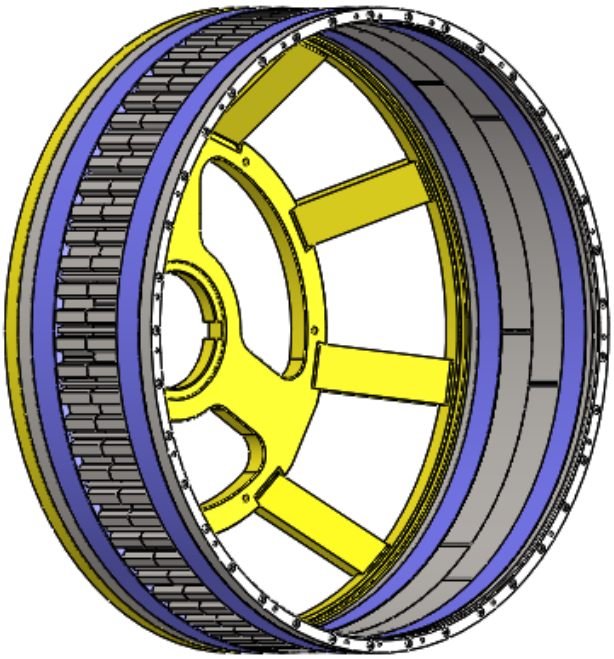

Figure 12. Modulator structure showing from left to right, fabricated end bell (yellow), SS end ring (gray) G11 stand-off (blue) lamination core (gray) ...

The design of the bridge thickness was based on a compromise between the electromagnetic requirements and handling requirements for the lamination segments. We did not attempt to model the resonant properties of the modulator due to its inherent mechanical complexity. However, an impulse test was performed to determine the resonant frequencies of the modulator after its construction and those results are shown in Figure 13.

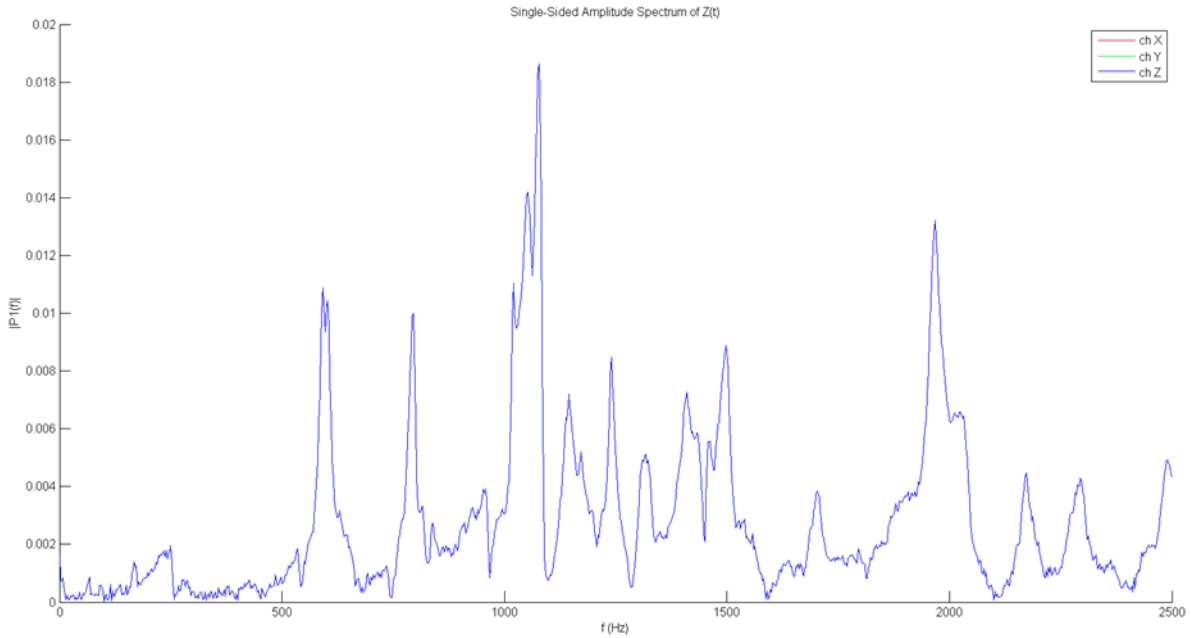

Figure 13. Assembled modulator impulse response test results

Because significant leakage flux was anticipated in the end-regions of the modulator the stand-offs are as large as was deemed practical. They are fabricated from 1.5in (37mm) G11 which presents a significant potential problem due to the mismatch of coefficient of thermal expansion (CTE) between the G11 and the tension bolts. (Glass-filled sheet has low CTE in the 1-1 and 2-2 directions; the 3-3 (through the thickness) CTE is similar to that of plastic.) With regards to the through bolts, two problems arise if traditional metal fasteners are used: (1) the conductivity of the material in the airgap adds to the losses in the machine and (2) a moderate temperature rise can result in yielding the fasteners.

To provide a more uniform stress distribution it was decided to place tension rods either every other slot (37 bolts) or every fourth slot (18 bolts). Although this machine is well ventilated, we targeted a temperature rise of 50℃ which we feel is representative of possible temperature rise in the full scale, non-ventilated machine. For this temperature rise we evaluated a variety of possible fastener choices. Stainless steel (SS) is the obvious choice. However, it does not provide sufficient strength under our loading condition. Silicon bronze (SiBr) was evaluated as another traditional fastener material as well as polyether ether ketone (PEEK) thermoplastic with 30% glass fill. PEEK provided the best performance but we opted to use a more traditional fastener with which we had more experience. A design using 18 silicon bronze rods provides the least amount of conductive material in the air gap which still survives the imposed loads and was chosen for the modulator.

Finally, the modulator was segmented since this would be necessary at the full scale. The modulator has 74 pole-pieces which has 2 and 37 as factors and two segments of 37 are not representative of a scalable design. As a result, we chose to use two unique laminations per layer: seven segments composed of 9 pole-pieces and one of 11. It is also worth noting that stress relief due to local heating during laser cutting caused small distortion of the arc of the segments; this would have been exacerbated if the modulator had been cut as a single piece. It is also necessary to electrically isolate the tension rods from the end rings otherwise the flux through the pole-

pieces will induce a current in the rods and the resulting magnetic field will oppose the field from the LS and HS rotor with the result of significantly reduced net torque and efficiency. Unfortunately during the manufacture of the modulator structure the isolation was compromised, the rods were cut and four additional SS rods were added just to withstand assembly forces although this compromises the thermal capability of the prototype. The modulator has fabricated end-bells.

Significant effort was required to produce components for the modulator that could be reliably machined. The large number of through holes required for the pins on both side of the G11 and end rings made these difficult to manufacture and made the final assembly difficult to clamp to perform the final machining operations on the assembly. Although a thicker annulus for the modulator will ultimately add some magnet cost and volume, it is desired for manufacturability.

Low Speed Rotor

The LS rotor has 136 poles and the laminations are 29 gauge electrical steel. Although the low speed rotor could have been laser-cut from a single lamination it was decided to segment into four pieces since segmentation would be necessary at the full scale. Unlike the modulator and HS rotor the low speed rotor uses castings for the outer most end-bells of the machine. The active components of the LS rotor are shown in Figure 14. The stand-off for the LS rotor is fabricated from 0.25 in G11.

Figure 14. Low speed rotor with magnets installed

Test Results and Predictions

The peak static torque measured 3,870 Nm, within 1% of the predicted value (3,905 Nm).

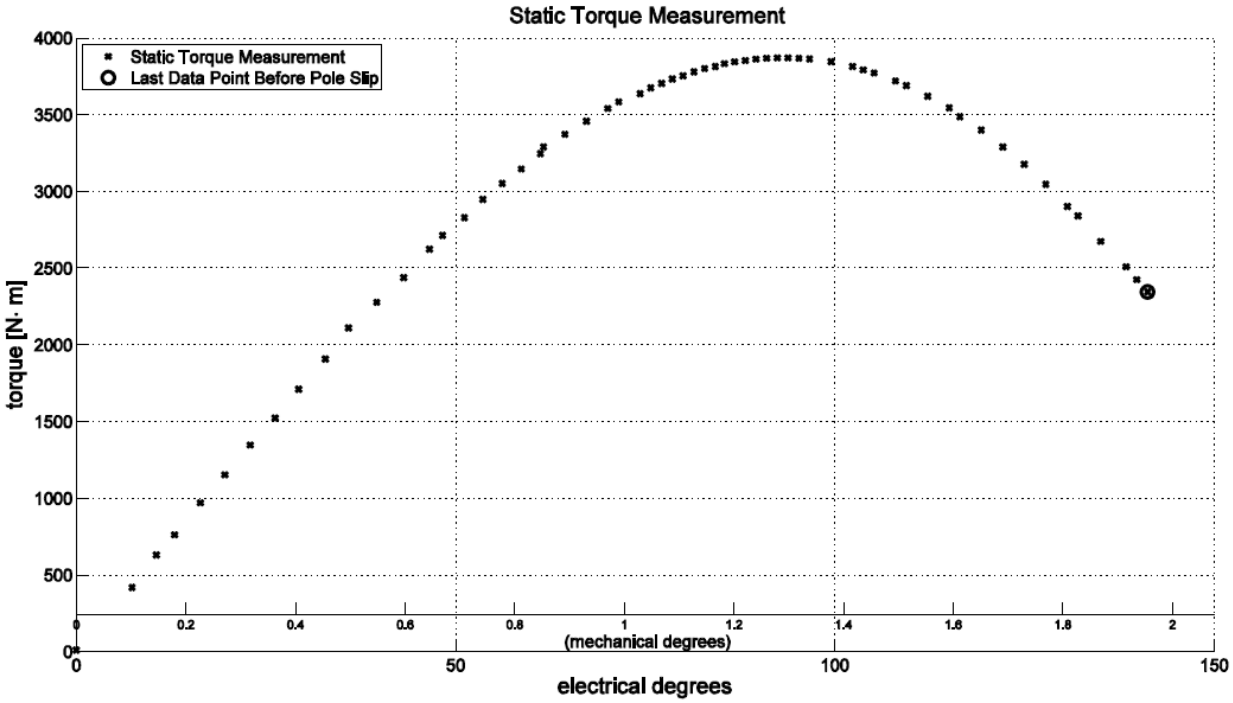

Figure 15. Static torque versus angle measurement

The static torque was measured by locking the high speed rotor and applying a load via a lever on the high speed side of the mechanical gearbox until the low speed rotor slipped. The lock consists of two 0.5 in pins which slide through blocks on the modulator end-bell and index into holes on the HS rotor. Angular displacement was measured on the low speed end bell using a Mitutoyo dial indicator with 0.001in gradations located on a magnetic base and reading from a known radius. It was found that the modulator-end-bell also rotated ~1˚ on its key under load. This created error in the measurement since the torque is produced via relative position of the modulator with respect to the low speed rotor. To measure the small displacement of the modulator a Mitutoyo dial indicator with 0.0001in gradations was placed in a similar manner to the first. The effective rotation of the low speed rotor with respect to the modulator was calculated and the peak torque was found to be 3,870±8.5 Nm. The full static torque curve is shown in Figure 15. Note that the measured torque curve has a peak at 3,870 N·m before the final measurement is recorded at 2,400 N·m. Although this can be measured in a static loading scenario (where the applied torque can be relaxed after the peak is reach) it not would be achievable when rotating under constant torque, i.e. the peak torque is the slip torque when a constant torque is applied.

No load testing was performed with open circuit configuration of the generator terminals. The drive motor provides input torque to spin the low speed rotor at constant speed from 2 rpm to 30 rpm. The generator losses are measured via the shaft torque and speed. To prevent slipping the machine during testing, the machine was kept below 95% of the slip torque. In Table 4, the test data for the power measurement are listed. The temperature included is the average stator winding temperature from the thermocouples built into the six stator phases.

Table 4. No load test data

IM Command (rpm)	LS Rotor Speed (rpm)	HS rotor speed (rpm)	Torque (lbs-in)	Torque (Nm)	Shaft Power (W)	LL V (V, rms)	I (A, rms)	Freq (Hz)	Temp (C deg)
43.04	2	22.67	900	101.70	21.30	23.1	0	7.56	21
86.08	4	45.33	1060	119.78	50.17	45.3	0	15.11	21.5
129.12	6	68.00	1200	135.60	85.20	67.6	0	22.67	21.5
172.16	8	90.66	1370	154.81	129.69	89.9	0	30.22	21.5
215.2	10	113.33	1500	169.50	177.50	112.3	0	37.78	22
258.24	12	136.00	1650	186.45	234.30	134.7	0	45.33	22.4
301.28	14	158.66	1780	201.14	294.89	157	0	52.89	22.6
322.8	15	170.00	1820	205.66	323.05	168.2	0	56.66	22.8
344.32	16	181.33	1900	214.70	359.73	179.4	0	60.44	23
387.36	18	203.99	2000	226.00	426.00	201.7	0	68.00	23.5
430.4	20	226.66	2130	240.69	504.10	224.1	0	75.55	24
473.44	22	249.33	2250	254.25	585.75	246.4	0	83.11	24.5
516.48	24	271.99	2375	268.38	674.50	268.7	0	90.66	25
559.52	26	294.66	2460	277.98	756.86	290.9	0	98.22	25.5
602.56	28	317.32	2580	291.54	854.84	313.4	0	105.77	26
645.6	30	339.99	2720	307.36	965.60	335.6	0	113.33	26.5

The calculate no load losses at 30 rpm from time-stepping finite element simulations are provided in Table 5 to provide a better idea of the expected breakdown between mechanical and electromagnetic losses under no load operation. Future iterations on all aspects of the mechanical supporting structure and bearing arrangement, even though initial solution worked well, could significantly reduce the bearing losses. The generator design tried to minimize induced eddy current losses in the structural components of the generator. These are expected to be low (a few 10's of Watts) in this case, but stray eddy current losses are another possible source of no load losses that is difficult to quantify.

Table 5. No load loss components at 15 and 30 rpm

Speed	**15 rpm**		**30 rpm**	
Low speed rotor core (FEA Calculation)	56 W	15%	148 W	15%
LS magnets (FEA)	82 W	23%	222 W	23%
Modulator (FEA)	18 W	5%	48 W	5%
HS rotor core (FEA)	18 W	0.6%	4 W	0.4%
HS magnets (FEA)	2 W	6%	56 W	6%
Generator stator core (FEA)	21 W	8%	117 W	12%
Generator magnets (FEA)	29 W	3%	28 W	3%
Total electrical no load loss (from FEA)	**218 W**	**60%**	**623 W**	**64%**
Mechanical loss (=Measured - FEA)	**144 W**	**40%**	**343 W**	**36%**
Test measured total loss	**362 W**	**100%**	**966 W**	**100%**

The constant load test was repeated with different loads ranging from 14.1 to 1.2 Ohms per phase, and the results are plotted in Figure 16. The low operating temperatures and consistently high efficiency are encouraging. Even though this stator was designed for a rated operating point at 10 kW at 30 rpm, it still performs well over a wide operating range of speed and load. This attribute is well matched for MHK applications where the input torque from the wave or water energy converter is highly variable.

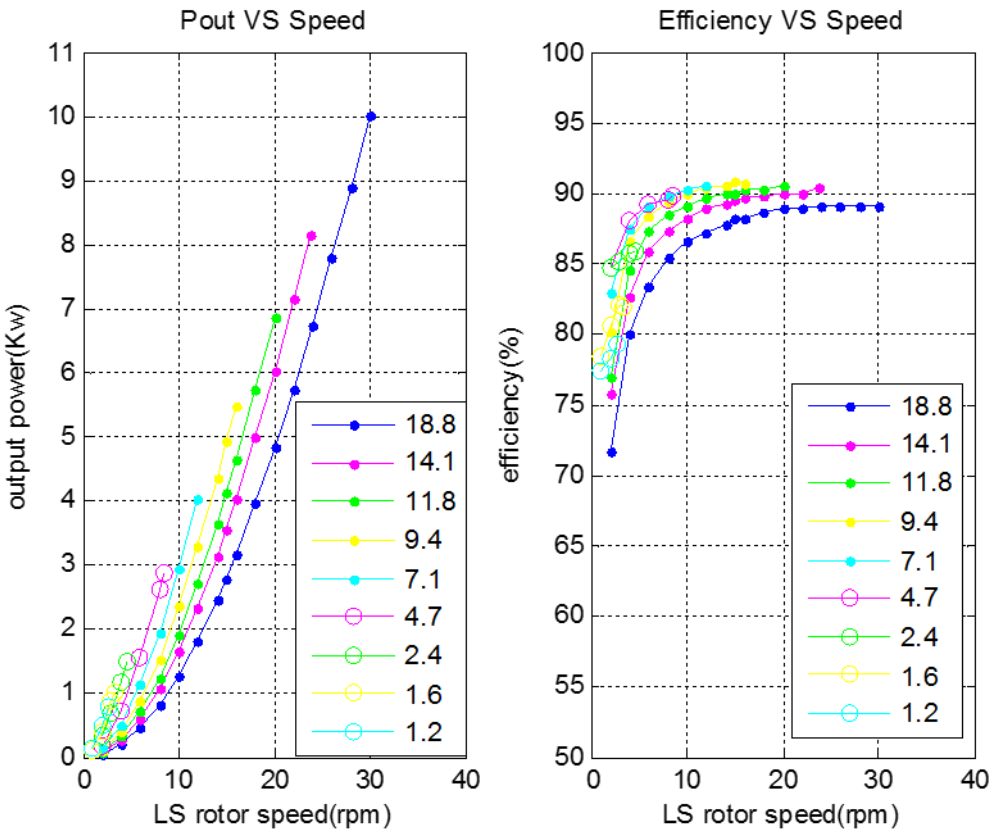

Figure 16. Generator output power and efficiency at different load resistance

The measured efficiency is slightly over 89% at the rated 10 kW, 30 rpm operating point, including the consideration of estimated mechanical drag losses at full speed (343 W obtained from the No Load test, primarily due to bearing losses). Apart from the mechanical losses, the measured electromagnetic system efficiency increases to 92%, which is the combined efficiency of the magnetic gearing (97%) and electrical generation (95%) sections of the integrated machine. In addition to the potential for reduced mechanical losses, the full scale machine, due to the larger size and power rating, is expected to have a slightly higher, around 95.1%, combined electromagnetic efficiency (neglecting bearing or mechanical losses) including both the magnetic gear (98.9%) and electrical generator (96.2%) components.

Despite being designed for a constant 30 rpm rated speed, the prototype was also tested under much slower oscillating speed waveforms. One logical but still interesting conclusion from these tests was that for the same average speed, both the constant speed and sinusoidal oscillation cases produced roughly the same average output power (see Figure 17 below). Similarly, the sinewave period also did not significantly impact the average power output. This data suggests the average speed is the most important parameter for estimating the full scale generator output over a given distribution of ocean wave periods and heights for a given wave energy site. The power output at the 5 rpm oscillation point shows lower power because the torque limit setting on the drive did not allow enough torque for the machine to follow the desired sinusoidal speed function.

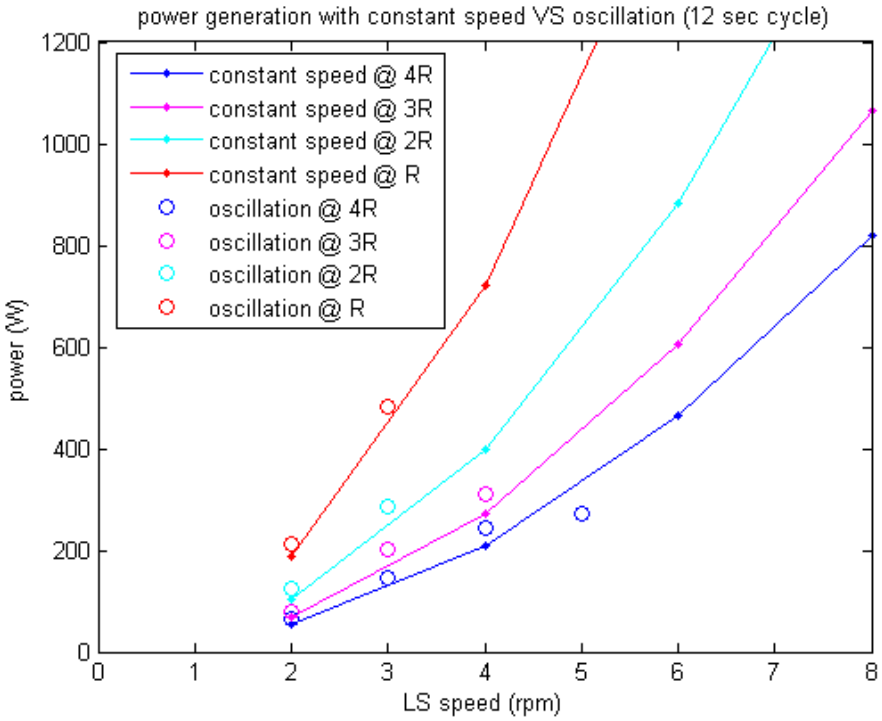

Figure 17. Power comparing oscillation and constant speed tests (R=4.7 Ohm load)

The final sets of testing included a power converter connected to the generator output instead of the resistive load. Unavoidably, the converter must reduce the system efficiency for any individual operating point. However, the reduction in efficiency would be more than compensated in a real system from the overall increase in power output from the ability to control the instantaneous generator load and torque for maximum power output. The system efficiency is expected to achieve as high as ~88% with the power converter when the power is extrapolated to 10 kW. The tests were performed with only three out of the six generator phases because of the converter limitation.

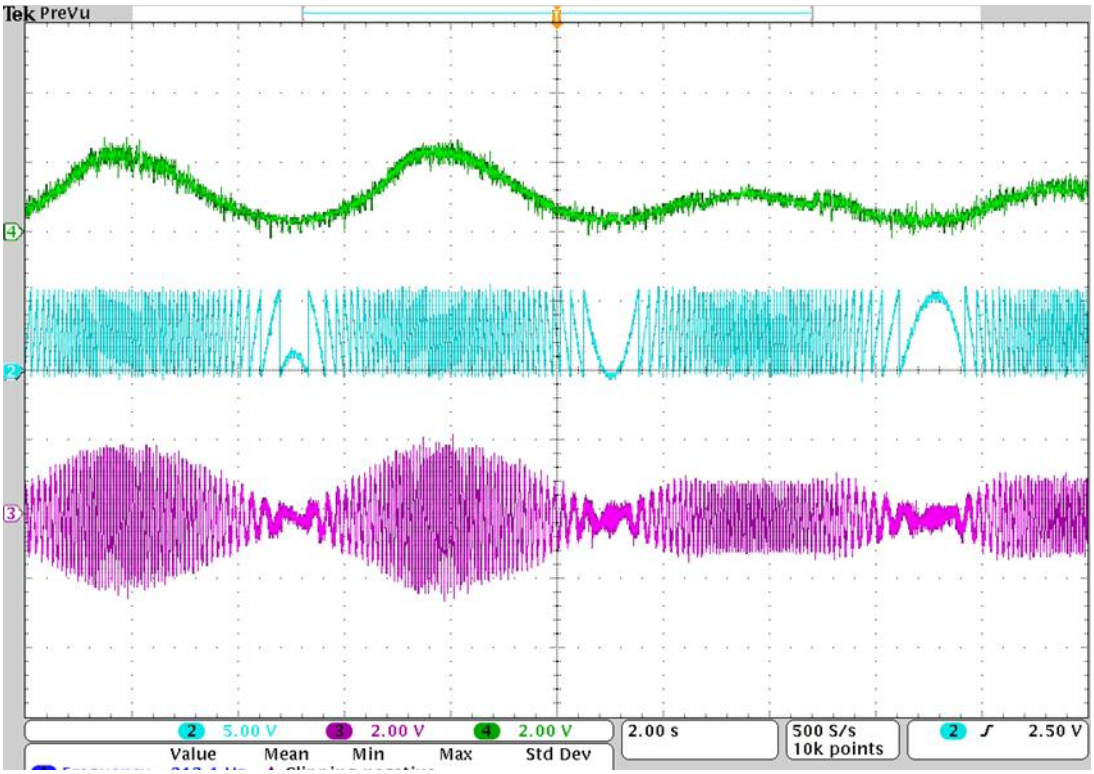

Figure 18. Current regulation for torque limiting in oscillation mode (green:torque, blue: rotor position, pink: current)

Finally, we have demonstrated the torque limiting control of the generator, as illustrated in Figure 18. In the test set-up we have only controlled the input speed for oscillating tests. The focus here is on the generator capability, not the control strategy, and for the same input speed we've demonstrated the ability to limit the generator current and torque. In real ocean wave applications, this torque limiting strategy can allow the generator to avoid the extreme peaks from the flap and ocean waves, benefitting the design and operation of the generator as well as slightly increasing average flap and generator speed.

Suggestions for Future Prototypes

Further work is necessary to scale up the prototype machine in size, torque, and power, for lower speeds. Manufacturability of the modulator is of principal concern at large diameters. Further designs should attempt to predict the resonant frequencies of the modulator before construction although the effect of this could be reduced by providing thicker bridges and a thicker annulus.

Magnetic gears can also have a driven modulator and fixed outer magnets. This results in a slight advantage in gear ratio (g + 1) but was not pursued for the first large prototype due to perceived mechanical complexity. The prototype machine was driven along its axis via the shaft extension, and driving the modulator should not be significantly more difficult if a sufficiently stiff modulator can be designed for the full-scale machine.

Further investigation into bearing arrangement and minimizing the mechanical losses could further improve the generator efficiency and reliability. Also, low cost and dependable strategies for operating the generators sub-sea also need to be developed and tested.

Task 6.0: Full Scale MHK System and Integration Studies

The design of the 40 kW, 1.7 rpm full scale generator is a scaled up version of the Phase II prototype development, with a concept picture in Figure 19 and design parameters given in Table 6 and Table 7. Additional information is provided in Appendix 5, the Task 6.2 Full Scale Generator Design Report.

The outer diameter of the full scale generator is limited to 1.6 meter in order to avoid impact to the hydrodynamic performance of the WEC flap. As with the Phase II design, estimated cost, torque density, and power capability are the main design criteria. After some initial general design sizing calculations, Finite Element Analysis (FEA) optimization routines are run to evaluate a large sample space of potential designs. The critical air gap parameters are selected at 4.5 mm as a reasonably aggressive value based on the Phase II prototype experience.

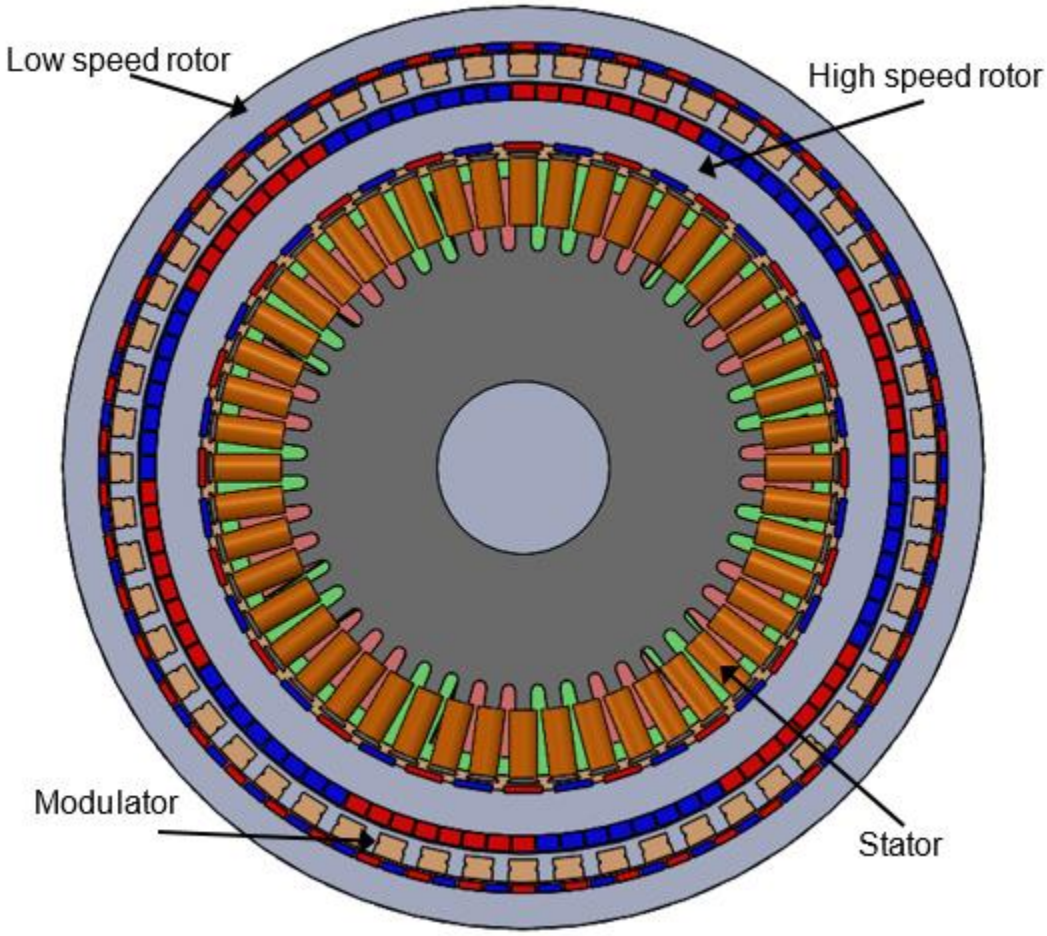

Figure 19. Full scale design concept

Table 6. Full scale design parameters

Parameter	**Value**
Gear Ratio	8.33:1
High Speed Rotor Pole Pairs	6
Low Speed Rotor Pole Pairs	50
Modulator Count	56
Overall Outer Radius	800 mm
High Speed Rotor Back Iron Thickness	101.9 mm
High Speed Rotor Magnet Thickness	28 mm
Modulator Air Gaps	4.5 mm
Modulator Thickness (Including Bridge)	50 mm
Modulator Bridge Thickness	10 mm
Low Speed Rotor Outer Magnet Thickness	14 mm
Low Speed Rotor Back Iron Thickness	50.5 mm
Modulator Fill Factor	0.35
High Speed Rotor Magnet Fill Factor	0.95
Low Speed Rotor Magnet Fill Factor	0.9
Gear Stack Length	1194 mm
High Speed Rotor Outer Radius	614 mm
High Speed Rotor Inner Radius	560.5 mm
Stator Outer Radius	556 mm
Stator Inner Radius	255 mm
Inner Air Gap Length	4.5 mm
Stator Lamination Stack Length	760 mm
Stator End Winding Length	124 mm
Total System Magnet Mass	1180 kg
Total System Mass	15,155 kg

Table 7. Additional design parameters

Electrical Parameters	**Full Scale Design**
Stator Poles	40
Stator Slots	48
LS Rotor inner magnet thickness (mm)	18
Rated VLL (V)	350
Rated Phase current (A)	35
Power Factor	>0.94
Frequency (Hz)	4.53
Connection	YY
Turns / coil	58
Phase Resistance (Ohms at 20º C)	0.17
Copper Loss (W)	1260
Iron Loss (W)	355
PM Loss (W)	30
Peak Torque (kNm)	320
Efficiency (without bearing loss)	95%

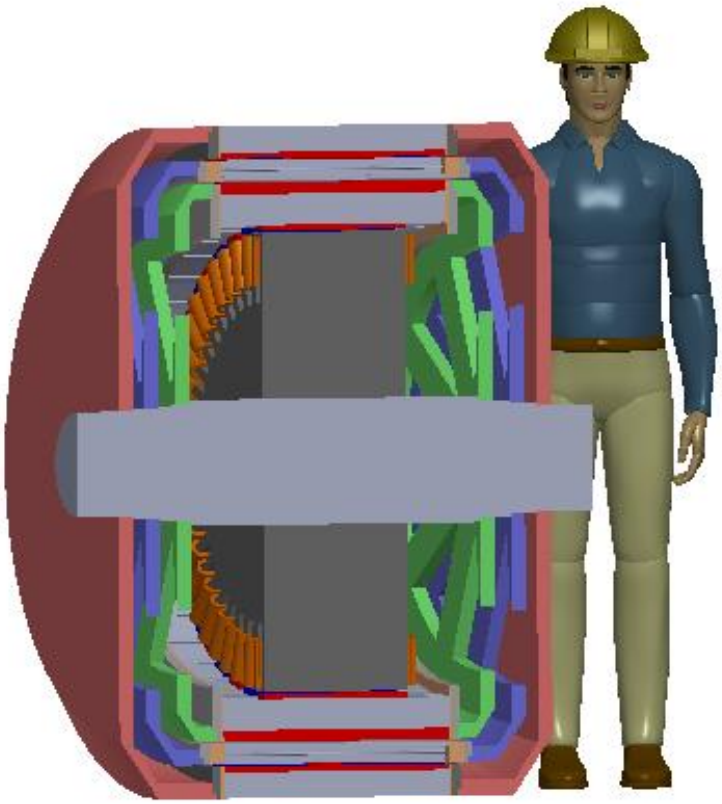

Figure 20. Full scale generator size and structure

For submersible operation, the bearings and sealing will be more challenging, but one option is for the outer rotor (LS rotor) to be integrated with a fully sealed frame. This may be simpler if the modulator is rotated and the outer magnets are held stationary along with the outer sealed housing.

The performance of the full scale generator was also calculated using the same modeling tools and strategy validated with the Phase II prototype. The example ocean wave speed profile is shown in Figure 21.

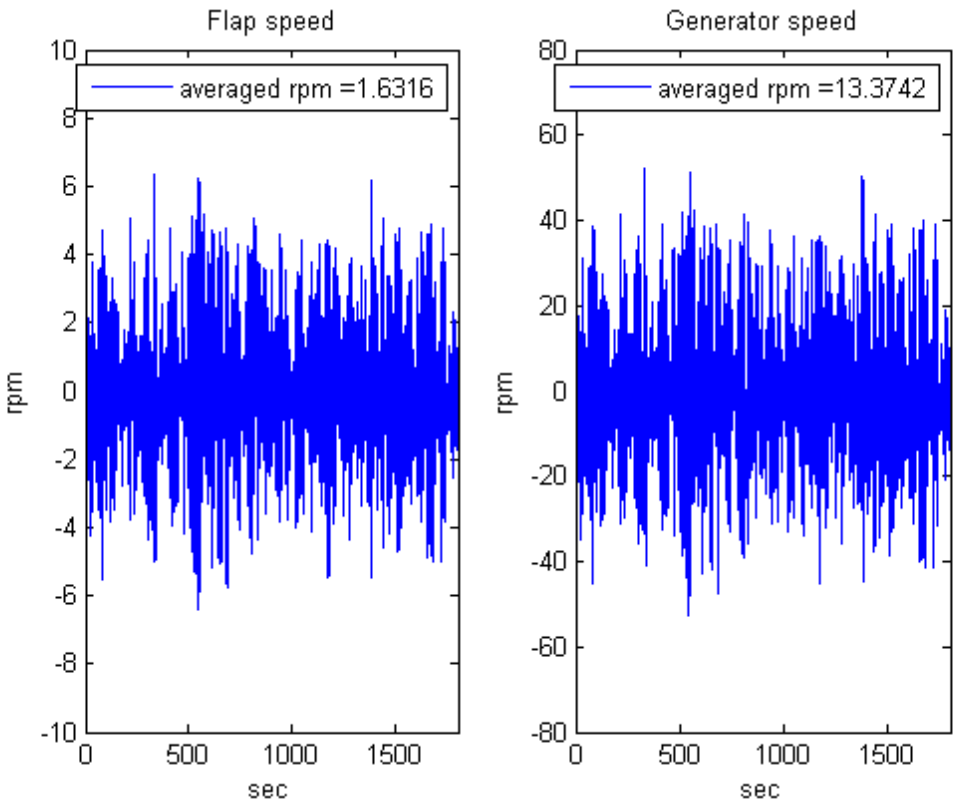

Figure 21. Example ocean wave speed profile

The predicted power output from the full scale generator design, without applying any torque limiting control, is expected to average about 37.3 kW from an average 40.6kW WEC input power. Additional energy conversion stages are required to condition the power for the grid, however this electrical power take off system can offer a significantly higher energy conversion efficiency, better matched to the variable peaked waveforms, than hydraulic-electric or other alternatives. The calculated generator output power is plotted in Figure 22.

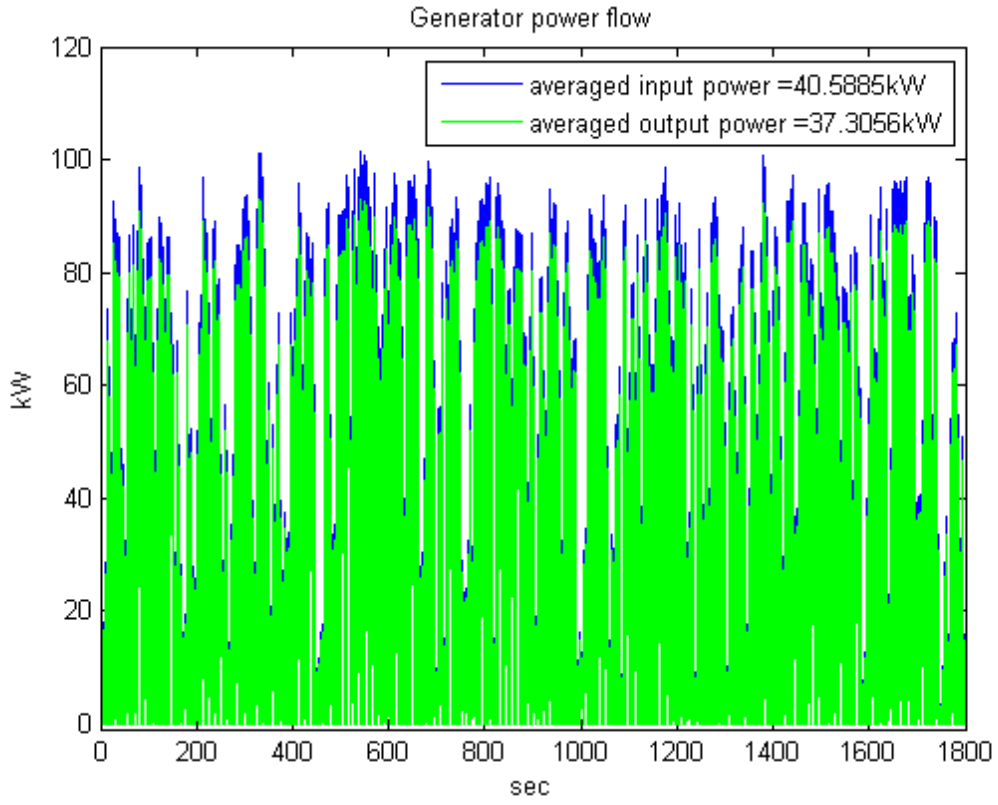

Figure 22. Full scale generator calculated output power

In summary, the full scale generator design, scaled up from the Phase II prototype, and developed using the design procedure validated by both Phase I and Phase II prototype is able to well exceed the project targets for the machine size and cost. In terms of active material cost, using the same $10/kg copper, $50/kg magnet, and $2/kg core cost estimates as in Phase I, the full scale generator design includes only about $82k for the active material, well under the $200k target, leaving plenty of margin for additional supporting structure and manufacturing costs. The volumetric and gravimetric torque density values are similarly encouraging. Table 8 compares the target, conventional off-the-shelf (COTS) reference motor, Phase II prototype, and final design in terms of volumetric and gravimetric torque density, considering just the active material or the full machine. The Phase II prototype does not compare well when looking at the full machine because of the short active length (less than 4 inches compared to an overall length of about 2 feet) and conservative amount of structural material to ensure the success of the prototype. However, taking advantage of additional design optimization and increased stack length, as in the full scale design, enables torque density values exceeding the project targets. The full scale design, despite the lower speed and power ratings, still offers an almost three times reduction in volume and six times reduction in weight compared to the commercial 250 hp, 125 rpm reference. This design is moving toward the required step-change reduction in electrical generator cost, size, and weight required to enable direct drive electrical PTO systems for low speed MHK applications.

Table 8. Torque density targets and values for Phase II prototype and full scale design

Component Metric	Target Value	Units	COTS Reference 250 hp (186.5 kW) 125 rpm	Phase II 10 kW 30 rpm	Full Scale 40 kW 1.7 rpm
Total Volume Density	46	kNm/m^3	18	12	88
Total Mass Density	10	Nm/kg	3.8	3.8	21
Active Volume Density	84	kNm/m^3	33	75	93
Active Mass Density	14	Nm/kg	5.5	17	33

Task 7.0: System Performance Impact Analysis

Detailed calculations of LCOE according to the NREL guidelines for both the Baseline Hydraulic and Direct Drive Electrical PTO Systems can be examined in the attached spreadsheets and summarized below in Figure 23 through Figure 28. In general, these projections remain difficult at this stage in the technology development. However, they do provide a useful comparison and encouraging estimation of some of the potential benefits of a direct drive electrical PTO system.

The summary values for the two PTO system alternatives are included below. The LCOE calculations show a reduction of more than the targeted 10% when comparing the $1.24/kWh value of with the baseline hydraulic PTO system (Figure 23 and Figure 24) to the $1.01/kWh value for the direct drive electrical system (Figure 25 and Figure 26). The main advantage of the direct drive electrical system is increased net power generation because of increased power conversion efficiency. This is consistent with industry trends toward more electric systems and reasonable considering the test results from the Phase II prototype and full scale generator design calculations.

These values are considering the same fixed, maximum 50kW generation capacity for both PTO systems. In reality, this fixed capacity makes sense for a hydraulic motor or pipe where there is no difference between the maximum and continuous ratings, but the electrical PTO system should have more flexibility in generation capability. The generator and electrical power converters can be sized for thermal limits to better take advantage of the pulsed power from the ocean waves. With similar initial investment requirements, the electrical PTO system can be designed for momentary peak output of 100 kW instead of the original 50kW (Figure 27). This one change makes for better use of the WEC and ocean wave energy, increasing the annual generation and further decreasing the LCOE to $0.80/kWh (Figure 28).

Significant research and development work remains before this type of magnetically geared generator and PTO system can be commercially available. Still, this project has demonstrated the significant potential this technology holds for low speed, high torque applications like ocean wave or similar MHK energy conversion.

Spreadsheet input and output			
Input		**Output**	Annual
WEC width	8 m	Average wave energy	30.5 kW
WEC rated cap.	50 kW	Average energy extracted by one WEC	33.9 kW
Number of WEC	18		
AEP Directional losses	10%	Operating time	78%
AEP Shallow water loss	10%	Capacity factor	68%
AEP Array losses	10%	Theoretical annual energy production	2,380 MWh
Conversion efficiency	61%	Actual energy capture	2,142 MWh
Availability	90%	**Annual Energy Production**	**1,928 MWh**

Figure 23. Baseline Hydraulic PTO LCOE Parameters

ICC	13,971,275 $
FCR	0.108 %
O&M	873,730 $
AEP	1,928 MWh
LCOE	**1.24 $/kWh**
CAPEX contribution	0.78 $/kWh
OPEX contribution	0.45 $/kWh

Figure 24. Baseline Hydraulic PTO LCOE Value

Spreadsheet input and output			
Input		**Output**	Annual
WEC width	8 m	Average wave energy per meter	30.5 kW
WEC rated cap.	50 kW	Average energy extracted by one 8m WEC	33.9 kW
Number of WEC	18		
AEP Directional losses	10%	Operating time	78%
AEP Shallow water loss	10%	Capacity factor	68%
AEP Array losses	10%	Theoretical annual energy production	3,121 MWh
Conversion efficiency	80%	Actual energy capture	2,809 MWh
Availability	90%	**Annual Energy Production**	**2,528 MWh**

Figure 25. Direct Drive Electrical PTO LCOE Parameters

ICC	14,305,670 $
FCR	0.108 %
O&M	1,017,475 $
AEP	2,528 MWh
LCOE	**1.01 $/kWh**
CAPEX contribution	0.61 $/kWh
OPEX contribution	0.40 $/kWh

Figure 26. Direct Drive Electrical PTO LCOE Value

Spreadsheet input and output				
Input			**Output**	Annual
WEC width	8	m	Average wave energy per meter	30.5 kW
WEC rated cap.	100	kW	Average energy extracted by one 8m WEC	43.0 kW
Number of WEC	18			
AEP Directional losses	10%		Operating time	78%
AEP Shallow water loss	10%		Capacity factor	45%
AEP Array losses	10%		Theoretical annual energy production	3,953 MWh
Conversion efficiency	80%		Actual energy capture	3,558 MWh
Availability	90%		**Annual Energy Production**	**3,202 MWh**

Figure 27. Direct Drive Electrical PTO LCOE Parameters with Increased Power Output

ICC	14,305,670 $
FCR	0.108 %
O&M	1,017,475 $
AEP	3,202 MWh
LCOE	**0.80 $/kWh**
CAPEX contribution	0.48 $/kWh
OPEX contribution	0.32 $/kWh

Figure 28. Direct Drive Electrical PTO LCOE Value with Increased Power Capability

MILESTONE DELIVERABLE

Task 1.0: Generator Specifications from System Aspects Including Wave Profiles, Wave Energy Converter (WEC) Characteristics, and Electrical PTO Requirements

Date of Completion: 3/21/2015

State of the art power take-off systems for flap-type wave energy converters use hydraulic PTO components. A direct-drive electrical generator and PTO system could offer significant advantages in terms of system simplicity and availability. However, the large generator size and cost for this extremely low and variable speed application is not currently available or competitive using conventional technology. The main challenge addressed by this project is the design of an electrical generator of a sufficiently reduced size and cost to be competitive with the hydraulic alternatives. One of the project goals addressed by the generator and system specifications is to determine roughly what is required from the generator and direct drive electrical PTO system in order to substitute for the hydraulic system.

1. SPECIFIED WAVE ENERGY CONVERTER MECHANICAL REQUIREMENTS:

This section discusses the specified mechanical requirements on the generator determined by the flap-type wave energy converter (WEC) device under the given wave profiles. Figure 1 illustrates the scale of the flap and generators, showing one possible configuration with the outer rotors of two separate generators joined to the base of the flap on either end of the common axis. Another alternative, depending on the generator length and final system bearing solution, could also use a single generator in the middle along the flap axis.

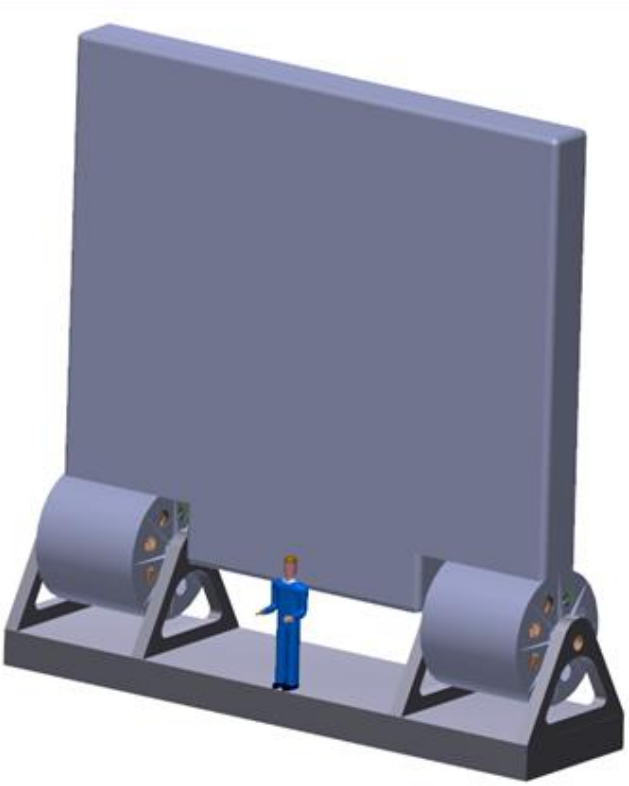

Figure 1. Concept illustration of flap integrated with two outer-rotor generators

A baseline flap and hydraulic PTO system have been defined for reference, target setting, and comparison to the proposed electrical PTO system. The reference system is rated for 30 kW electrical power output to the grid using a single 8 m wide by 7 m tall flap at rated sea conditions of 2.5 m wave height and 12 sec wave period. Both rated wave conditions as well as an annual distribution of wave conditions have been defined as input. Additionally, representative half-hour, data sets of simulated flap torque and speed for both rated sea conditions and a few reduced wave heights have been provided for partial load calculation and comparison.

The motion of the flap and directly coupled generator are unique for this application. Instead of the constant speed, continuous rotation typical for most electric motors and generators, the direct drive generator in this case will oscillate, rotating back and forth with the flap, stopping and changing direction twice every cycle. The average speed is low but the oscillations contribute highly variable peak values of speed and torque at irregular intervals. For the phase one and phase two prototype development at reduced scale, the generators are designed and tested with an increased constant speed in order to make the prototypes more manageable. However, for the target application of the generator directly coupled with the flap in the sea bed, the actual motion is oscillating back and forth, as shown in Figure 2. The slow motion averages around 0.18 rad/sec and the rotation angle varies within ±70 degrees, usually much less. The peak to average speed ratio for this data set is nearly 4:1.

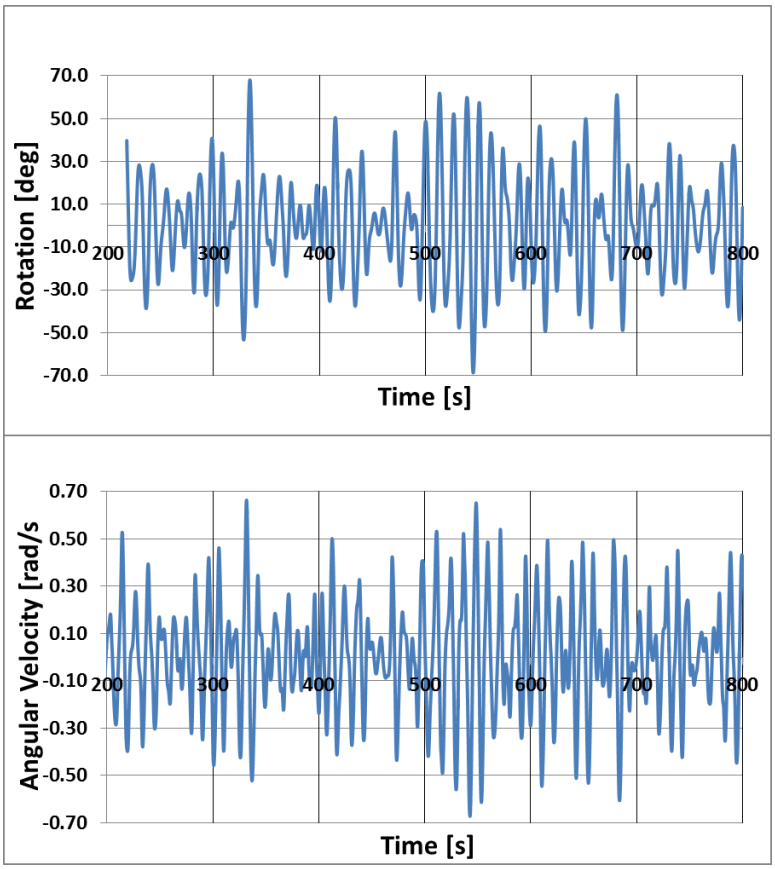

Figure 2. Example flap angle and velocity for 10 min interval with load torque limited to 320 kNm

The peak and average flap values under the rated wave conditions and with the load torque applied to the flap by the PTO system limited to no more than 320 kNm are provided below in Table 1. With no limit on the load torque applied to the flap, the peak torque can reach nearly four times the average value, and the peak power more than nine times the average.

Table 1. Wave energy converter flap characteristics with PTO torque limiting

Mechanical PTO Load Torque			**Rotaional Angle**				
Ave PTO Torque	240	kNm	Ave Rotation Angle	18.4	deg		
Peak PTO Torque	320	kNm	Peak Rotation Angle	68.7	deg		
Peak/Ave Torque Ratio	1.3	pu	Peak/Ave Angle Ratio	3.7	pu		
Flap Mechanical Output Power			**Angular Velocity**				
Ave Mech Flap Power	53	kW	Ave Angular Velocity	0.18	rad/sec	= 1.7	rpm
Peak Mech Flap Power	215	kW	Peak Angular Velocity	0.67	rad/sec	= 6.4	rpm
Peak/Ave Power Ratio	4.1	pu	Peak/Ave Velocity Ratio	3.83	pu		

Limiting the torque applied to the flap by the PTO system can significantly reduce the generator peak torque and peak power output with a comparatively small reduction in average torque and power. For example with the same flap, limiting the peak generator torque from about 1,180 kNm to no more than 320 kNm reduces the average torque only from 320 to 240 kNm. Similarly, the peak mechanical power output reduces from 564 kW to 215 kW while the average mechanical output drops only from about 64 kW to 53 kW. With the limited generator torque, since the wave input does not change, the average angular flap speed also increases from about 0.13 rad/sec to 0.18 rad/sec (1.2 to 1.7 rpm), helping to reduce the generator size and cost.

The load torque can be limited by bypassing the pumps in the hydraulic case. In the electrical PTO case there are a number of possible strategies to limit the torque including reducing the field current in field wound synchronous machines, reducing the generator phase winding current by controlling the conduction time of the solid state switches used to rectify the generator output power for permanent magnet machines, or slipping poles in a magnetic gear. This topic will be discussed in more detail as part of the comparison between generator alternatives.

2. ELECTRICAL PTO SYSTEM REQUIREMENTS:

This section describes the target values for the electrical PTO system including power output, efficiency, and cost. The baseline hydraulic PTO system is the starting point for the electrical PTO system requirements. The overall specifications of the electrical PTO system are defined in order to provide at least equal electrical power output to the grid, using the same flap under the same wave conditions (rated for 30 kW output in this case for a single 8x7m flap).

a. Baseline Hydraulic PTO System Overview

The full description is available and under continued development from the project partner Resolute Marine Energy and has been removed here for the publically released full report. The description did not include the flap prime-mover and its foundation or the interface to the utility grid or anything that is common to both cases since the goal is a comparison between the hydraulic and electrical systems.

a. Electrical PTO System Initial Overview

The variable current and voltage waveforms produced by the direct-drive generator with the periodic and bidirectional waves require customized power conversion technology. The wave energy variability must be supplemented with an energy storage system in order to maintain a constant output voltage and limited output power ramp rate. The energy storage system acts as an energy buffer, smoothing the power output at the grid-tie. Figure 3 shows the potential direct-drive system interconnected with the grid.

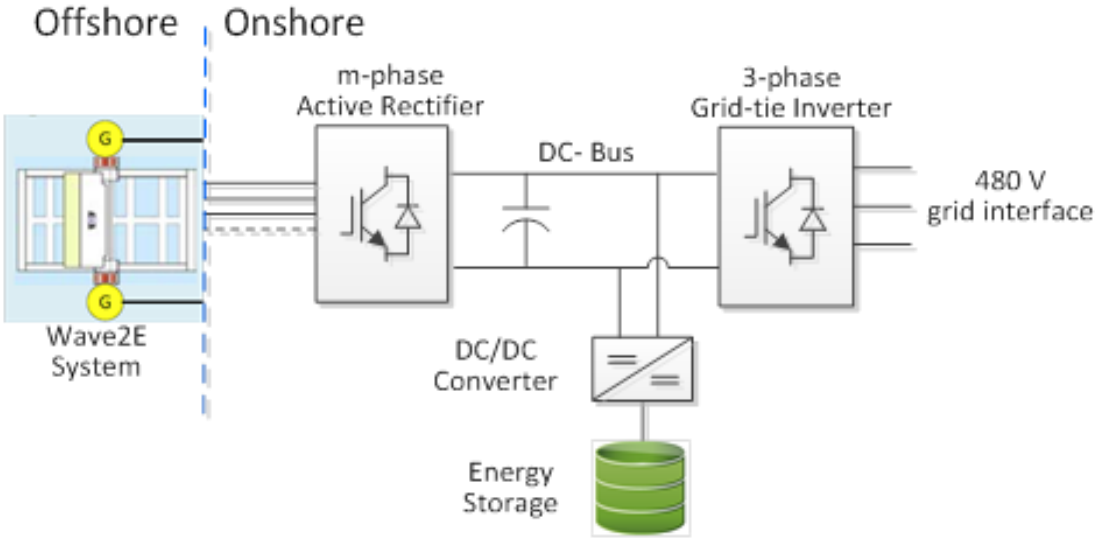

Figure 3 . Electrical PTO system configuration

In this configuration the dc-link is an essential intermediary between the low and variable frequency generator and the 60 Hz grid. The energy storage is a requirement of the power conversion and needs to be sized only large enough to maintain the output voltage level and minimum power ramp rates required by the grid. Additional energy storage could be included for both hydraulic and electrical PTO systems to provide power during extended periods of no or light waves, but this is not included at this stage.

One of the typical challenges in integrating such a variable output power to the grid is in controlling the dc-link voltage stability within the power conversion system. The stability of the dc voltage can be ensured by having a fast dynamic energy storage system connected directly to the dc-link [1]. The energy storage system improves dc bus voltage regulation by using a bidirectional dc/dc buck-boost converter to dynamically control the charging/discharging of the super-capacitors proportionally to any variation in the generator output.

The principal components and estimated costs are provided in Table 2. Estimates are based on commercial products from various vendors for the given rating. In this case the estimated material cost of the direct-drive generator has been doubled to roughly account for manufacturing costs.

Table 2. Estimated cost of electrical PTO system components

DESCRIPTION	EST Rating	QTY	UNIT COST	EST COST	MANUFACTURER
Direct Drive Generator	40 kW	1	400,000	400,000	ABB
AC-DC Rectifier	125 kW	1	60,000	60,000	ABB, ZBB
Cable	3-core 775 meters	2	7,175	14,350	Mercury Wire
Capacitors - DC Bank	350 - 450 V, 220uF	30	130	3,900	AVX
Bidirectional DC -DC Converter	125 kW	1	60,000	60,000	ABB, ZBB
Grid side DC - AC Converter	80 kW	1	60,000	60,000	ABB, ZBB
Super Capacitor Module	125 V, 144Whr	16	6,500	104,000	Maxwell Technologies
System Controller		1	20,000	20,000	ABB/ZBB
Aux - System Protection	-	-	50,000	50,000	
TOTAL				**$ 772,250**	**$25,700/kW**

These values suggest a reasonable, direct-drive electrical PTO system can be cost competitive with the baseline hydraulic PTO system. The final electrical PTO system design will be reviewed and updated with the Phase II prototype testing and delivered at the end of Task 6.

In addition to equal or lower cost, the electrical PTO system must also provide equal or greater electrical output power to the grid as the rated 30 kW hydraulic solution under similar wave conditions. Since the input mechanical power from the flap is also the same for both systems, this requires equal or higher power conversion efficiency for the electrical PTO system. In order to meet this goal, each major component of the electrical PTO system requires at least the minimum efficiency values as given in Table 3.

Table 3. Electrical PTO system component minimum efficiency requirements

PTO System Component	Min Efficiency
Generator	80%
AC/DC Rectifier	93%
Cabling & Connections	94%
DC-DC Converter	96%
Energy Storage	92%
Grid Inverter	97.5%
Electrical PTO System:	**60%**

Efficiency values can also be traded between components as long as the system total remains at or above the 60% target, ensuring at least 30 kW of the roughly 50 kW (The average flap mechanical power from Table 1 is actually 53 kW, so 50 kW is a conservative and convenient value to use for clearer calculations.) of mechanical power available from the flap is delivered to the electrical grid. The next section narrows the focus down to the generator, as the source behind the electrical power output as well as the main new and enabling component of the electrical PTO system solution.

3. DIRECT DRIVE ELECTRICAL GENERATOR REQUIREMENTS:

The previous section included a minimum generator efficiency requirement of at least 80%. This is a low efficiency value for a typical 40 kW electrical machine. This efficiency is not expected to be a challenge or limiting factor for a permanent magnet generator. A higher generator efficiency would increase the electrical power output or allow for a slightly smaller generator design. The 80% generator efficiency requirement can be

reexamined for the final generator and system design in Task 6, but for now provides a reasonable and conservative starting point and builds in some margin for unexpectedly low efficiency anywhere else in the system. Starting with around 50 kW of mechanical power delivered from the flap, a minimum 80% efficiency results in a minimum generator rating of 40 kW. These are net, total values, and depending on the aspect ratio and supporting structure requirements, the 40 kW could be from a single generator mounted in the center of the flap or two separate generators symmetrically attached to the flap as illustrated in Figure 1 and Figure 3.

Also from the previous section, the cost for the total 40 kW direct drive electrical generator material should be less than about $200,000. From the first section, the rated generator speed dictated by the torque-limited flap averages about 1.7 rpm with the generator average torque 240 kNm with the peak torque limited to 320 kNm.

One starting point for the generator design is to first consider a generator with constant rotating speed equal to the average speed of the actual flap. The low but constant rotational speed case is simpler to model and compare to machines rated for other values of speed and power output. In particular, constant rotation at higher speeds and lower power output compared to the full scale design is required in order to make the reduced scale Phase I and Phase II prototypes more manageable. Still, it is critical to also consider how the constant speed, rotational case relates to the motion of the actual application.

The torque, size, weight, and cost of the Phase I and Phase II prototype generators are significantly reduced by increasing the rated speed and running the machines continuously rotating. This enables multiple prototypes to be built and tested within a limited time and budget but also requires some examination of the difference in performance between the constant speed versus oscillation.

Initial examination during the second quarter found a 15% reduction in average torque when using a sinusoidal speed waveform with a 1 rpm average value compared to a constant 1 rpm speed.

A more detailed comparison of the generator performance under constant speed and oscillations using a 40 kW design is included below as shown in Figure 4. Values are selected from the baseline flap for a 12 second cycle time and a 1.7 rpm average speed for both cases. For this calculation, a simplified sinusoidal waveform is used instead of the more complicated actual flap torque waveforms. Besides simplifying the process, the sinusoidal oscillation, with a peak to average ratio of only about 1.6 provides a conservative estimation of the impact on the power output. An increased peak to average ratio will only increase the average power output for the oscillation case. The generator and power conversion equipment must be designed to handle the peak current values. If the peak torque is limited, the generator power output can increase with the increased flap speed during the intervals of maximum applied torque. Comparison of the generator current, torque and power are shown in Figure 5, Figure 6, and Figure 7.

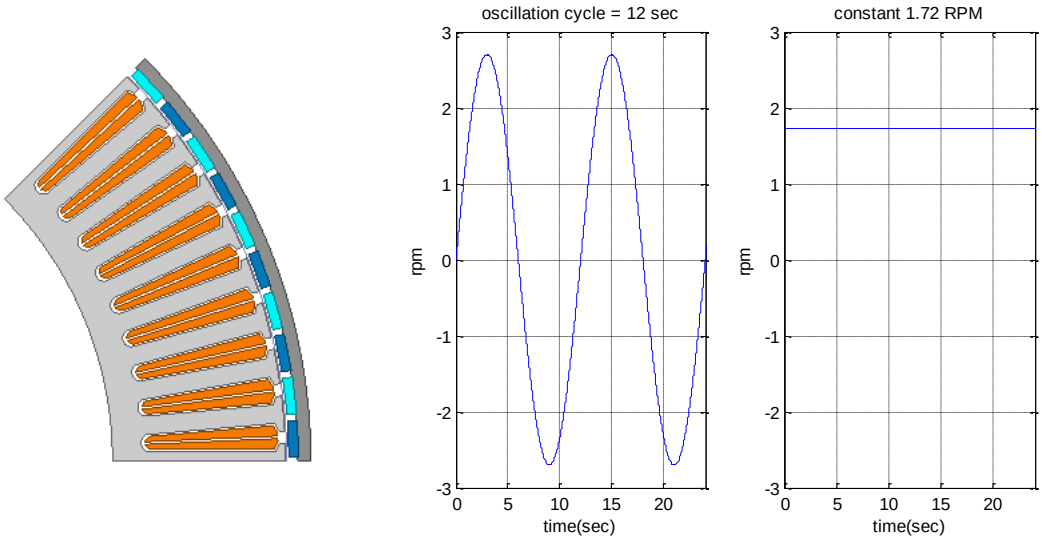

Figure 4. Geometry and speed for constant vs oscillation calculations

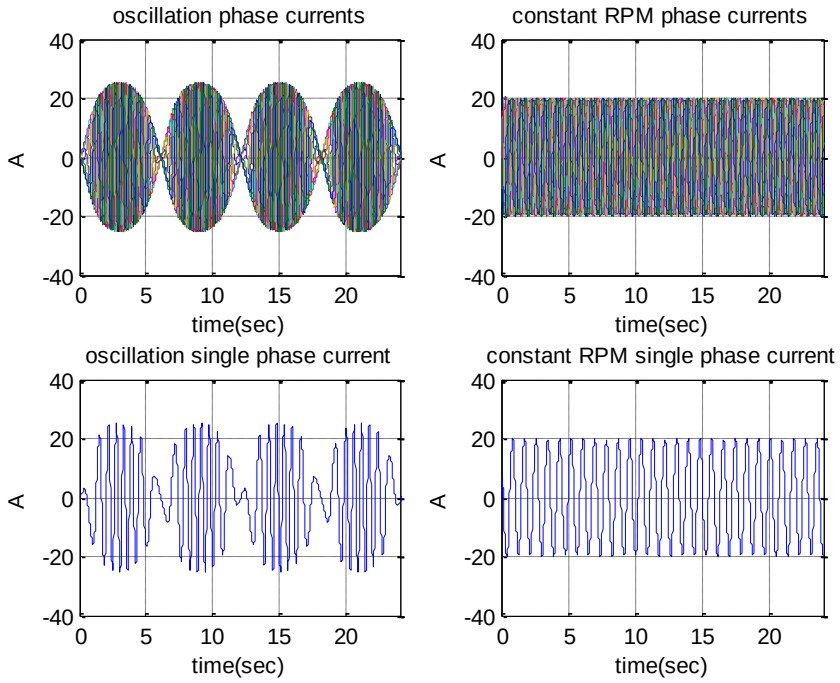

Figure 5. Generator phase current for sinusoidal oscillation (left) and constant speed (right)

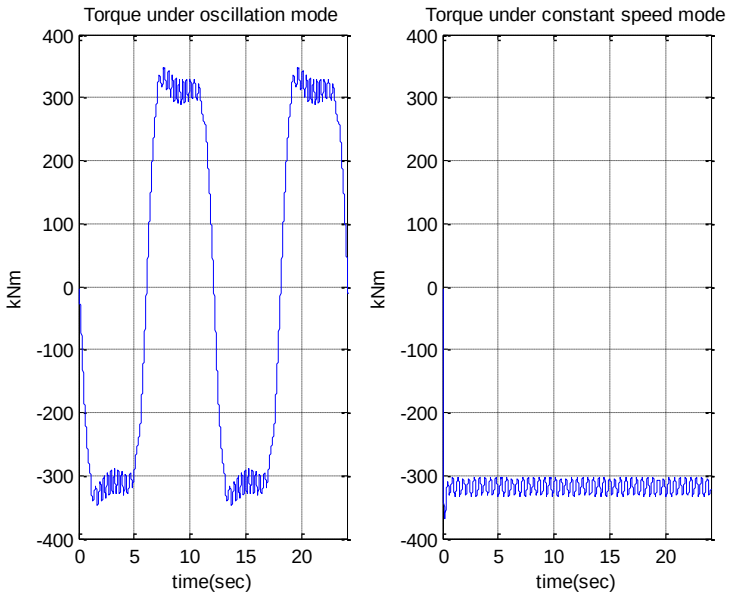

Figure 6. Generator torque for sinusoidal oscillation (left) and constant speed (right)

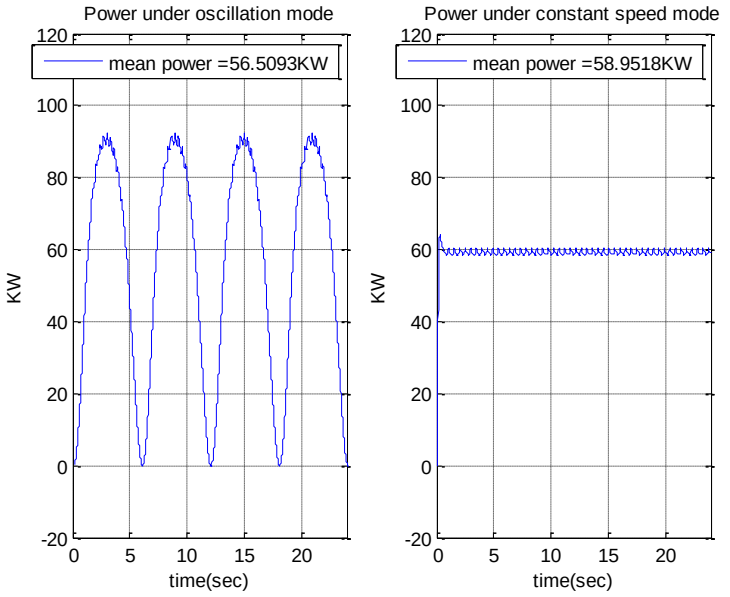

Figure 7. Generator output power for sinusoidal oscillation (left) and constant speed (right)

The average torque values in this case are about 270 kNm and 320 kNm for the sinusoidal and constant speed cases. The average torque in the sinusoidal case is about 18.5% lower, similar to the 15% calculation in the Quarter 2 Report. The power output, as a function of both the torque and the speed, is a better value for comparison. The average power here only reduces by 4% in the sinusoidal oscillation case, and higher power output will result from the actual flap torque and speed waveforms, with the increased peak values. We have also already run simulations using sections of the flap torque and speed waveforms when evaluating a field wound alternative rotor with no surprises. The same performance trends and design tradeoffs apply for either the

constant or highly variable generator speed, provided the generator and power converter components are correctly sized for the increased peak, periodic currents. The simulated torque and speed flap waveforms as in Figure 2 will also be used to estimate the power production of the final generator design in Task 6.

Specific, initial torque density requirements for the full scale and prototype generators have been defined for this project based on doubling the mass and volume torque density values of state-of-the-art direct drive industrial motors with ratings as similar as possible. This goal has not changed, but the target values given in the original proposal and later SOPO have varied slightly, depending on how the values were calculated. The active volume calculation used for the rest of the project will be a function of the outer and inner diameters of active material and the core length plus any axial extension of the end windings.

This calculation is applies equally well for both prototype and full scale designs. Moving forward, the greatest of the torque density values previously given will be used as the torque density targets

Table 4. Baseline motor and target torque density values

BASELINE MACHINE DESCRIPTION					
	Output Power	Speed	Torque	Active Mass	Volume (OD-ID, L+Ends)
	[Watts]	[rad/sec]	[N.m]	[kg]	[m^3]
Full Scale Reference	186,500	13.09	14,248	2,600	0.430
Prototype Reference	5,222	31.42	166	91	0.020
TORQUE DENSITY VALUES					
	Output Power	Speed	Torque	Active Mass Density	Volume Density
	[Watts]	[rad/sec]	[N.m]	[N.m/kg]	[kN.m/m^3]
Full Scale Reference	186,500	13.09	14,248	5.5	33
Prototype Reference	5,222	31.42	166	1.8	8
TORQUE DENSITY TARGETS (USING GREATEST OF PROPOSAL, SOPO, OR DOUBLE BASELINE VALUES)					
	Output Power	Speed	Torque	Active Mass Density	Volume Density
	[Watts]	[rad/sec]	[N.m]	[N.m/kg]	[kN.m/m^3]
Full Scale Reference	40,000	0.18	224,689	**14**	**84**
Prototype Reference	1,000	31.42	32	**4**	**16**

All else being equal, the higher the torque density and the smaller the generator the better. However, the cost for the required power output at the given torque and speed is the most important factor. There is a rough, general correlation between machine size and weight and material cost, but making a smaller and lighter generator with increased power density (for example with increased permanent magnet material) is not beneficial if the total cost is not still competitive. The cost for the required average power output and speed is the most critical requirements on the direct drive generator designs. A fixed 80% minimum efficiency target is also included, but is not particularly challenging (can this be justifiably scaled for Phase I and Phase II prototypes?)

Table 5. Direct drive generator targets

Parameter	Final Generator Design	Phase II Prototype
Min Rated Ave Power [W]	40,000	10,000
Min Rated Ave Speed [rpm]	1.7	30
Min Rated Ave Torque [Nm]	240000	3180
Min Rated Ave Efficiency [%]	80	80
Max Generator Material Cost [$]	200,000	2,750

The Phase II and Phase I prototype requirements are determined using the scaling procedure described in the next section.

4. GENERAL SCALING PROCEDURE:

The full scale generator design and requirements cannot be directly scaled down to the prototype levels, at lower power and higher speed ratings. The generator outer diameter and air gap length are two significant parameters requiring special scaling consideration. The other machine parameters may generally be assumed constant or simply adjusted logically consistent with the adjusted geometry and air gap length. The volume and cost of any machine can vary significantly based on the aspect ratio and the air gap length. Electric machines generally favor designs with increased diameter and decreased air gap length, pushing the limits until some other constraint is reached. A consistent scaling approach for the machine diameter then enables defining the length and aspect ratio for a given power, speed, and torque, and this, together with any defined change in air gap length are enough to roughly scale a given machine design

The air gap length, as one of the most critical parameters in any electric machine design, is typically sized as small as mechanically possible. Realistic air gaps can vary from less than half a millimeter in small, fractional horsepower machines to more than a centimeter in large, multi-megawatt machines. The air gap in the Phase I prototypes, at 1.5mm for the outer rotor designs and 2-4mm for the multiple air gaps in the axial flux integrated gear generator, have been sized conservatively large in order to reduce the chance of mechanical issues. On the other hand, full scale calculations use a more aggressive air gap value for the given machine size, around 5mm, to minimize the machine size, weight, and cost. The range of reasonable air gap values is relatively small, but the design impact is significant. Instead of trying to determine a simple, straightforward, and general method to account for differences in air gap length, the different air gap values will be separately assigned as given input values for the machine designs at any given scale.

It is a challenging task to consistently compare machines of different power rating, different rated speed, or different design topology, and there is not one unique, simple and clear method. One traditional method of comparison is to use the volume ($D_g^2 L_e$) sizing equation [1], which compares the machine power on the basis of the air gap volume, where D_g is the air gap diameter and L_e is the effective stack length. However, the machine outer diameter D_o is more directly coupled with the volume and thus to the cost and size of the machine. The general-purpose sizing and power density equations based on the main machine dimensions $D_o^2 L_e$ instead of air gap dimension $D_g^2 L_e$ have been developed for machine evaluations and previously validated by comparison with a wide range of machines [2], [2].

From the work presented in [4], the electromagnetic torque in a machine can be approximated by:

$$T_e \approx \left(\pi r_{ag}^2 l\right)\left(\hat{A}_s B_{rg}\right) = \lambda_0^2 v_m \left(\hat{A}_s B_{rg}\right) \quad (1)$$

Where

$$\lambda_0 = r_{ro} / r_{ag} \quad (2)$$

is a conversion ratio to get from air gap radius and volume to outer radius and total machine volume, v_m, with

$$v_m = \pi r_{ro}^2 l \quad (3)$$

In these equations r_{ag} is the center of the air-gap radius, r_{ro} is the machine outer radius (rotor outer radius for our outer rotor machines), l is the stack length, $\hat{A}_s$ is the peak stator current loading, and B_{rg} is the flux density in the air-gap due to the rotor magnets.

The machine torque and generator output power are a result of the interaction between the stator current (represented as $\hat{A}_s$) and the rotor magnets (B_{rg}).

From (1), the electromagnetic torque is approximately linearly proportional to machine volume for a fixed speed. Furthermore, the volumetric torque density is directly proportional to the energization quantities $\hat{A}_s$ and B_{rg}. which can be assumed roughly constant for consistent magnetic and electrical machine loading. The current is limited by the maximum current density, losses, and cooling strategy. The air gap flux is limited by the electrical steel magnetic saturation, air gap length, and magnets. The equation for power is obtained from the torque as

$$P_e = \omega_{rm} T_e = \omega_{rm} \lambda_0^2 v_m \left(\hat{A}_s B_{rg}\right) \quad (4)$$

where ω_{rm} is the angular velocity of the rotor.
Or equivalently expressing the torque as in (5) shows the dependence of the torque on both the rated power and speed.

$$T_e^* = P_e^* / \omega_{rm}^* \quad (5)$$

Since the torque is a function of the radius cubed, and accounts for changes in both power and speed, it is a convenient parameter for roughly consistent scaling machine dimensions. The outer radius can be roughly scaled as the cube root of the ratio of the torques. However, this by itself does not account for the typical and somewhat arbitrary change in air gap lengths for different machines. The scaling in radius should also be adjusted by dividing by the ratio of air gap lengths, since torque is roughly inversely proportional to the air gap length.

This provides a scaled generator outer diameter requirement, which can then be used to derive a machine design, analytically or using FEA, and approximate active material mass and cost.

As one example, assuming a 2 m outer diameter for the full scale generator design, Table 6 below shows the resulting values for the Phase II prototype. In this case the cube root of the ratio of torque is almost ¼, about 0.24, and dividing this by the 1:2 ratio

of air gap lengths gives about 0.48, which is remarkably consistent with the rough ratio of 1 m to 2 m outer diameters from finite element calculations of these machines. Active material mass and cost can then be estimated from the finite element model or an equivalent analytical design. This scaling procedure has not been widely verified but seems reasonable and is consistent with finite element calculations of the Phase II generator in this case, as shown in Figure 8.

Table 6. Generator scaling example

	Power [kW]	Speed [rpm]	Torque [kNm]	Air gap [mm]	Outer Diamter [m]	Cost [$]
Full Scale Design	40	1.7	225	5	2	200,000
Phase II Prototype	10	30	3.2	2.5	1	2,750

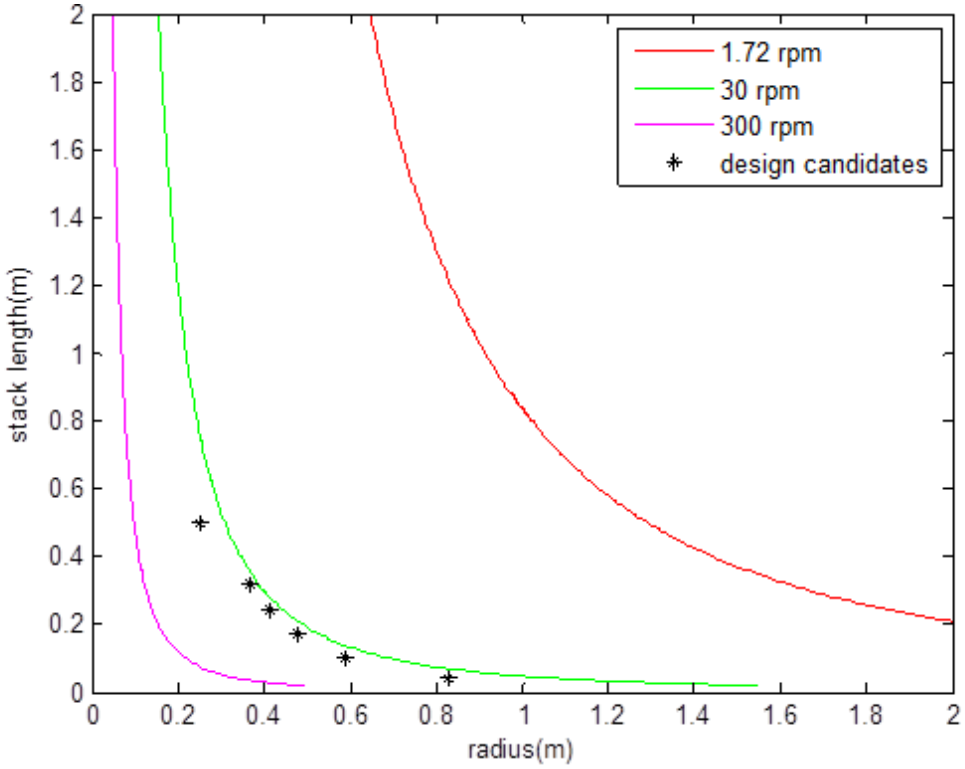

Figure 8. 10kW generator sizing with different aspect ratio

In Figure 8, the solid lines are analytical sizing equations and the *'s represent particular finite element models with different active material aspect ratio. The active material costs for these same designs are estimated below in .

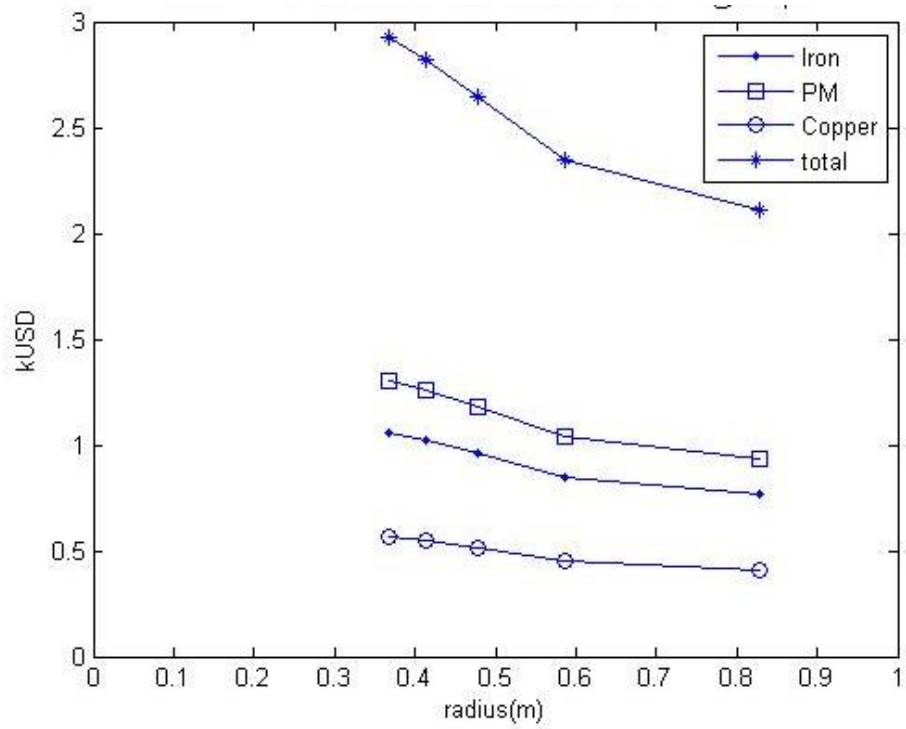

Figure 9. Active material cost estimation of 10 kW, 30 rpm FEA models

5. ESTIMATED SYSTEM RELIABILITY:

Assuming the direct drive electrical PTO system can deliver similar power output and performance at a similar system cost, then the main advantage claimed over the hydraulic PTO system is increased reliability and availability. This claim is consistent with conventional wisdom and general trends in the automotive and aerospace industry, where safety and reliability are critical, but this section provides more specific data and justification.

The reliability data is gathered from recent papers covering topics on power electronics in renewables (wind, wave, etc.), a comprehensive survey on reliability performed by the Army Corp of Engineers, and ABB internal documents and citations. The numbers are presented in the form of Mean Time Between Failures (MTBFs) and Mean Time to Repair (MTTR) statistics from literature and communications with vendors and experts in their respective fields, for components similar to those planned for the electrical PTO system.

The IEEE 493 Standard for the Design of Reliable Industrial and Commercial Power Systems published in 2007 cites a comprehensive review of hydraulic and electric component reliability and downtime produced by the US Army Corps of Engineers and Reliability Analysis Center. The study, referred to as Annex Q in gathered over 6,000 records of O&M data from commercial and industrial facilities, manufacturing utilities, universities, and others for a variety of equipment in service during a span of 30 years.. The study concluded in 1997 and consists of dated data for certain parts of the electrical system; hydraulics, in contrast, have been well established and changed less since the study started. Therefore, MTBF and MTTR have been updated to replace outdated values for the converter and inverter MTTR and a field for supercapacitors has been added, which were not widely available at the time of publication. The results for MTBF and MTTR are presented in Table 7 and Table 8 below.

Table 7. Estimated hydraulic PTO system component reliability data

Category	MTBF [hrs]	MTTR [hrs]	Reliability for a period of 20 Yrs
Accumulator	1336648	8.22	88%
Induction Motor < 600V	791448	1	80%
Piping, Water, >2<=4 inch	426692	14.08	66%
Positive Displacement Pump	1066720	8	85%
Valve, Check	33963360	1	99%
Valve, Pressure Relief	6587760	2	97%

Table 8. Estimated electrical PTO system component reliability data

Category	MTBF	MTTR	Reliability for a period of 20 Yrs
Cable Connection	23624073	0.75	99%
DC-DC Converter	6500894	1	97%
Rectifier	1960032	0.5	91%
Inverter	1817016	0.5	90%
Cable-Below Ground, 1000 ft	1512727	6.77	89%
Super Capacitor Bank	1.33E+10	0.5	99%
Capacitor Bank	5022133	0.5	96%

These tables quantitatively describe the advantage of an electrical PTO system in terms of MTBF and MTTR of components versus a similar hydraulic system. The column titled "Reliability for a period of 20 Yrs" uses the well-known formula for comparing likelihood a component will successfully run for 20 years according to the formula below:

$$Reliability = e^{\frac{-20*8760}{MTBF}}$$

Based on the reliability numbers, the average likelihood that a hydraulic component and system will meet a 20-year lifespan is reduced compared to the same measure for a comparable electrical system. To improve the hydraulic PTO system reliability requires more frequent scheduled maintenance, but at the same time, this will increase the downtime and decrease the availability. Based on the MTTR, maintenance and repair of the hydraulic system also requires nearly four times longer on overall average. The complete system projected downtime and availability are summarized in Table 9 below. Since the actual availability of the electrical direct drive generator is still unknown, for this calculation it is assumed equivalent to the "Induction Motor" included in Table 7 of the hydraulic system components.

Table 9. Estimated hydraulic vs electrical yearly PTO system availability

PTO type	Typical availability over a year
Hydraulic	96.70%
Electrical	99.10%

The system availability is calculated mathematically as:

$$p(0) = 1 - p(x_1) - p(x_2) - \cdots ..$$

where, $p(0)$ is the probability that all components are in service (total availability of the system), it is equal to the 1 minus the sum of the unavailability of the other components in the list and $p(x_j)\,p(x_j)$ is the unavailability of component x_j. The unavailability of component x_j is equal to 1 minus its availability, and the component x_j operational availability is given as:

$$p'(x_j) = \frac{MTBF}{MTBF + MTTR} - SEU$$

where, SEU is scheduled unavailability. The scheduled unavailability is assumed to be one day a year for the electrical PTO system and four times this for the hydraulic PTO system from a combination of increased frequency and duration of required maintenance.

As argued in the original proposal, if maintenance costs make up 18% of the levelized cost of energy (LCOE) for a wave energy farm as estimated by the UK Carbon Trust in 2012 [5], then a 60% reduction in downtime and maintenance results in a 10% decrease in LCOE. The relative increase in availability for the electrical PTO system in this calculation shows roughly a 75% reduction in downtime and maintenance, consistent with a more than 10% reduction in LCOE. This argument also requires equivalent electrical power output from the interchangeable hydraulic and electrical PTO systems.

The reliability reference data and calculated availability estimates for both hydraulic and electrical PTO systems will become more realistic as the technology becomes more established. However, even in the near-term, the relative comparison still provides a reasonable calculation for the potential improvement in availability and reduction in LCOE for the direct drive electrical PTO system compared to the hydraulic baseline.

6. REFERENCES:

[1] Muhamad Zalani Daud, Azah Mohamed, and M. A. Hannan “An Optimal Control Strategy for DC Bus Voltage Regulaiton in PV System with BES”, Vol. 2014, The Scientific Wrold Journal of Hindwai Publishing Corporation

[2] Surong Huang, Jian Luo, Franco Leonardi, T.A.Lipo, “A general Approach to Sizing and Power Density Equations for Comparison of Electrical Machines”, IEEE Transactions on Industry Applications, Vol.34, No. 1, Jan 1998

[3] Wen Ouyang, “Modular Permanent Magnet Machine Drive System with Fault Tolerant Capability”, PhD thesis, University of Wisconsin-Madison, 2007.

[4] M. G. Say, *Alternating Current Machines*, 5th ed., Halsted Press, John Wiley & Sons, Inc., ISBN 0-470-27451-4, 1983.

[5] IEEE Gold Book 493 – Design of reliable industrial and commercial power systems, 2007.

[6] Carbon Trust report, “UK wave energy resource,” October 2012.

MILESTONE DELIVERABLE

Task 2.2: 1 kW Generator Prototype Test Results

Date of Completion: 03/20/2015

1. GENERAL DESCRIPTION:

This document describes the results of the experimental performance evaluation of the pole-modulated, 300 rpm generator prototype as well as a tooth wound stator using the same surface permanent magnet outer rotor. The primary goals of these tests are to

- Demonstrate the feasibility of the novel rotor design
- Compare the mass and volumetric torque density of the prototype against the baseline targets
- Measure test data for calibration and validation of performance calculations
- Identify potential risks and opportunities to improve the electromagnetic, mechanical, structural, or thermal performance of the larger second prototype

Following an initial description of the test-set-up and generator configurations, the rest of the report compares mechanical, electromagnetic, and thermal measured test data to finite element calculated predictions.

Finally, a comparison is made between the two configurations of the Phase I prototype and the baseline reference values.

2. TEST SET UP:

After some initial load tests driving the generator rotor directly using the 20 hp motor where the generator is face-mounted, the test set-up was reconfigured in order to add an in-line torque transducer. A DC drive dyno which can provide direct torque measurements of the shaft is utilized for the remainder of the prototype testing. A bare shaft has been substituted in place of the rotor inside the 20 hp induction machine. The same 20hp induction motor frame and bearings are used to support the prototype generators under test. The general layout of the test set-up is shown in Figure 1.

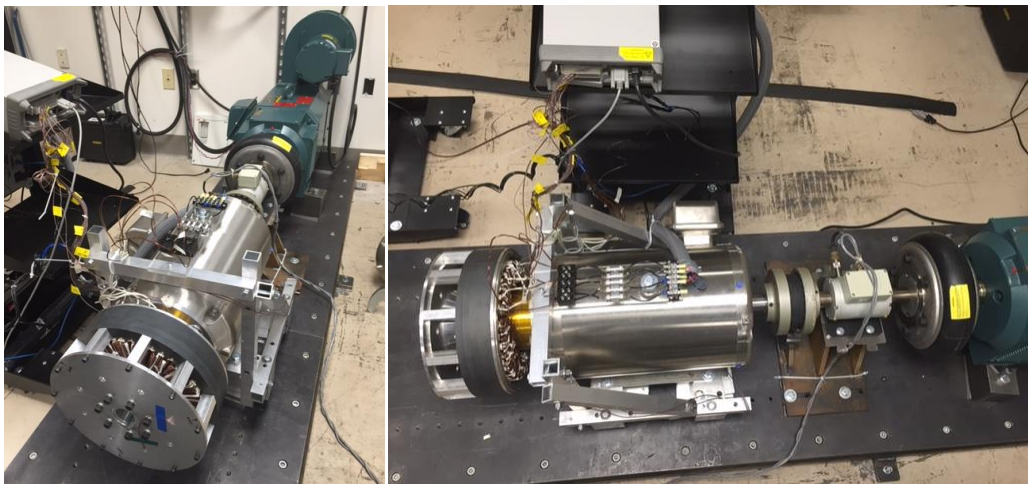

Figure 1. Reconfigured test set-up

Table 1. Dyno components

Tooth Wound Prototype	AC Induction Machine	Torque Meter	DC Drive Machine
4 KW / 300 rpm	as frame/shaft only	400Nm / 8,500 rpm	45 KW / 4,000 rpm

For this setup, the generator torque can be directly measured with the face-mounted AC induction machine frame. The dragging torque / power characteristics are provided in Figure 2.

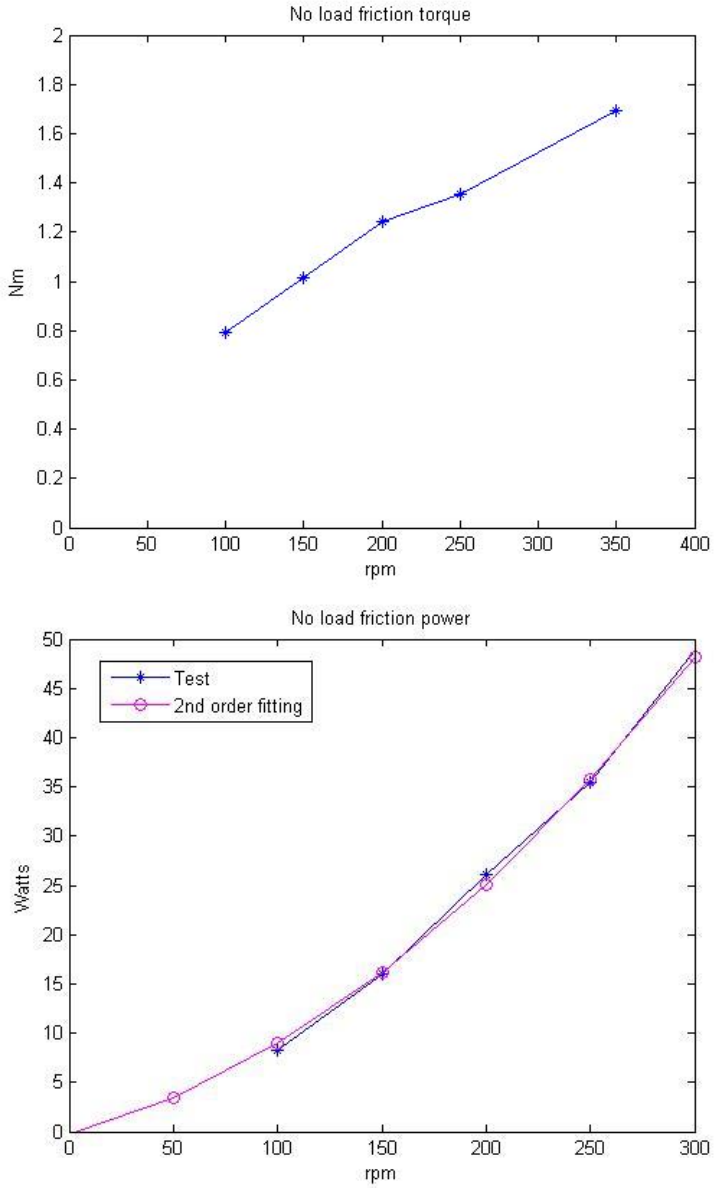

Figure 2. Dyno shaft torque at no load

3. PROTOTYPE CONFIGURATIONS

The pole modulated and tooth wound prototype concepts are shown below in Figure 3 and Figure 4.

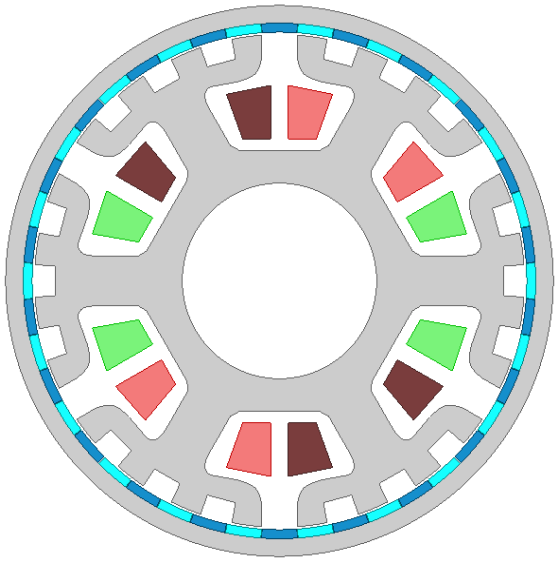

Figure 3. Pole modulated stator generator configuration

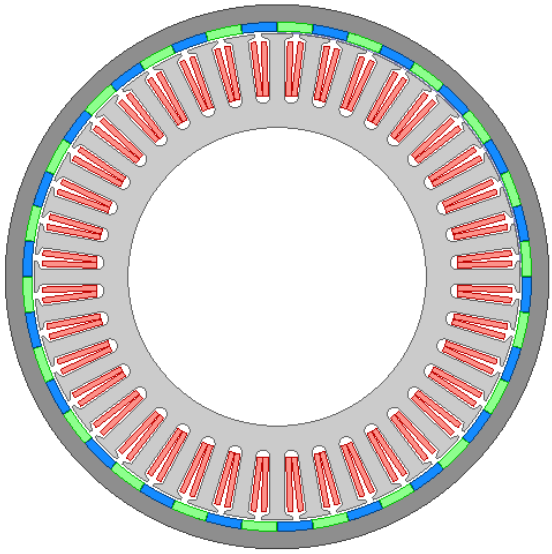

Figure 4. Tooth wound stator generator configuration

Table 2. 300 rpm pole modulated generator characteristics

Rotor OD (mm)	310	Stator OD (mm)	277.3
Stack Length(mm)	60	Rotor pole number	44
Phase number	3	PM thickness(mm)	5
PM width (mm)	19	PM length (mm)	60
Winding type	Y	Turns/Coil	75
Modulation Poles	48	Air gap (mm)	1.5
PM weight (kg)	1.8	Lam weight (kg)	17.2
Raw Active Material $	290	Winding weight (kg)	2.4

Table 3. 300 rpm tooth wound generator characteristics

Rotor OD (mm)	310	Stator OD (mm)	277.3
Stack Length(mm)	60	Rotor pole number	44
Phase number	5	PM thickness(mm)	5
PM width (mm)	19	PM length (mm)	60
Winding type	Star	Turns/Coil	48
Stator slot #	40	Air gap (mm)	1.5
PM weight (kg)	1.8	Lam weight (kg)	15.1
Raw Active Material $	276	Winding weight (kg)	2.1

4. MECHANICAL CHECK AND FREQUENCY RESPONSE:

First, the rotor runout was checked by partially mounting the rotor on the drive machine, leaving space so that a plunger style deflection gauge attached to a magnetic base could be placed on the interior of the rotor. The rotor was engaged on the shaft roughly one shaft diameter (1.375”) and then rotated by hand. The rotor eccentricity was measured to be 0.008”, or about 10% of the air gap diameter.

Next, modal modeling and frequency response testing have been performed to examine the prototype rotor resonant frequencies. Finite element analysis on the rotating components of the prototype generator, as well as the supporting shaft and bearing structures were validated by experimentally measuring impulse response data for the rotating components of the Phase I prototype using a small, three-axis accelerometer. Figure 5 shows the ANSYS model of the rotating components. The accelerometer placement is shown in Figure 6. A comparison between the calculated and measured modal frequencies is given in Figure 7. The two major modes occur at about 62 and 112 Hz. The mode frequencies were modeled within 7% of experimental data. The calculated amplitude values are arbitrary and should be disregarded since no attempt was made to measure the impulse force or calculate the vibration amplitudes. No vibration issues are expected during generator testing since no modes are close to the operating range up to 300 rpm, or 5 Hz. Calculated mechanical air gap deflections, too small to measure in the Phase I prototype case, can also be applied to the larger generator designs.

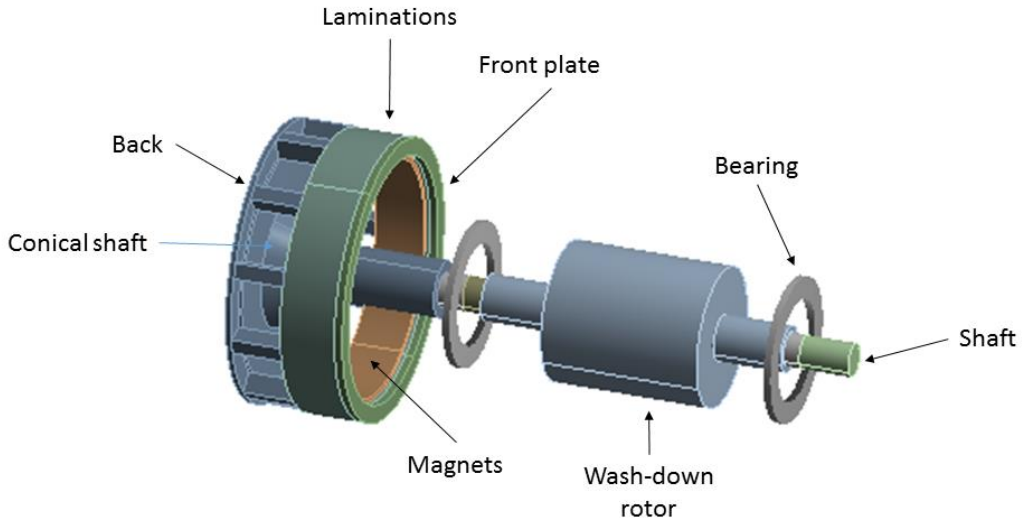

Figure 5. ANSYS model for the generator rotor and supporting induction motor rotor, shaft, and bearings

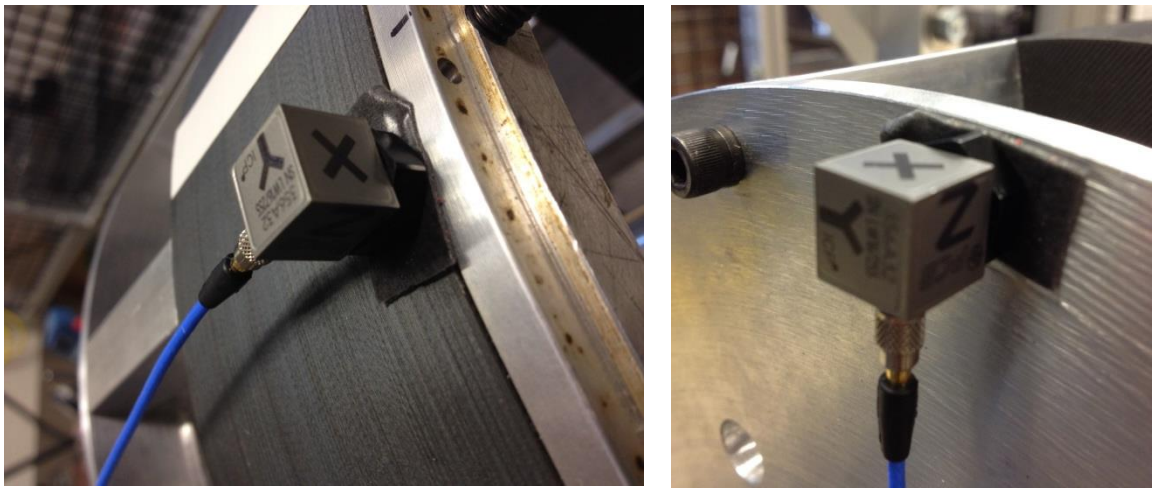

Figure 6. Accelerometer locations

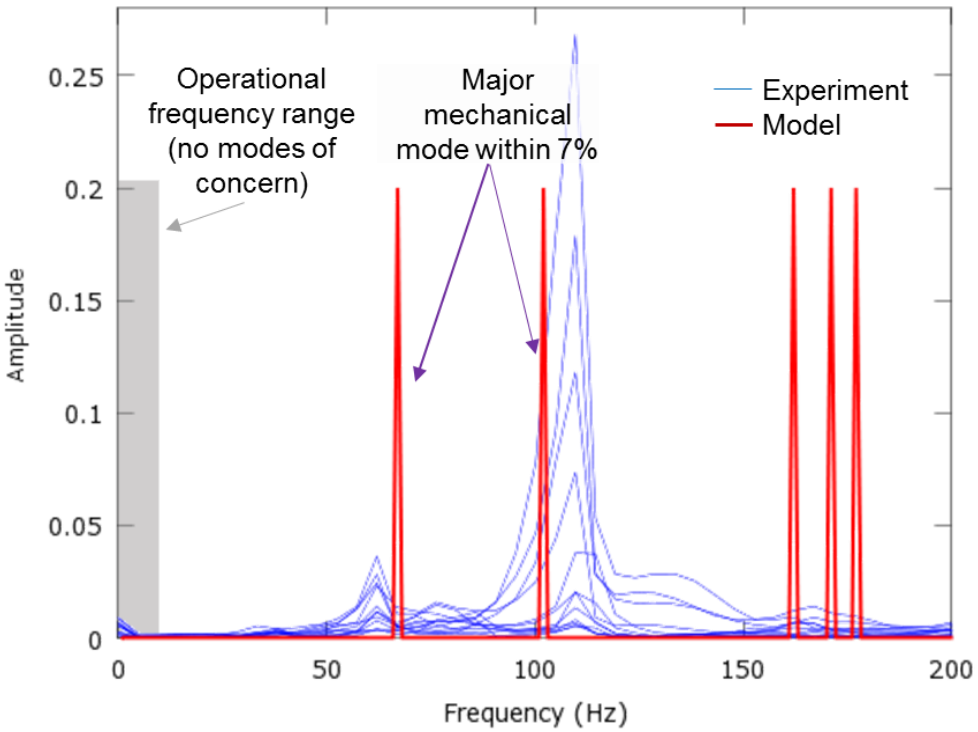

Figure 7. Comparison of modal modeling and test data

5. Back EMF: Measurement vs Calculation

The open circuit line to line voltage waveforms at 300 RPM for the pole-modulated prototype are overlaid with FEA simulation data as shown in Figure 8. The harmonic component peak values from fundamental up to 30th are insignificant, as shown on the right.

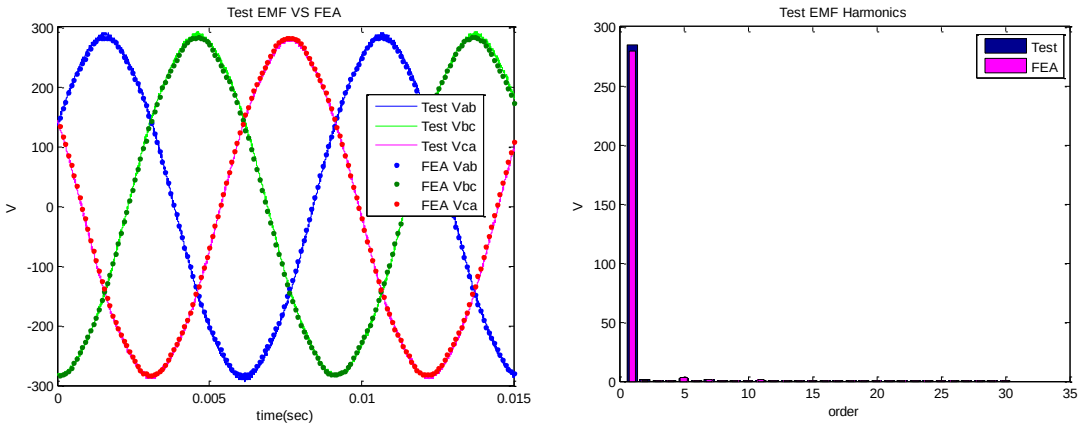

Figure 8. Pole-modulated stator open circuit back EMF waveforms

The details of the waveforms are summarized in the table below.

Table 4. Pole-modulated stator open circuit back EMF waveform characteristics

Back EMF Test	Fundamental (V)	THD
Test	284.5	0.88%
FEA	280.0	1.07%
Error	1.6%	-

Similarly, with phase windings disconnected from the load bank, the prototype tooth wound stator was also tested under no load condition. The measured EMF waveforms are overlaid with FEA simulation data as shown in Figure 9. The harmonic component peak values from fundamental up to 30th are include at the right side for detailed comparison.

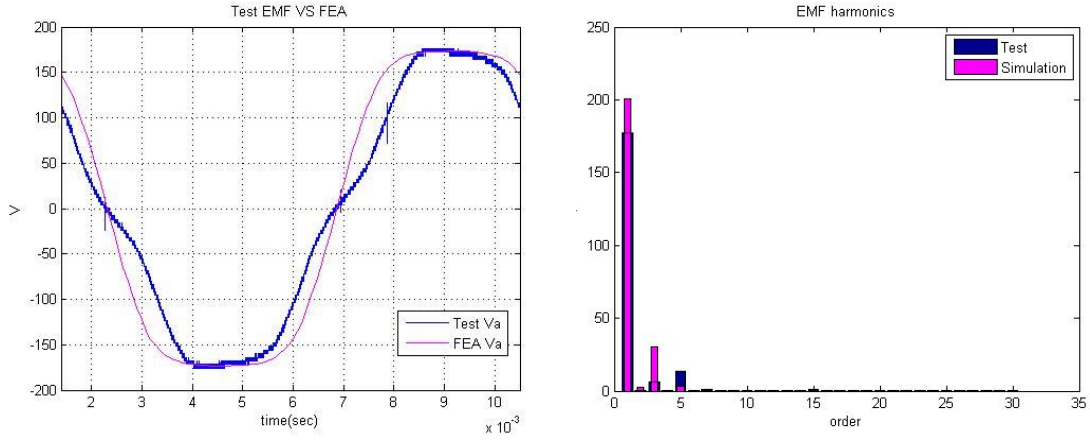

Figure 9. Tooth-wound stator open circuit back EMF waveforms

The details of the waveforms are summarized in the table below.

Table 5. Tooth-wound stator open circuit back EMF waveform characteristics

NL Test	Fundamental (V)	THD
Test	177	8.4%
FEA	200	15.3%
Error	13%	

6. POLE MODULATED RESISTIVE LOAD TESTING:

The pole modulated generator has been tested at 1kW while feeding a resistive load. In Figure 10 the load voltage and current are illustrated, with a comparison of measured and predicted power, losses, efficiency and torque density listed in Table 6.

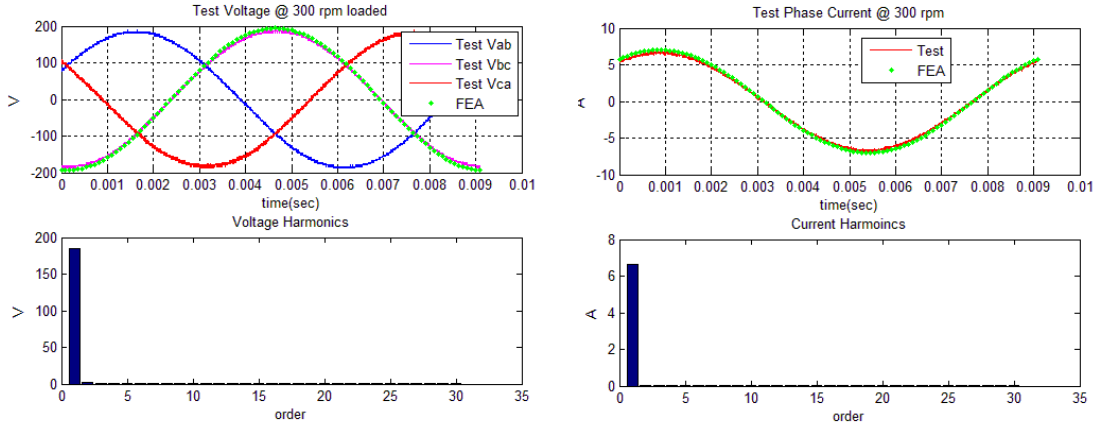

Figure 10. 1kW resistive load voltage and current comparison

Table 6. 1kW resistive load design and test data comparison (300 rpm)

	Power (KW)	Voltage (V,rms)	Current (A,rms)	Total Loss (W)	Effi (%)	Temp Rise (C deg)
Design	1.0	133.5	4.9	138	89.6	60
Test	1.1	131.2	4.8	85	92.7	15
Error	-	1.8%	2%	-	-	-

It should be noted that the pole modulated prototype losses are significantly reduced compared to the original design estimations because of two major design changes during the final design/manufacturing phase: 1) thinner laminations were applied (0.25mm instead of 0.5mm in thickness) for iron loss reduction. 2) The winding configuration was adjusted to achieve as low a phase resistance as possible. With these adjustments, the prototype losses are reduced by about 40% if compared with the original design value.

With different load bank configurations, the Pole Modulated prototype is tested under different resistive loads at 300 rpm as shown in Figure 11. There is generally only a small mismatch in the voltage and current at different operating points. However, an

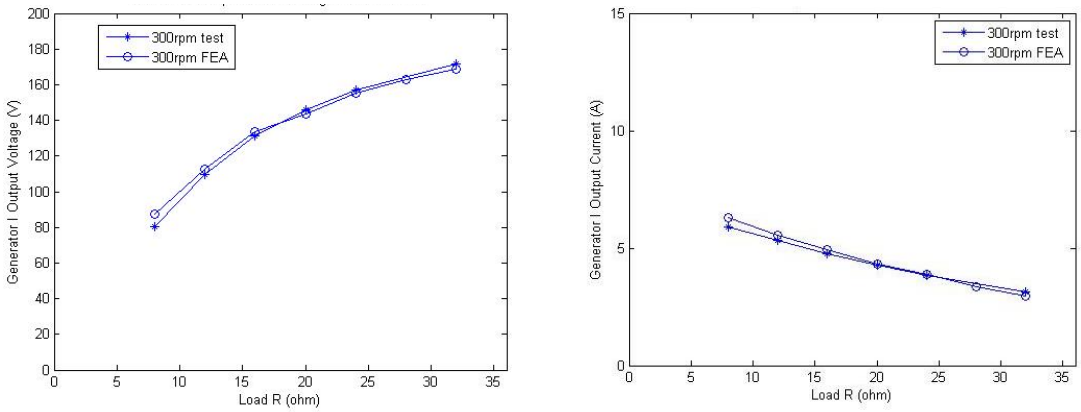

Figure 11. Pole modulated prototype V/I characteristics with FEA comparisons

increased difference can be observed as the generator saturates at lower load resistance values and higher load currents, as well as in the power comparisons due to the multiplication of error with the product of voltage and current, as shown in Figure 12.

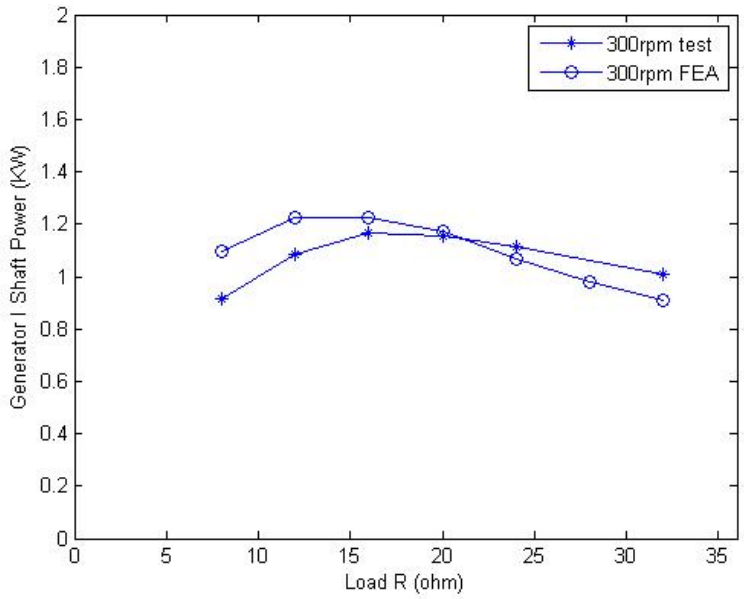

Figure 12. Pole modulated output power characteristics with FEA comparisons

At rated 300rpm speed, the pole modulated generator can deliver 1 kW of power over a large range of load resistance, from 10 ohms to over 30 ohms. The breakdown of the generator loss is also investigated with the results plotted in Figure 13.

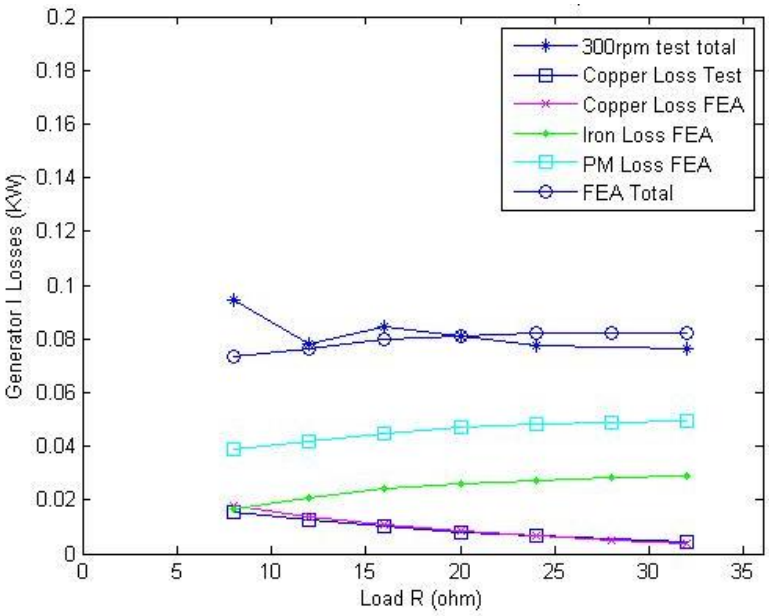

Figure 13. Pole modulated prototype losses with FEA comparisons

The pole modulated prototype efficiency is above 90% over a wide resistive load range as indicated in Figure 14, with left plot VS load resistance and right plot VS output power.

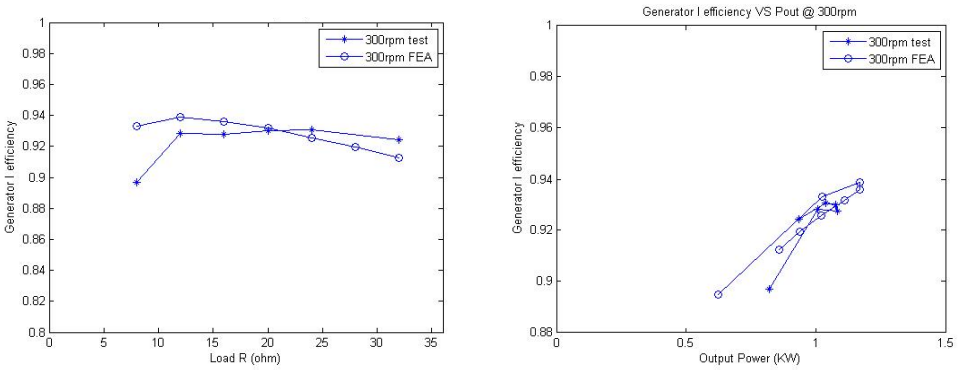

Figure 14. Pole modulated prototype efficiency with FEA comparisons

With load power factor adjustment, the pole modulated prototype can be operated in the "over-excited mode" which is expected to deliver significantly higher power and thus higher torque density. With only one prototype rotor built for testing, this over-excited mode is scheduled at the end of the Phase I testing after completing testing of the tooth wound stator.

7. POLE MODULATED RESISTIVE-CAPACITIVE LOAD TESTING:

As predicted in the design phase, the pole modulated generator has higher power output capability when it is operated in the leading power factor domain. With different capacitor bank configurations, the pole modulated prototype is tested under a few different RC loads at 300 rpm and the major characteristics are shown in Figure 15.

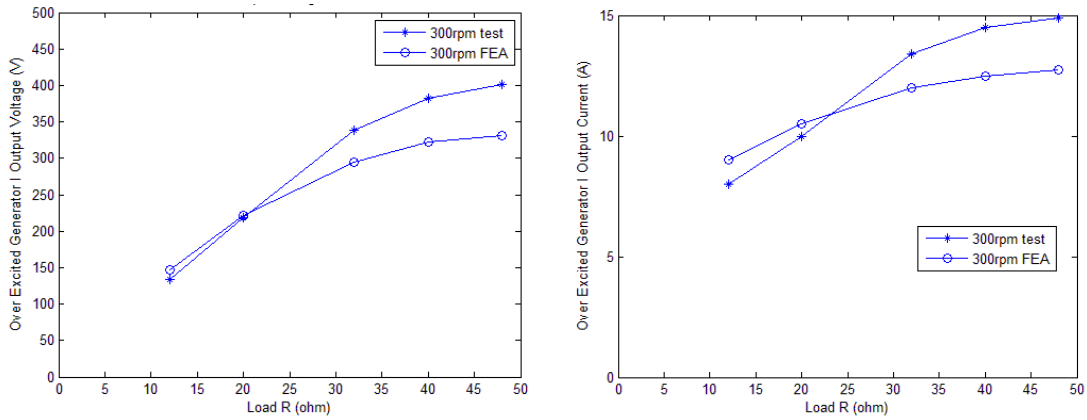

Figure 15. Pole modulated prototype V / I characteristics with over excitation operation

With non-constant characteristics of the capacitor bank in different operation domain, there are significant gaps between the simulation results and test data, especially at higher currents. The efficiency characteristics for these operation points are provided in Figure 16.

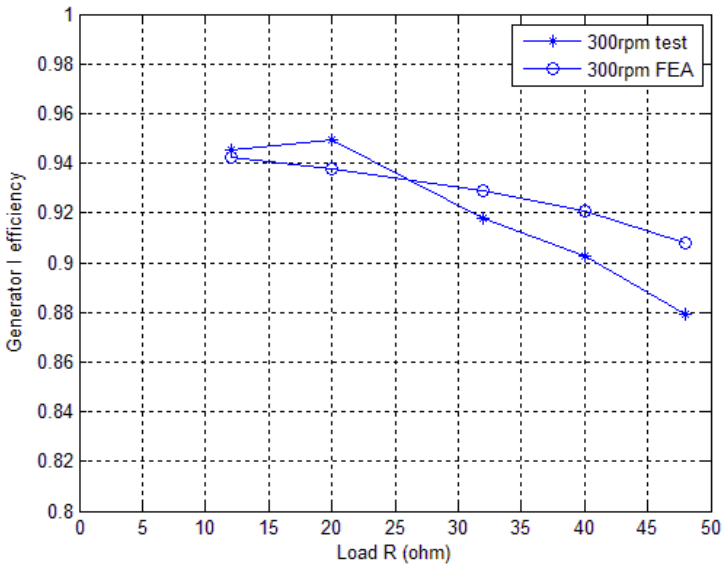

Figure 16. Pole modulated efficiency characteristics with over excited operation

The highest power output observed with the RC load combinations is provided in Table 7.

Table 7. Pole modulated performance under over excited operation

	Power (kW)	Voltage (V)	Current (A)	PF	Efficiency (%)
Pole Modulated Design	4.1	300	12.5	0.52	92.9
Pole Modulated Test	3.7	330	14.2	0.46	91.8

8. POLE MODULATED HEAT RUN:

The magnet and stator winding temperatures were monitored during all tests, but specific heat runs were also performed using the pole modulated stator operating at about 1.2 kW feeding a resistive load and about 3.65 kW with a resistive-capacitive load. For the lower power case, the generator temperature rise was insignificant, and the drive motor operating at the low speed was a significant source of heat. Both lumped parameter and finite element models were used to predict the motor temperature distribution at about 3.65 kW power output.

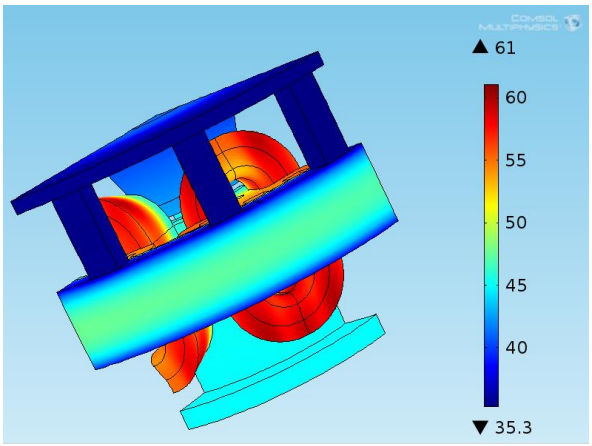

(A)

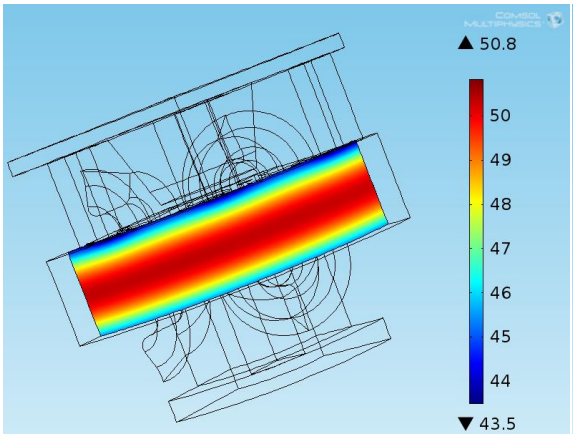

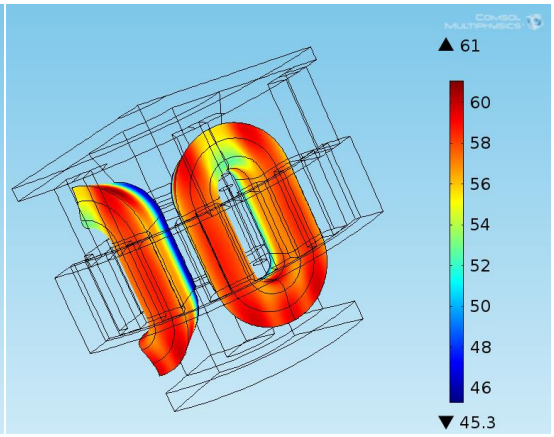

(B) (C)

Figure 17. Pole modulated steady state thermal modeling at 3.65 kW

Results in Figure 12 (3.65 kW) are summarized as below:

I. Temperature distribution on different parts of the 3.65 kW generator indicates the highest temperature occurs on the stator windings

II. The center part is the hottest part of the magnets since the supporting rotor structure components on both sides act as heat sinks

III. The face mounting surface (20hp stainless steel induction motor) functions as a heat sink, and consequently the parts of the winding which are in contact with stator shaft (stand) show lower temperatures. The highest temperature on the winding is about 60 C on the surface facing to air, and the lowest temperature is about 46 C on the surface facing and connecting to the face-mounting induction motor frame (Fig. 12(C))

Table 8 compares average temperatures as results of steady state lumped parameter and steady state finite element thermal modeling for the 3.65 kW power rated case.

Table 8. Comparison between average temperatures as the results of LPM and FEM

Part	Average temperature (degC)		
	LPM	FEM	T_{LP} - T_{FE}
End winding inside rotor	54	56	-2
Winding inside stator	54	56	-2
End winding outside rotor	53	56	-3
Stator back iron	51	53	-1.5
Stator teeth	52		
PM	46	49	-3
Rotor back iron	42	46	-4

Next, the thermal model results will be compared with measured temperatures during the heat run tests. During the experimental studies, seven J-type wired thermocouples have been installed for measuring the temperatures of the end windings (inside and outside the rotor), on the end plate of the drive motor, inside the drive motor (on the end windings), and facing toward the air (inside and outside the rotor, and toward the air gap). Also one J-type wireless thermocouple has been installed on the rotor end plate where its sensor has been placed between magnets for monitoring the magnets' temperature. Figures 13 and 14 illustrate the positions of some of the thermocouples.

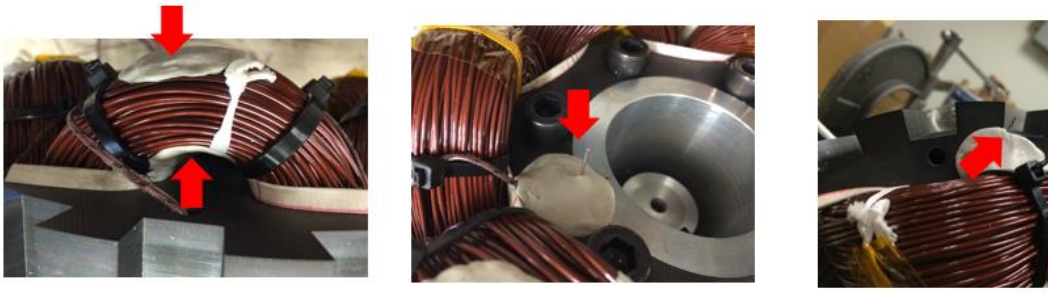

(A) (B) (C)

Figure 18. Wired thermocouples for measuring temperatures, (A) end winding, (B) air inside the rotor, (C) air in the entrance of the air gap

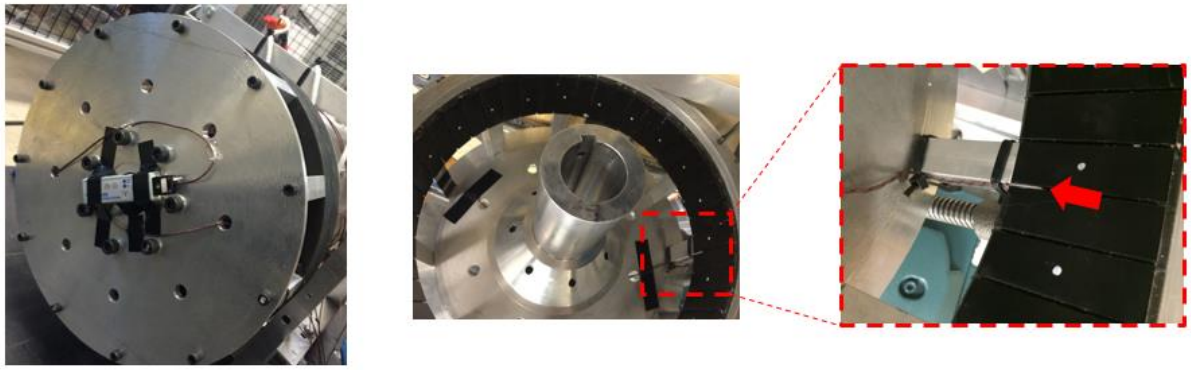

Figure 19.Wireless thermocouple for measuring magnets' temperature on the rotor

As comparisons between simulation and measurement show:

- Results of finite element modeling are in good agreement with experimental results (less than 10% difference, and the finite results over estimate the experimental results)
- Difference between numerical simulation and experimental results might be from error in thermocouple reading (thermocouple's surface attachments, rotational motion effect on wireless transmission), error in calculating convection coefficients (lack of precise semi-empirical correlations for the complicated machine geometry), error in calculating thermal losses, or error in calculations of thermal properties of the materials
- Experimental and numerical results showed internal diameter of the end windings are in higher temperatures than outer diameter of the end winding. (These results might be because of weaker convection effect on internal surfaces)
- Highest measured temperature is on the face mounting motor end plate surface

Table 9 presents steady state finite element temperature results versus steady state experimentally measured temperatures for different parts of the pole modulated generator at 3.65 kW.

Table 9. Steady state FE temperature results versus steady state experimentally measured temperatures for different parts of the 3.65 kW power rated generator

	Experimental (degC)	FE model (degC)	T_{exp} - T_{FE}
End winding inside rotor _2	53	55	-2
End winding inside rotor _1	58	56	+2
End winding outside rotor _2	52	57	-5
PM	56	51	+5

A prototype pole modulated, exterior rotor permanent magnet machine was thermally studied using steady state lumped parameter analysis (applying SIMULINK/MATLAB software), transient and steady state three dimensional finite element modeling (using

COMSOL software), and experimental examinations using wired and wireless thermocouples. Comparison between transient simulation and experimental thermal results has been carried out. Results of FE modeling were in good agreement with the experimental results. Similar thermal analysis and measurement can be applied to the Phase II design and testing in order to push the temperature limits for the generator design while also maintaining safe operation.

9. TOOTH WOUND RESISTIVE LOAD TESTING:

A tooth wound stator has been developed to utilize the same 44 pole, surface PM outer rotor, which allows investigation of another generator topology with reduced engineering design efforts and prototype cost. The tooth wound stator is designed with five phases in order to maximize the winding factor while still using the same 44 pole rotor originally designed for the pole modulated stator. The tooth wound stator can deliver higher power output at unity power factor compared with the pole modulated stator.

Generator performance was measured under a range of resistive loads. In Figure 20, the generator full load voltage and current are illustrated, with the comparison of full load power, losses, and efficiency listed in Table 10.

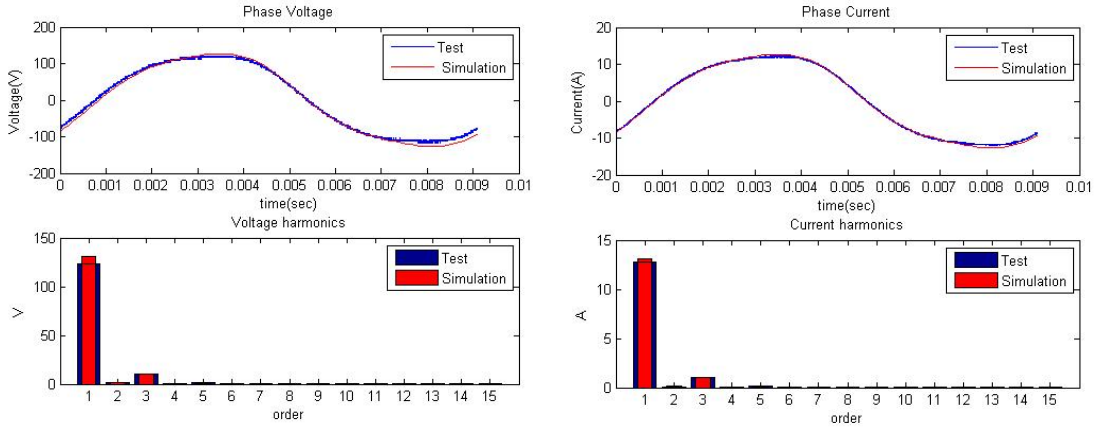

Figure 20. Tooth wound voltage and current waveform comparison

Table 10. Tooth wound design calculations compared to test data

	Pout (KW)	Voltage (V,rms)	Current (A,rms)	Total Loss (W)	Effi (%)	Temp Rise (C deg)
Design	4.0	90	9	396	91	100
Test	4.07	89	8.9	350	92.1	90
Error	-	1.1%	1.1%	-	-	-

It should be noted that the Tooth Wound prototype losses are reduced compared to the original design estimations because thinner laminations were applied (0.25mm instead of 0.5mm in thickness) for iron loss reduction. With this adjustment, the prototype losses are reduced 13% if compared with the calculated values. The direct benefit of loss reduction is that the tooth wound prototype exhibits less than predicted temperature rise. The generator hot spot temperature rise is less than 90 C degree in the 3 hour thermal run without extra cooling method applied in the lab environment.

With different load bank configurations, the tooth wound prototype is tested under different resistive loads as illustrated in Figure 21.

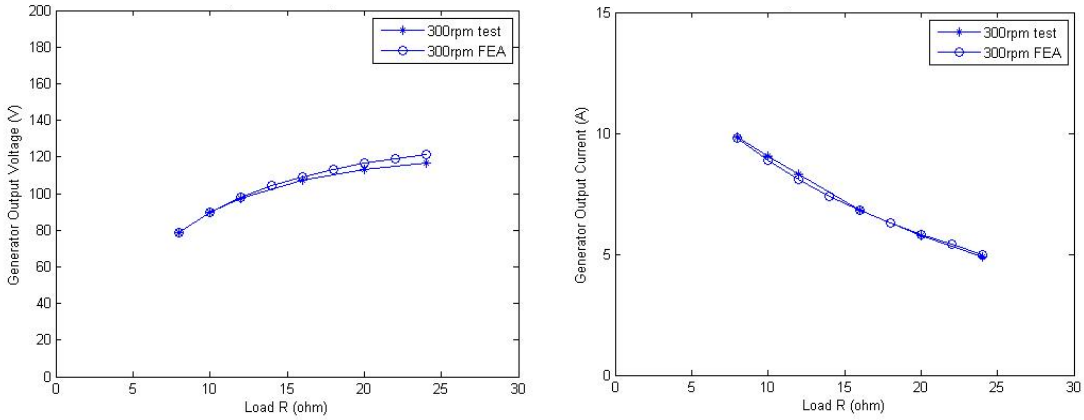

Figure 21. Tooth wound prototype V / I characteristics with FEA comparison

With only slightly over-estimated voltage and current at most operating points, the difference is still magnified for the power comparison due to the squaring effect from the product of the voltage and current, as shown in Figure 22.

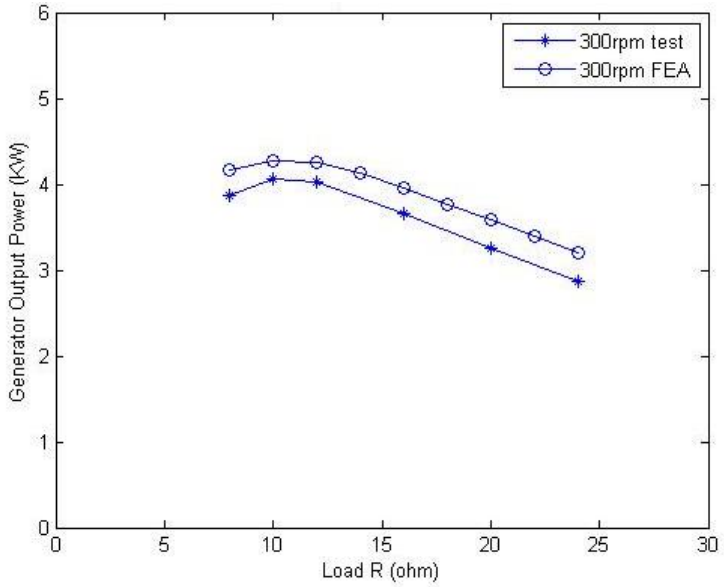

Figure 22. Tooth wound prototype output power characteristics with FEA comparison

At rated speed, the generator can deliver 4 kW power output over a range of load resistance from 8 ohms to about 15 ohms. The breakdown of the loss is also investigated with the results plotted in Figure 23.

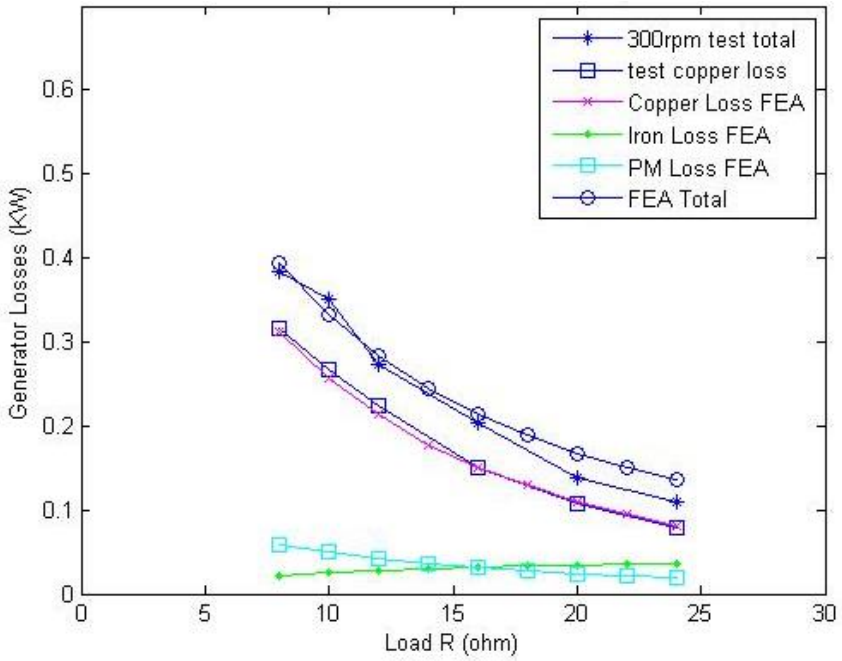

Figure 23. Tooth wound prototype losses with FEA comparisons

The tooth wound prototype efficiency is also above 92% for a broad load range as indicated in Figure 24, plotted versus load resistance on the left and versus output power on the right.

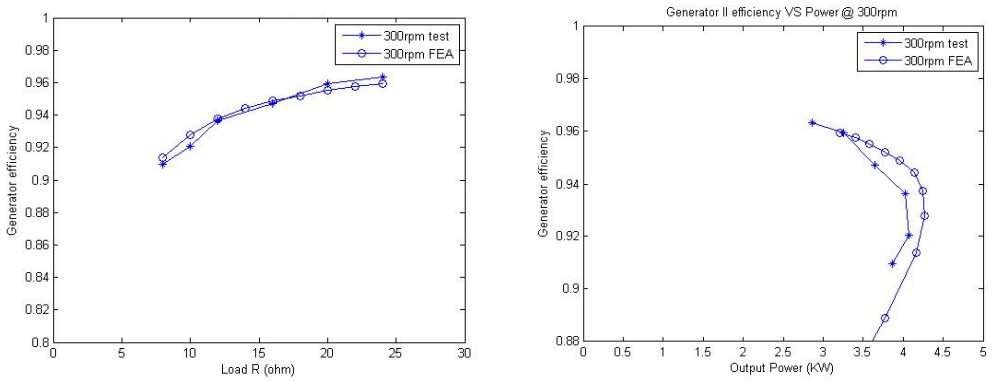

Figure 24. Tooth wound prototype efficiency with FEA comparisons

For the targeted wave energy conversion power generation application, the DC link is a required power conversion stage between generator and fixed frequency output electric power feed to the grid. Thus, the power characteristics of the rectified operation are also interesting for the system level investigation, which is performed next.

10. TOOTH WOUND DIODE RECTIFIER LOAD TESTING:

With rectified load bank configurations, the Tooth Wound prototype is tested under different resistive loads and speed as illustrated in Figure 25.

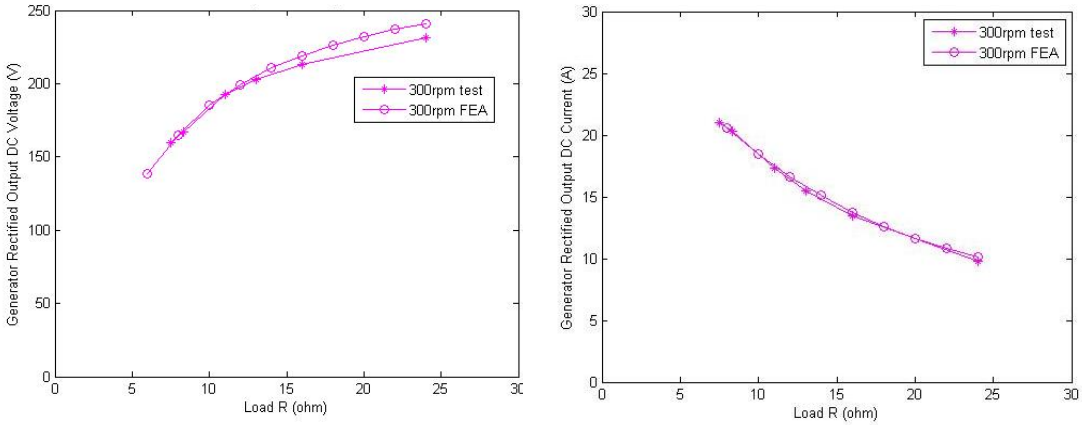

Figure 25. Tooth wound prototype rectified V / I characteristics with FEA comparison

Similarly to the AC operation, the machine also observes slightly higher output power if compared with FEA simulations, as shown in Figure 26.

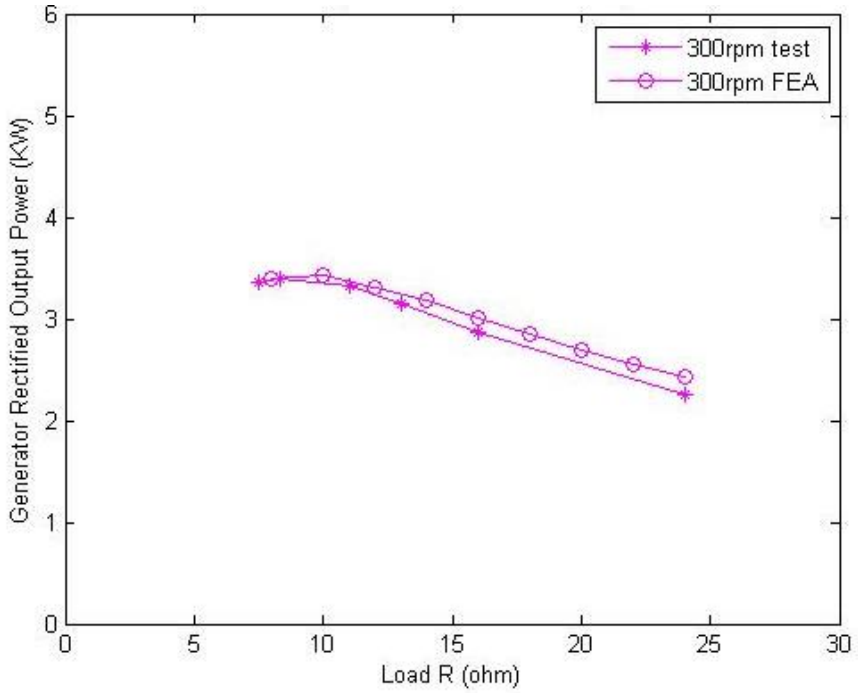

Figure 26. Tooth wound prototype rectified output power with FEA comparison

The breakdown of the loss is also investigated with the results plotted in Figure 27.

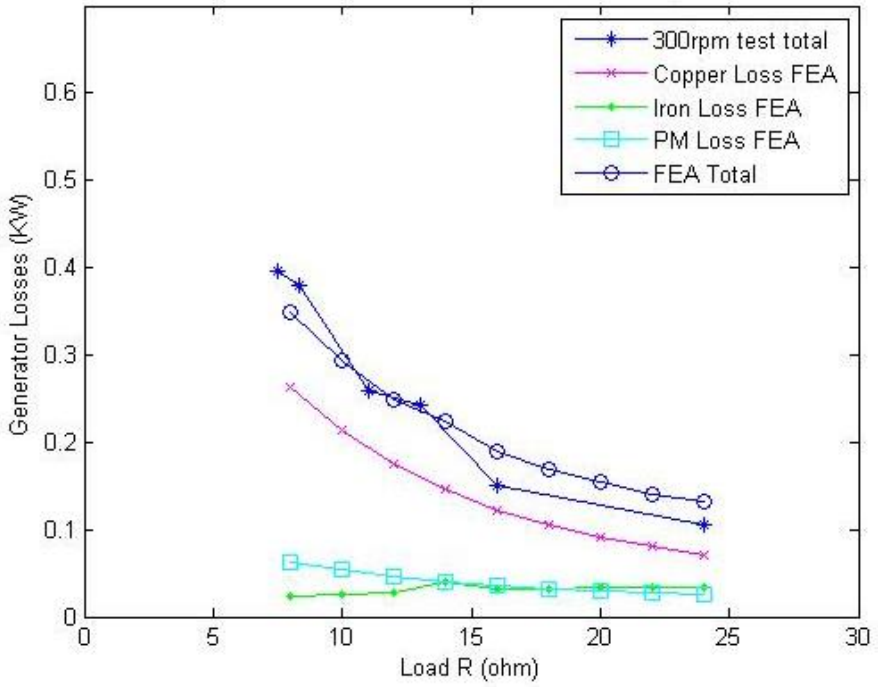

Figure 27. Tooth wound prototype rectified operation losses with FEA comparison

The tooth wound prototype efficiency under rectified load is above 90% for a wide load range as indicated in Figure 28.

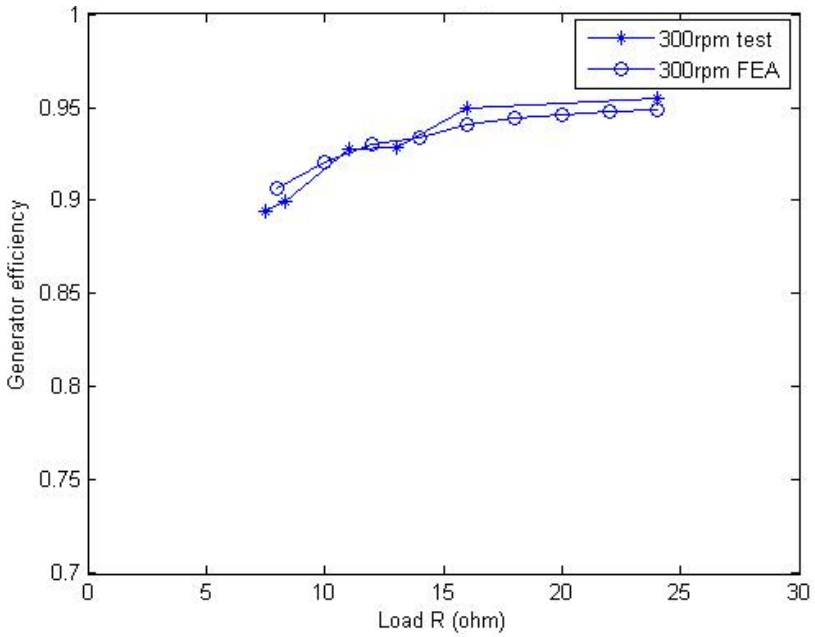

Figure 28. Tooth wound prototype rectified operation efficiency with FEA comparison

For comparison, the measured DC bus voltage profile at 300 rpm is plotted versus FEA simulations as shown in Figure 29.

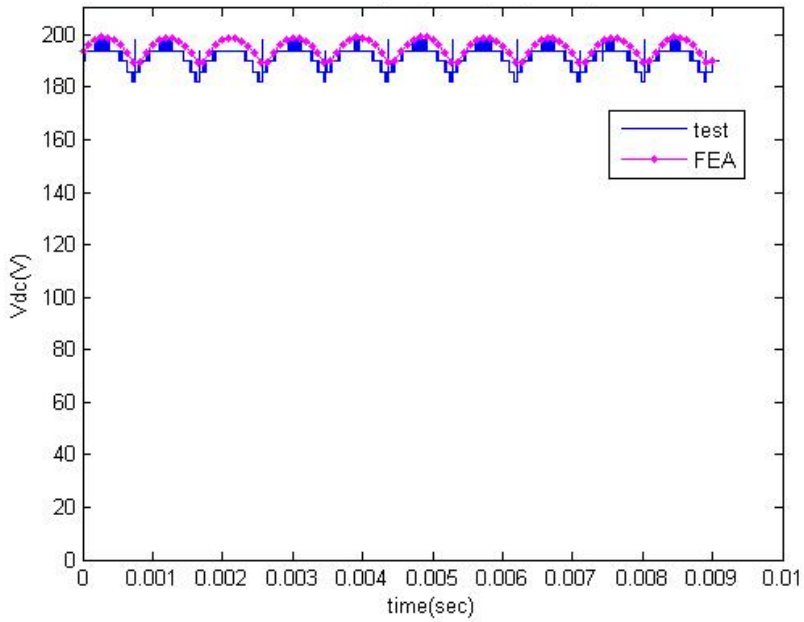

Figure 29. Tooth wound prototype rectified Vdc with FEA comparison

11. PROTOTYPE TEST COMPARISON, SUMMARY, AND CONCLUSIONS

In Table 11, the machine major design dimensions, performance index on the shear stress and torque density are provided for comparisons. The torque volume density is evaluated including the length of the the end winding section. The torque weight density is assessed with the active material weight in for these designs.

Table 11. Generator topology comparison

	Base PM Machine	Pole Modulated	Tooth Wound	Target
Machine OD (mm)	310	310	310	-
Air gap OD (mm)	184.2	278.8	278.8	-
Air gap length (mm)	0.89	1.5	1.5	-
Stack length (mm)	152.4	60	60	-
Power (KW)	5.2	1.0 (PF=1) 3.8 (PF = 0.5)	4.1 (PF=1)	-
Torque (Nm)	165.5	31.8 (PF=1) 121.0 (PF=0.5)	130.5 (PF=1)	-
Efficiency	87%	92% (PF=1) 90% (PF = 0.5)	92% (PF =1)	
Shear Stress (kN/m^2)	20.5	4.3 (PF=1) 16.5 (PF=0.5)	17.8 (PF=1)	-
Torque Volume Density (kNm/m^3)	8.2	3.4 (PF = 1) 13 (PF = 0.5)	19 (PF = 1)	**16**
Torque Weight Density (Nm/kg)	1.8	1.5 (PF=1) 5.7 (PF = 0.5)	6.9 (PF = 1)	**4**

1) Both prototypes have been designed and tested and the results are consistent with the design predictions

2) The inline torque transducer was necessary for accurate torque and efficiency measurements.

3) The pole modulated design uses the iron pole harmonics in the air gap region. The stator structure is simple and easy to manufacture. It can achieve high power and torque under low, leading power factor operation, which introduces extra loss and cost from the system side for power factor conditioning and higher currents.

4) The tooth wound design features a high winding factor which contributes to the target power generation density with the power factor close to unity. While the stator winding coils will be more effort to manufacture than with the pole modulated design, a modular design and machine winding process can be applied to significantly reduce the manufacturing cost.

5) The PM loss is not a major loss component as observed in these prototype tests. Large thermal margin and low rotor temperature were observed during tests on both prototypes. The iron and PM losses are not concerns for the targeted low speed application. The stator winding loss is the most significant source of generator loss.

MILESTONE DELIVERABLE

Task 3.2: 1 kW Alternate Generator Prototype Test Results

Date of Completion: 9/30/2015

1. GENERAL DESCRIPTION:

This document describes the results of the experimental performance evaluation of the "Alternative Phase I Prototype," the 300 rpm integrated axial flux magnetic gear and generator. The primary goals of these tests are to

- Demonstrate the feasibility of the novel machine design
- Measure test data for calibration and validation of performance calculations
- Identify potential risks and opportunities to improve the electromagnetic, mechanical, structural, or thermal performance of the larger second prototype

Following an initial description of the test-set-up and generator configurations, the rest of the report compares measured test data to finite element calculated predictions.

Finally, a comparison is made between the alternative Phase I prototypes and the baseline reference values. Full scale calculations are also presented, along with the selection and justification of a generator topology proposed for the Phase II prototype.

2. TEST SET UP:

The test bed for evaluating the axial field magnetically geared machine has been set up and is shown in Figure 1 with the prototype machine in position.

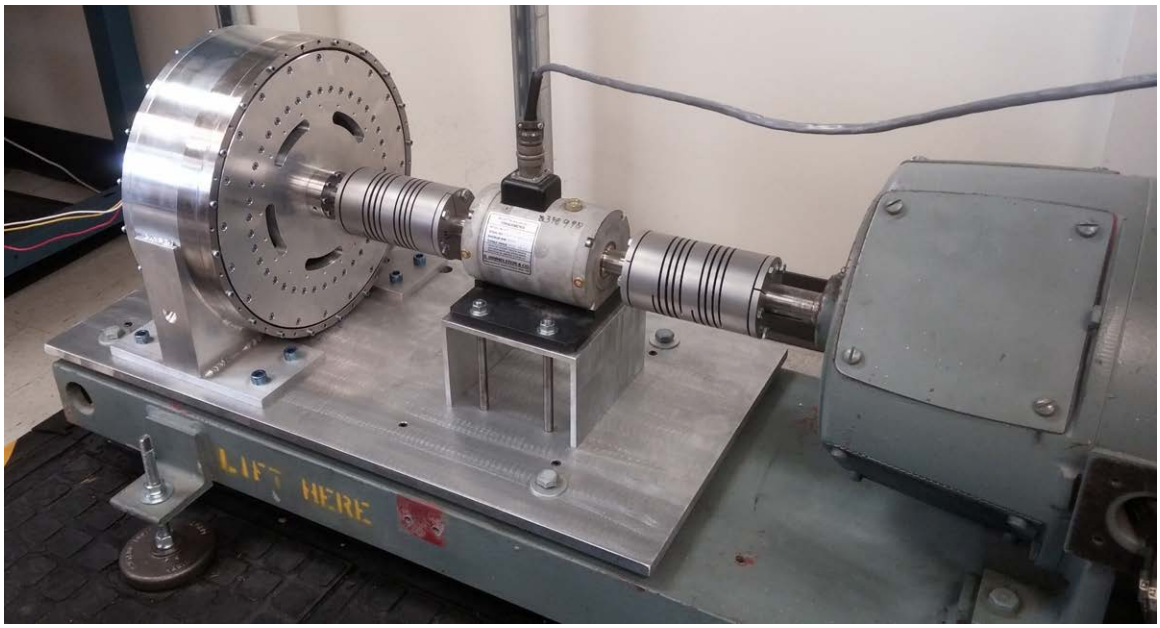

Figure 1. Test bed for Phase I Axial Flux Prototype

3. PROTOTYPE TOPOLOGY OVERVIEW

The axial field magnetically geared machine consists of four primary subassemblies: the high speed rotor, the low speed rotor, the stationary middle section, and the housing. The first three of these subassemblies are illustrated in the models in Figure 2 and make up the active magnetic circuit of the system. In Figure 2, the modulator pole pieces and the generator stator are the active parts of the stationary middle section. The housing, illustrated by the model in Figure 3 of the fully assembled machine, is not part of the active magnetic circuit, but serves as the base fixture, bearing support, and frame which holds everything together.

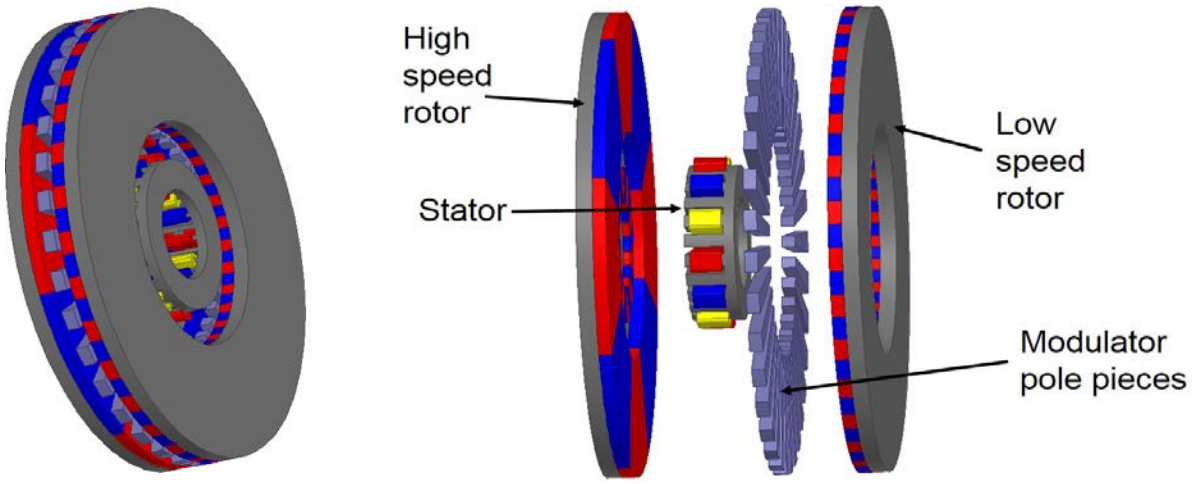

Figure 2. Axial field magnetically geared machine topology active structure

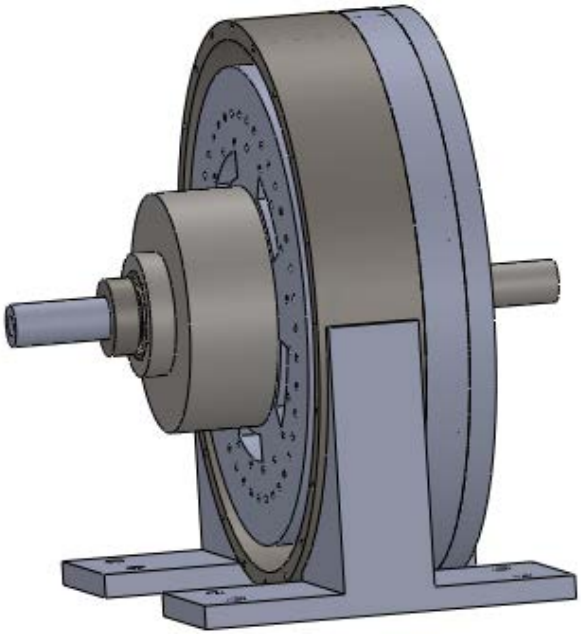

Figure 3. Model of the fully assembled axial flux magnetically geared generator with housing

The high speed rotor consists of two subcomponents fixed on the same supporting structure, Rotor 1 and Rotor 0 as illustrated by the model in Figure 4. Rotor 1 is the magnetic gear's high speed rotor, and Rotor 0 is the integrated generator's high speed rotor tacking advantage of the available space inside the inner diameter of the gear components. Rotor 1 was assembled by attaching a laminated steel coil onto an aluminum backing used for structural support. The tape-wound steel coil, which serves as the Rotor 1 back iron in the active magnetic circuit, is attached to the aluminum backing with screws and epoxy. The high speed, low pole count gear magnets were then epoxied to the top surface of the laminated steel coil in the appropriate alternating North, South configuration, as depicted in Figure 4. The magnets were aligned on the coil in the desired positions using the plastic retainer shown in Figure 4.

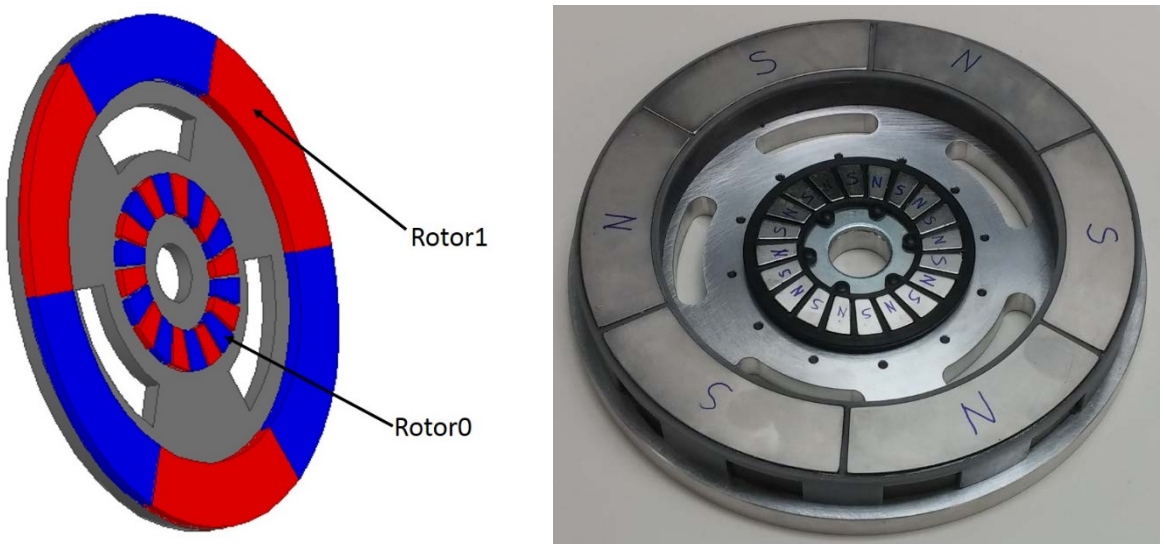

Figure 4. High speed rotor with Rotor 1 (gear) and Rotor 0 (generator) on aluminum backing

The low speed rotor, or Rotor 2, is the low speed, high torque, high pole count rotor of the magnetic gear. Whereas the high speed magnetic gear rotor has 3 magnetic pole pairs, the low speed rotor has 28 magnetic pole pairs. Rotor 2 was constructed in a similar manner to Rotor 1.

First, a laminated steel coil was attached to the aluminum backing. The aluminum backing is purely for structural support and the steel coil serves as the Rotor 2 back iron in the active magnetic circuit. The steel back iron coil is attached to the aluminum backing using both screws and epoxy. Next, the low speed, high pole count gear magnets were epoxied to the top surface of the laminated steel coil in the appropriate alternating North, South configuration, as depicted in Figure 5. The magnets were aligned on the coil in the desired positions using the plastic retainer shown in Figure 5.

This completed the assembly of the active magnetic circuit portion of the low speed rotor. During the final assembly of the full machine, there are a few additional parts which will be connected to the low speed rotor, such as its shaft and its large outer bearing which rides on the perimeter of the aluminum backing for the final assembly of the full machine.

Figure 5. Low speed Rotor 2

The two primary components of the stationary middle subassembly are the integrated axial field generator's stator and the axial field magnetic gear's modulators. This subassembly also includes the cup in which the stator is mounted and the modulator spacer which holds the modulator pieces, as shown in Figure 6.

The modulator pieces themselves have been cut to their basic rectangular dimensions and then tapered to trapezoidal shapes to achieve the proper harmonic modulation and radial extensions cut out of the modulator pieces to help with mechanically holding the pieces in place. These extensions provide a surface for the two support rings shown in Fig 6 to clamp the modulators into the modulator spacer.

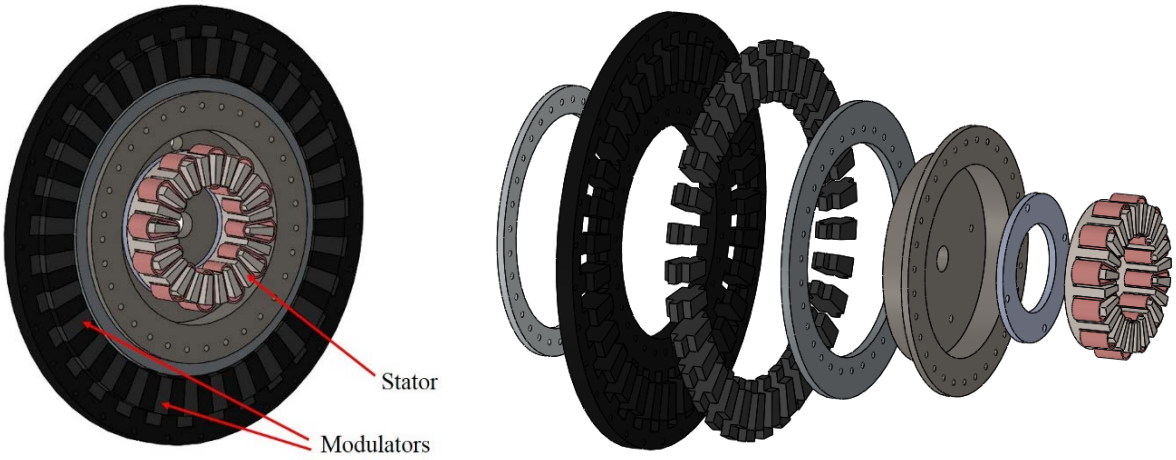

Figure 6. Models of the stationary middle assembly

The housing subassembly primarily consists of a large circular ring with mounting feet attached to it. Both the housing ring and mounting feet are shown together on the machine shop work bench in Figure 7. The housing ring provides a structural frame for the axial field magnetically geared machine, and the mounting feet provide a mechanism for attaching the machine to the test bed base.

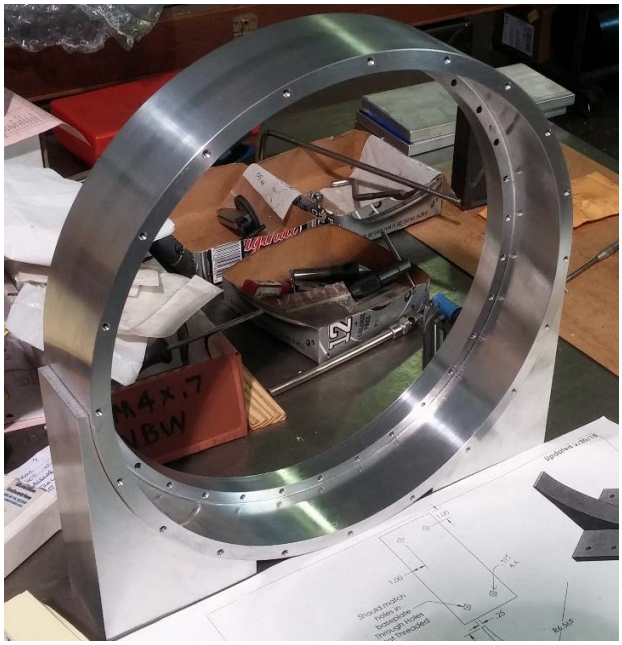

Figure 7. Housing ring and mounting feet

The assembly and initial testing of the alternative, axial-field magnetically geared machine (MGM) prototype is shown in Figure 8. The prototype operated well under initial verification tests and no load testing as detailed in the next section.

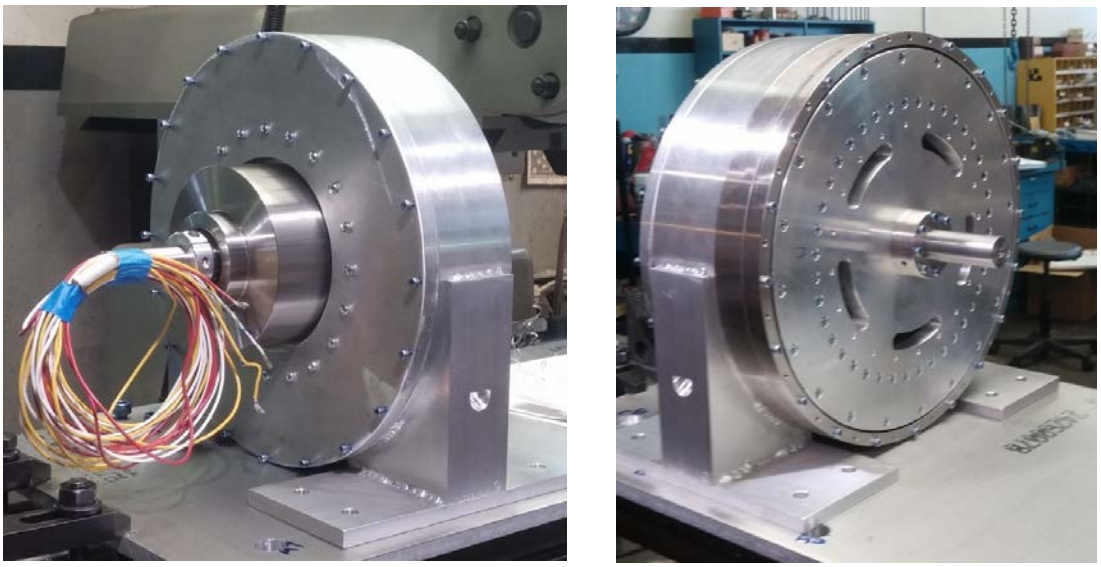

Figure 8. Assembled magnetically geared generator prototype

4. BACK EMF AND NO LOAD: MEASUREMENT VS CALCULATION:

In order to characterize the torque transmission properties of the axial field magnetic gear in the prototype, a locked high speed rotor (HSR) test was conducted by fixing the HSR in place and rotating the low speed rotor (LSR) to different angular positions. The resulting LSR torques are shown in Figure 9 as a function of the relative electromagnetic angle (or torque angle) between the LSR and the HSR. The corresponding simulated torque characteristics obtained from static 3D FEA simulations at different torque angles are also shown in the same graph. This clearly proves that the 3D FEA model accurately predicts the gear's static torque transmission capability, as the simulated and experimental results indicate a maximum torque of 42.1 N·m and 42.2 N·m, respectively before the gear poles slip.

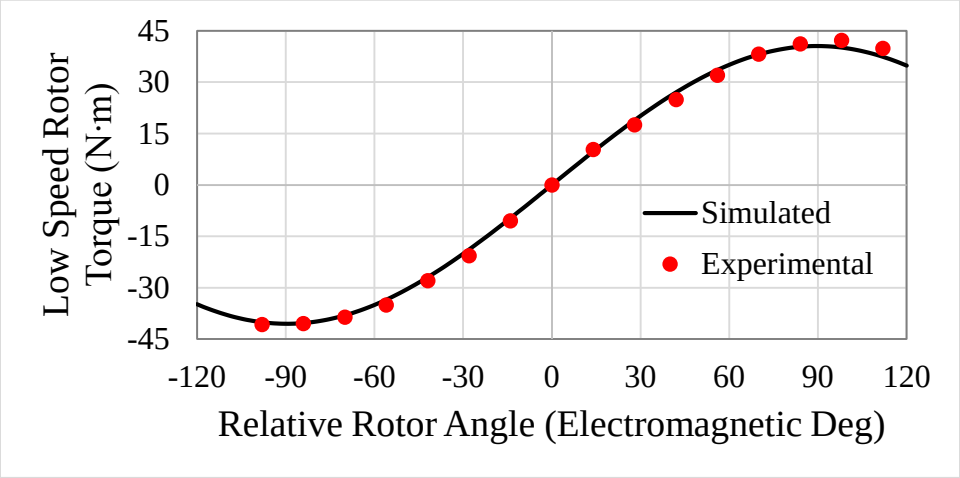

Figure 9. Static torque vs rotor position

Predicted calculations of static torque are very consistent with experimental measurements. As shown in Figure 10, the gear ratio was about 9.33, which matches the theoretically anticipated results based on the 28:3 pole pair combination on the rotors and torque ripple was negligible.

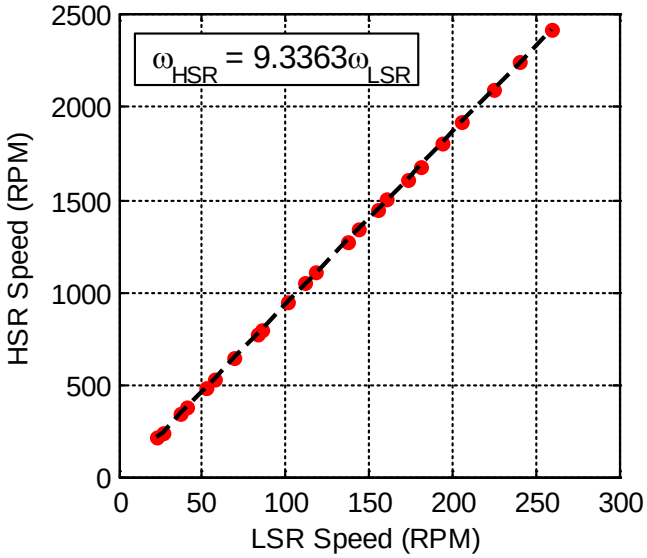

Figure 10. Axial Flux Prototype Gear Ratio Measurements

The no load, open circuit back EMF produced by the integrated machine prototype was measured at several different speeds and the results are summarized by the graph in Figure 11. The same graph also depicts the simulated back EMF amplitude characteristics obtained from a 3D FEA model. The data illustrates a high degree of consistency between the simulated and experimental results, and the relatively small deviations are likely due to a very minor difference between the actual generator air gap size and the designed size. Additional 3D FEA simulations suggest that the differences in predicted and measured back EMF amplitudes could be accounted for by less than 0.2 mm of variation in the generator air gap, which is less than 10% of the 2 mm design value.

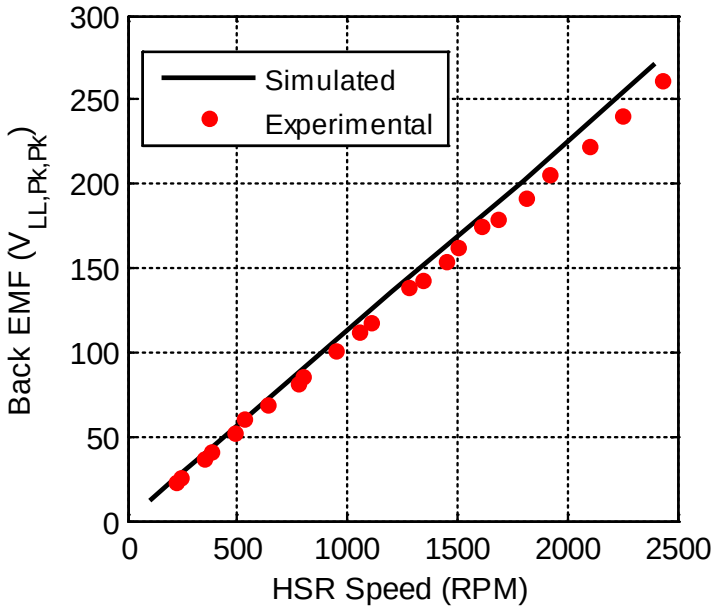

Figure 11. Experimental and Simulated AFMGM No Load Back EMF Amplitude Characteristics

Experimental and simulated no load, open circuit back EMF waveforms produced at an HSR speed of 1800 rpm are shown in Figure 12. Not only are the simulated and experimental waveforms a good match for each other, but they are also very smooth sine waves with negligible harmonic content. This observation is important for two reasons, first and most importantly, it demonstrates that the axial flux magnetic gear and integrated generator are magnetically isolated, as desired. If the two were not isolated, the EMF would contain harmonic content from the three pole pairs of the magnetic gear HSR.

Second, the quality of the sine wave indicates how smoothly the HSR was rotating. This smooth operation is due in part to the lack of direct mechanical contact between the HSR and the LSR, as well as the prototype's low cogging torque from the design of pole pairs. The HSR peak to peak torque ripple is a mere 3.5% of the HSR stall torque, while the LSR peak to peak torque ripple is only 1.3% of the LSR stall torque. These minor torque ripples are easily damped out by the machine's inertia.

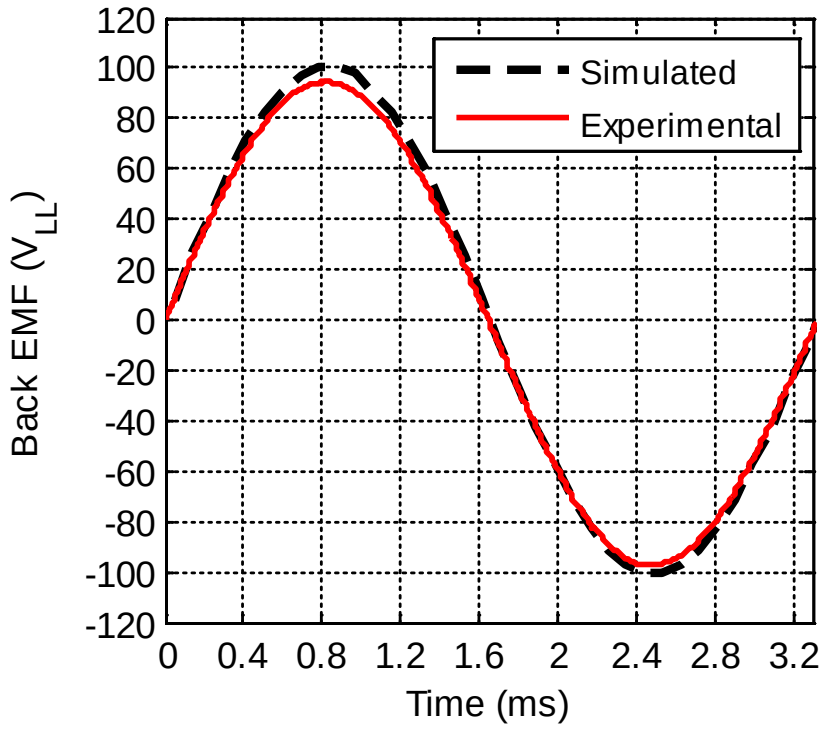

Figure 12. No Load Back EMF Waveforms at an HSR Speed of 1800 rpm

The prototype's no load losses were recorded at several different LSR input speeds, and the information is shown in Figure 13 along with the magnetic loss predictions obtained from transient 3D FEA simulations in Infolytica MagNet. This graph demonstrates that the experimental losses are significantly higher than the simulated losses.

The additional losses experienced in the experimental prototype are believed to be a result of the large diameter, thin-section four-point contact bearing used on the LSR. This hypothesis is based on rotation of the individual rotors before the prototype was fully assembled. Although the strong magnetic axial forces do place a significant thrust load on both the HSR and LSR bearings, this issue is not believed to be an intrinsic characteristic of the topology but specific to the prototype LSR bearing solution not rated for sufficient axial loading.

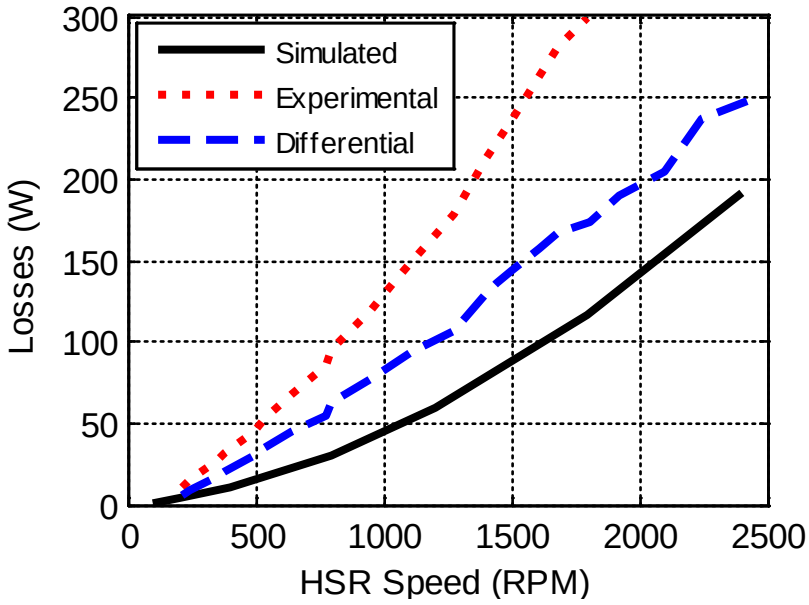

Figure 13. Experimental and Simulated No Load AFMGM Losses

A breakdown of the simulated no load and full load electromagnetic loss components is provided in Figure 14. This data demonstrates that the full load and no load magnetic losses are very similar except for the iron core losses. In particular, that variation is due to the losses in the integrated generator rotor back iron, which was the only non-laminated back iron in the machine. These findings suggest that with appropriate design, the no load and full load magnetic losses should be very similar, so the no load losses can provide a good estimation of the full load loss, after adjusting mechanical losses and for the increased copper losses.

The loss components breakdown in Figure 14 also indicates that one of the largest magnetic loss components is eddy current losses produced by leakage flux in some of the structural aluminum. This was a known potential issue during the prototype development process and is primarily associated with aluminum structural reinforcement components that were added due to concerns over the large axial forces in accordance with a very conservative design approach. Based on insight gained during the prototype's construction and experimental operation, along with information from 3D mechanical FEA models, this aluminum is unnecessary and can be eliminated from future designs.

The measured test data from Figures 15 and 16 again demonstrate the smooth design and magnetic isolation of the gear and generator components from the sinusoidal line-to-line back EMF of the integrated generator.

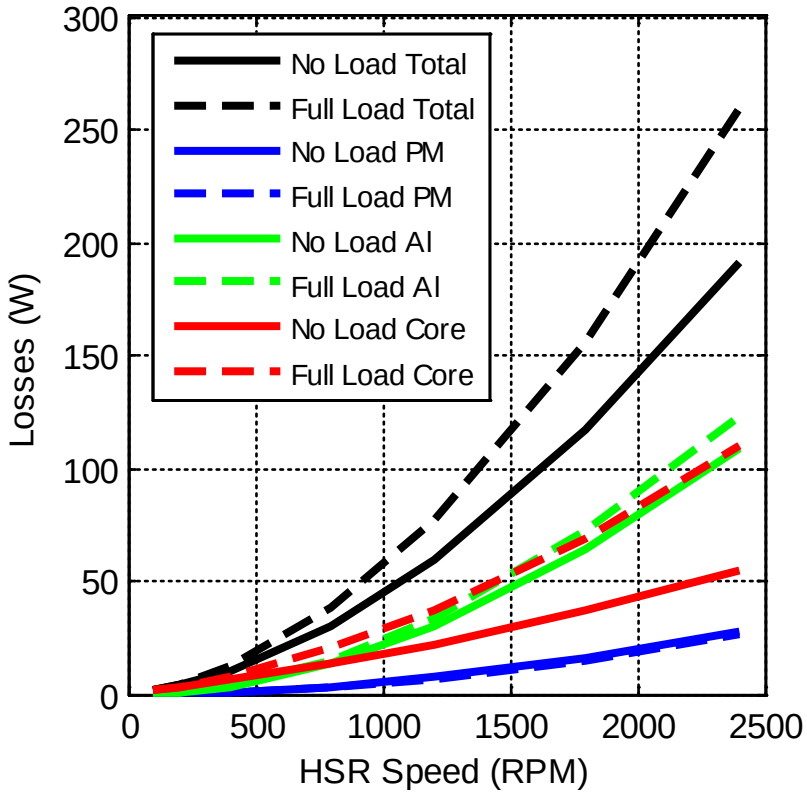

Figure 14. Simulated No Load and Full Load Magnetic Loss Components

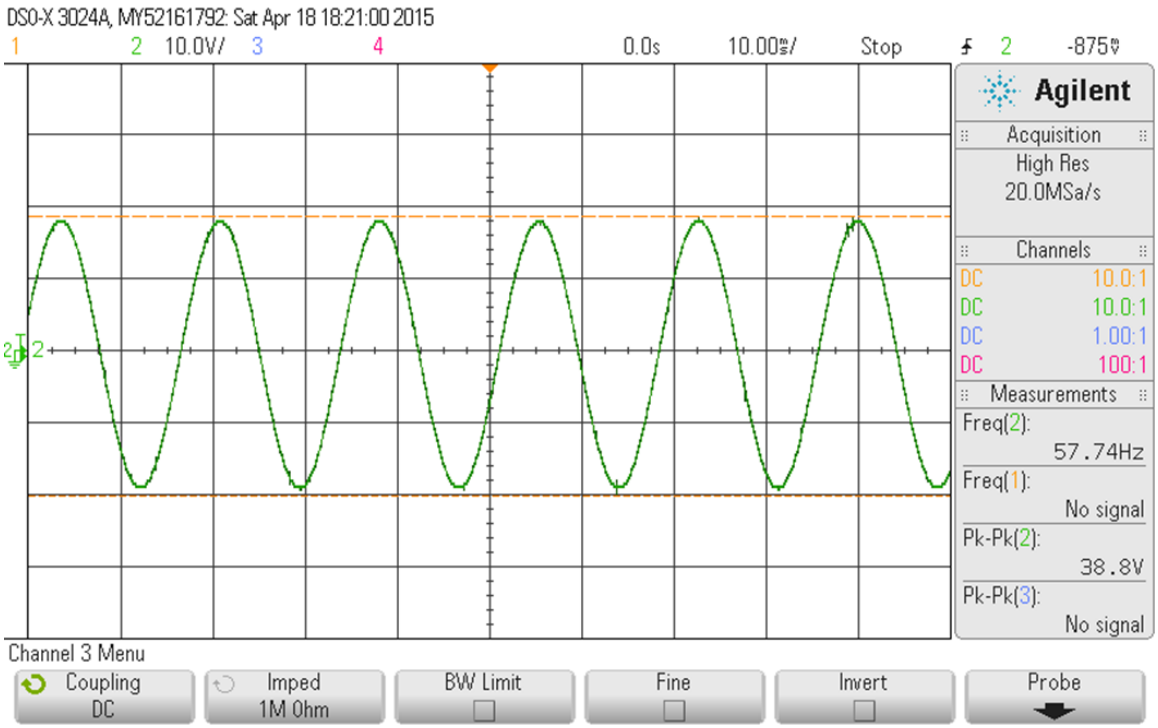

Figure 15: No load rotor back EMF at 37.1 / 346 RPM

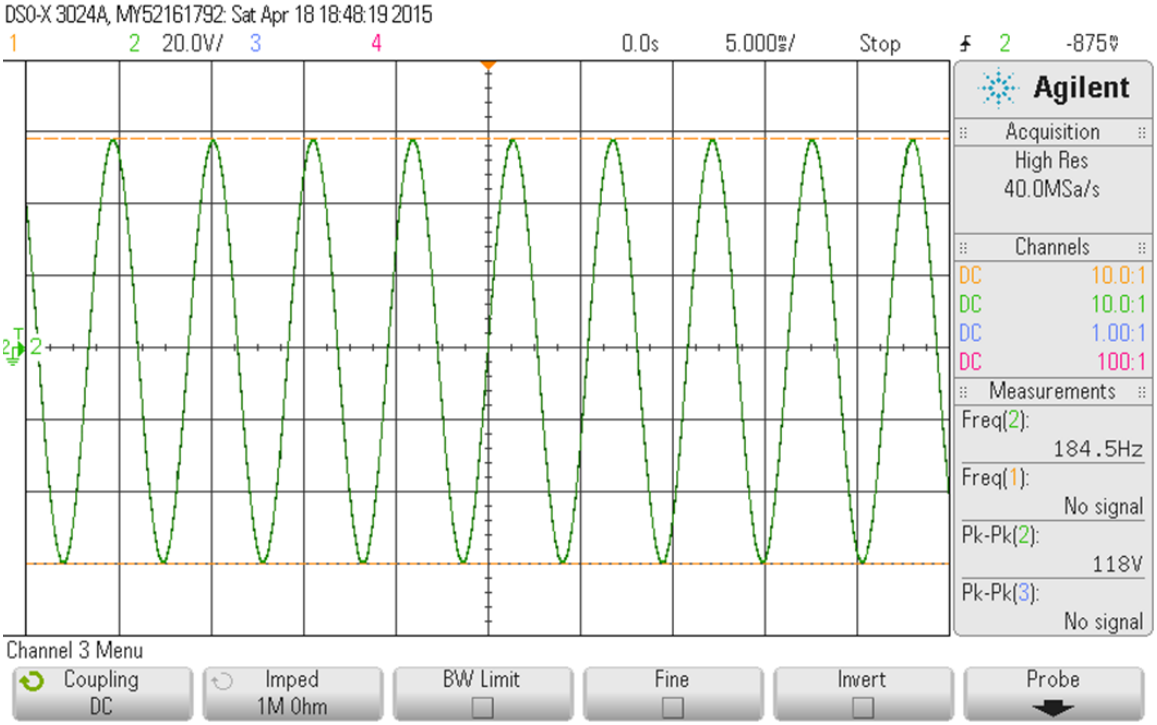

Figure 16: No load rotor back EMF at 118.6 / 1107 RPM

5. LOAD TESTING:

The axial-flux, magnetically-geared alternative Phase I prototype, provided invaluable information for the selection and design of the Phase II prototype. The experience with the design and performance calculations, the bearing system, magnet retention, multiple rotor assembly, and eddy-current losses in conductive structural material from the Phase I prototype improve our chances of a successful Phase II prototype. Unfortunately, the alternative Phase I prototype was damaged by a dislodged magnet during initial load testing. Not only the magnet but the bearings and structural assembly were damaged from the severe shock of the sudden stop caused by the loose magnet lodging between the modulator and rotor.

Calculated values of output power and efficiency for the Phase I integrated, axial-flux magnetically geared-machine are displayed in Figure 17 and 18 below. These values are based on the no-load voltage measurements and armature resistance measurements. No additional testing is necessary from this Phase I prototype.

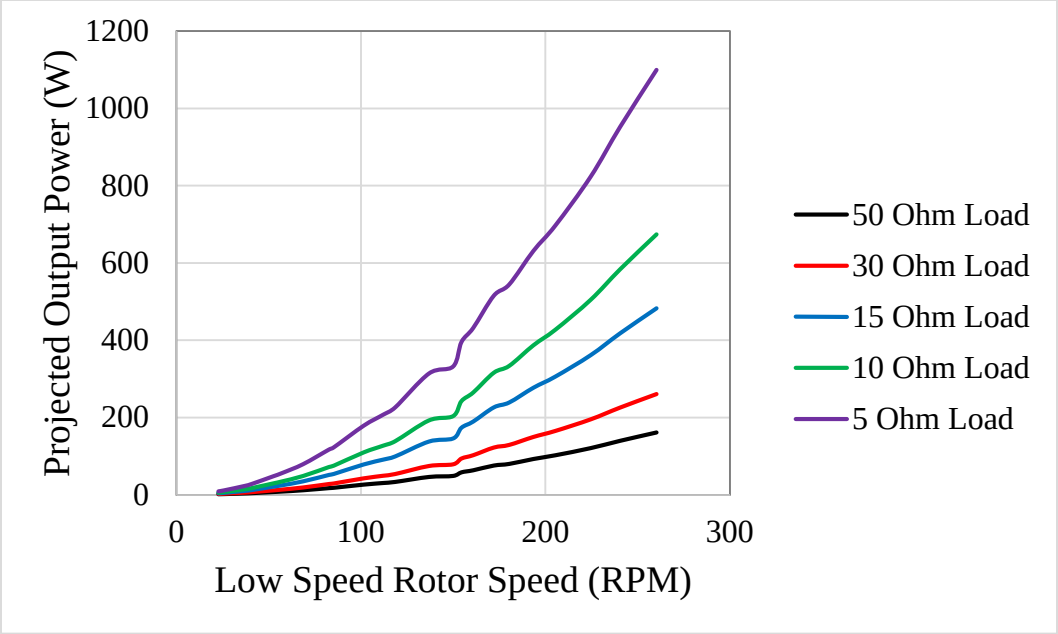

Figure 15: Phase I projected output power

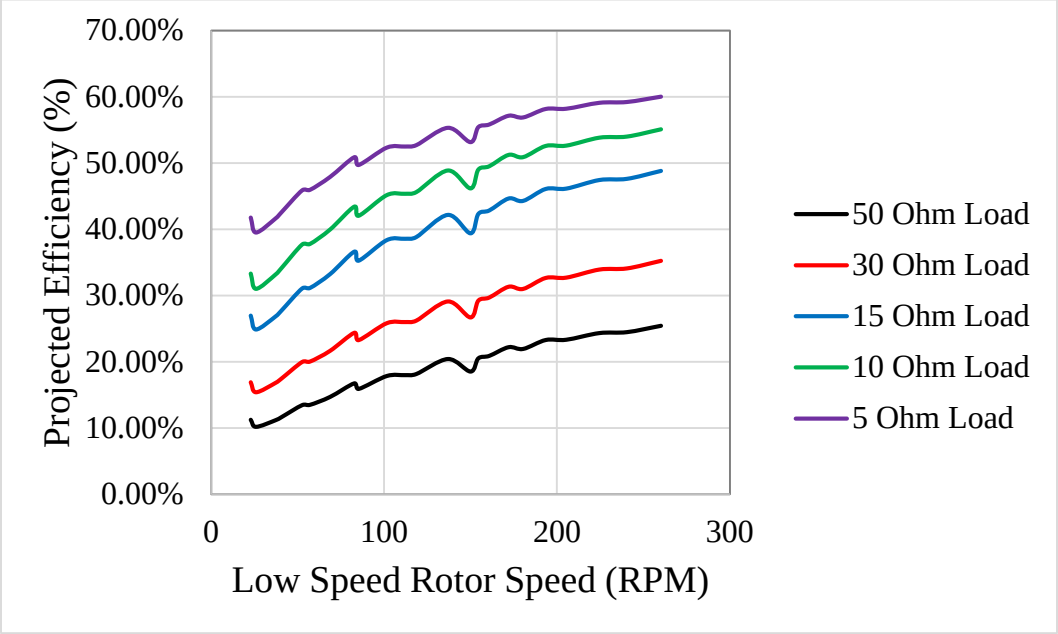

Figure 16: Expected Phase I prototype efficiency

The full load efficiency of the Phase I prototype integrated, axial flux magnetically geared generator is expected to be about 60%, with electrical efficiency values of about 80% for the magnetic gear and about 75% for the off the shelf generator. Higher efficiencies are achievable with reduced bearing loss, minimizing eddy current losses in structural material, dedicated design of the generator components (reduced winding resistance, higher quality laminations, and design for low harmonics for example) as well as additional focus on efficiency of the magnetic gear from steps like magnet segmentation, pole-combination selection, and laminating the modulator segments. These strategies will be applied to increase the efficiency of the Phase II radial flux, magnetically geared generator prototype.

6. PHASE II PROTOTYPE SELECTION:

A summary of the Phase I prototypes is shown below in Table 1. The integrated axial flux magnetically geared generator values are the calculated performance predictions, not yet validated with the test results. Similar values for the full scale generator are shown on the next page in Table 2. The material costs in both tables are calculated assuming $50/kW for the magnets, $10/kW for the copper, and $2/kW for the lamination electrical steel.

Table 1. Phase 1 300 rpm, 1 kW generator prototype summary

Design Parameters	Integrated Axial Flux Gear+Generator	Pole Modulated	Tooth Wound	COTS Reference 7 hp (5.2 kW) 300 rpm
Gear Ratio	9	-	-	-
Outer Diameter (m)	260	310	310	305
Inner Diameter (m)	60	95.25	95.25	62
Stack Length (m)	55	60	60	152
Est. Coil Head Length [m]	0	37.5	20	69
Magnet Material (kg)	1.7	1.8	1.8	4.1
Electrical Steel Core Material (kg)	9.1	17.2	15.1	71.1
Copper Material (kg)	0.45	2.4	2.1	15.8
Total Active Weight (kg)	11	21	19	91
Continuous Power Output (kW)	1	3.8	4.1	5.2
PM per kW (kg/kW)	1.7	0.5	0.4	0.8
Iron per kW (kg/kW)	9.1	4.5	3.7	13.6
Copper per kW (kg/kW)	0.5	0.6	0.5	3.0
Total Active Weight per kW (kg/kW)	11	6	5	17
Torque Density (kNm/m^3) Target ≥ 16 kNm/m^3	12	13	19	8
Torque Density (Nm/kg) Target ≥ 4 Nm/kg	2.8	5.7	6.9	1.8
Active Material Cost (USD)	108	148	141	505
Active Material Cost per kW (USD/kW) Target ≤ $100 USD/kW	108	39	34	97

Table 2. Full Scale, 40 kW, 1.7 rpm design projections

Design Parameters	Integrated Axial Flux Gear+Generator	Pole Modulated Generator	Tooth Wound Generator	Integrated Radial Flux Gear+Pole Modulated	Integrated Radial Flux Gear+Tooth Wound Generator	COTS Reference 250 hp (186.5 kW) 125 rpm
Gear Ratio	9	-	-	11	11	-
Outer Diameter (m)	2.5	2	2	2	2	0.73
Inner Diameter (m)	0.9	1.24	1.28	0.2	0.23	0.18
Stack Length (m)	0.38	3.2	3	0.9	0.9	0.81
Est. Coil Head Length [m]	0	0.4	0.25	0	0	0.14
Magnet Material (kg)	2,160	1,750	1,650	2,420	2,370	88
Electrical Steel Core Material (kg)	4,700	14,300	15,400	9,350	9,050	2,220
Copper Material (kg)	160	9,100	6,600	180	130	292
Total Active Weight (kg)	7,020	25,150	23,650	11,950	11,550	2,600
Torque Density (kNm/m^3) Target ≥ 84 kNm/m^3	139	29	35	80	81	33
Torque Density (Nm/kg) Target ≥ 14 Nm/kg	32	9	10	19	19	5.5
Active Material Cost (kUSD) Target ≤ $200 kUSD	119	207	179	142	138	12

In summary, these are important points from the tables above:

- The pole-modulated generator did not provide an advantage in terms of torque density, but did show a significant PTO system disadvantage not included in the tables, from a low power factor (~0.5 leading) for maximum power output.
- The single air gap machines are not expected to be able to meet the full scale torque density targets.
- The axial flux integrated magnetic gear generator requires a larger diameter, which will be more difficult to integrate with the flap.
- The air gaps will be challenging to maintain with the full scale axial flux topology. The mechanical assembly and supporting structure will be more complicated and expensive than with a radial flux topology.

Based on these points and our progress over Phase I, we propose an integrated radial flux magnetic gear with an inner, radial flux tooth-wound generator for the Phase II prototype. The radial flux topology simplifies the mechanical complications delaying the axial flux prototype. This mechanical disadvantage would be an even more serious drawback at larger scale. Initial examinations based on our Phase I effort predict a radial flux integrated magnetically geared generator topology has potential to meet the torque density targets and meet the project goals by enabling an all-electric PTO system.

MILESTONE DELIVERABLE

Task 4.1: Phase 2 Generator Prototype Test Plan

Date of Completion: 1/16/2016

1. GENERAL DESCRIPTION:

This document outlines the experimental performance evaluation of the magnetically geared 10 kW, 30 rpm generator prototype. The primary goals of these tests are to

- Evaluate the prototype performance
  - At constant speed up to 30 rpm, including power output, loss, and efficiency
  - Under oscillating input and emulating actual wave conditions
- Compare the power, efficiency, and mass and volumetric torque density of the prototype against the baseline targets
- Measure test data for calibration and validation of performance calculations
- Validate the generator torque limiting, power conversion, and energy storage strategy focusing on the measured impact to generator performance
- Identify potential risks and opportunities to improve the electromagnetic, mechanical, structural, or thermal performance of the full scale design

The generator will be tested first under continuous rotation up to 30 rpm before testing under oscillating and emulated ocean wave speed and torque waveforms. The general layout of the test set-up is shown in Figure 1.

The drive motor will be coupled to the gearbox high speed shaft, with the 10 kW magnetically geared generator prototype coupled to the gearbox low speed shaft through the torque transducer and a variable speed drive used to control the low speed of the drive motor.

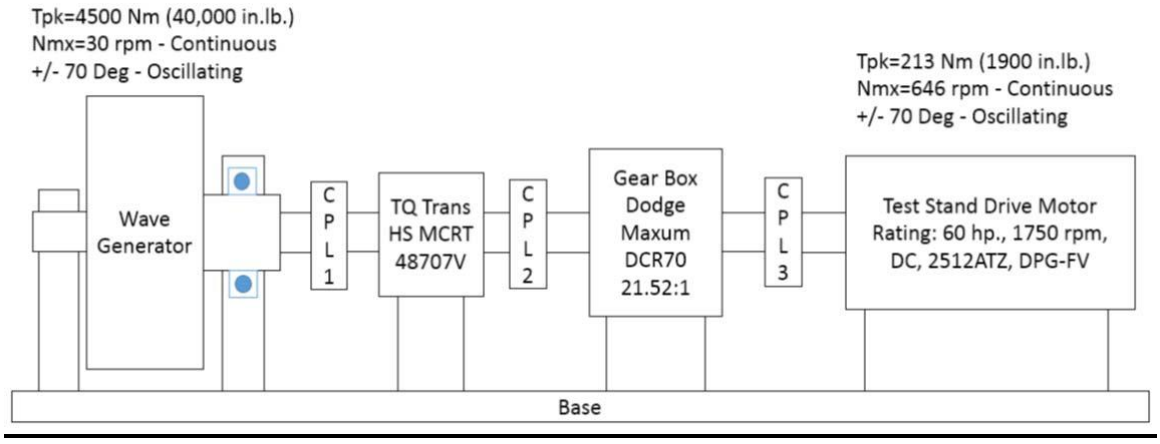

Figure 1. Schematic of Phase 2 Prototype Test Set-up

As a high level summary of the planned testing, the experiments to be conducted start

with characterization of the prototype and commissioning of the test stand to control the drive motor and variable speed drive. Constant speeds can be set as in Phase 1. Controllable speed and torque waveforms will be added for Phase 2 testing. The prototype will first be examined to verify critical electrical and mechanical parameters of the generator design including gear characteristics with open circuit stator windings and no load rotational testing. Next, oscillating testing will start with simple periodic input speed waveforms and then programmed to emulate the example ocean wave speed profile, first to a resistive load and then including the output power converter and energy storage components. Finally, the generator performance will be measured under input torque emulating the ocean wave torque profile and generator torque limiting through output current control.

2. LIST OF TEST EQUIPMENT:

- Baldor 60hp DC motor and ABB DCS800 drive
- Baldor/Dodge DCR70 21:1 Gearbox
- ParaFlex flexible plus 2 rigid couplings
- Himmelstein MCRT 48707V torque meter
- Fluke multimeters
- Tektronix and Yokogawa oscilloscopes and power meter
- Agilent data acquisition
- Thermocouples (J Type), Fluke IR thermometer, FLIR IR camera
- Tachometer
- Adjustable resistive load bank
- Active Rectifier
- Super capacitors and DC/DC charge controller

3. LIST OF TEST OBJECTS:

- Prototype 10 kW, 30 rpm magnetically geared generator

4. DRIVE MOTOR AND ACTIVE RECTIFIER CONTROL:

- Verify drive settings for control of speed and torque waveforms
    - First for speed control, program a ramp function with ~12 sec period and dead time for 6.4 rpm peak speed and 1.7 rpm average speed
    - Then, similarly program a ramp function for torque control with a ~4:3 ratio of peak to average torque
    - Next, program the flap speed values from RME's flap simulation, emulating actual ocean wave conditions
    - Finally, program a scaled version (with amplitude reduced consistent with the prototype performance) of the flap torque from RME's non-torque limited flap simulation to emulate actual wave conditions
- Verify active rectifier operation for generator output current and torque limiting

5. INITIAL DESIGN VERIFICATION/CHARACTERIZATION:

- Rotation clearance tests
- Static measurement of torque vs angle with fixed high speed rotor
- Gear ratio measurement
- Room temperature resistance of each stator phase
- Maximum static torque limit

6. PROTOTYPE PERFORMANCE TESTS – FIXED SPEED:

- Back emf voltage measurements up to 30 rpm input
- No Load losses vs speed

- Performance measurements for a range of fixed speeds and resistive loads
  - Waveforms and average values for speed, torque, current, voltage, power, power factor, and efficiency
  - Stator winding and rotor temperature monitoring

- Steady state heat run at 10 kW and 30 rpm

7. PROTOTYPE PERFORMANCE TESTS – OSCILLATING:

- Performance measurements under periodic speed ramp function
  - For range of resistive loads and power conversion system
  - Speed and torque waveforms and average values
  - Output voltage, current, and power waveforms and all average values including power factor and efficiency

- Performance measurements with speed function simulating ocean wave oscillations
  - For range of resistive loads and power conversion system
  - Speed and torque waveforms and average values
  - Output voltage, current, and power waveforms and all average values including power factor and efficiency

- Performance measurements with torque ramp and ocean wave oscillations
  - For range of resistive loads and power conversion system
  - Speed and torque waveforms and average values
  - Output voltage, current, and power waveforms and all average values including power factor and efficiency

8. SUMMARY OF DATA TO BE SUBMITTED:

Prototype Characterization

- Static Torque vs Angle Curve
- Measured gear ratio

Constant Speed Testing

- Open circuit stator performance waveforms and average values (speed, torque, voltage, losses)
- Performance waveforms and average values for range of input speed and resistive loads (speed, torque, current, voltage, power, power factor, efficiency)
- Operating temperature measurements

Oscillation Testing

- Speed and torque waveforms and average values
- Output voltage, current, and power waveforms and average values including power factor

DE-EE0006400
MILESTONE DELIVERABLE

TASK 5.1 Phase II Generator Test Report

Report Main Author: Wen Ouyang

Table of Content

1 General information

A prototype magnetically geared generator was developed under DOE contract (DE-EE0006400) as a proof of concept development for wave energy conversion low speed, high torque applications. The generator is a direct drive electrical power generating device which integrates a magnetic gear and a permanent magnet generator within the same nested machine.

The generator includes four electromagnetically active components:

- Low speed (LS) rotor
- Modulator
- High speed (HS) rotor
- Stator

The LS rotor is the outer most component of this generator and can be directly connected with a flap-type or other wave energy capture device. In the prototype case, the LS rotor is coupled via a stub shaft to the test bed drive train. The modulator, HS rotor, and stator are nested in the same order inside the LS rotor. For ocean wave energy applications, the LS rotor operates at a very low speed range typically averaging about 1~2 rpm, with a peak speed less than 10 rpm. To generate significant power, the torque observed by this LS rotor is large, which makes the development of this type of generator a challenging task. This initial proof of concept investigation is focused on prototype demonstration and dry laboratory testing to validate modeling and calculations for a full scale design. The additional challenges of operating submerged in a marine environment are outside the scope of this project.

With the magnetic gear effect, the HS rotor rotates in the opposite direction of the LS rotor at higher speed, with the speed (and also torque) ratio determined by the designed magnetic gear ratio.

This report describes the prototype design data and test results for the 10 kW, 30 rpm Phase II magnetically geared generator prototype. The testing was performed at the ABB Corporate Research lab for the characterization and validation of the proposed design concept.

1.1 Magnetically Geared Generator Design Information

The generator concept is illustrated in Figure 1.1.1.

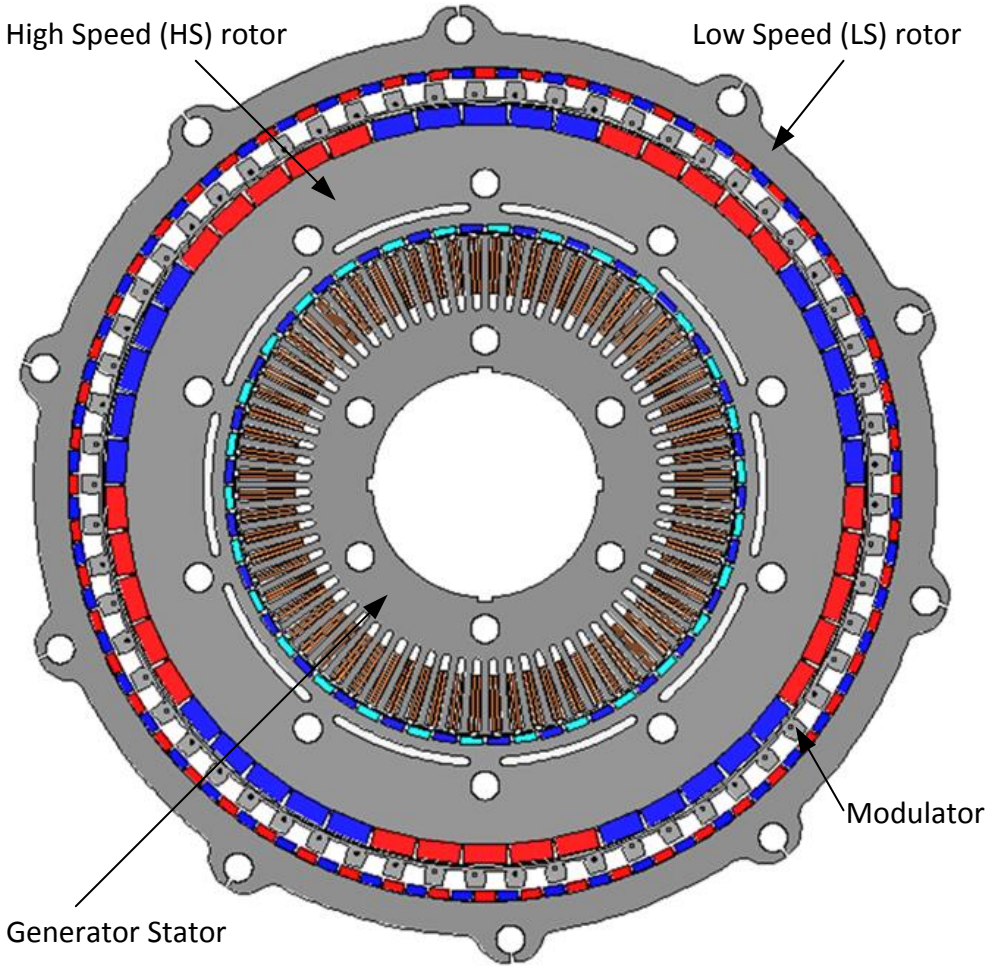

Figure 1.1.1: Magnetically Geared Generator Concept View

The outer most rotor is the low speed (LS) rotor, which is directly coupled via an input stub shaft to the test-bed drive train. Next is the thin electrical steel modulator layer, fixed in position between the outer low speed rotor and the inner, high speed (HS) rotor. The high speed rotor includes thicker magnets on the outer diameter for the magnetic gear operation as well as a magnetically isolated thinner set of magnets on the inner diameter to interact with the inner generator stator for generating electrical power. The stator is mounted on a fixed supporting shaft running through the center of the machine. The generator is designed with three air gaps. The two LS and HS rotors rotate in opposite directions, with a magnetic gear speed ratio of 11.2.

The prototype design information is provided in Table 1.1.1 below.

Parameter	Value	Parameter	Value
LS rotor OD (mm)	800	Pole #	40
LS rotor ID (mm)	736.6	Stator slot #	48
Modulator air gaps (mm)	3	Inner air gap (mm)	2.5
LS rotor magnet thickness(mm)	7.5	Stator phase resistance @ 20 deg C (Ohm)	0.235
LS rotor pole #	136	Stator phase #	6
HS rotor iron OD (mm)	649.6	Stator winding type	YY
HS rotor outer magnet thickness (mm)	15	HS rotor inner magnet thickness (mm)	7.5
HS rotor outer pole #	12	HS rotor torque (Nm)	310
Modulator iron pole	74	HS rotor speed (rpm)	336
Rotors stack length (mm)	93	Stator stack length (mm)	53
LS rotor peak torque (kNm)	3.87	Stator rated frequency (Hz)	112
Total Weight (kg)		1,008	
Overall OD (mm)		1,680	
Rated Input Speed (rpm)		30	
Rated Voltage (V LL)		300	
Rated Current (A)		10	
Rated Power (W)		10	

Table 1.1.1: Generator Design Information

2 Test Equipment & Setup

2.1 Equipment

The equipment list is provided in Table 2.1.1. The ABB drive information is provided in Table 2.1.2.

Power Meter	Yokogawa WT1800
AC induction motor	ABB/Baldor 60 HP general purpose
AC Drive	ABB ACS 850
Torque Meter	Himmelstein MCRT 48707V
Temperature Reader	Keysight 34972A
Current Sensor	Tektronix TCPA300
Scope	Tektronix mso4054b
Gear Box	Baldor/Dodge DCR70
Adjustable resistive load bank	Customized power resistor bank
Voltage Meter	Fluke multi-meters
Generator encoder	Customized built
Thermal coupler	J type
SiC MOSFET- 1200V, 100A	Cree
Control board	Oztek
Interface board and converter	Customized built
Super-capacitors	Maxwell
DC Power supply	Chroma 3120

Table 2.1.1: Test Equipment List

Nominal ratings		No-overload use			Light-duty use				Heavy-duty use				Type designation	Frame size
I_{2N} (A)	I_{Max} (A)	P_N (kW) $U_{N=400V}$	P_N (kW) $U_{N=500V}$	P_N (hp) $U_{N=480V}$	I_{Ld} (A)	P_{Ld} (kW) $U_{N=400V}$	P_{Ld} (kW) $U_{N=500V}$	P_{Ld} (hp) $U_{N=480V}$	I_{Hd} (A)	P_{Hd} (kW) $U_{N=400V}$	P_{Hd} (kW) $U_{N=500V}$	P_{Hd} (hp) $U_{N=480V}$		
3	4.4	1.1	1.5	1.5	2.8	1.1	1.1	1	2.5	0.75	1.1	1	ACS850-04-03A0-5	A
3.6	5.3	1.5	1.5	2	3.4	1.5	1.5	2	3	1.1	1.5	1.5	ACS850-04-03A6-5	A
4.8	7	2.2	2.2	3	4.5	1.5	2.2	2	4	1.5	2.2	2	ACS850-04-04A8-5	A
6	8.8	2.2	3	3	5.5	2.2	3	3	5	2.2	2.2	3	ACS850-04-06A0-5	A
8	10.5	3	4	5	7.6	3	4	5	6	2.2	3	3	ACS850-04-08A0-5	A
10.5	13.5	4	5.5	5	9.7	4	5.5	5	9	4	4	5	ACS850-04-010A-5	B
14	16.5	5.5	7.5	7.5	13	5.5	7.5	7.5	11	5.5	5.5	7.5	ACS850-04-014A-5	B
18	21	7.5	11	10	16.8	7.5	7.5	10	14	7.5	7.5	10	ACS850-04-018A-5	B
25	33	11	15	15	23	11	11	15	19	7.5	11	10	ACS850-04-025A-5	C
30	36	15	18.5	20	28	15	15	20	24	11	15	15	ACS850-04-030A-5	C
35	44	18.5	22	25	32	15	18.5	20	29	15	18.5	20	ACS850-04-035A-5	C
44	53	22	30	30	41	22	22	30	35	18.5	22	25	ACS850-04-044A-5	C
50	66	22	30	30	46	22	30	30	44	22	30	30	ACS850-04-050A-5	C
61	78	30	37	40	57	30	37	40	52	22	30	40	ACS850-04-061A-5	D
78	100	37	45	60	74	37	45	50	66	37	45	50	ACS850-04-078A-5	D
94	124	45	55	60	90	45	55	60	75	37	45	50	ACS850-04-094A-5	D
103	138	55	55	75	100	55	55	75	83	45	55	60	ACS850-04-103A-5	E0
144	170	75	90	100	141	75	90	100	100	55	55	75	ACS850-04-144A-5	E0
166	202	90	110	125	155	75	90	125	115	55	75	75	ACS850-04-166A-5	E
202	282	110	132	150	184	90	110	150	141	75	90	100	ACS850-04-202A-5	E
225	326	110	132	150	220	110	132	150	163	90	110	125	ACS850-04-225A-5	E
260	326	132	160	200	254	132	160	200	215	110	132	150	ACS850-04-260A-5	E
290	348	160	200	200	286	160	200	200	232	132	160	150	ACS850-04-290A-5	E
387	470	200	250	300	377	200	250	300	300	160	200	200	ACS850-04-387A-5	G1
500	560	250	315	350	480	250	315	350	355	200	250	250	ACS850-04-500A-5	G1
580	680	315	355	450	570	315	355	450	414	200	250	350	ACS850-04-580A-5	G1
650	730	355	400	500	634	355	400	500	477	250	315	400	ACS850-04-650A-5	G1
710	850	400	500	600	700	400	500	600	566	315	400	450	ACS850-04-710A-5	G2
807	1020	450	560	700	785	450	560	600	625	355	450	500	ACS850-04-807A-5	G2
875	1100	500	560	700	857	450	560	700	680	400	450	600	ACS850-04-875A-5	G2

Table 2.1.2: ABB drive options (phase II test bench drive is enclosed in red)

In Table 2.1.2, ABB provides a series of drives at different power ratings with different current capability. With low speed high load operation, the drive selected needs to be well matched with the induction motor capability with good margin for the current rating. The Baldor induction motor details are listed in Table 2.1.3.

Nameplate 000613007HV										
CAT NO	ZDVSM4314T	SPEC NO.	P36G3219							
SER.NO.		FRAME	364T							
	HP	RPM		VOLTS		AMPS		HZ	TYPE	P
BASE	60	1785		230/460		142/71.2		60	SF	1.00
MAX	60	2675		230/460		138/69.1		90	INSUL.CLASS	F
DRIVE END BEARING	65BC03J30X	CONSTANT TORQUE		DUTY	CONT	AMB	40			
OPP D.E. BEARING	65BC03J30X	1000 1		ENCL	TEFC	PHASE	3			
DESIGN NO.	A36WG0566-R002	FLUX AMPS	48.6/24.3							
MAX SPEED/RPM	3600	OVERTEMP PROT	2	WK2	14.32	POLES	4	WEIGHT	907	

Table 2.1.3: Baldor induction motor specifications

The induction motor is connected with 460 Volt configuration and rated current of 71.2 Amps, which is well within the nominal current rating (94 amps) from drive. The induction motor characteristics are provided in Figure 2.1.1.

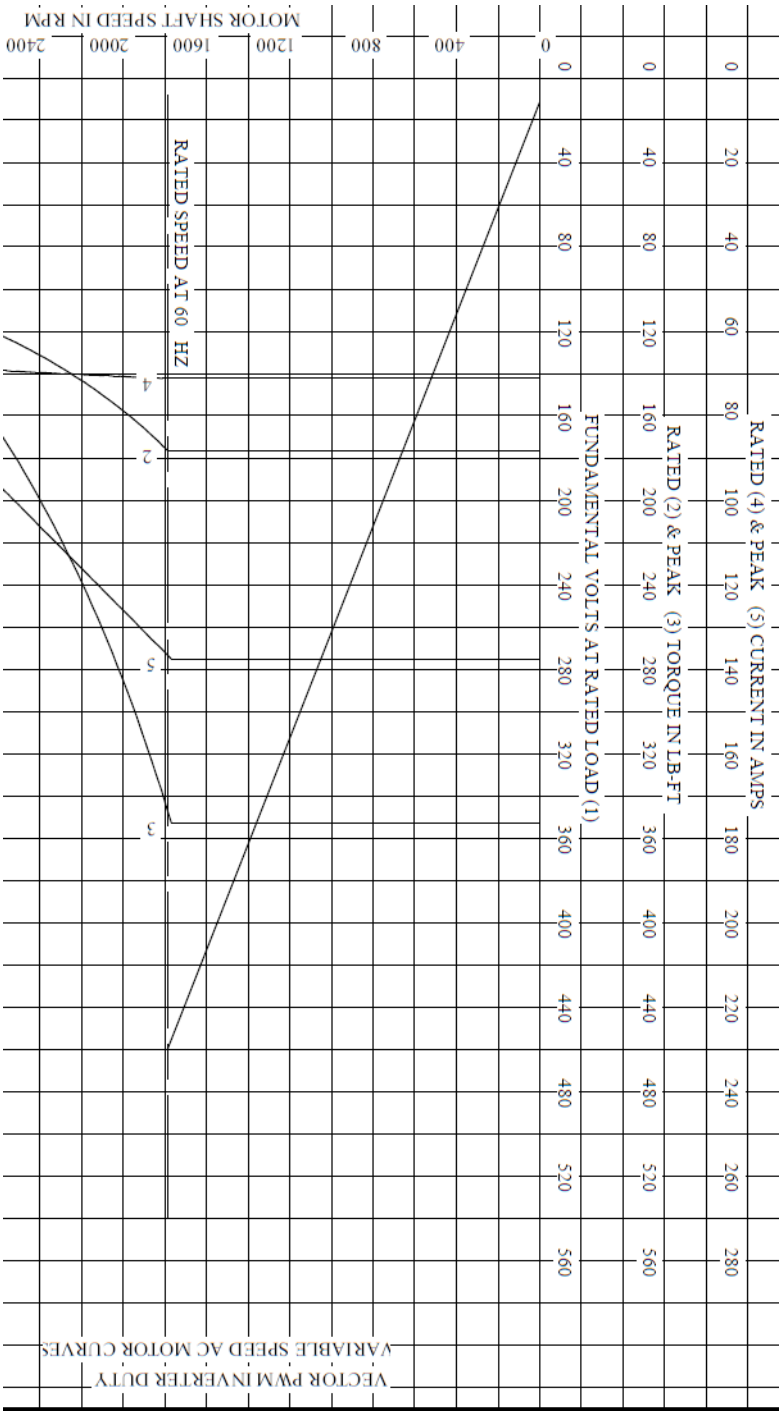

Figure 2.1.1: Baldor induction motor characteristics

2.2 Setup

The test bed setup for the prototype Phase II testing is shown in Figure 2.2.1.

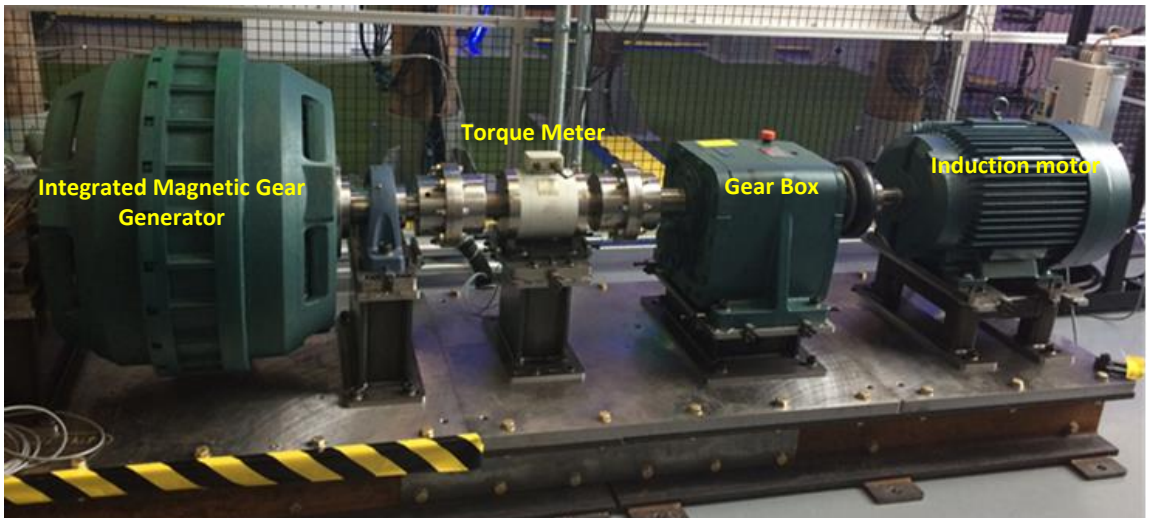

Figure 2.2.1: Phase II test bed setup

Due to the low speed and high torque requirements of this machine it was necessary to design a purpose-built test stand. The stand uses a Baldor/ABB 60hp (44.7kW) RPMAC induction motor as a prime mover, a Dodge/ABB Maxum XT 21.52:1 gear reducer, a Himmelstein torque transducer rated at 50,000 in·lbs (5,649 N m) and a 45 kW ABB ACS850 drive to control the induction motor. The drive may be programmed independently but it may also be controlled via an Agilent 33500B waveform generator permitting specification of custom torque wave-forms, like sinewaves or more random ocean waveforms. The torque transducer is coupled to the generator and gearbox with Dodge rigid-rigid couplings which were chosen to provide accurate torque measurements during oscillating tests. (Torsionally compliant couplings would create a phase shift between the measured and applied torque). The drive machine is coupled to the gearbox via a Dodge Paraflex coupling which adds compliance to the drivetrain and reduces peak-torques imposed on the gearbox.

The use of rigid couplings requires precision alignment of the drivetrain, and it should be noted, is not the typical method for mounting a torque transducer in a drive-train where precision measurements are desired. Due to inherent manufacturing inaccuracies, “perfect” alignment is not possible: shaft run out, mis-alignment of the machine shaft extension with the machine axis, etc. contribute to the error. The final error in the torque measurement is assumed to be ±75in·lbs (8.5N·m) and was determined by rotating the machine and measuring the static torque at the 12, 3, 6, and 9 o’clock positions.

2.3 Static Torque

The static torque capability of the magnetically geared generator was the first measurement after completing the test bed setup. The static torque was measured by locking the HS rotor and applying a load via a lever on the HS side of the mechanical gearbox until the LS rotor slipped. The motor was not used for torque application in order to have finer control and to be able to stop the torque immediately after exceeding the peak torque and slipping a pole. The lock consists of two 0.5in pins which slide through blocks on the modulator end-bell and index into holes on the HS rotor. This locking feature was specifically added to the design to help measure the static torque profile of the machine. Angular displacement was measured on the LS end bell using a Mitutoyo dial indicator with 0.001in gradations located on a magnetic base and reading from a known radius. It was found that the modulator-end-bell also rotated ~1˚ on its key under load. This created error in the measurement since the torque is produced via relative position of the modulator with respect to the LS rotor. To measure the small displacement of the modulator a Mitutoyo dial indicator with 0.0001in gradations was placed in a similar manner to the first. The effective rotation of the LS rotor with respect to the modulator was calculated and the peak torque was measured to be 3,870 N·m and the full static torque curve is shown in Figure 2.3.1.

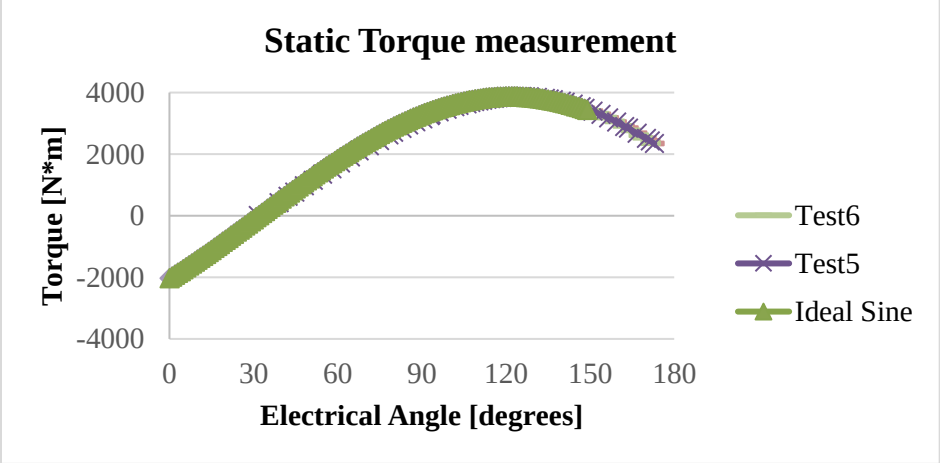

Figure 2.3.1: Magnetically geared generator static torque characteristic

The slip torque for this integrated magnetic gear generator measured 3870 Nm, which is only 1% less than the designed value.

This maximum slip torque is a very important value for the generator characterization and operation. If the load torque exceeds this peak torque, the relative position between rotors will suddenly shift, slipping to the next equilibrium point once the applied torque is reduced. This “pole slipping” is observable as a noisy sudden jolt. And this slip will continue to happen if the load torque remains higher than the slip torque. This pole slipping is a an inherent safety feature of magnetic gears, but still repetitively stresses

the mechanical structure of the machine in ways that are difficult to model and could reduce the useful lifespan of the single prototype. Therefore, to be cautious, the loaded torque in this testing is maintained below this torque limit for the tests performed in this report.

3 Constant Speed Testing

Constant speed testing provides the steady state operation characteristics of the prototype generator. The generator is first tested at no load and then incrementally loaded over the full speed range to provide performance data over the full range of operating conditions.

3.1 No Load

No load testing was performed with open circuit configuration of the generator terminals. The drive machine provides input torque to spin the low speed rotor at constant speed from 2 rpm to 30 rpm. The generator losses are measured via the shaft torque and speed. In Table 3.1.1, the test data for the power measurement are listed.

IM Command (rpm)	LS Rotor Speed (rpm)	HS rotor speed (rpm)	Torque (lbs-in)	Torque (Nm)	Shaft Power (W)	LL V (V, rms)	I (A, rms)	Freq (Hz)	Temp (C deg)
43.04	2	22.67	900	101.70	21.30	23.1	0	7.56	21
86.08	4	45.33	1060	119.78	50.17	45.3	0	15.11	21.5
129.12	6	68.00	1200	135.60	85.20	67.6	0	22.67	21.5
172.16	8	90.66	1370	154.81	129.69	89.9	0	30.22	21.5
215.2	10	113.33	1500	169.50	177.50	112.3	0	37.78	22
258.24	12	136.00	1650	186.45	234.30	134.7	0	45.33	22.4
301.28	14	158.66	1780	201.14	294.89	157	0	52.89	22.6
322.8	15	170.00	1820	205.66	323.05	168.2	0	56.66	22.8
344.32	16	181.33	1900	214.70	359.73	179.4	0	60.44	23
387.36	18	203.99	2000	226.00	426.00	201.7	0	68.00	23.5
430.4	20	226.66	2130	240.69	504.10	224.1	0	75.55	24
473.44	22	249.33	2250	254.25	585.75	246.4	0	83.11	24.5
516.48	24	271.99	2375	268.38	674.50	268.7	0	90.66	25
559.52	26	294.66	2460	277.98	756.86	290.9	0	98.22	25.5
602.56	28	317.32	2580	291.54	854.84	313.4	0	105.77	26
645.6	30	339.99	2720	307.36	965.60	335.6	0	113.33	26.5

Table 3.1.1: No Load Test Data

For this prototype development, the HS and LS rotor frame are designed with significant margin to provide a robust structure for high input torque. The extra

size and weight contribute non-negligible bearing friction and windage mechanical losses to the total no load loss shown in Figure 3.1.1.

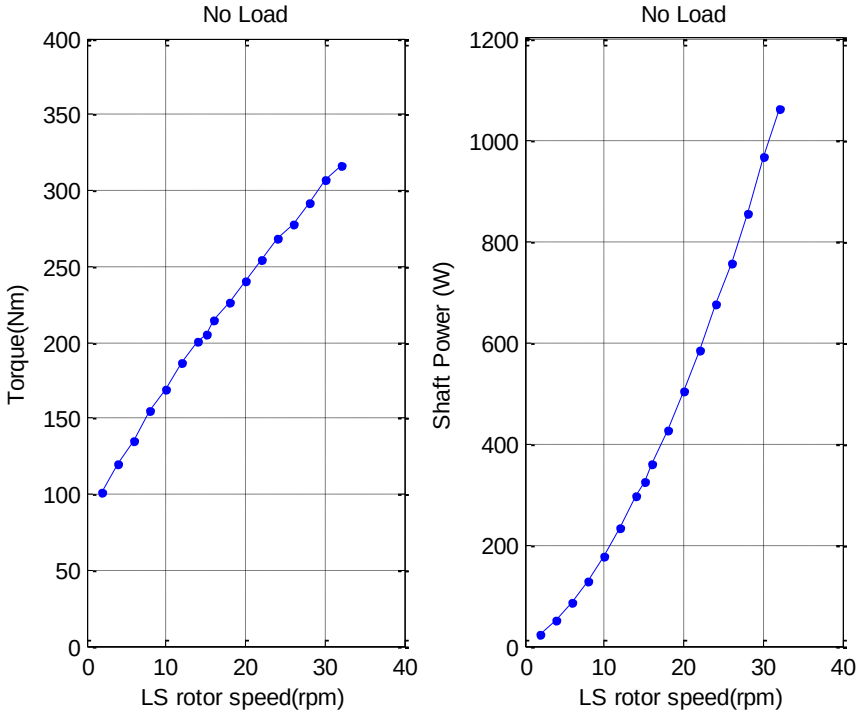

Figure 3.1.1: No load torque and shaft power characteristics

The static friction torque is estimated to be about 75 Nm if the torque versus speed curve in Figure 3.1.1 is extrapolated to 0 rpm. It should be noted that the high speed rotor is also spinning under no load operation. Thus the torque measured at no load actually combines the effects of the low speed rotor friction and windage torque, the high speed rotor friction and windage losses, and the laminated core and magnet losses due to flux variations.

The simulated no load losses at 30 rpm are provided in Table 3.1.2 to provide a better idea of the expected breakdown between mechanical and electromagnetic losses under no load operation. Further iterations on the mechanical supporting structure and bearing arrangement could significantly reduce the bearing losses. The generator design tried to minimize induced eddy current losses in the structural components of the generator. These are expected to be low (a few 10's of Watts) in this case, but this is another possible source of no load losses that is difficult to quantify.

Speed	15 rpm		30 rpm	
LS rotor core (FEA Calculation)	56	15%	148	15%
LS magnets (FEA)	82	23%	222	23%
Modulator (FEA)	18	5%	48	5%
HS rotor core (FEA)	18	0.6%	4	0.4%
HS magnets (FEA)	2	6%	56	6%
Generator stator core (FEA)	21	8%	117	12%
Generator magnets (FEA)	29	3%	28	3%
Total electrical no load loss (FEA)	**218**	**60%**	**623**	**64%**
Mechanical loss (=Measured - FEA)	**144**	**40%**	**343**	**36%**
Test measured total loss	**362**	**100%**	**966**	**100%**

Table 3.1.2: No load loss components at 15 and 30 rpm

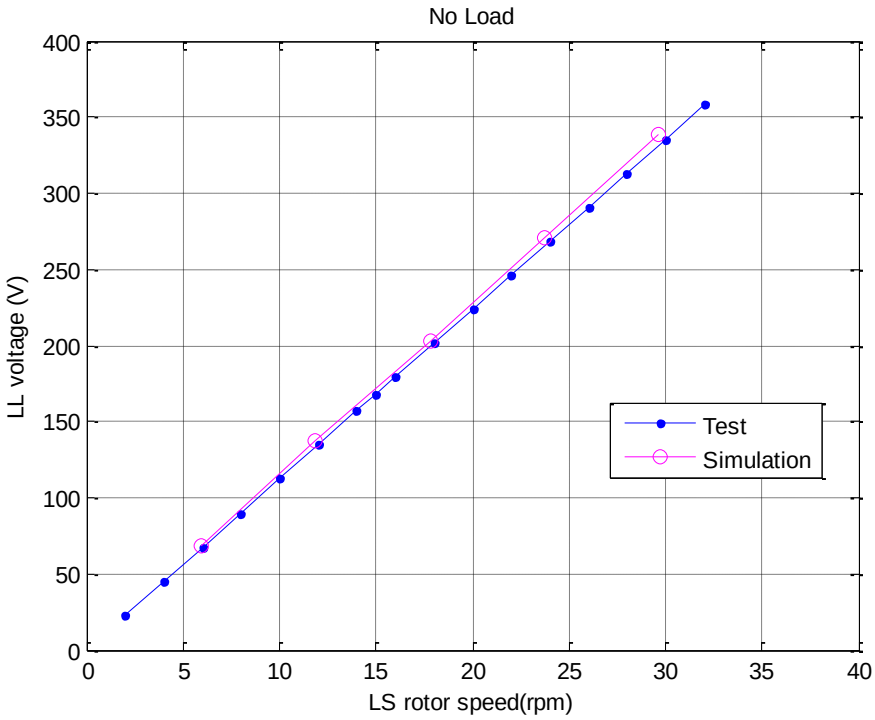

Figure 3.1.2: No load generator terminal voltage

With no current in the generator windings, the open circuit terminal voltage is proportional to the speed of the high speed rotor as indicated in Figure

3.1.2. At this speed range, the calculated magnet eddy current loss induced from relative rotation between stator teeth and generator magnets is low, increasing up to only about 28W at 30 rpm as shown in Table 3.1.2. The slightly higher simulated voltage results are based on ideal lamination characteristics and magnetization, while the prototype is built with the material provided by vendors with minor manufacturing tolerance. For example, the lamination is finished by laser cutting, which usually will change the magnetic property along the edge of the lamination profile. Moreover, the actual lamination stacking factor, the lamination and air gap dimensional tolerance, and magnet remanence variation all can impact the induced voltage, which is beyond the discussion scope of this prototype investigation. Anyway, the measured no load voltage is consistent with the predicted value.

3.2 Loaded

The Phase II prototype load tests were performed using the resistive load bank shown in Figure 3.1.3. Table 3.2.1 includes the test data with constant resistive load of 18.8 Ohms per phase at speed range from 2 rpm up to 30 rpm is provided.

Figure 3.1.3: No load generator terminal voltage

IM Command (rpm)	LS Rotor (rpm)	HS rotor (rpm)	Torque (lbs-in)	Torque (Nm)	Shaft Power (W)	VLL (V, rms)	I (A,ms)	Freq (Hz)	Temp (C deg)	Meter (W)	Effi (%)
43.04	2.00	22.67	3120	352.56	73.84	22.8	0.68	7.56	25.6	53.0	71.78
86.08	4.00	45.33	5530	624.89	261.75	44.4	1.35	15.11	25.6	209.5	80.04
129.12	6.00	68.00	7850	887.05	557.35	66.3	2.01	22.67	25.6	465.0	83.43
172.16	8.00	90.66	10150	1146.95	960.87	89.2	2.67	30.22	25.6	820.5	85.39
215.20	10.00	113.33	12400	1401.20	1467.34	109.6	3.32	37.78	25.7	1270.0	86.55
258.24	12.00	136.00	14630	1653.19	2077.46	131.0	3.97	45.33	26.0	1813.0	87.27
301.28	14.00	158.66	16800	1898.40	2783.21	152.2	4.60	52.89	26.5	2445.0	87.85
322.80	15.00	170.00	17850	2017.05	3168.38	162.6	4.95	56.67	26.9	2794.0	88.18
344.32	16.00	181.33	18920	2137.96	3582.19	173.0	5.25	60.44	27.6	3160.0	88.21
387.36	18.00	203.99	20950	2367.35	4462.36	194.0	5.86	68.00	28.5	3957.0	88.68
430.40	20.00	226.66	22920	2589.96	5424.41	214.0	6.50	75.55	29.5	4825.0	88.95
473.44	22.00	249.33	24850	2808.05	6469.30	234.5	7.11	83.11	29.0	5757.0	88.99
516.48	24.00	271.99	26680	3014.84	7577.14	254.1	7.70	90.66	30.0	6749.0	89.07
559.52	26.00	294.66	28410	3210.33	8740.83	273.3	8.27	98.22	31.0	7795.0	89.18
602.56	28.00	317.32	30100	3401.30	9973.16	291.8	8.83	105.77	32.0	8890.0	89.14
645.60	30.00	339.99	31660	3577.58	11239.33	309.8	9.38	113.33	33.0	10013.0	89.09

Table 3.2.1: Constant load variable speed test data

The temperature of the innermost rotor magnets and stator windings was a potential concern brought up during the project Phase I Go/No Go Review Meeting. With low current density design for the generator stator winding, the winding losses measured 130 W with the corrected winding resistance and winding current, which results in very low temperature rise for the end winding section. The 33 C degree indicated in Table 3.2.1 is the typical end winding temperature for the full load test with continuous operation mode. The large dimensions of this low speed prototype (compared to an industrial 1800 rpm 10 kW machine) also helps to dissipate the heat from the generator losses. Moreover, the air cooling effect from the relative movement from both low speed rotor and high speed rotor via the large windows between structure frames also contributes to this “cool” generator.

Figure 3.2.1 provides the generator input torque and output power characteristics with constant resistive load of 18.8 Ohms.

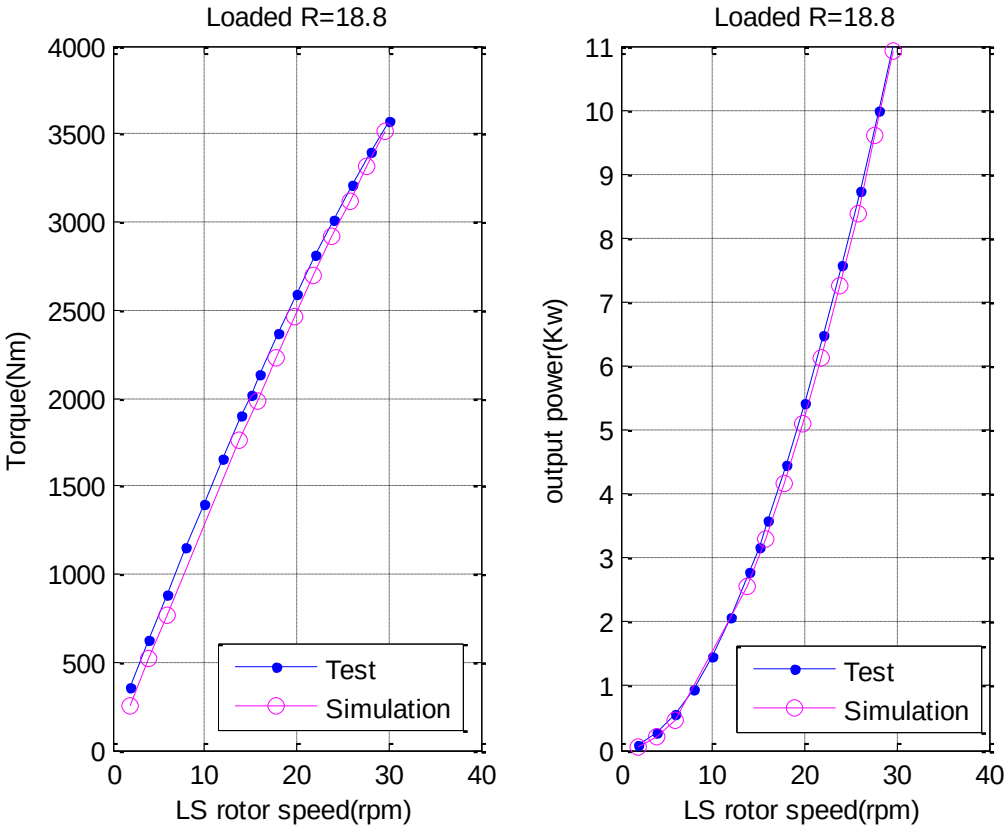

Figure 3.2.1: Gear Generator Torque (LS) & drive shaft output power at constant load

For this constant load test, the rated 10 kW power is achieved at 30 rpm. With increased speed, the generator input torque increases rather linearly, with a minor impact from winding armature reaction when the phase current is on the high end. Also, the increasing voltage drop due to leakage inductance with increased frequency becomes more significant when the generator speed approaches the rated speed. The FEA predicted phase leakage inductance and measured value are provided in Table 3.2.2

Phase leakage inductance	FEA	Test
mH	4.4	5.2

Table 3.2.2: Phase leakage inductance estimation

With 2D simulation, the phase leakage inductance is lower than the measured value due to the 3D effect of the end coil. Additionally, the prototype measurement was performed with a low current, which can give a higher inductance measurement with less saturation, although in this design, the generator saturation is not severe due to the large effective air gap.

The leakage inductance with the corresponding voltage trop for this constant load test is provided in Table 3.2.3. Figure 3.2.2 plots the generator phase current and efficiency with constant 18.8 Ohm resistive load.

Frequency	Current	Vls
7.56	0.68	0.17
15.11	1.35	0.67
22.67	2.01	1.49
30.22	2.67	2.64
37.78	3.32	4.10
45.33	3.97	5.88
52.89	4.60	7.95
56.67	4.95	9.17
60.44	5.25	10.37
68.00	5.86	13.02
75.55	6.50	16.04
83.11	7.11	19.31
90.66	7.70	22.81
98.22	8.27	26.54
105.77	8.83	30.51
113.33	9.38	34.73

Table 3.2.3: Leakage inductance voltage drop

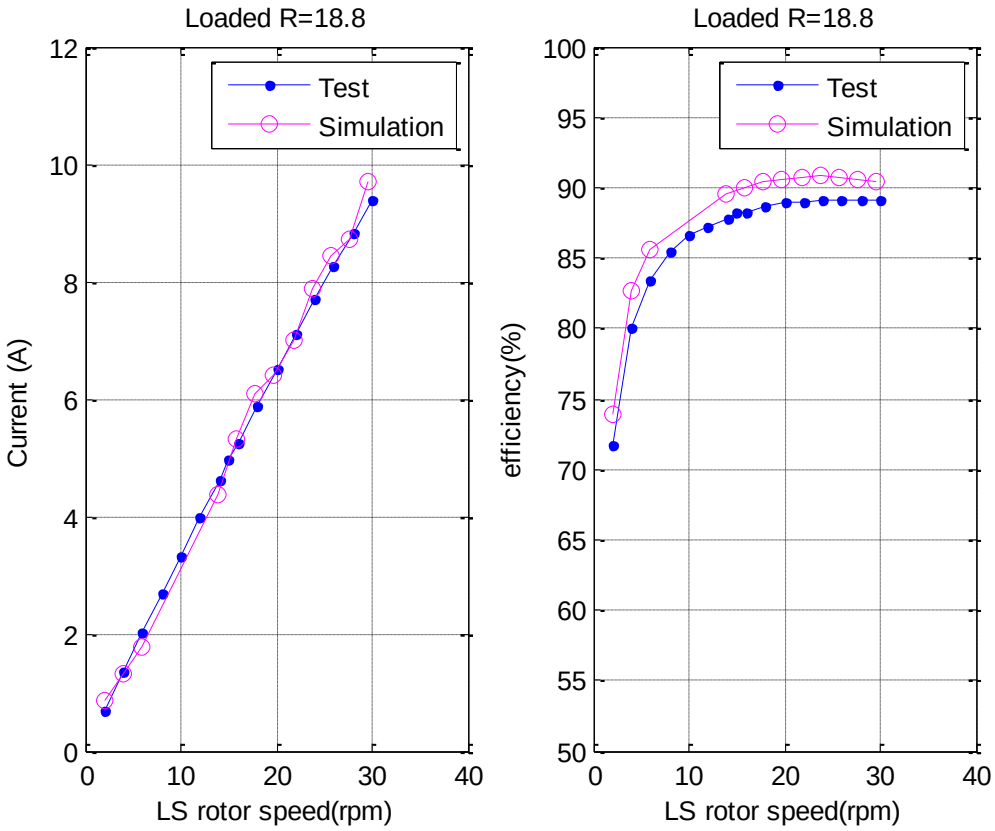

Figure 3.2.2: Generator current & efficiency at constant load

The current characteristics is similar to the linear torque characteristic due to the fact that torque production in this unity power factor loaded test is determined by the Q axis current, which is primarily the phase current.

The measured efficiency is slightly over 89% at the rated 10 kW, 30 rpm operating point, including the consideration of estimated mechanical drag losses at full speed (343 W obtained from the No Load test). Apart from the mechanical losses, the measured electromagnetic system efficiency increases to 92%, which is the combined efficiency of the magnetic gearing (97%) and electrical generation (95%) sections of the integrated machine. In addition to the potential for reduced mechanical losses, the full scale machine, due to the larger size and power rating, is expected to have a slightly higher, around 95.1%, combined electromagnetic efficiency divided 98.9% from the gear and 96.2% from the electrical generator sections.

The constant load test was repeated with different loads ranging from 14.1 to 1.2 Ohms per phase, and the results are listed in Table 3.2.4. The low operating temperatures and consistently high efficiency are encouraging. Even though this stator was designed for a rated operating point at 10 kW at 30 rpm, it still performs well over a wide operating range of speed and load. This attribute is well matched for MHK applications where the input torque from the wave or water energy converter is highly variable.

IM Comm	LS Rotor S	HS rotor s	Torque (lb	Torque (N	Shaft Pow	LL V (V, rm	I (A, rms)	Freq(Hz)	Temp (C d	Meter(W)	Effi(%)
43.04	2	22.67	3900.00	440.70	92.30	22.00	0.90	7.56	31.00	70.00	75.84
86.08	4	45.33	6950.00	785.35	328.97	44.00	1.78	15.11	31.00	272.00	82.68
129.12	6	68.00	9920.00	1120.96	704.32	66.00	2.66	22.67	30.00	605.00	85.90
172.16	8	90.66	12880.00	1455.44	1219.31	87.00	3.53	30.22	30.00	1065.00	87.34
215.2	10	113.33	15740.00	1778.62	1862.57	108.00	4.38	37.78	30.00	1642.00	88.16
258.24	12	136.00	18490.00	2089.37	2625.59	129.00	5.23	45.33	30.00	2335.00	88.93
301.28	14	158.66	21190.00	2394.47	3510.48	150.00	6.05	52.89	31.00	3133.00	89.25
322.8	15	170.00	22450.00	2536.85	3984.88	160.00	6.46	56.67	31.00	3566.00	89.49
344.32	16	181.33	23700.00	2678.10	4487.21	170.00	6.85	60.44	32.00	4022.00	89.63
387.36	18	203.99	26110.00	2950.43	5561.44	190.00	7.64	68.00	33.00	4998.00	89.87
430.4	20	226.66	28370.00	3205.81	6714.25	209.00	8.39	75.55	33.00	6045.00	90.03
473.44	22	249.33	30520.00	3448.76	7945.39	227.00	9.13	83.11	34.00	7150.00	89.99
510.2392	23.71	268.71	32100.00	3627.30	9006.26	242.00	9.72	89.57	36.00	8140.00	90.38

(a)

IM Comm	LS Rotor S	HS rotor s	Torque (lb	Torque (N	Shaft Pow	LL V (V, rm	I (A, rms)	Freq(Hz)	Temp (C d	Meter(W)	Effi(%)
43.04	2	22.67	4450.00	502.85	105.32	22.00	1.06	7.56	34.00	81.00	76.91
86.08	4	45.33	8050.00	909.65	381.03	44.00	2.10	15.11	34.00	322.00	84.51
129.12	6	68.00	11520.00	1301.76	817.92	65.00	3.15	22.67	33.00	714.00	87.29
172.16	8	90.66	14950.00	1689.35	1415.27	87.00	4.18	30.22	33.00	1252.00	88.46
215.2	10	113.33	18260.00	2063.38	2160.77	107.00	5.18	37.78	33.00	1925.00	89.09
258.24	12	136.00	21400.00	2418.20	3038.81	128.00	6.16	45.33	33.00	2725.00	89.67
301.28	14	158.66	24400.00	2757.20	4042.28	148.00	7.11	52.89	33.00	3636.00	89.95
322.8	15	170.00	25850.00	2921.05	4588.39	157.00	7.58	56.67	34.00	4130.00	90.01
344.32	16	181.33	27180.00	3071.34	5146.09	167.00	8.03	60.44	34.00	4645.00	90.26
387.36	18	203.99	29770.00	3364.01	6341.02	186.00	8.92	68.00	35.00	5729.00	90.35
430.4	20	226.66	32100.00	3627.30	7597.02	204.00	9.76	75.55	36.00	6875.00	90.50

(b)

IM Comm	LS Rotor S	HS rotor s	Torque (lb	Torque (N	Shaft Pow	LL V (V, rm	I (A, rms)	Freq(Hz)	Temp (C d	Meter(W)	Effi(%)
43.04	2	22.67	5375.00	607.38	127.21	22.00	1.34	7.56	21.60	102.00	80.18
86.08	4	45.33	9750.00	1101.75	461.50	44.00	2.64	15.11	22.00	400.00	86.67
129.12	6	68.00	14060.00	1588.78	998.26	65.00	3.92	22.67	22.00	883.00	88.45
172.16	8	90.66	18200.00	2056.60	1722.94	86.00	5.18	30.22	22.50	1540.00	89.38
215.2	10	113.33	22100.00	2497.30	2615.17	106.00	6.39	37.78	23.00	2352.00	89.94
258.24	12	136.00	25700.00	2904.10	3649.41	124.00	7.57	45.33	24.00	3301.00	90.45
301.28	14	158.66	29050.00	3282.65	4812.63	145.00	8.69	52.89	25.00	4362.00	90.64
322.8	15	170.00	30550.00	3452.15	5422.64	154.00	9.23	56.67	26.00	4924.00	90.80
344.32	16	181.33	32000.00	3616.00	6058.68	163.00	9.73	60.44	28.00	5497.00	90.73

(c)

IM Comm	LS Rotor S	HS rotor s	Torque (lb	Torque (N	Shaft Pow	LL V (V, rm	I (A, rms)	Freq(Hz)	Temp (C d	Meter(W)	Effi(%)
43.04	2	22.67	6720.00	759.36	159.04	22.00	1.73	7.56	26.00	132.00	83.00
86.08	4	45.33	12390.00	1400.07	586.46	43.00	3.44	15.11	26.50	513.00	87.47
129.12	6	68.00	17800.00	2011.40	1263.80	64.00	5.09	22.67	27.00	1127.00	89.18
172.16	8	90.66	22900.00	2587.70	2167.87	84.00	6.69	30.22	27.00	1946.00	89.77
215.2	10	113.33	27460.00	3102.98	3249.44	103.00	8.21	37.78	27.00	2935.00	90.32
258.24	12	136.00	31500.00	3559.50	4473.01	121.00	9.62	45.33	28.00	4048.00	90.50

(d)

IM Comm	LS Rotor S	HS rotor s	Torque (lb	Torque (N	Shaft Pow	LL V (V, rm	I (A, rms)	Freq(Hz)	Temp (C d	Meter(W)	Effi(%)
43.04	2	22.67	9280.00	1048.64	219.63	21.00	2.50	7.56	28.00	186.00	84.69
86.08	4	45.33	17300.00	1954.90	818.87	42.00	4.95	15.11	28.00	721.00	88.05
129.12	6	68.00	24550.00	2774.15	1743.05	61.00	7.27	22.67	28.00	1555.00	89.21
172.16	8	90.66	30780.00	3478.14	2913.85	79.00	9.40	30.22	28.50	2610.00	89.57
182.2744	8.47	95.99	32000.00	3616.00	3207.31	84.00	9.86	32.00	30.00	2881.00	89.83

(e)

IM Comm	LS Rotor S	HS rotor s	Torque (lb	Torque (N	Shaft Pow	LL V (V, rm	I (A, rms)	Freq(Hz)	Temp (C d	Meter(W)	Effi(%)
43.04	2	22.67	16200.00	1830.60	383.40	20.00	4.70	7.56	28.00	325.00	84.77
64.56	3	34.00	23150.00	2615.95	821.83	29.00	6.90	11.33	28.00	700.00	85.18
86.08	4	45.33	29120.00	3290.56	1378.35	38.00	8.98	15.11	29.00	1182.00	85.75
98.00208	4.554	51.61	32000.00	3616.00	1724.45	43.00	10.04	17.20	32.00	1480.00	85.82

(f)

IM Comm	LS Rotor S	HS rotor s	Torque (lb	Torque (N	Shaft Pow	LL V (V, rm	I (A, rms)	Freq(Hz)	Temp (C d	Meter(W)	Effi(%)
21.52	1	11.33	11850.00	1339.05	140.23	9.50	3.40	3.78	29.00	110.00	78.45
43.04	2	22.67	21750.00	2457.75	514.75	19.00	6.50	7.56	30.00	415.00	80.62
64.56	3	34.00	30120.00	3403.56	1069.26	27.00	9.40	11.33	31.00	877.00	82.02
70.00456	3.253	36.87	31930.00	3608.09	1229.11	29.00	10.08	12.29	32.00	1007.00	81.93

(g)

IM Comm	LS Rotor S	HS rotor s	Torque (lb	Torque (N	Shaft Pow	LL V (V, rm	I (A, rms)	Freq(Hz)	Temp (C d	Meter(W)	Effi(%)
21.52	1	11.33	14400.00	1627.20	170.40	9.00	4.20	3.78	24.00	132.00	77.46
43.04	2	22.67	26200.00	2960.60	620.07	17.50	8.00	7.56	24.00	485.00	78.22
56.0596	2.605	29.52	31900.00	3604.70	983.35	22.00	10.10	9.84	27.00	780.00	79.32

(h)

Table 3.2.4: Test data for different loads
(a~h refers to load resistance 14.1, 11.8, 9.4, 7.1,4.7,2.4,1.6,1.2)

With lower load resistance, the maximum LS rotor input test speed was reduced due to the torque limit consideration to avoid pole slipping. In the tests performed, the constant speed phase current is limited at about 10 amps to avoid rotor slipping.

The torque and power characteristics under different loads are provided in Figure 3.2.3.

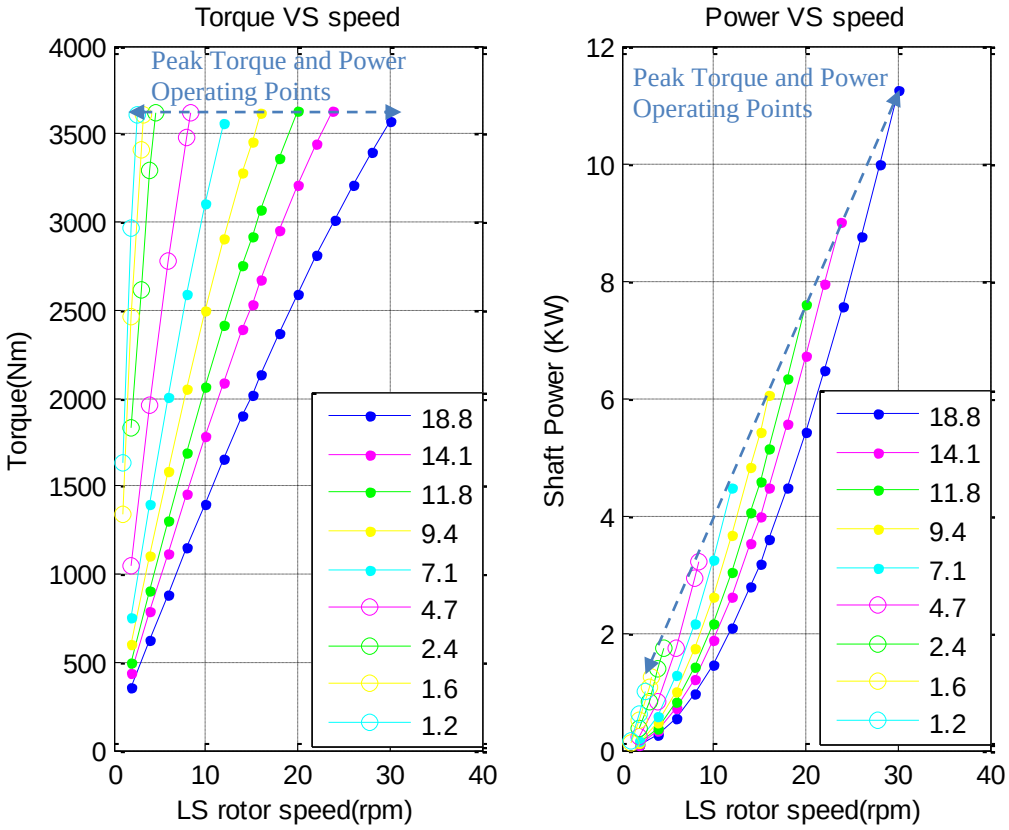

Figure 3.2.3: Torque (LS) & shaft power with different loads

With lower load resistance, the generator current will be higher for the same speed. Due to the slip torque limit, the highest load torque applied with different loads is set at around 3600 Nm, as indicated in Figure 3.2.3. These current and torque limits correspondingly limit the output power, with the lowest load resistance achieving up to about 1 kW power at 2.6 rpm before reaching the torque and current limits.

With a power electronics drive emulating a continually variable resistance load, one possible control strategy is to aim for constant torque operation as the input speed changes. The generator current and load torque acting against the WEC flap can be can be adjusted, for example, to operate in a near straight line through the top points near 3600 Nm in the Figure 3.2.3 Torque vs Speed plot. This increases the effective load resistance as the generator speed increases, also corresponding to the maximum power output operating points, along the top points of each colored curve in the Figure 3.2.2 Power vs Speed plot.

The generator voltage / current characteristics are provided in Figure 3.2.4.

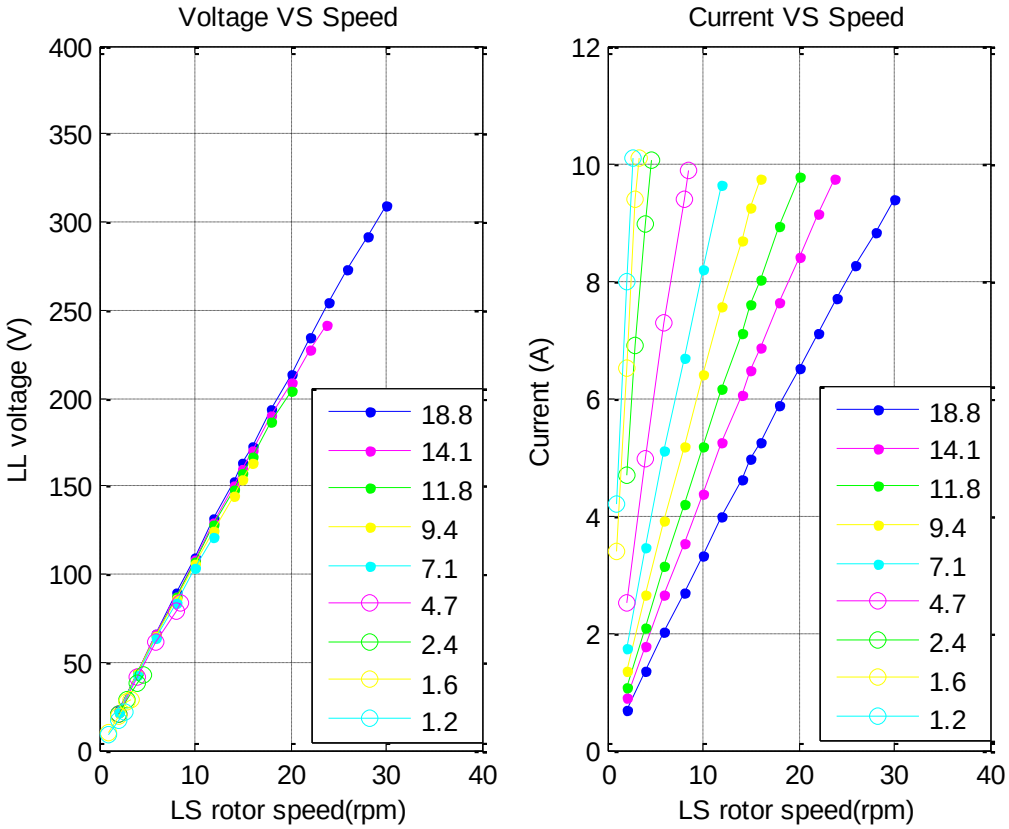

Figure 3.2.4: Generator voltage & current at different loads

As indicated in the voltage characteristic plot in Figure 3.2.4, the generator terminal voltage is linear with the rotor speed and not sensitive to load resistance. When current and the speed are higher, the combined effect of leakage inductance voltage drop as well as winding armature reaction begins to exhibit the slightly sagging voltage (below a straight line) in the higher speed end of each test data line.

To stay below the 3600 Nm imposed maximum torque to avoid pole slipping, the current of each load configuration gradually increases to the peak current rating (10A) as input speed is increased, as illustrated in the current plot for different load in Figure 3.2.4.

It was found that there is a resonance near 20 and 28 rpm. The source of the resonance appears to be the modulator, however, the root cause has not been confirmed. Operation near these resonant speeds was avoided as much as possible because of the noise and potential risk to the generator

It should also be emphasized that to avoid pole slipping, it is not enough to just limit the constantly applied speed and torque, but the rate of change in speed must also be limited. The ramp rate for the prototype testing was limited to 3 rpm/sec. As the load increases, there is less margin available to ramp the speed up or down.

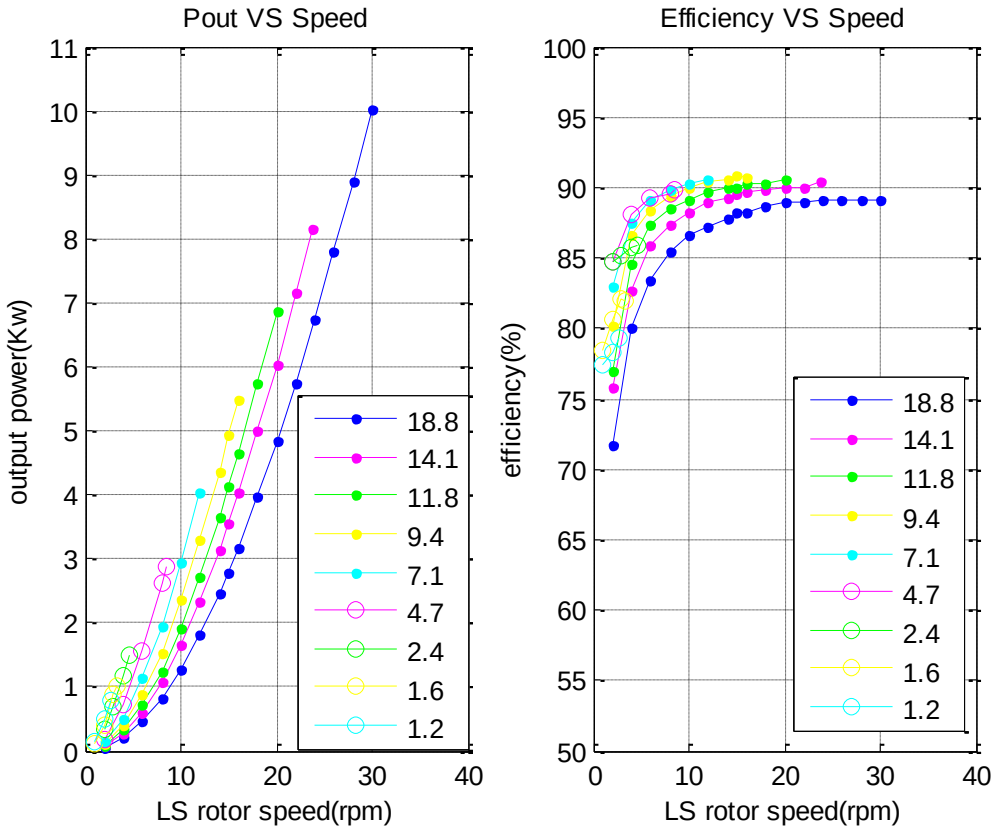

Figure 3.2.5: Generator output power & efficiency at different load resistance

The output electrical power and efficiency are related to the generator speed as shown in Figure 3.2.5. With the selected phase resistance of 18.8 ohm, the generator can provide 10 kW at 30 rpm with 9.4 A phase current, which is the rated design point, consistent with the design calculations and performance predictions. With reduced load resistance, the generator speed as well as power are bounded by the generator torque limit. This validation of the Phase II generator performance strengthens our confidence that the full scale generator design will similarly meet the expected performance.

As indicated in the efficiency curves, the peak efficiency is not observed at the peak load region. With lower speed and higher torque, the generator sees less losses compared with same torque at higher speed, due to the rise of the significant mechanical losses with increasing speed.

4 Oscillation Test

The oscillation test mode simulates the actual ocean wave operation. The drive machine is first operated to follow a regular sine speed profile at different peak speeds and cycle time periods. Alternatively, any defined waveform can also be programed for the drive motor to follow within the control limit, as done in the second step to emulate the example ocean wave speed waveforms provided by project partner Resolute Marine Energy.

The high inertia of this type of generator has an impact on the observable waveforms for oscillating tests, and should be kept in mind when sizing the prime mover motor and drive.

4.1 Range of Speed and Load

The oscillation tests were conducted with different fixed load resistances and different generator speeds. The rotor peak sine speed and total cycle period can be adjusted for different average oscillation speeds. For comparison purposes, average oscillating rotor speed can be compared to the fixed speeds used in the constant speed tests. In Figure 4.1.1, the typical generator output voltage under oscillation test is illustrated for an average oscillation speed of 3 rpm (10 sec period, 4.7 rpm peak).

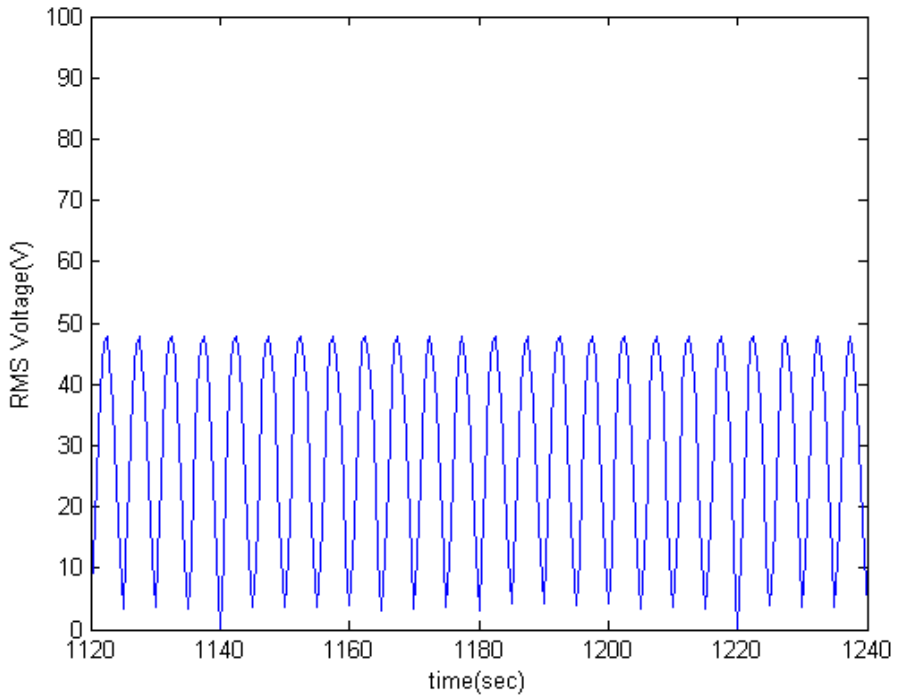

Figure 4.1.1: Generator output voltage at oscillation test (cycle time = 10 sec)

It should be noted that the profile in Figure 4.1.1 is the averaged voltage for all the loaded phases, which is proportional to generator speed. Each pulse in Figure

4.1.1 represents a generator rotation from start to stop in one direction, which also contains multiple voltages pulses for each phase under the same RMS voltage pulse envelop. Similarly, the output current and power of this generator is provided in Figure 4.1.2 and Figure 4.1.3 respectively.

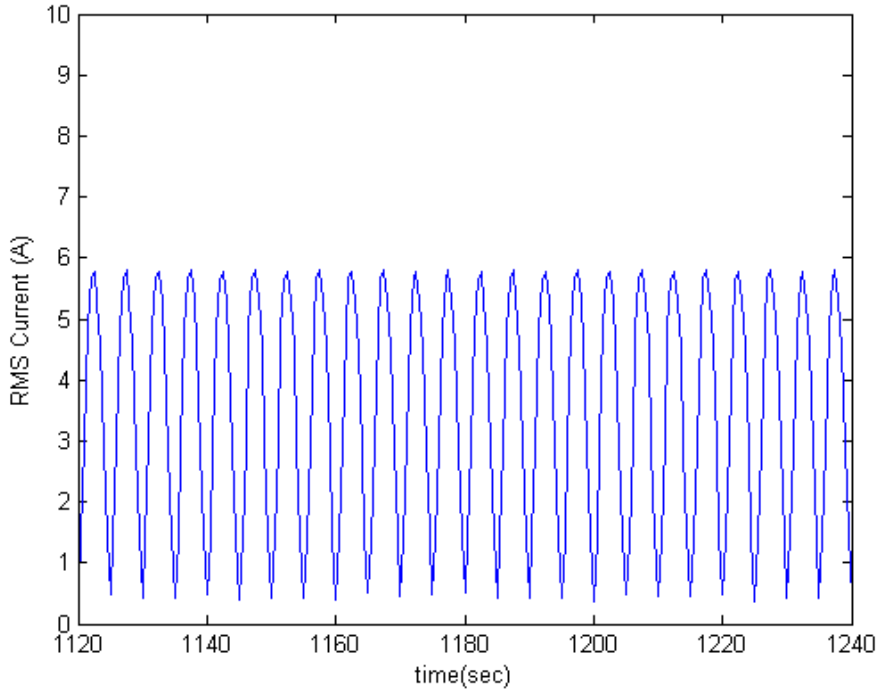

Figure 4.1.2: Generator output current at oscillation test (cycle time = 10 sec)

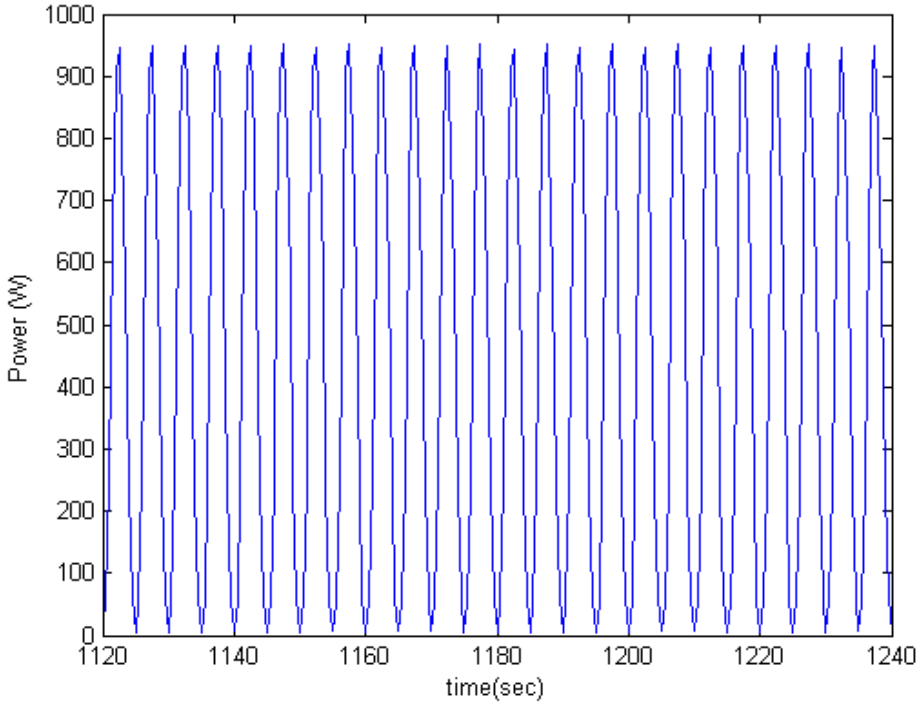

Figure 4.1.3: Generator output power at oscillation test
(cycle time = 10 sec)

In order to compare the performance of oscillation mode power generation with constant speed power generation, the output power under these two modes are compared in Figure 4.1.4.

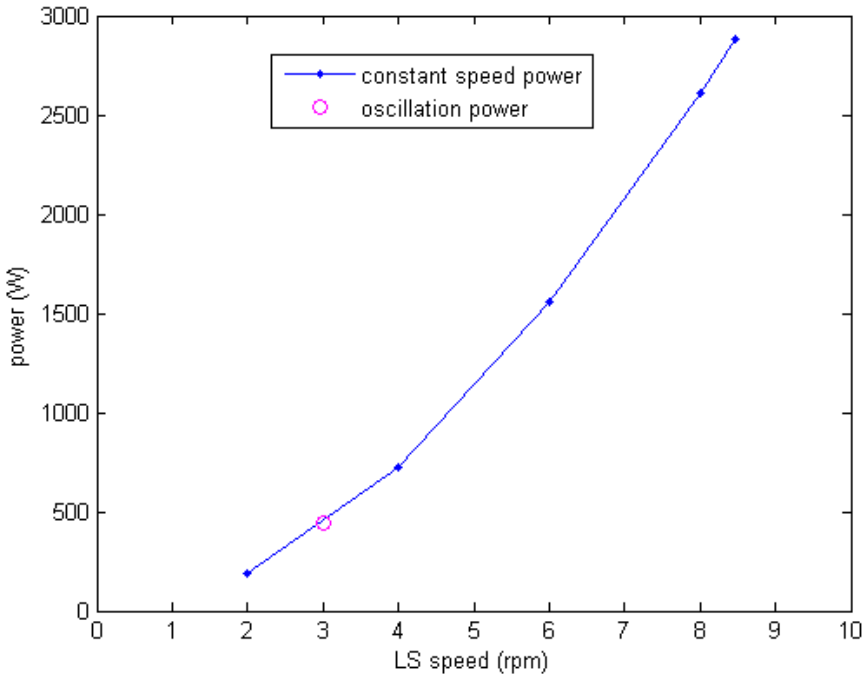

Figure 4.1.4: Generator output power at oscillation test Compared with constant speed test results. (oscillation cycle time = 10 sec)

With the input information on the ocean wave characteristics, it is identified that 12 second oscillation cycle time is the most typical time period for the target wave energy conversion. Thus, oscillation tests under different load conditions have been performed with the test data summarized in Figure 4.1.5.

Due to the high inertia design of the LS rotor, the torque required for the reversal type operation is significant. The torque limit set for the constant speed operation is still applied in the oscillation type testing to avoid pole slipping. Thus, the oscillation tests can be only be performed at a lower speed range before the torque limit is reached.

Important to note, the averaged output power produced in the oscillation mode is quite comparable with the constant speed operation in the target low speed range. This provides a useful design reference for the full scale generator development or scaling to other powers and sizes. This also greatly simplifies the machine design, since it is enough to initially design electromagnetically for an average rated speed and power, provided that the peak speed and torque values are included in the mechanical design.

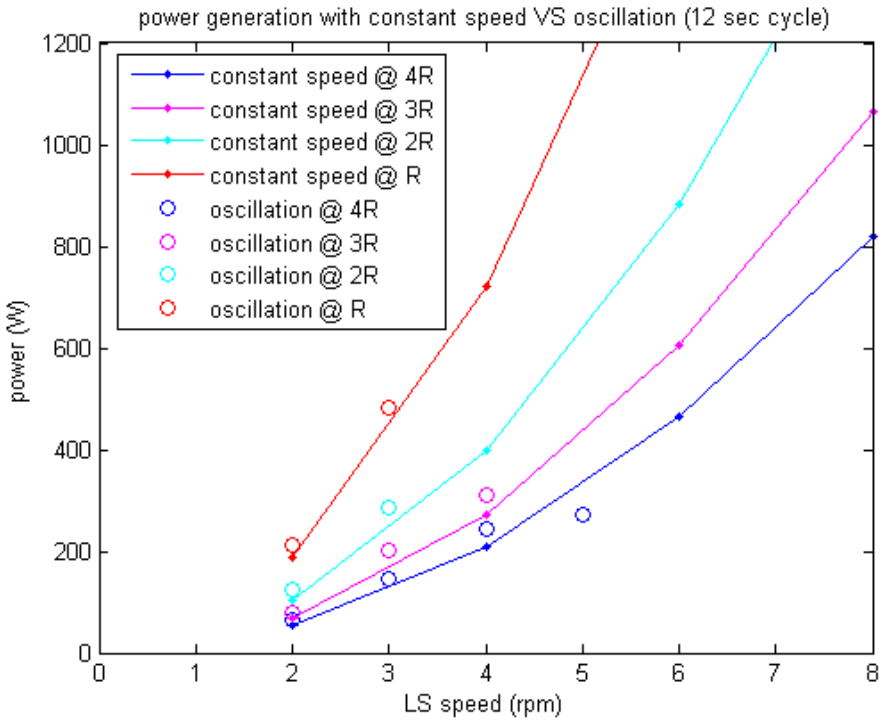

Figure 4.1.5: Generator output power at oscillation test Compared with constant speed test results. (R = 4.7 ohm)

The observed data is well matched in the low speed range up to 4 rpm as

indicated in Figure 4.1.5. A deviation point for high load resistance is observed for 5 rpm, which is primarily attributed to the drive control characteristics under high inertia load and the torque limiting setting. In other words, the speed reference for the LS rotor at 5 rpm is not achieved due to the torque limit setting for the drive motor side and thus the average speed and power generated are less than expected.

4.2 Variable Cycle Time

With randomly distributed ocean wave energy speed profile characteristics, the testing with different cycle time of the wave movement is performed to investigate the impact on the power generation capability.

In Figure 4.2.1, the oscillation mode for different cycle times at 2 and 3 rpm speed are illustrated.

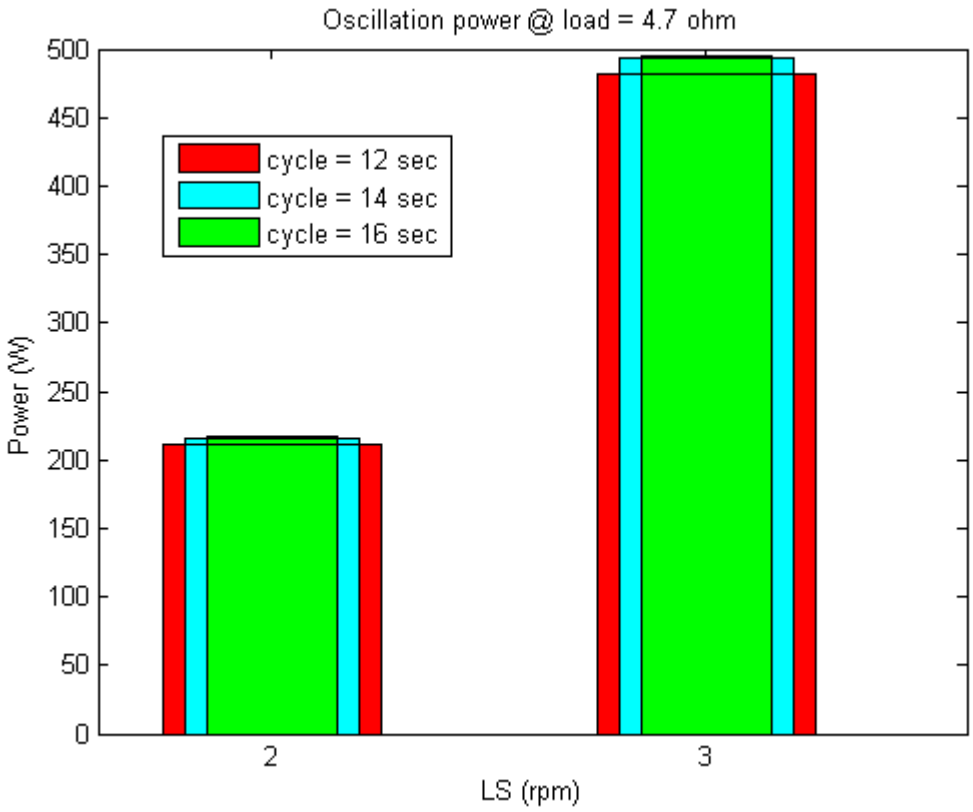

Figure 4.2.1: Power generation with load 4.7 ohm at 2 rpm & 3 rpm oscillation modes.

The cycle time impact is tested under different speed at different loads as illustrated in Figure 4.2.2 and Figure 4.2.3. With only very small variations observed in the averaged power production from the generator, the power generation capability is not explicitly dependent on the cycle time variations in the interested wave period length range. Again, this data is useful for estimating the full scale generator output for a given distribution of ocean wave periods and peak heights at a given location.

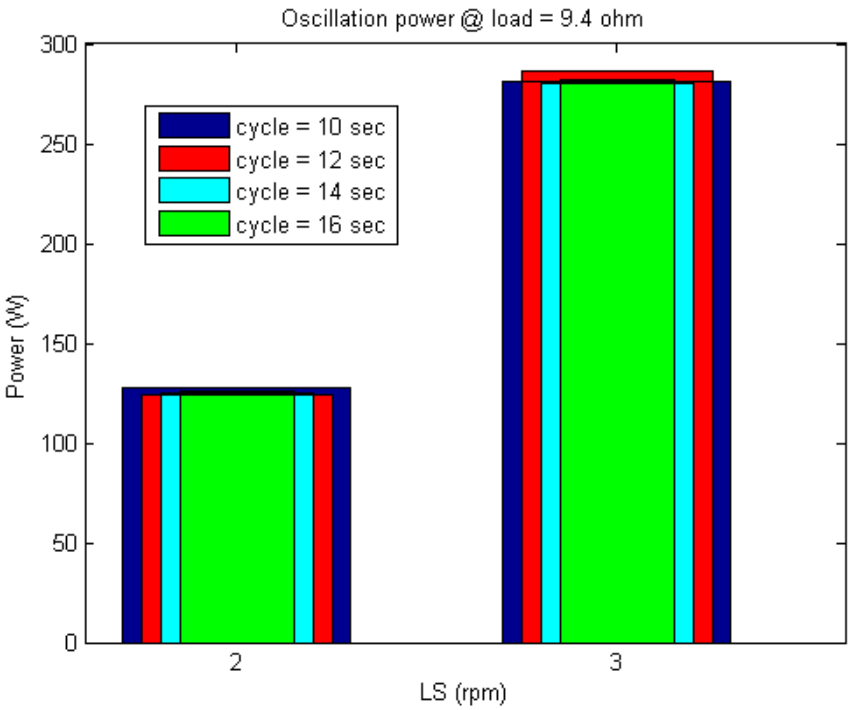

Figure 4.2.2: Power generation with load 9.4 ohm at 2 rpm & 3 rpm oscillation modes.

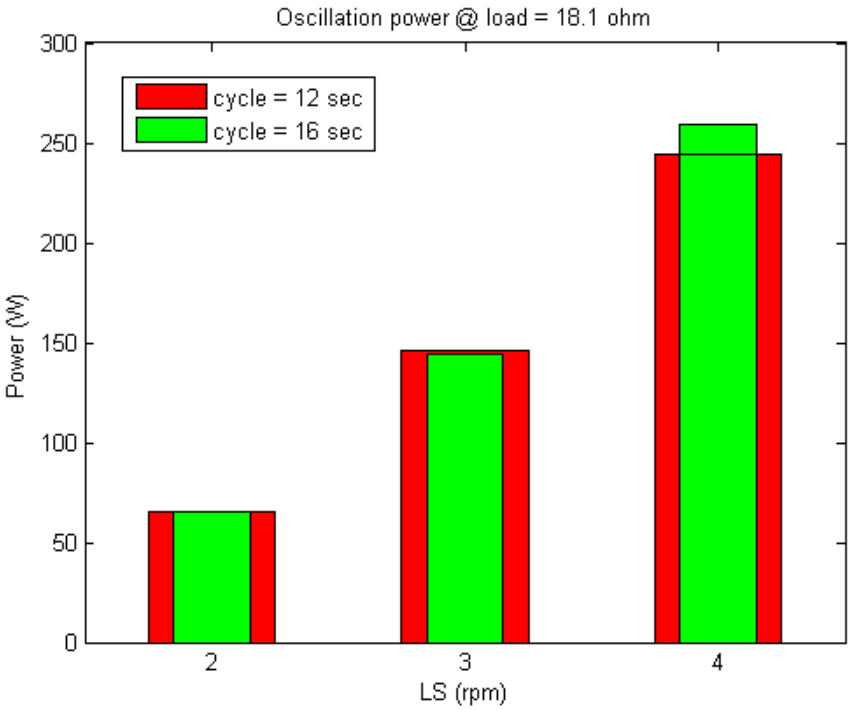

Figure 4.2.3: Power generation with load 18.1 ohm at 2 rpm, 3 rpm & 4rpm oscillation modes.

5 Power Converter Torque Limiting

The generator has the inherent torque limiting feature of slipping poles when the maximum torque is exceeded. This is a good safety and survival feature, but is not intended for normal operation. The ability to control and limit the generator load torque, independent of the applied torque from the WEC and ocean wave, can be a useful feature for increasing the generator speed and reducing the mechanical requirements on the generator design.

To this end, the generator was also tested with an actively controlled converter as illustrated in Figure 5.1.1 supplied from North Carolina State University.

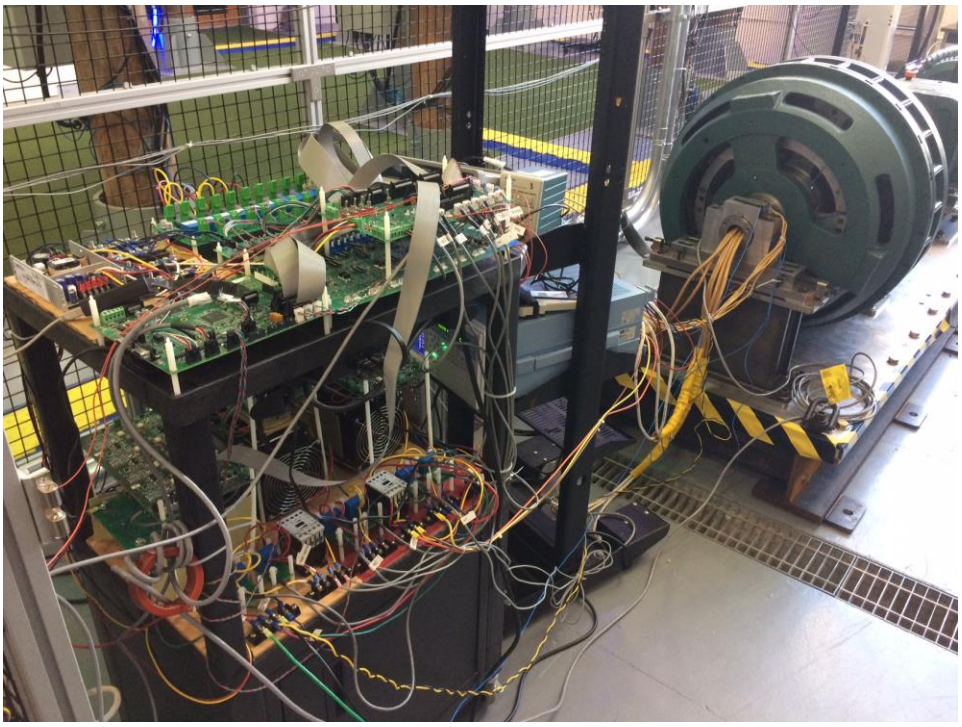

Figure 5.1.1: Generator with converter interface

The converter rectifies and boosts the variable frequency, variable amplitude generator output power to a fixed DC voltage, with the option of additional power smoothing using a combination of super capacitors, batteries, or alternative energy storage system. The DC power is then converted to the constant frequency constant output voltage to be directly fed into the grid system. This project utilized a power converter designed and built by North Carolina State University from a previous project. The detailed investigation of the power converter itself is outside the scope of this project, but the focus is on the interaction of the generator and power converter, specifically the impact of the torque limiting function on the generator performance in this test section.

5.1 Constant Speed

The tests are performed with constant speed and current regulated in full range up to 120% of the rated current (~11.25 A). Maximum torque per amp control is applied in the testing as indicated in Figure 5.1.1 and Figure 5.1.2.

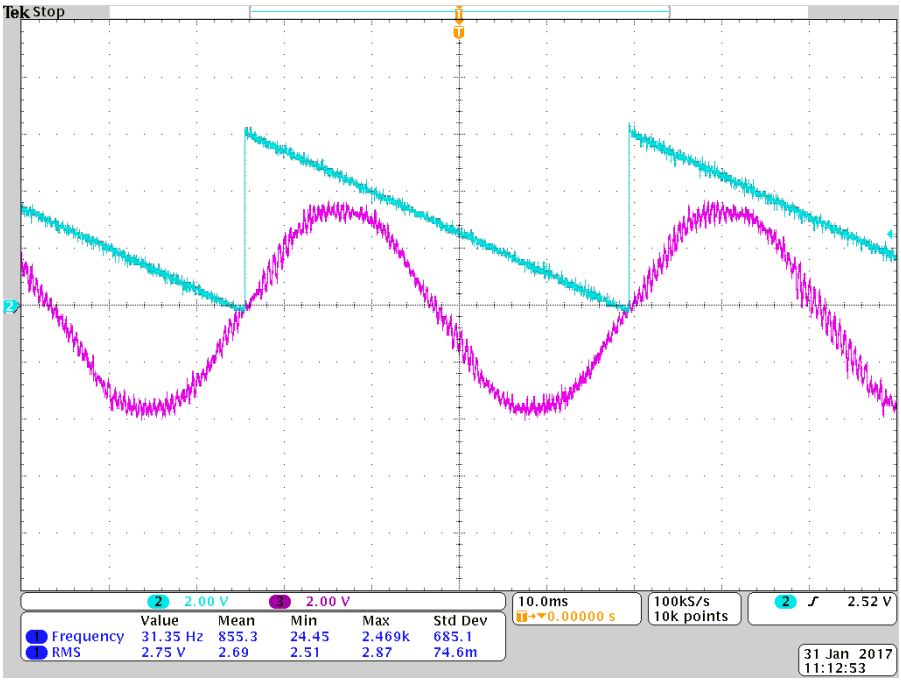

Figure 5.1.1: Current (pink) and generator rotor position (blue)

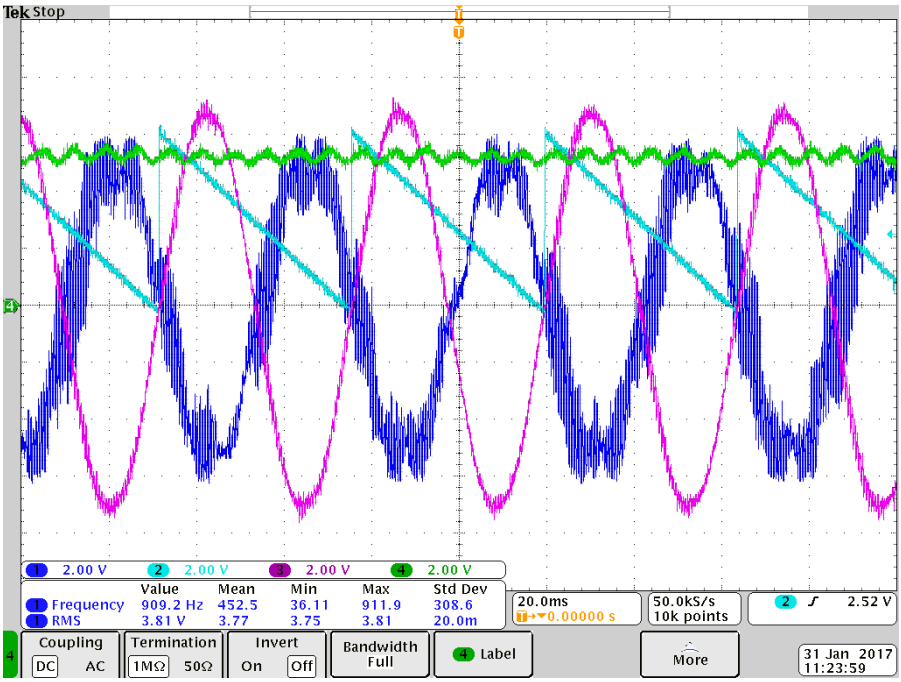

Figure 5.1.2: Voltage (dark blue), DC bus voltage (green), Current (pink) and generator rotor position (blue)

For the prototype, the torque characteristics in the actively controlled converter load tests are linearly dependent on the generator current as tested before with the passive, resistive loads. In Figure 5.1.3, the torque response under different speed and load with active regulation is provided.

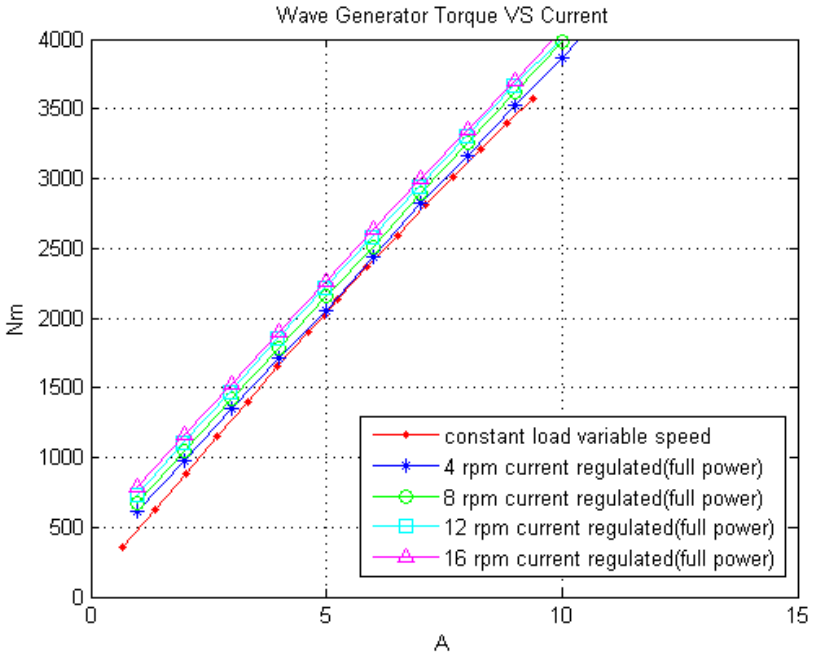

Figure 5.1.3: Torque versus current under active and passive loads

The system efficiency with the converter engaged is listed in Table 5.1.1.

IM Cmd (rpm)	LS Rotor (rpm)	HS rotor (rpm)	Torque (lbs-in)	Torque (Nm)	Shaft Power (W)	VLL (V, rms)	I (A, rms)	Freq (Hz)	Temp (C deg)	Meter (W)	Effi (%)
344.32	**16.00**	**181.3**	**3525**	**398.3**	**667.4**	**179.0**	**1.0**	**60.44**	**27.6**	**317**	**47.5**
344.32	**16.00**	**181.3**	**5150**	**581.9**	**975.1**	**178.6**	**2.0**	**60.44**	**28.5**	**620**	**63.6**
344.32	**16.00**	**181.3**	**6800**	**768.4**	**1287.5**	**178.4**	**3.0**	**60.44**	**29.5**	**920**	**71.5**
344.32	**16.00**	**181.3**	**8400**	**949.2**	**1590.4**	**178.2**	**4.0**	**60.44**	**29.0**	**1215**	**76.4**
344.32	**16.00**	**181.3**	**10050**	**1135.6**	**1902.8**	**178.2**	**5.0**	**60.44**	**30.0**	**1510**	**79.4**
344.32	**16.00**	**181.3**	**11700**	**1322.1**	**2215.2**	**178.2**	**6.0**	**60.44**	**31.0**	**1800**	**81.3**
344.32	**16.00**	**181.3**	**13300**	**1502.9**	**2518.1**	**178.2**	**7.0**	**60.44**	**31.0**	**2085**	**82.8**
344.32	**16.00**	**181.3**	**14900**	**1683.7**	**2821.1**	**178.6**	**8.0**	**60.44**	**31.0**	**2370**	**84.0**
344.32	**16.00**	**181.3**	**16500**	**1864.5**	**3124.0**	**178.7**	**9.0**	**60.44**	**32.0**	**2650**	**84.8**
344.32	**16.00**	**181.3**	**18050**	**2039.6**	**3417.5**	**179.2**	**10.0**	**60.44**	**32.0**	**2930**	**85.7**
344.32	**16.00**	**181.33**	**19550**	**2209.1**	**3701.5**	**179.5**	**11.0**	**60.44**	**32.0**	**3200**	**86.5**
344.32	**16.00**	**181.33**	**21100**	**2384.3**	**3994.9**	**180.0**	**12.0**	**60.44**	**32.0**	**3450**	**86.4**

Table 5.1.1: System efficiency test data

The plot comparing efficiency versus power under active current regulation and passive resistive loads is provided in Figure 5.1.4.

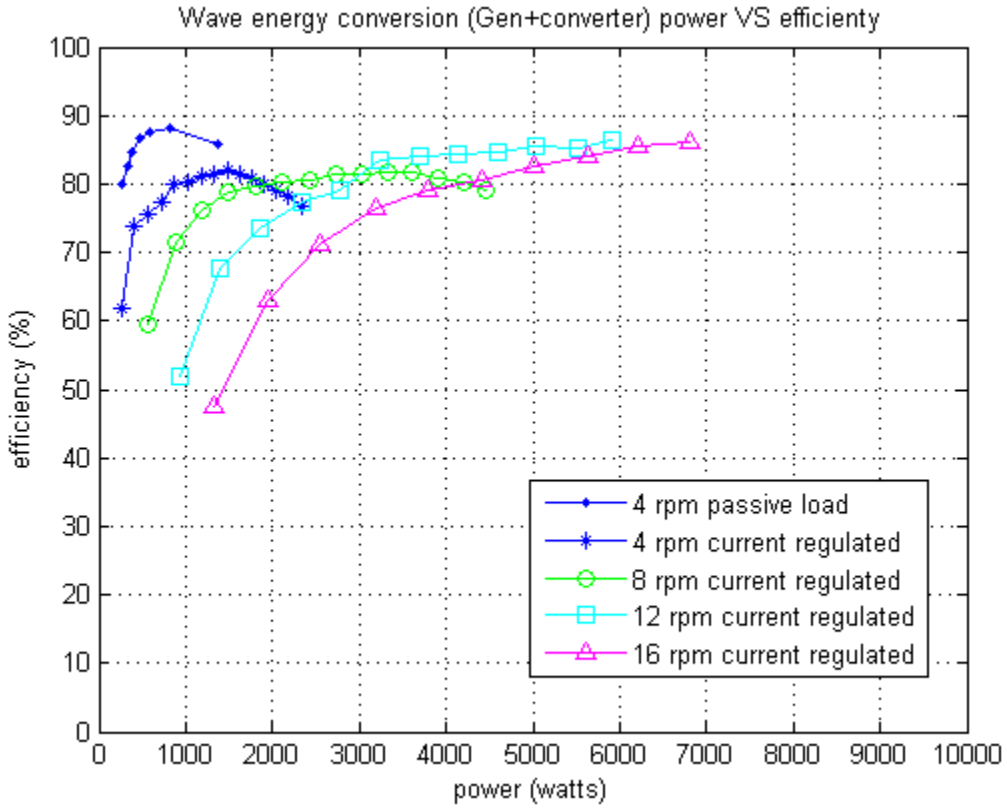

Figure 5.1.4: Efficiency by current regulation under different power and speed

The efficiency must decrease with the addition of the converter into the system, and this converter has not been optimized. However, the reduction in efficiency would be more than compensated in a real system from the increase in power output from the ability to control the instantaneous generator load and torque for maximum power output. As indicated in Figure 5.1.4, the system efficiency can achieve as high as ~88% with the power extrapolated to 10 kW. The tests were performed with three out of the six generator phases because of the converter limitation. It should also be noted that the system efficiency is higher at lower speed range due to the less dragging loss from the mechanical bearing and less magnetic losses in the lamination material and magnets.

5.2 Oscillation

With current regulation engaged from the converter side, the generator torque can be effectively regulated to maintain a safe operating range as illustrated in Figure 5.2.1.

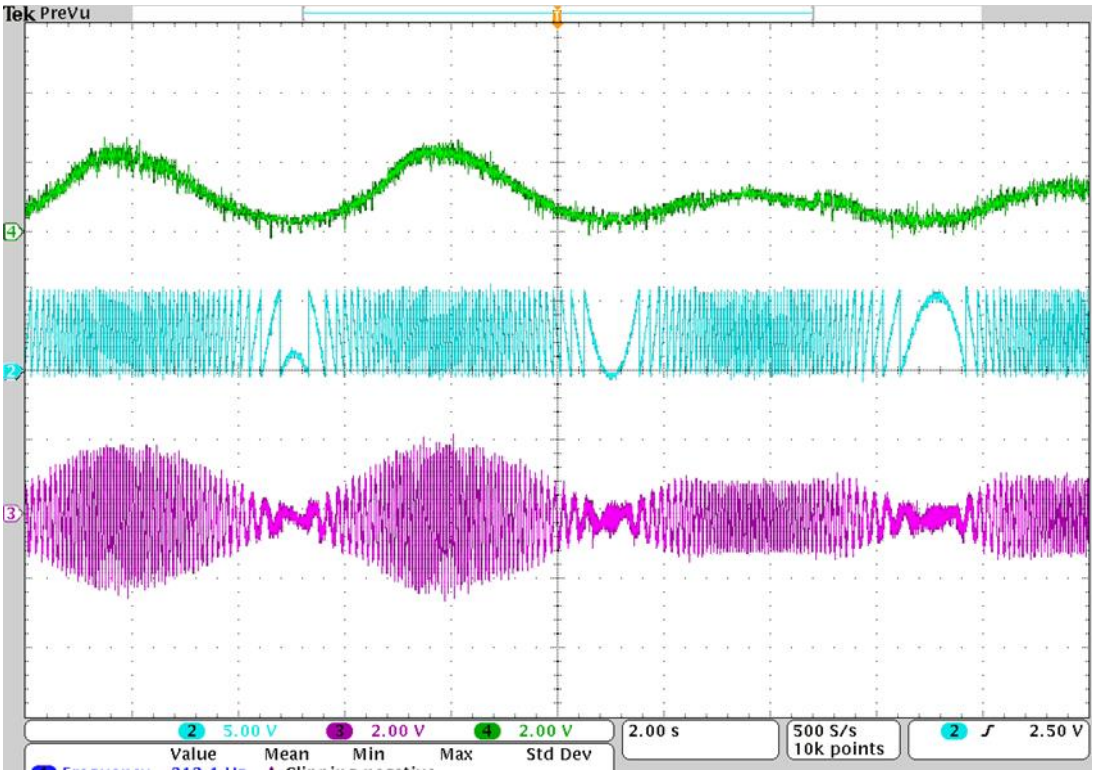

Figure 5.2.1: Current regulation for torque limiting in oscillation mode (green**:** torque, blue: rotor position, pink: generator current)

With current limiting, peak torque can be controlled as demonstrated in Table 5.2.1.

sine Peak(rpm)	condiction	LS Rotor Average Speed	Torque pe	Torque (N	Shaft Pow	V (V, rms)	I (A, rms)
135.21	Without torque Limit	4	15000	1695.00	Variable	47(peak)	7(peak)
135.21	With torque limit	4	13000	1469.00	Variable	52(peak)	3.5(peak)

Table 5.2.1: Current regulation for torque limiting demonstration

The torque in Table 5.2.1 is the torque observed from the low speed rotor side as input shaft torque, which is a combination of the generator torque and the inertial torque to change the speed of the low speed rotor under oscillation mode. In the test set-up we have only controlled the input speed for oscillating tests. For the same input speed we've demonstrated the ability to limit the generator current and torque. In real ocean wave applications, this torque limiting strategy avoids the extreme peaks from the WEC flap and ocean waves, benefitting the design and operation of the generator as well as slightly increasing in average WEC and generator speed.

Appendix A
Oscillation mode reference speed

time [s]	rotation [deg]	ang vel [rad/s]	PTO torque [MNm]	flap pwr [kW]
0.1	-2.275	-0.079	-0.197	15.673
0.2	-2.735	-0.081	-0.200	16.188
0.3	-3.198	-0.080	-0.199	16.028
0.4	-3.655	-0.078	-0.194	15.249
0.5	-4.095	-0.075	-0.186	13.929
0.6	-4.512	-0.070	-0.174	12.196
0.7	-4.898	-0.064	-0.159	10.161
0.8	-5.245	-0.057	-0.140	7.947
0.9	-5.547	-0.048	-0.120	5.793
1.0	-5.799	-0.039	-0.097	3.805
1.1	-5.995	-0.029	-0.071	2.049
1.2	-6.130	-0.018	-0.044	0.791
1.3	-6.201	-0.007	-0.016	0.108
1.4	-6.206	0.005	0.013	0.071
1.5	-6.140	0.018	0.045	0.804
1.6	-6.003	0.030	0.075	2.287
1.7	-5.794	0.043	0.106	4.555
1.8	-5.513	0.055	0.137	7.554
1.9	-5.162	0.067	0.167	11.268
2.0	-4.744	0.079	0.195	15.395
2.1	-4.261	0.089	0.222	19.847

Table A.1: Generator speed sample reference

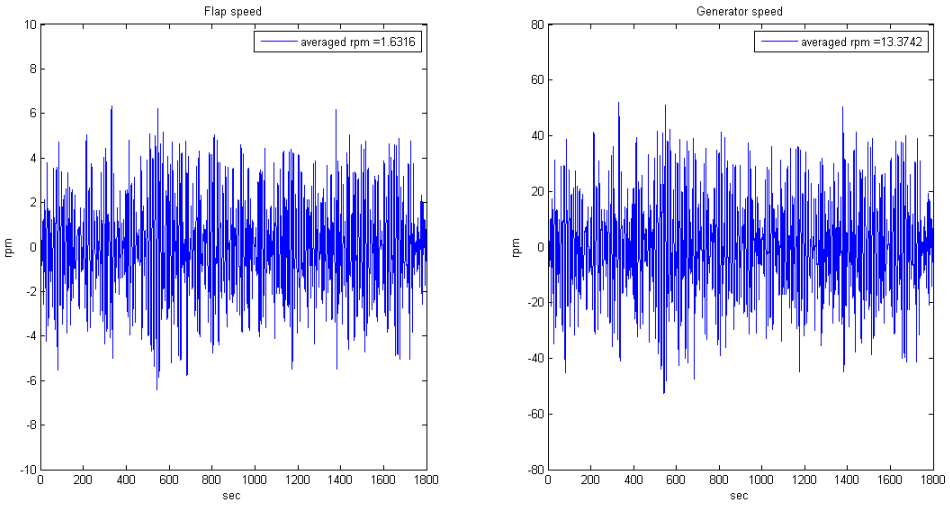

Figure A.1: Generator reference speed plot

DWIGHT LOOK
COLLEGE OF ENGINEERING

Department of Electrical and Computer Engineering

Advanced Direct Drive Generator for Improved Availability of OWSC Power Generation Systems

Full Scale Design Report

By

Dr. Hamid Toliyat
Matthew Gardner
Matthew Johnson
Electric Machines & Power Electronics (EMPE) Lab

September 16, 2016

020 Wisenbaker Engineering Building
3128 TAMU
College Station, Texas 77843-3128

Tel. 979.862.3034 Fax. 979.845.6259
http://www.ece.tamu.edu/~empelab/

MAGNETIC GEAR DESIGN METHODOLOGY

The magnetic gear sub-system of the full scale magnetically geared generator was designed using the trends observed and modeling infrastructure created during the development of the intermediate scale Phase II prototype. Additionally, practical considerations based on "lessons learned" during the Phase II prototype construction were also incorporated into the full scale machine design process to produce a high-performance magnetically geared generator which is also realistic and mechanically viable. Design sizing, optimization, and performance prediction information is included to provide a comprehensive overview of how the full scale design was selected and the resulting impact on its sizing, cost, and operating behavior.

System level considerations dictate that 1.6 m is the maximum diameter the magnetically geared generator can use without negatively impacting the performance of the oscillating wave surge converter and further complicating the system integration. Based on this information, the known required operating torque of 225 kN·m, and the design trends observed during the development of the intermediate scale prototype, all full scale magnetic gear design simulations used the maximum outer radius of 0.8 m. Furthermore, based on the experience gained from the construction of the intermediate prototype, 4.5 mm was selected as the minimum practical air gap size at this diameter and that value was also employed in all full scale design simulations.

The modulator assembly and the attached mechanical support infrastructure proved to be some of the most difficult aspects of the magnetically geared generator prototype construction. These challenges stemmed from the use of relatively radially thin modulators and a relatively thin modulator bridge which produced a narrow annulus structure at a large radius. To address and mitigate these issues in the full scale machine, all 13,320 design possibilities specified by the various combinations of parameter values in Table I were analyzed using static 2D finite element analysis (FEA) models. Multiple different modulator and modulator bridge thickness options were included in this study to evaluate the size and cost penalties associated with using thicker and easier to build modulator and modulator bridge design combinations.

Because there are strong interdependencies between the effects of different dimensions, the values of certain variables were coupled through derived parameters, which are included in Table I. Because the low speed rotor (LSR) has more magnetic poles than the high speed rotor (HSR), there is significantly more flux leakage between adjacent poles on the LSR than on the HSR. Therefore, it is prudent to concentrate most of the magnet material on the HSR. Thus, the radial thickness of the LSR magnets, T_{LSPM}, is determined by the radial thickness of the HSR magnets, T_{HSPM}, and a derived parameter, k_{PM}, as shown in (1). Additionally, a second derived parameter, G_r, represents the approximate gear ratio and is used to relate the number of pole pairs on the HSR and LSR, P_{HS} and P_{LS}, respectively, according to (2). This relationship keeps the number of modulators even, which symmetrically eliminates the net radial forces on each rotor, and maintains a relatively high least common multiple (LCM) between P_{HS} and P_{LS}, which reduces the gear's torque ripple. Finally, the HSR and LSR back iron thicknesses, T_{HSBI} and T_{LSBI}, were sized based on the appropriate permanent magnet pole arcs and the derived scaler parameters, k_{HSBI} and k_{LSBI}, as indicated in (3) and (4), where R_{HSPM} denotes the inner radius of the HSR permanent magnets and R_{LSPM} denotes the outer radius of the LSR permanent magnets. The term k_{HSBI} represents the idealized ratio of the HSR permanent flux density to the HSR back iron permanent magnet flux density, based on an overly simplified, single pole pair model of the magnetic flux

paths in the HSR. Thus the thickness of the HSR back iron is sized based on the HSR permanent magnet pole arc and k_{HSBI}, where a larger value of k_{HSBI} indicates a thicker HSR back iron with lower magnetic loading. While the necessary sizing of the HSR back iron is dominated by the HSR permanent magnet pole arc, the necessary sizing of the LSR back iron is impacted by the pole arcs of both the HSR and LSR permanent magnets. Thus, as indicated in (4), the thickness of the LSR back iron is sized based on an analogous approach using k_{LSBI} and the average of the HSR and LSR permanent magnet pole arcs, where a larger value of k_{LSBI} indicates a thicker LSR back iron with lower magnetic loading.

Table I: Parametric Design Study Ranges

Name	Description	Values	Units
G_r	Nearest integer gear ratio	4:2:12	
P_{HS}	HSR pole pairs		
	For $G_r = 4$	12:2:32	
	For $G_r = 6$	8:2:22	
	For $G_r = 8$	4:2:16	
	For $G_r = 10$	4:2:14	
	For $G_r = 12$	4:2:12	
R_{out}	Gear's active outer radius	800	mm
k_{HSBI}	HSR back iron thickness coefficient	0.3	
T_{HSPM}	HSR magnet thickness	12:4:28	mm
T_{AG}	Air gap thickness	4.5	mm
T_{Mods}	Modulator thickness	25:25:100	mm
T_{Bridge}	Modulator bridge thickness	0:5:10	mm
k_{PM}	LSR magnet thickness ratio	0.35, 0.5, 0.75	
k_{LSBI}	LSR back iron thickness coefficient	0.6	

$$T_{LSPM} = T_{HSPM} \cdot k_{PM} \tag{1}$$

$$P_{LS} = \begin{cases} G_r \cdot P_{HS} + 1, & \text{for } (G_r+1)\cdot P_{HS} \text{ odd} \\ G_r \cdot P_{HS} + 2, & \text{for } (G_r+1)\cdot P_{HS} \text{ even} \end{cases} \tag{2}$$

$$T_{HSBI} = k_{HSBI} \cdot \left(\frac{\pi \cdot R_{HSPM}}{P_{HS}}\right) \tag{3}$$

$$T_{LSBI} = \frac{k_{LSBI} \cdot \pi \cdot R_{LSPM}}{\left(\frac{P_{HS}+P_{LS}}{2}\right)} \tag{4}$$

Aside from improving mechanical feasibility, the primary objectives of the parametric design study were to maximize the volumetric torque density (VTD), with a goal of exceeding 84 $kN \cdot m/m^3$, maximize the gravimetric torque density (GTD), with a goal of exceeding 14 $N \cdot m/kg$,

and to minimize the active material cost (ACM), with a target of less than $200,000. A relatively wide range of gear ratios was considered in order to perform a true system level optimization. Increasing the gear ratio decreases the size of the integrated generator, but beyond a certain initial range, increasing the gear ratio also results in a larger and more expensive magnetic gear. The overall system level optimum design is achieved in part by selecting the gear ratio that strikes the appropriate balance between these two considerations.

Each design specified in Table I was evaluated using static 2D FEA and the stack lengths were selected to achieve an LSR stall torque of 320 kN·m, which was also used to calculate the volumetric and gravimetric torque densities. This conservative sizing approach was employed to create a safety factor so that the nominal operating torque of 225 kN·m only corresponds to 71% of the stall torque and a torque angle of 45°. This operating torque requirement and the previously specified diameter restriction result in designs with stack lengths that are much larger than the outer radius and thus, 3D effects do not significantly impact their torque ratings. As a result, a 3D FEA model was only used to characterize the axial leakage flux associated with the final selected design. For each magnetic gear design, the size of the required integrated machine was determined from the machine's design curves based on the gear ratio and the magnetic gear's inner radius (the integrated machine's outer radius). This information was then used to determine the overall volume and mass of the magnetically geared generator and its constituent materials for each parametric design case. Finally, these constituent material masses were used with the fixed material cost rates specified in Table II to calculate the active material cost for each design.

Table II: Constituent Active Material Characteristics

Material	Density	Cost Rate
N42 NdFeB	7400 kg/m^3	$50/kg
M19 Steel (29 Gauge)	7870 kg/m^3	$2/kg
Copper	8933 kg/m^3	$10/kg

MAGNETIC GEAR DESIGN TRENDS AND SELECTION

Figure 1 shows the overall system active material cost, volumetric torque density, and gravimetric torque density for a subset of the 13,320 evaluated magnetically geared generator designs. This data clearly indicates that there are several options capable of achieving all three of the primary performance goals and, as a result, an emphasis was placed on maximizing the volumetric torque density which also reduces the requisite amount of inactive material. The variation of the maximum system volumetric torque density with gear ratio is shown for different modulator bridge thicknesses in Figure 2(a) and for different modulator thicknesses in Figure 2(b). Increasing the modulator bridge thickness, T_{Bridge}, or the modulator thickness, T_{Mods}, increases the reluctance of the primary torque producing flux paths and decreases the reluctance of the leakage flux paths, which results in a significant reduction in the maximum attainable system torque density; however, increasing these thicknesses also improves the machine's mechanical integrity and simplifies its construction. In response to the challenges experienced with the modulators during the construction of the intermediate scale prototype, the relatively conservative design combination of 50 mm thick modulators (T_{Mods} = 50 mm) and a 10 mm thick bridge (T_{Bridge} = 10 mm) was selected for use in the full scale machine, since all of the performance objectives can still

be achieved with these parameter values. All subsequent simulation results are based on this modulator thickness and bridge thickness combination.

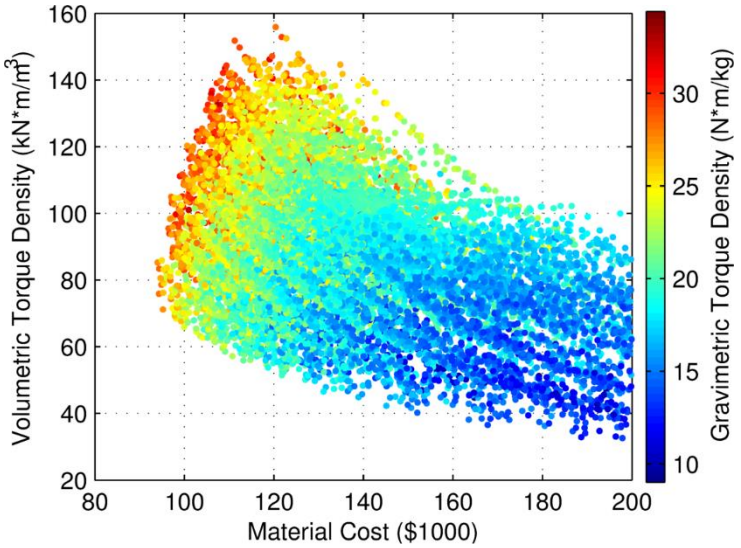

Figure 1: Overall System Metrics for a Subset of the Highest Performance Full Scale Magnetically Geared Generator Design Options

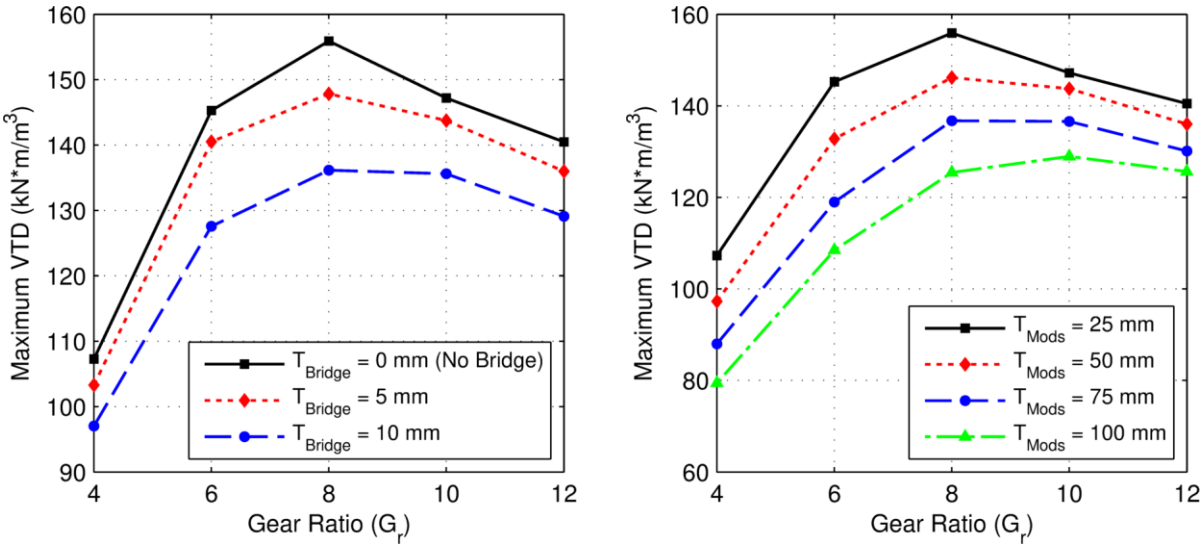

(a) (b)

Figure 2: Variation of Maximum Overall System Volumetric Torque Density with Gear Ratio for (a) Different Bridge and (b) Modulator Thicknesses

The data in Figure 2 indicates that a gear ratio of 8 results in the highest torque density for all considered bridge and modulator thicknesses; however, the advantage of a gear ratio of 8 over a gear ratio of 10 become less pronounced at larger modulator and bridge thicknesses. Figure 3(a) shows the variation of the maximum overall system volumetric torque density with the HSR pole pair count for the different gear ratios, using the selected modulator thickness of 50 mm and the selected bridge thickness of 10 mm. Figure 3(b) indicates the corresponding overall system active material cost for each of these same design points. Similarly, Figure 4(a) shows the variation of

the maximum overall system volumetric torque density with the HSR permanent magnet thickness for the different gear ratios at the same modulator and bridge thickness combination. Again, Figure 4(b) illustrates the corresponding overall system active material cost for each of these design points. One key distinction between the trends depicted in Figures 3 and 4 is that while there is an optimum HSR pole count with respect to torque density, which also results in the lowest corresponding active material cost, the optimal HSR magnet thickness with respect to torque density is simply the largest considered value and it results in the highest corresponding active material cost. Using thicker magnets does increase the torque density, but only with diminishing returns, as it significantly increases the leakage flux, which results in less effective magnet utilization and higher active material costs. The increase in active material cost with magnet thickness is less pronounced for this design, over the considered range, because of the extremely thick modulator bridge. Using a thicker modulator bridge means that more flux is required to saturate the bridge and increase the reluctance of that leakage path. Thus, while increasing the HSR magnet thickness increases the effective HSR air gap, which results in greater leakage flux, it also further saturates the modulator bridge which helps to increase the reluctance of that leakage flux path. However, once the bridge becomes fully saturated, this positive trend subsides and the active material cost increases much more rapidly with magnet thickness. Furthermore, increasing the magnet thickness can also elevate the axial leakage flux and eddy current losses in addition to complicating the construction process. As a result of these considerations, HSR magnet thicknesses of more than 28 mm were not considered for the full scale machine design.

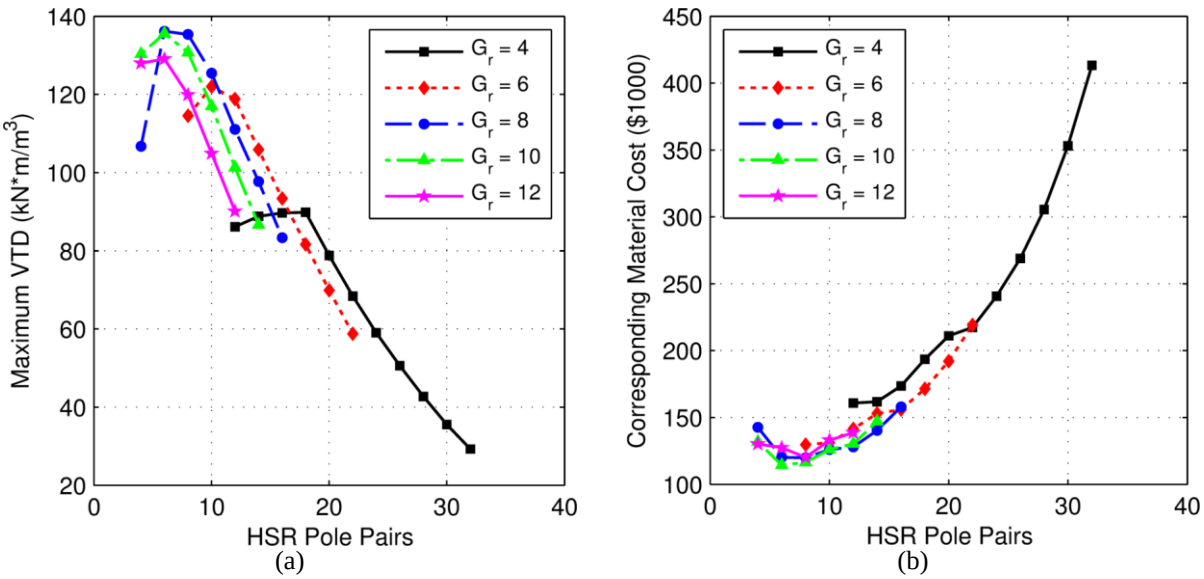

Figure 3: Variation of (a) Maximum Overall System Volumetric Torque Density and (b) Corresponding System Active Material Cost with HSR Pole Pair Count for Different Gear Ratios at a Modulator Thickness of 50 mm and a Bridge Thickness of 10 mm

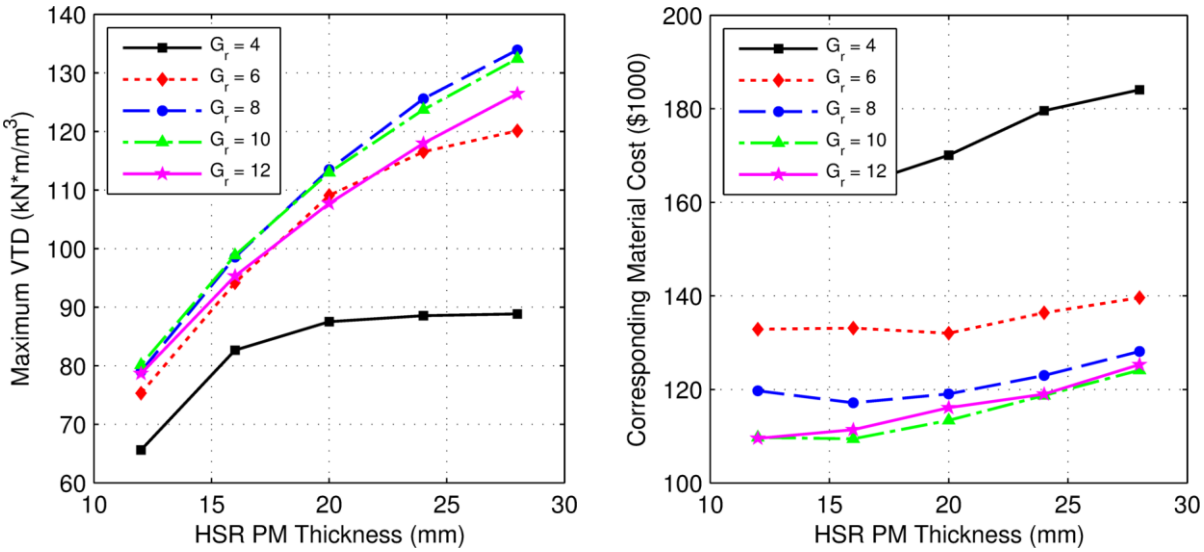

Figure 4: Variation of (a) Maximum Overall System Volumetric Torque Density and (b) Corresponding System Active Material Cost with HSR Permanent Magnet Thickness for Different Gear Ratios at a Modulator Thickness of 50 mm and a Bridge Thickness of 10 mm

Figure 5(a) illustrates the variation of the maximum overall system volumetric torque density with the LSR magnet thickness ratio for the different gear ratios, using the selected modulator thickness of 50 mm and the selected bridge thickness of 10 mm. Figure 5(b) indicates the corresponding system active material cost for each of these same designs. As previously noted, it is generally desirable to use thinner magnets on the LSR than on the HSR ($k_{PM} < 1$) because the higher pole count on the LSR results in elevated leakage flux on that rotor, a problem which becomes more pronounced with thicker LSR magnets and thus a larger effective air gap. For a fixed outer radius, using thinner LSR magnets also offers the benefit of a larger LSR air gap radius, which is analogous to using a larger torque arm. As shown in Figure 5(b), the active material cost tends to increase with the LSR magnet thickness at an even faster rate than it increases with the HSR magnet thickness because of the higher pole count, increased leakage flux, and the associated reduction in the outer air gap radius. Additionally, for all designs, the modulator bridge is located on the inner edge of the modulators as far away as possible from the higher pole count LSR to minimize leakage flux; therefore, increasing the LSR magnet thickness does not offer any significant help in saturating the bridge. In addition to all of these considerations, when evaluating the optimal LSR magnet thickness ratio, it is also important to make sure that the HSR magnets are not so much thicker than the LSR magnets that they demagnetize them. All depicted designs were evaluated to ensure that the LSR magnets are not demagnetized.

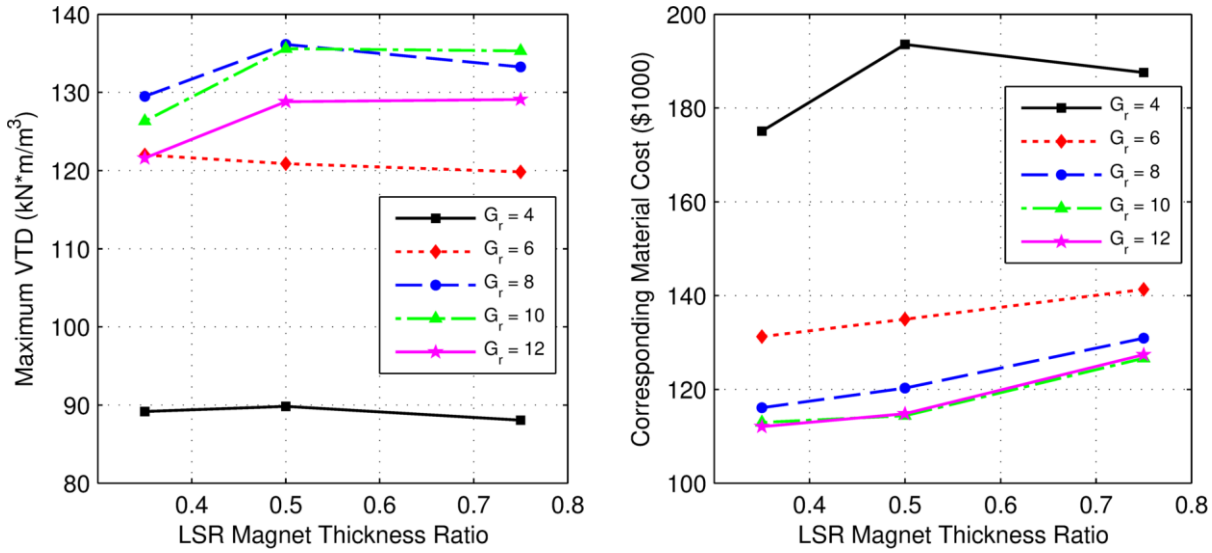

(a) (b)

Figure 5: Variation of (a) Maximum Overall System Volumetric Torque Density and (b) Corresponding System Active Material Cost with LSR Magnet Thickness Ratio for Different Gear Ratios at a Modulator Thickness of 50 mm and a Bridge Thickness of 10 mm

Based on the trends illustrated in Figures 1-5 the magnetic gear design specified in Table III was selected for use in the full scale magnetically geared generator. Although Figures 2-5 indicate that, based on the chosen modulator and bridge thicknesses, comparable performances can be achieved using either a gear ratio of approximately 8 or 10, a gear ratio of approximately 8 was selected because it results in lower modulator and LSR permanent magnet pole counts which would simplify construction. A full cross-sectional view of the magnetic gear sub-system for this design is shown in Figure 6, and a detailed view of the magnetic gear cross-section is provided in Figure 7. For practical purposes, the HSR permanent magnets would be segmented in an actual physical prototype, but this change would not have a significant impact on performance. Based on a 3D static FEA simulation, the resulting system volumetric torque density, gravimetric torque density, and active material cost for this design are 133.3 kN·m/m^3, 23.0 N·m/kg, and $122,400, respectively. All of these metrics surpass the corresponding target values. The stall torque predicted by the 3D FEA model is 97.9% of that predicted by the 2D FEA model; thus, using 2D FEA models was a reasonable approach to the optimization process. The information provided in Table III presumes the use of a single magnetically geared machine stack, but in practice it might be prudent from a system integration perspective to use two magnetically geared generators, each with half of the full stack.

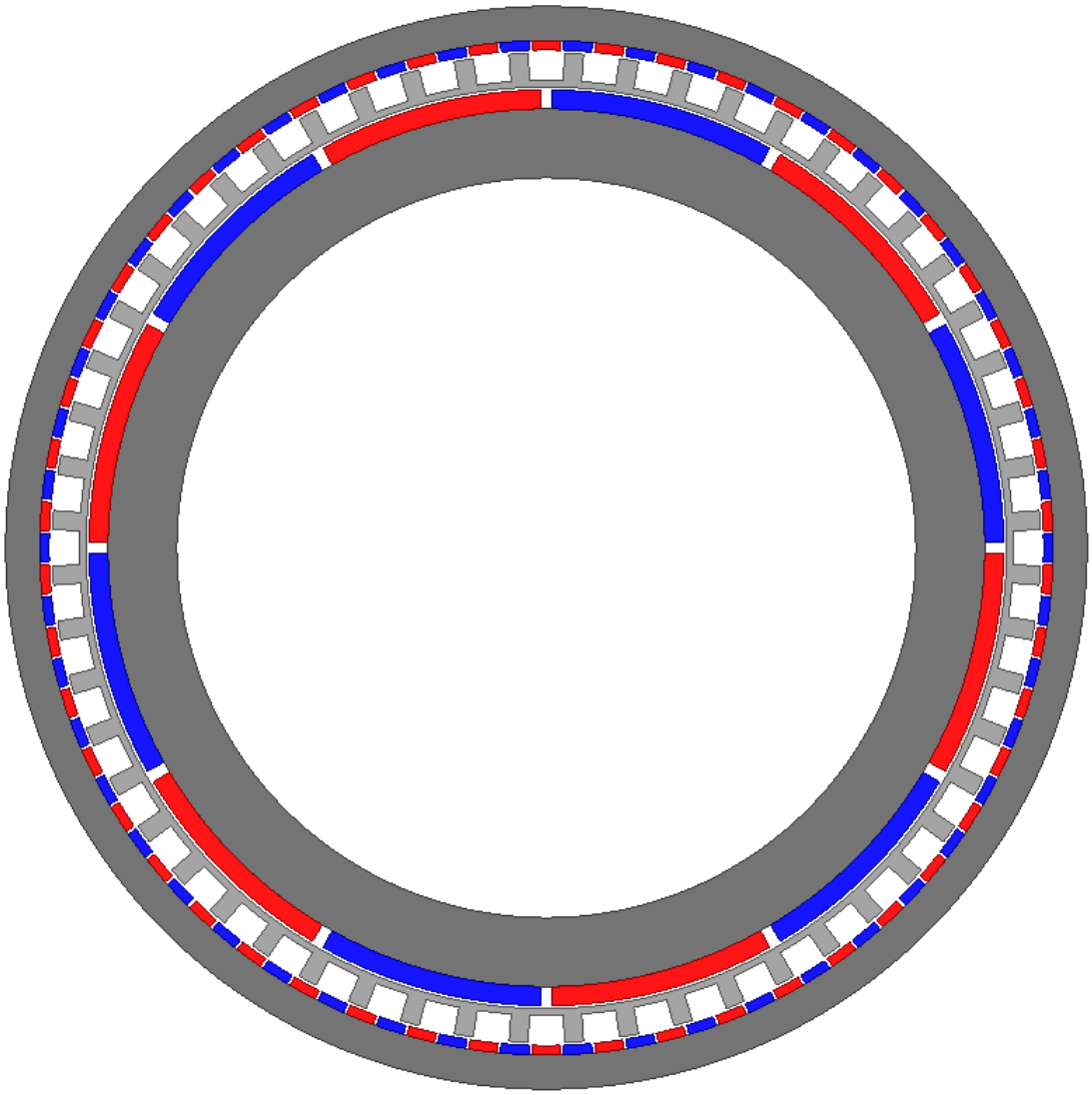

Figure 6: Full Cross-Sectional View of Full Scale Magnetic Gear Design

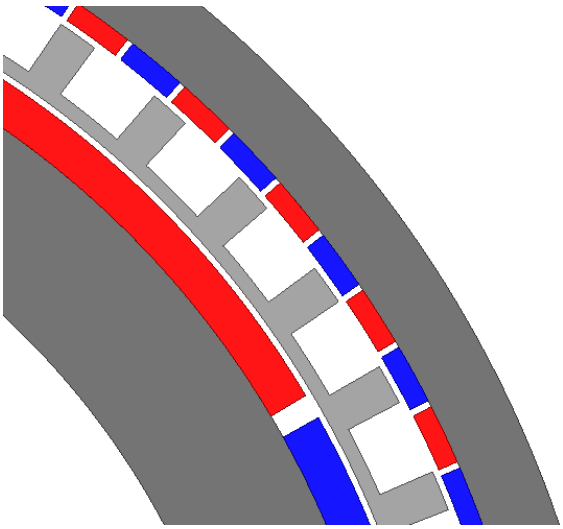

Figure 7: Detailed Cross-Sectional View of Full Scale Magnetic Gear Design

Table III: Full Scale Magnetic Gear Design

Parameter	Value
Gear Ratio	8.33
HSR Pole Pairs	6
LSR Pole Pairs	50
Modulator Count	56
Outer Radius	800 mm
HSR Back Iron Thickness	101.9 mm
HSR PM Thickness	28 mm
HSR Air Gap	4.5 mm
Modulator Thickness (Including Bridge)	50 mm
Modulator Bridge Thickness	10 mm
LSR Air Gap	4.5 mm
LSR PM Thickness	14 mm
LSR Back Iron Thickness	50.5 mm
Modulator Fill Factor	0.35
HSR PM Fill Factor	0.95
LSR PM Fill Factor	0.9
Gear Stack Length	1194 mm
Total System PM Mass	1801.3 kg
Total System Mass	15,155.2 kg
Total System GTD	23.0 N·m/kg
Total System VTD	133.3 kN·m/m^3
Total System Active Material Cost	$122,400

MAGNETIC GEAR LOSS ANALYSIS

Transient 2D FEA simulations were used to evaluate the magnetic gear losses at different loads and speeds and the results are summarized in Figures 8 – 10. The data in Figure 8 demonstrates that the gear exhibits a predicted electromagnetic efficiency of better than 95% for all considered (non-zero) loads and speeds and a predicted electromagnetic efficiency of 99% at the rated load and speed. The contour plot in Figure 9 illustrates the gear's predicted total electromagnetic losses under different operating conditions. This data clearly indicates that while the losses do change significantly with operating speed, they are relatively constant with respect to steady state load variation. This is consistent with past simulated and experimental results. Figure 10(a) shows the variation of the full load permanent magnet and iron losses with operating speeds. The permanent magnet losses vary quadratically with speed because they are entirely eddy current losses and the iron losses vary linearly with speed because they are dominated by hysteresis losses. The losses are relatively low (and the efficiency is relatively high), despite the use of

extremely thick magnets, because of the thick modulator bridge and the exceptionally low operating speed. As discovered during the design of the Phase II prototype, the bridge effectively serves as a filter to attenuate some of the LSR magnetic flux harmonics which would otherwise result in eddy current losses in the HSR permanent magnets. Because all of the losses are frequency (speed) dependent, the low operating speed decreases all of the loss components. Figure 10(b) shows the variation of the full load losses in the HSR, modulators, and LSR with operating speeds. The LSR losses are the most significant loss component and occur because of the relatively large asynchronous magnetic flux harmonics produced by the thick, low pole count HSR magnets which travel through the LSR. The HSR rotor losses are the least significant because the thinner, higher pole count LSR magnets naturally produce weaker magnetic flux harmonics and these are further attenuated by the substantial modulator bridge.

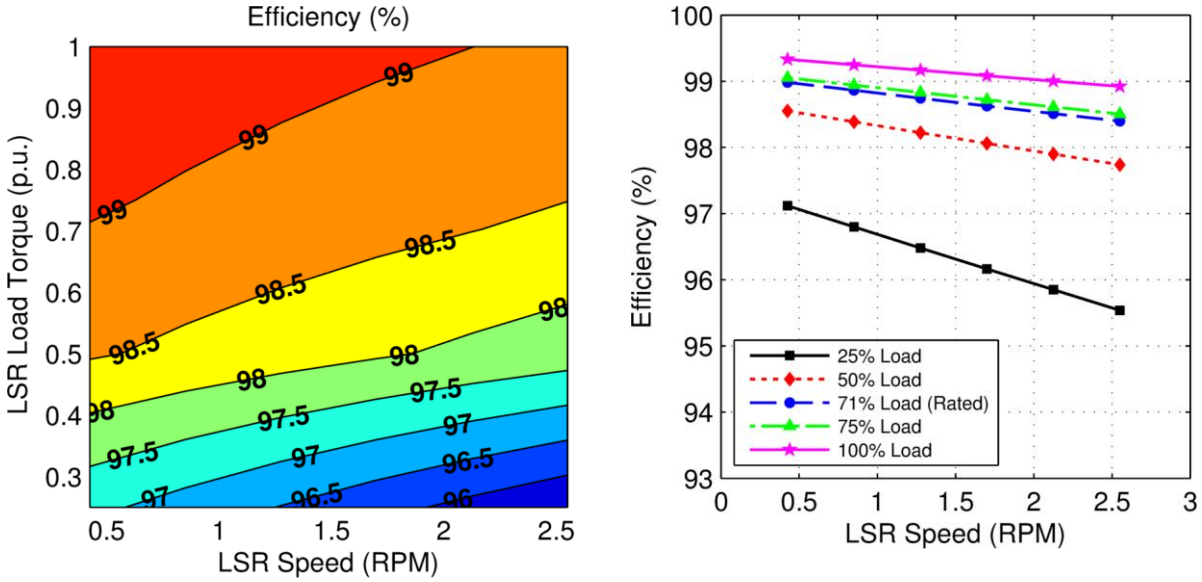

(a) (b)

Figure 8: (a) Contour and (b) Line Plot Illustration of Full Scale Design Magnetic Gear Efficiency Variation with Load and Speed

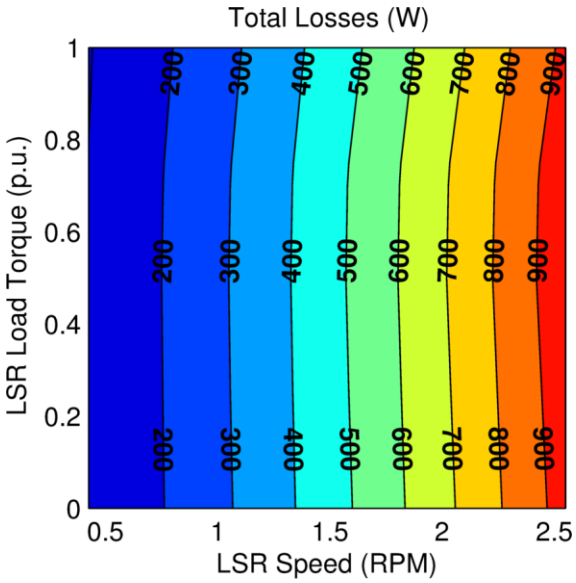

Figure 9: Full Scale Design Magnetic Gear Total Loss Variation with Load and Speed

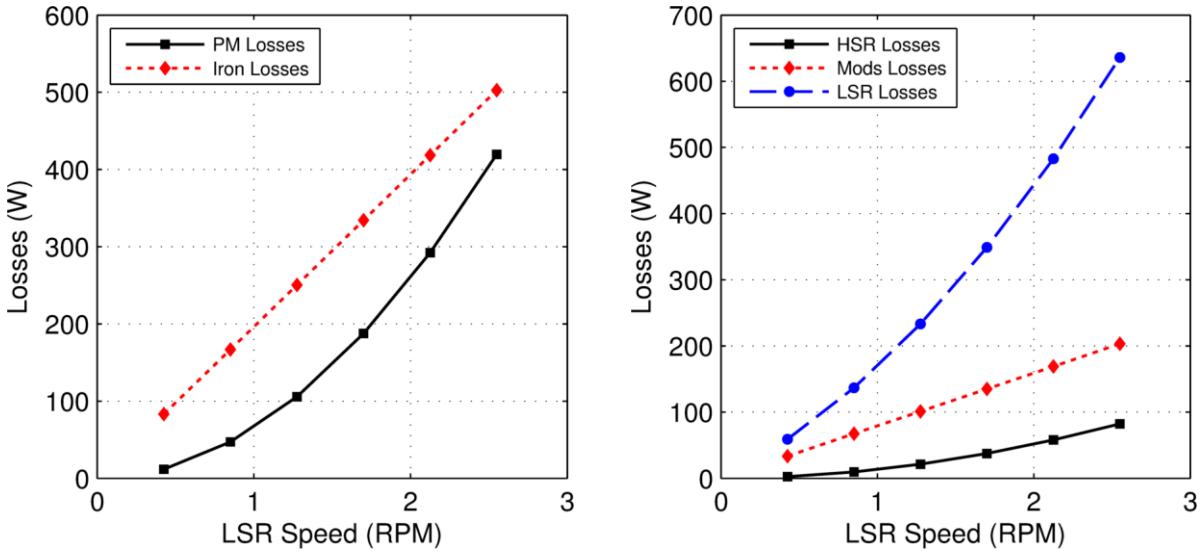

(a) (b)

Figure 10: Full Scale Magnetic Gear Design Full Load Loss Breakdown by (a) Type and by (b) Location

MAGNETIC GEAR AXIAL LEAKAGE FLUX EVALUATION

In addition to the basic design details and performance attributes summarized in Table III, axial leakage flux characteristics were also determined for the full scale magnetic gear design. Figure 11 illustrates the RMS flux densities along circular paths at various axial distances beyond the end of the modulators for this design. As discovered during the design of the Phase II prototype, this axially escaping leakage flux is very important for practical magnetically geared machine design considerations because it dictates how much non-conducting, non-magnetic buffer material must be used at the end of the active magnetic stack to prevent additional electromagnetic losses in the inactive material. Although the full scale design uses extremely thick magnets which tend to result in greater axial flux leakage, the full scale design stack length is also extremely long; therefore, the necessary non-conducting, non-magnetic buffer axial buffer space is a much smaller fraction of the stack length.

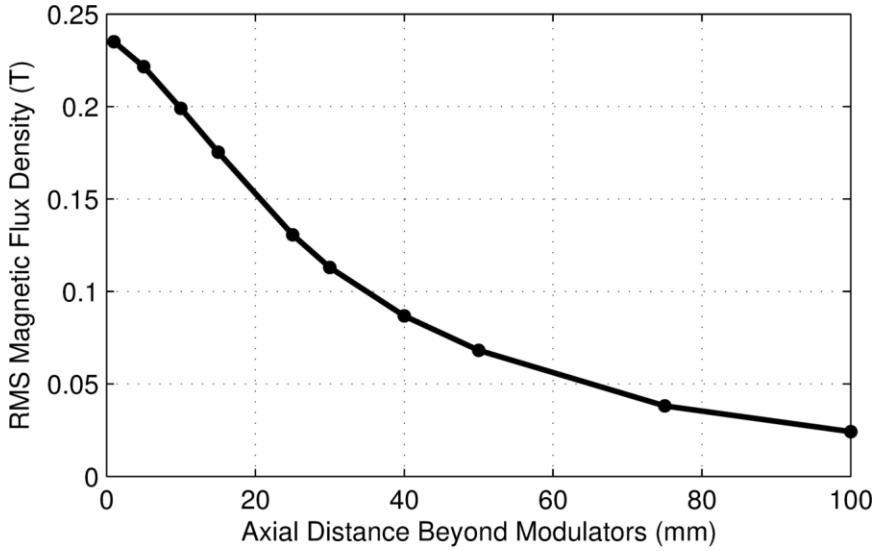

Figure 11: Axial Leakage Flux Characteristics for Full Scale Magnetic Gear Design

DE-EE0006400
MILESTONE DELIVERABLE

TASK 6.2: Full-Scale Generator Design Report

Report Main Author: Wen Ouyang

Table of Contents

1 General information

A prototype magnetically geared generator was developed under DOE contract (DE-EE0006400) as a proof of concept development for wave energy conversion low speed, high torque applications. The generator is a direct drive electrical power generating device which integrates a magnetic gear and a permanent magnet generator within the same nested machine.

The generator includes four electromagnetically active components:

- Low speed (LS) rotor
- Modulator
- High speed (HS) rotor
- Stator

The LS rotor is the outer most component of this generator and can be directly connected with a flap-type or other wave energy capture device. In the prototype case, the LS rotor is coupled via a stub shaft to the test bed drive train. The modulator, HS rotor, and stator are nested in the same order inside the LS rotor. For ocean wave energy applications, the LS rotor operates at a very low speed range typically averaging about 1~2 rpm, with a peak speed less than 10 rpm. To generate significant power, the torque observed by this LS rotor is large, which makes the development of this type of generator a challenging task. This initial proof of concept investigation is focused on prototype demonstration and dry laboratory testing to validate modeling and calculations for a full scale design. The additional challenges of operating submerged in a marine environment are outside the scope of this project.

With the magnetic gear effect, the HS rotor rotates in the opposite direction of the LS rotor at higher speed, with the speed (and also torque) ratio determined by the designed magnetic gear ratio.

This report describes the prototype design data and test results for the 10 kW, 30 rpm Phase II magnetically geared generator prototype. The testing was performed at the ABB Corporate Research lab for the characterization and validation of the proposed design concept.

This report details the 40 kW, 1.7 rpm full scale generator design.

1.1 Full Scale Design Requirements

The full scale generator design requirements are provided in Table 1.1.1 below.

Averaged Power (kW)	40
Averaged Speed (rpm)	1.7
Peak Speed (rpm)	10
Outer Diameter (m)	1.6
Overall Length (m)	1.8
Peak Torque (Nm)	320 kNm

Table 1.1.1: Full scale requirements

The design of the full scale generator is a scaled up version, based on the Phase II prototype development, with a concept picture in Figure 1.1.1.

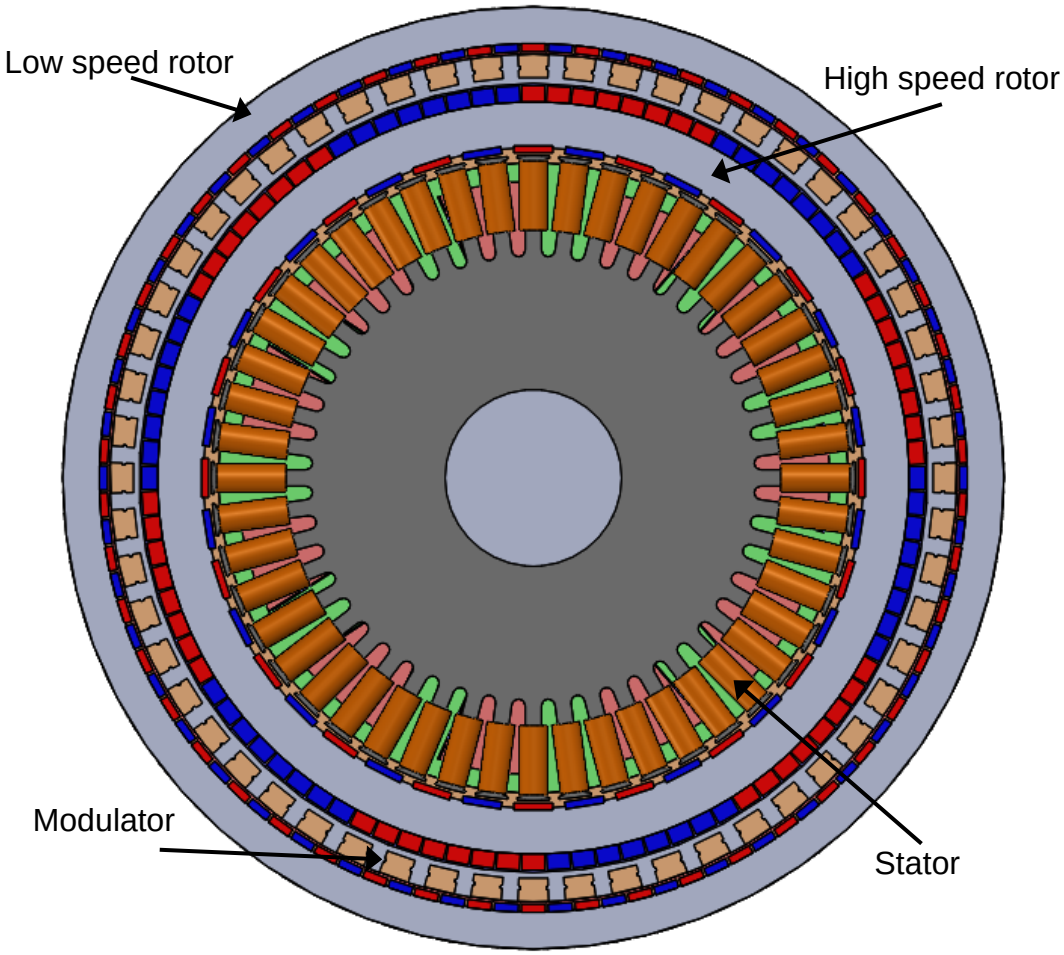

Figure 1.1.1: Full scale design concept

The outer most rotor is the low speed (LS) rotor, which is directly coupled via an input stub shaft to the test-bed drive train. Next is the thin electrical steel modulator layer, fixed in position between the outer low speed rotor and the inner, high speed (HS) rotor. The high speed rotor includes thicker magnets on the outer diameter for the magnetic gear operation as well as a magnetically isolated thinner set of magnets on the inner diameter to interact with the inner generator stator for generating electrical power. The stator is mounted on a fixed supporting shaft running through the center of the machine. The generator is designed with three air gaps. The two LS and HS rotors rotate in opposite directions, with a magnetic gear speed ratio of 8.33.

2 Magnetic Gear Design

2.1 Physical Dimension

As an installation limitation for integration with the paddle type wave energy harvesting device, the generator outer diameter is limited in order to avoid increasing the height of the base of the 8 m x 9 m paddle and altering the hydrodynamics of the system. Meanwhile, with different installation options, the generator could be configured as one single generator centered on the paddle axis or as two separate generators per paddle. In this report, a single generator per flap configuration is applied for discussion.

The major physical dimension limitations from the flap installation are listed in Table 2.1.1.

Generator Dimensions	Preferred values
Outer Diameter (m)	< 1.6
Axial Length (m)	< 1.8

These dimensions of the generator generally have negligible impact on the flap hydrodynamic performance.

2.2 Electrical Design

With the target speed range and power rating, the magnetic gear design parameters are provided in Table 2.2.1.

Parameter	Value
Gear Ratio	8.33
HSR Pole Pairs	6
LSR Pole Pairs	50
Modulator Count	56
Outer Radius	800 mm
HSR Back Iron Thickness	101.9 mm
HSR PM Thickness	28 mm
HSR Air Gap	4.5 mm
Modulator Thickness (Including Bridge)	50 mm
Modulator Bridge Thickness	10 mm
LSR Air Gap	4.5 mm
LSR PM Thickness	14 mm
LSR Back Iron Thickness	50.5 mm
Modulator Fill Factor	0.35
HSR PM Fill Factor	0.95
LSR PM Fill Factor	0.9
Gear Stack Length	1194 mm
Total System PM Mass	1801.3 kg
Total System Mass	15,155.2 kg
Total System GTD	23.0 N·m/kg
Total System VTD	133.3 kN·m/m3
Rated Efficiency	98.9%

Table 2.2.1: Magnetic Gear Design Parameters List

The magnetic gear side loss estimation is illustrated in Figure 2.2.1.

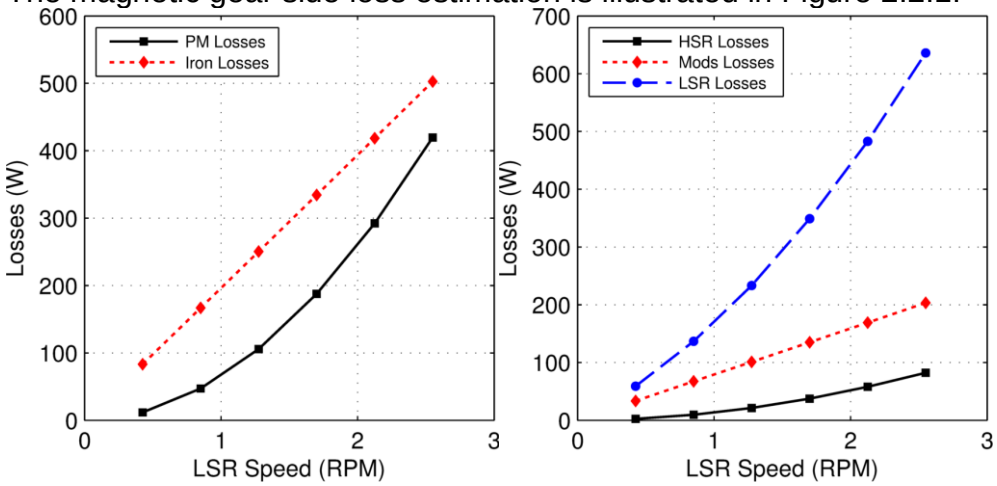

Figure 2.2.1: Magnetic Gear Loss Estimation

3 Generator Design

The generator design is constrained by the inner diameter of the magnetic gear, since the HS rotor of magnetic gear is integrated with the generator rotor. The active stack length of generator is less than the gear side lamination stack length, which makes it possible to integrate the stator end winding sections within the active stack length of the gear side.

3.1 Physical Dimension

The generator major physical dimensions are provided in Table 3.1.1. For full scale development, the LS rotor frame can provide containment of the generator for submersible operation.

Rotor equivalent OD (mm)	1228
Rotor ID (mm)	1121.3
Stator OD (mm)	1112.3
Stator ID (mm)	510
Air gap length (mm)	4.5
Active lamination stack length (mm)	760
End Winding Length (mm)	124

Table 3.1.1: Generator Physical Dimensions

3.2 Electrical Design

The full scale design is based on the averaged value of the wave oscillation conditions. A previous study indicates that the generator output power at constant speed mode and oscillation mode can be matched with their averaged speed. Table 3.2.1 provides main design parameters for the generator.

Electrical Parameters	**Full Scale Design**
Poles	40
Slot #	48
PM thickness (mm)	18
Rated VLL (V)	350
Rated Phase current (A)	35
Power Factor	>0.94
Frequency (Hz)	4.53
Connection	YY
Turns / coil	58
Phase Resistance (20 C deg)	0.17
Copper Loss (W)	1260
Iron Loss (W)	355
PM Loss (W)	30
Rated Torque (kNm)	28,000
Rated Efficiency	96%

Table 3.2.1: Full Scale Generator Main Design Parameters

4 Integrated Magnet Gear Generator Design

With integration of magnetic gear and generator, the gear high speed rotor and generator are mechanically coupled, both sharing the high speed rotor laminations, with magnets fixed to the outer diameter and inner diameter of the common rotor. Therefore, the interaction of these two components needs to be carefully considered, and the design strategy was to magnetically isolate the function of the high speed magnetic gear rotor and the electrical generator rotor. This magnetic isolation requires additional space and material, but maximizes the system performance and is a simpler starting point for early prototypes.

4.1 Rotor Integration

The integration of the HS gear rotor and generator rotor needs to be carefully considered for the magnets sitting on both the gear and generator sides of the rotor. Both gear and rotor functions must be performed using the different sets of magnets, rotating at the same speed on the same single rotor. Meanwhile, the isolation of the PM flux between these two layer of PMs need to be addressed. Figure 4.1.1 (from the Phase II design) illustrates the integrated generator cross view along with the magnetic isolation between magnetic flux between the two magnet layers from the proper size and positioning of the bolt holes and flux barriers.

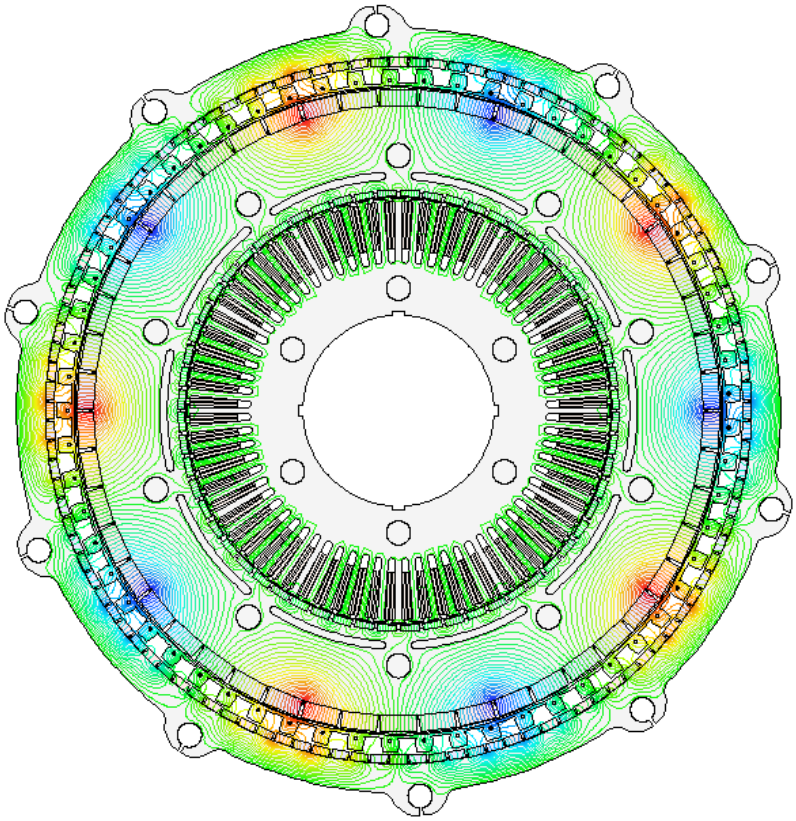

Figure 4.1.1: Generator cross view

It should be noted that the flux barrier slots are punched on the lamination close to the generator side with the segment number same as the HS rotor pole number. The circular bolt holes between these curve slots are primarily designed for clamping bolts, and also provide an additional flux barrier and local saturation function to minimize the interaction and leakage flux between the two sets of HS rotor magnets.

4.2 Structure

Figure 4.2.1 shows the generator cross section view with supportive frame and shaft. The the nested structure from outside to the inside with LS rotor, modulator (stationary), HS rotor, and generator stator.

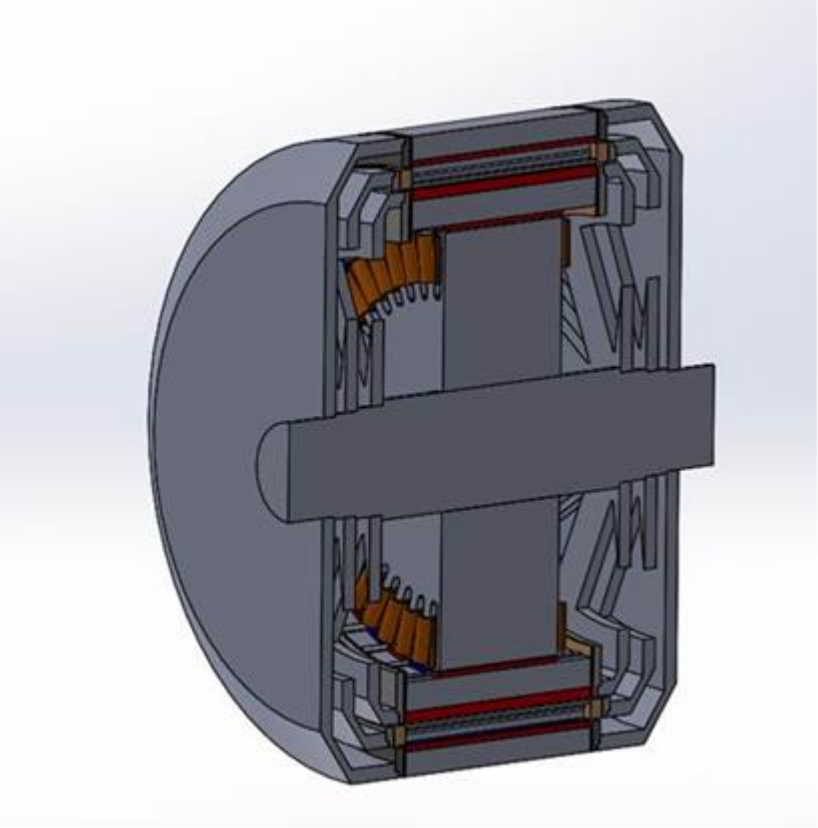

Figure 4.2.1: Cross sectional view of full scale generator structure

With submersible operation, the outer rotor (LS rotor) is integrated with a fully sealed design frame. The sealing and bearing needs to be carefully designed for such application needs, which is beyond the discussion scope of this report.

In Figure 4.2.2, the exploded view of the full scale generator structure is illustrated.

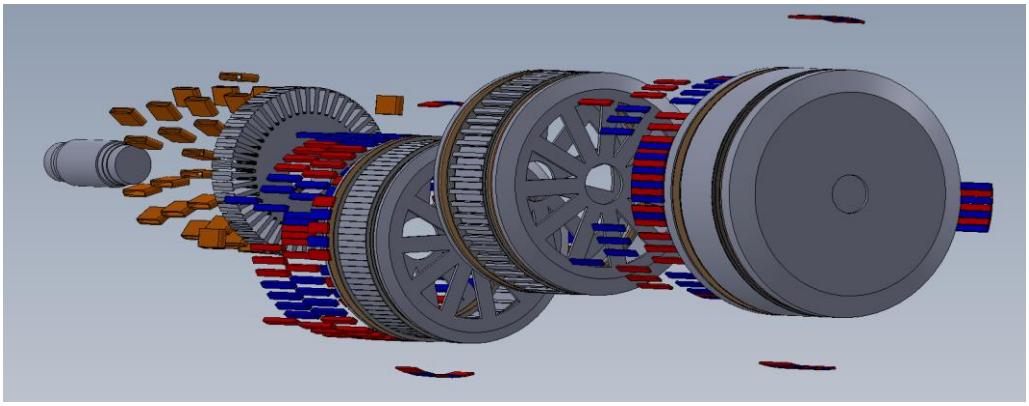

Figure 4.2.2: Exploded view of full scale generator structure

5 Generator Performance Simulations

With the proposed full scale design, the generator performance under non-torque limiting and torque limiting under oscillation mode have been studied with finite element analysis (FEA) based method to investigate the operation.

5.1 Non Limiting Torque

The generator set is following a typical oscillation wave profile (Appendix) to simulate the natural wave movement. In Figure 5.1.1, the non-torque limiting speed reference is provided for the LS rotor (left) and HS rotor (right) respectively. The speed ratio between HS and LS rotor is the gear ratio. Torque limiting is the function applied from control side to limit the actual torque can be observed from the flap/generator system.

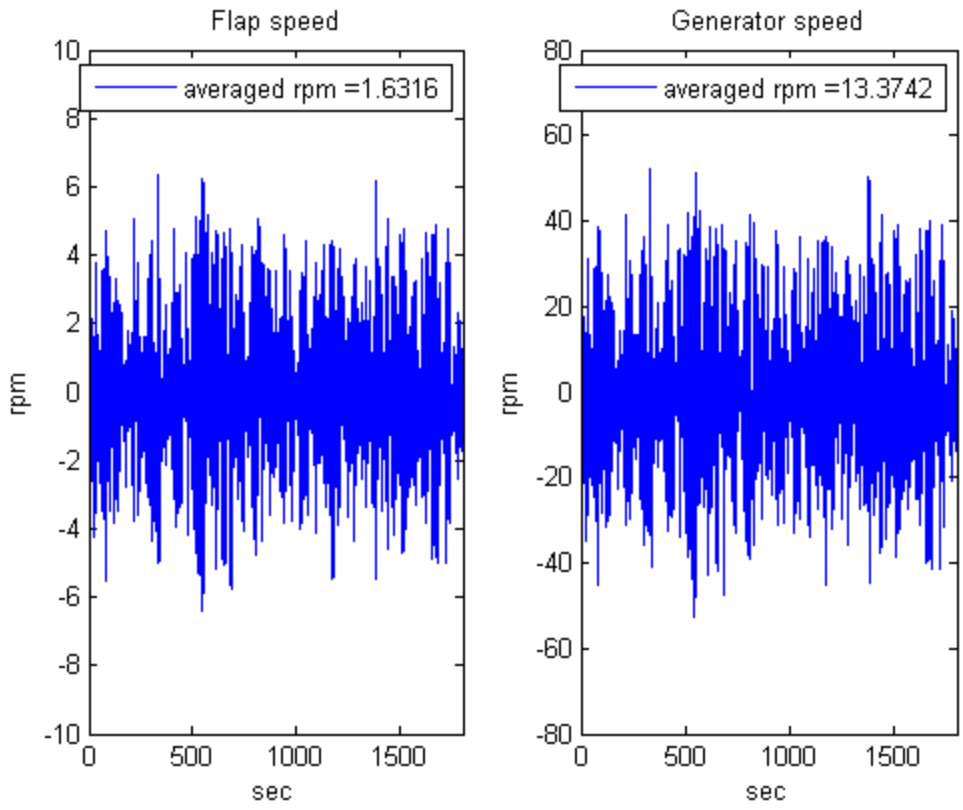

Figure 5.1.1: Generator speed reference. Left: LS rotor. Right: HS rotor

With rotor movement, the water energy is converted to the electric power in stator winding via the electro-magnetic torque generated in the generator air gaps.

In Figure 5.1.2, the simulated generator phase voltage and current are illustrated.

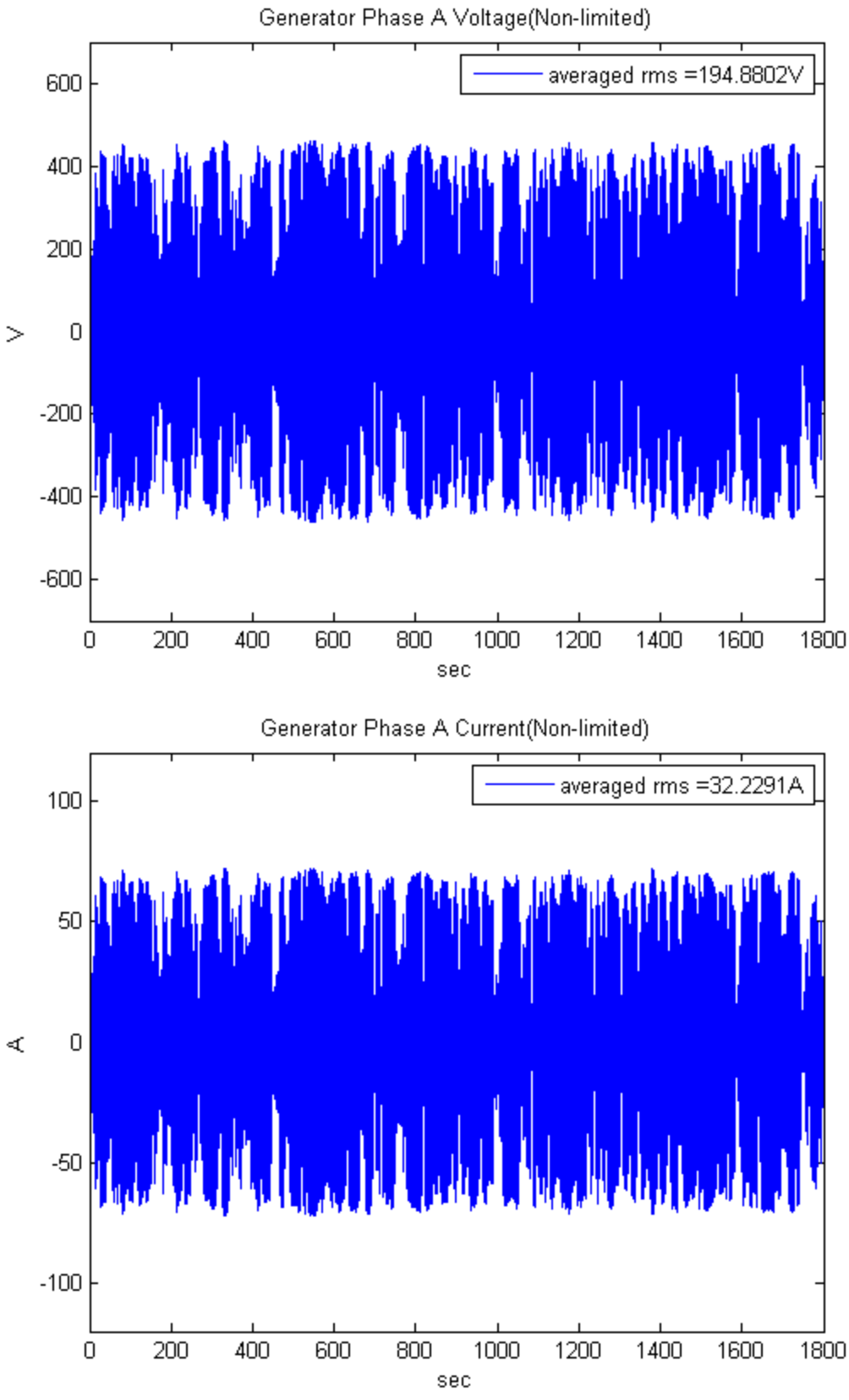

Figure 5.1.2: Generator phase voltage/current under non-limiting torque mode

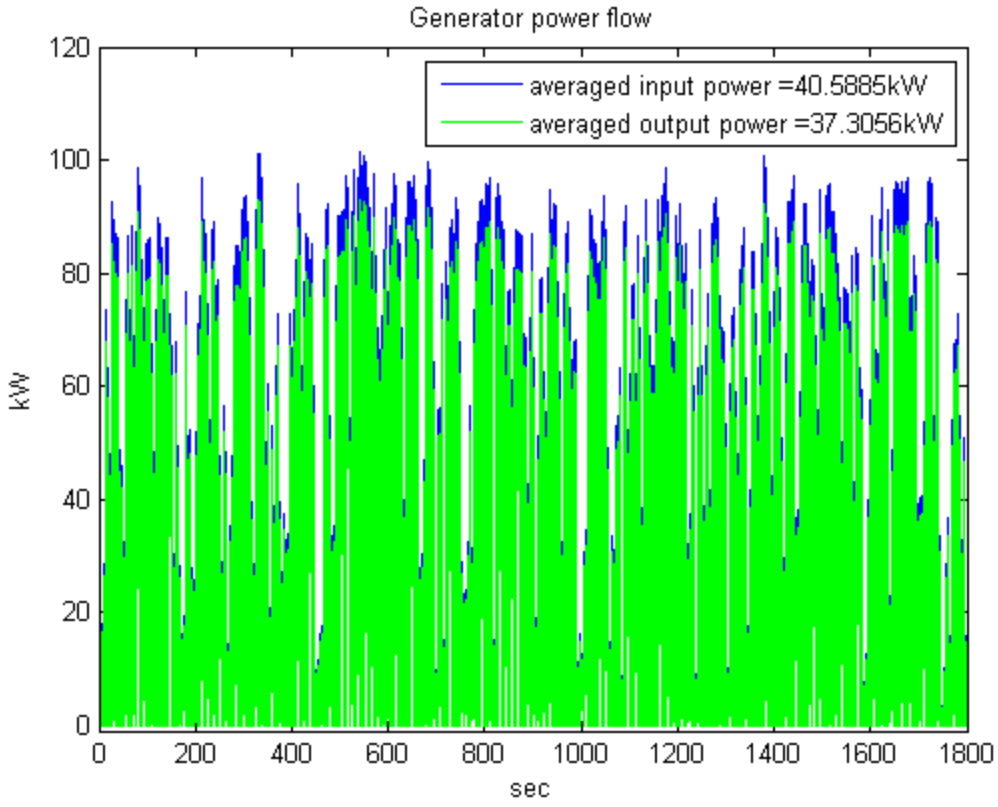

Figure 5.1.2: Simulated generator power input and output

In Figure 5.1.2, the power generation capability is simulated. It should be noted that the instant generator output power can be as high as 90kW due to the high input speed for short time, which is implemented with generator design as the short time overload capability.

5.2 Limiting Torque

Limiting torque capability is to provide system protection of the generator to avoid damage by dangerous high torque observed from both gear side and generator side.

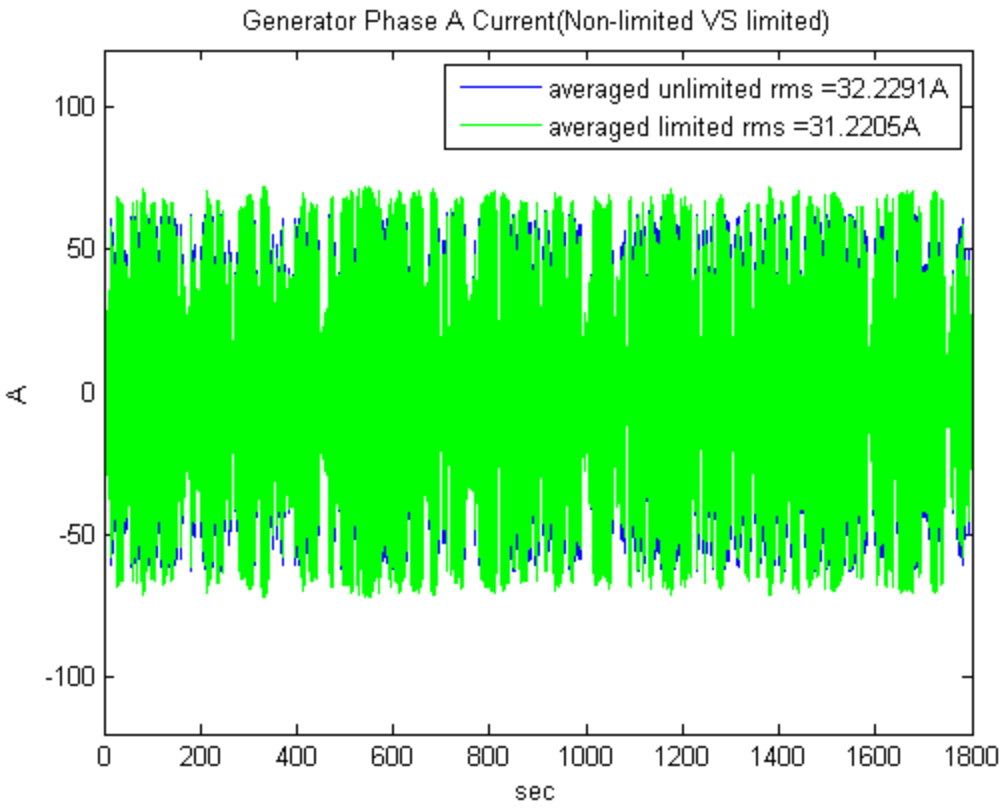

Figure 5.2.1: Limiting Torque mode generator current

In Figure 5.2.1, the generator torque is limited by the phase current of generator winding, mostly the peak current over protection threshold is modulated and controlled to be maintained within the safe range, which reduces the averaged output current as well.

In Figure 5.2.2, the generator output power is provided under limiting torque operation mode. The averaged output power under this mode is reduced for the eliminated high pulse type power generation.

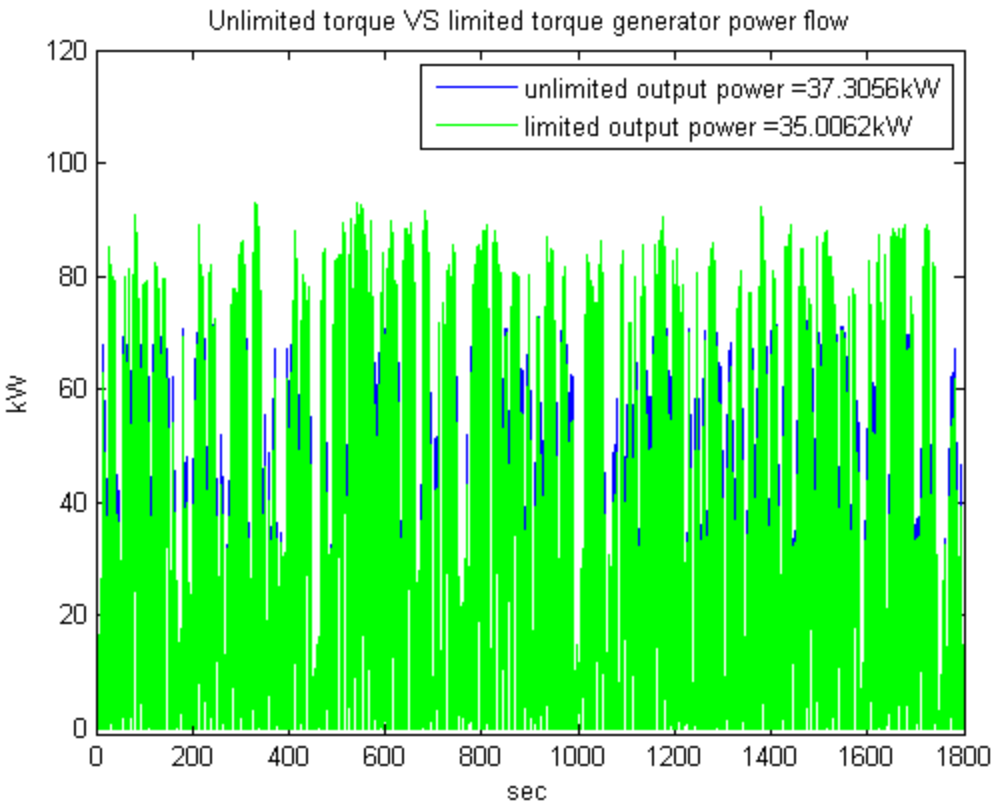

Figure 5.2.2: Limiting Torque output power

Appendix A
Oscillation mode reference speed

time [s]	rotation [deg]	ang vel [rad/s]	PTO torque [MNm]	flap pwr [kW]
0.1	-2.275	-0.079	-0.197	15.673
0.2	-2.735	-0.081	-0.200	16.188
0.3	-3.198	-0.080	-0.199	16.028
0.4	-3.655	-0.078	-0.194	15.249
0.5	-4.095	-0.075	-0.186	13.929
0.6	-4.512	-0.070	-0.174	12.196
0.7	-4.898	-0.064	-0.159	10.161
0.8	-5.245	-0.057	-0.140	7.947
0.9	-5.547	-0.048	-0.120	5.793
1.0	-5.799	-0.039	-0.097	3.805
1.1	-5.995	-0.029	-0.071	2.049
1.2	-6.130	-0.018	-0.044	0.791
1.3	-6.201	-0.007	-0.016	0.108
1.4	-6.206	0.005	0.013	0.071
1.5	-6.140	0.018	0.045	0.804
1.6	-6.003	0.030	0.075	2.287
1.7	-5.794	0.043	0.106	4.555
1.8	-5.513	0.055	0.137	7.554
1.9	-5.162	0.067	0.167	11.268
2.0	-4.744	0.079	0.195	15.395
2.1	-4.261	0.089	0.222	19.847

Table A.1: Generator speed example reference

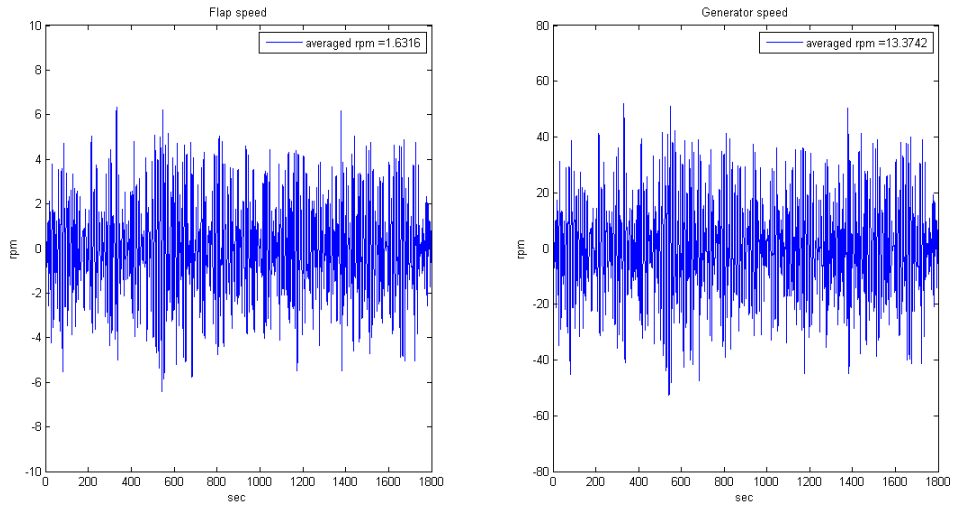

Figure A.1: Generator reference speed plot

UPDATE

Task 7.1 and 7.3: Initial PTO System Availability Calculations

2/8/2016

Wave Energy Conversion Power Take-Off System Availability

Summary:

**NOTE* These availability calculations demonstrate the approach but the values are still a work in progress. More effort is required on the prototype magnetically geared generator and adjustments for subsea/nearshore operation, as well as scheduled maintenance, and weather delays. These refinements are being made together with the LCOE calculations.*

This report provides initial reliability and availability analysis for an oscillating water column surge wave energy conversion system with either a hydraulic or a direct drive electrical power take-off (PTO) system. Reliability data was gathered for each PTO system component from industry surveys. The MTBF was found to be between 1 failure every 4 years down to 4 failures every 1 year. The availability was found to be above 95% in all cases. The main source of down time was found to be the hydraulic motor for the hydraulic PTO system and the magnetically geared direct drive generator for the direct drive electrical PTO system.

INTRODUCTION

This document provides initial reliability analysis for hydraulic and direct drive electrical PTO solutions for near shore wave energy conversion. Section 2 describes the PTO systems of the two solutions, including a single line diagram and component list. Section 3 explains the reliability calculation methods. Section 4 presents a reliability block diagram of each solution and gives reliability data for each component from the literature. Since reliability can be variable depending on environmental and manufacturing variables, a range of values representing a nominal, optimistic, and pessimistic case are included for each component. These values are used in Section 5 to calculate and simulate the reliability of each solution for each of the three cases. The results provide a robust picture of the range of reliability of each solution. Section 6 concludes the report.

Note on Methodology and Scope of Analysis

Regular maintenance and weather related delays are not included in this initial availability data, as these will vary from site to site. As a consequence of this, the reported availability is more optimistic than what will be experienced in the field. For one example, an on-shore availability of 97% can drop to less than 80%, or an availability of 99% becomes 96% when inaccessibility due to wind and waves is taken into account [1]. As a fist shot at accounting for offshore weather and related delays, the MTTR for all offshore equipment is increased by 12 hours for the optimistic case, 24 hours for the nominal case, and 48 hours for the pessimistic case. Based on offshore wind experience from [1], this initial adjustment does not add enough additional time. More comprehensive values including total downtime will be used for the LCOE calculations.

SYSTEM DESCRIPTION

The hydraulic and direct drive electrical wave energy conversion systems are described below. A single line diagram is provided for each along with a parts list. These are used to generate a reliability block diagram which can be used to determine the reliability and availability of each system as per the techniques described in Section 3.

Hydraulic System Definition

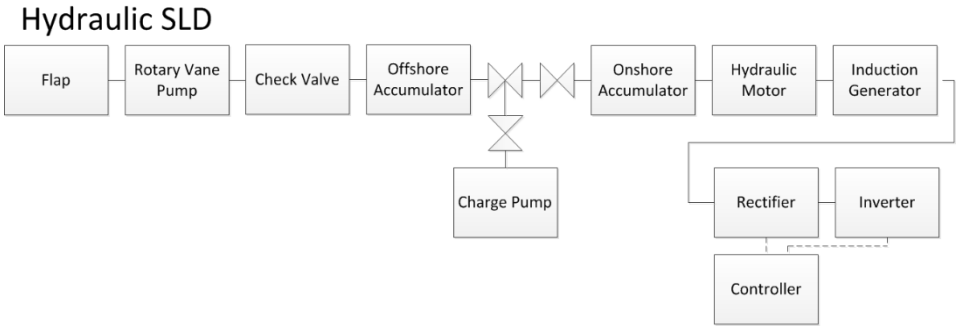

Figure 1: Hydraulic Wave Energy PTO System Single Line Diagram

A single line diagram of the hydraulic PTO system is shown in Figure 1. The mechanical flap is moved by the waves and applies pressure in low speed pulses to a hydraulic fluid in the rotary vane pump. The fluid moves into the pipes through a set of check valves which serve to force the fluid to flow in one direction regardless of the motion of the waves. There is an offshore accumulator that collects the hydraulic fluid pulses in a storage tank, then releases them at a constant rate. The fluid then moves through a subsea pipe until it reaches the shore.

On shore, there is a set of pressure relief valves that help protect the hydraulic system against excess pressure. These can be manually activated to allow a technician to perform maintenance on the onshore equipment. Another function of these valves is to connect to a charge pump. This equipment injects a steady flow of extra fluid into the pipes to replace fluid lost through small leaks.

After the protective equipment, the fluid moves into another accumulator to further smooth the power generation. It is then fed into a hydraulic motor, a converted axial piston pump, which converts the hydraulic pressure into rotating motion. This drives an induction generator to produce electric power, which is injected into the grid by a matrix converter. The converter includes a control board.

The equipment in the hydraulic system is listed below for reference:

- Rotary Vane Pump
- Check Valve
- Accumulator
- Pipe
- Pressure Relief Valve
- Charge Pump
- Hydraulic Motor
- Induction Generator
- Power Converter
- Converter Control Board

Direct Drive Electrical System Description

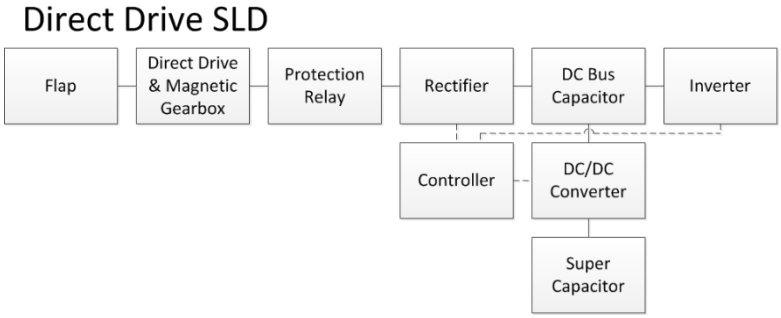

Figure 2: Direct Drive Electrical PTO System Single Line Diagram

A single line diagram of the direct drive electrical PTO system is shown in Figure 2. The mechanical flap is moved by the waves, with the oscillating motion driving the outer rotor of the integrated magnetic gear plus generator integrated along the pivot axis of the flap. An overcurrent relay protects the system from overheating. The power produced by the generator is sent to shore over a set of undersea cables. A controlled rectifier is used to limit the generator load torque and output current. On shore, the power is converted to line frequency by a converter. The converter consists of an active rectifier, DC bus capacitor bank, and an inverter, all regulated by a controller. A super capacitor bank or alternative electrical energy storage component provides power to smooth the power pulsations produced by the waves and limit the ramp rates of the output power to the grid. The energy storage equipment is connected to the converter's DC bus through a DC/DC converter. The converter controller also regulates the DC/DC converter.

The equipment in the direct drive wave generator is listed below for reference:

- Magnetically-Geared, Direct Drive Generator
- Protection Relay
- Cables
- Active Rectifier
- DC Bus Capacitor
- Inverter
- Controller
- DC/DC Converter
- Super Capacitor or Alternative Energy Storage

RELIABILITY CALCULATIONS

There are several methods to determine reliability and availability that have been presented in the literature. The IEEE 493 Standard for the Design of Reliable Industrial and Commercial Power Systems [2] provides a basic method to estimate reliability and availability. Monte Carlo simulations are used by the software BlockSim in order to observe the impact of real time events such as maintenance and work crew availability. BlockSim uses a reliability model called Reliability Block Diagrams (RBDs) in these simulations. These methods are described in more detail below.

Estimation from Equations

In IEEE 493, the reliability of the system is defined as the probability that a component or system is functioning as intended after a given time. If a constant failure rate is assumed, then the reliability of a component can be calculated to be:

$$R(t) = e^{-t/MTBF} \tag{1}$$

The availability is defined as the probability that a given component is operating as intended at a particular instant in time. It can be calculated by:

$$A = \frac{MTBF}{MTBF + MTTR} \tag{2}$$

Series Reliability and Availability

If a system consisting of a pair of components A and B fails if either A or B fails, then the two components are said to have series reliability. The reliability of the whole system is equal to the product of the reliability of the two components, or

$$R(t) = R_A(t) * R_B(t) = e^{-t/MTBF_A} * e^{-t/MTBF_B} = e^{-\left(\frac{1}{MTBF_A} + \frac{1}{MTBF_B}\right)t} \tag{3}$$

The equivalent MTBF of the system can be found as:

$$\frac{1}{MTBF} = \frac{1}{MTBF_A} + \frac{1}{MTBF_B} \rightarrow MTBF = \frac{1}{\frac{1}{MTBF_A} + \frac{1}{MTBF_B}} \tag{4}$$

The equivalent availability of the system can be somewhat complex, depending on how likely it is that two components are failed at the same time. If it is assumed that each component is repaired before the next fails, then the equivalent availability of the system is the product of the availability of each component in the system:

$$A = \frac{MTBF_A}{MTBF_A + MTTR_A} * \frac{MTBF_B}{MTBF_B + MTTR_B} \tag{5}$$

This will produce a conservative estimate of the availability of the system, as a real system is likely to have at least a few periods of overlap where two or more components can be repaired in the same work action. This would reduce the overall downtime of the system.

Parallel Reliability and Availability

If a system consisting of a pair of components A and B fails only if both A and B fails, then the two components are said to have parallel reliability, or more simply, are said to be redundant. The reliability of this system is most easily found by calculating the unreliability of the components (1 – R(t)), multiplying them, and then subtracting the result from 1. This gives:

$$R(t) = 1 - \left[\left(1 - R_A(t)\right) * \left(1 - R_B(t)\right)\right] \quad (6)$$
$$= 1 - \left[\left(1 - e^{-t/MTBF_A}\right) * \left(1 - e^{-t/MTBF_B}\right)\right]$$
$$= e^{-\left(\frac{1}{MTBF_A} + \frac{1}{MTBF_B}\right)t} - e^{-t/MTBF_A} - e^{-t/MTBF_B}$$

The equivalent MTBF cannot be easily calculated from this expression.

The availability of a redundant system depends on the operation and maintenance strategy of the system. If the two redundant components are run at the same time and repaired when both fail, then the availability is roughly equivalent to the best availability of the two components. The real power of redundancy, however, is that one component may be repaired while the other is still running. If the repair time is short enough, then it may be assumed that any damage to one component is repaired before the other component fails. The system will therefore always be available. This is of course optimistic, but in any event the down time of such systems tends to be at least an order of magnitude lower than the down time of the constituent components. This can be calculated more precisely by determining the probability that the second component fails while the first is being repaired, but such calculations become cumbersome. At this point it is more common to use reliability simulation tools to find the availability of such systems.

Reliability Block Diagrams and Monte Carlo Simulations

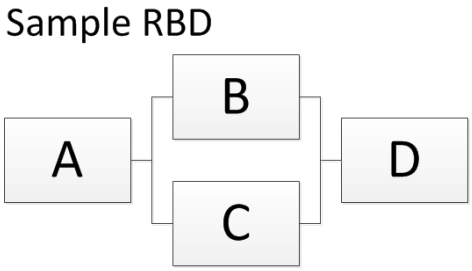

Figure 3: Example Reliability Block Diagram

A reliability block diagram shows the essential path for the equipment in the system. A continuous path must be available from the beginning of the diagram to the end in order for the system to function. It can easily be seen from this diagram where equipment failures can cause the whole system to cease functioning.

The example RBD shown in Figure 3 illustrates a system with four components: A, B, C, and D. The system is functioning as long as a continuous path exists from A to D. Components A and D are series connected; a failure of either component will cause the continuous path to break, resulting in a system failure. Components B and C are parallel connected; a failure in one component does not cause the system to fail, as a continuous path exists through the other component. In logic terms, the system functions only if A AND D are functioning, but continues to function if B OR C is functioning. It can be seen, then, that the RBD is a way to visually represent a logic diagram. It is also a quick way to see the key components in the reliability of the system.

One advantage of RBDs is that they can easily be checked by a computer to determine if the system is up or down. If rules are written for each block, such as a probability of failure and the time needed to restore the block, then the computer can determine whether each

block is up or down at a particular time. The RBD can then be checked for a continuous path to see fi the system is up or down.

Monte Carlo Analysis makes use of the RBD to find reliability and availability of a system. In this analysis, the system is simulated many times for a given time period with a given time step. A random number is generated at each time step for each event in the RBD which has a probability of occurring; most commonly, this means the probability of a block failing. If the random number is less than the probability, the event occurs. These probabilities can be time dependent, using something like an exponential function to represent the increasing probability that a component fails over time. The simulation can also take into account duration of events, such as using a Mean Time To Repair to determine when a component comes back online after a failure. It can be seen that these functions provide a powerful tool to evaluate the behavior of a system, and easily incorporate and analyze the impact of time dependent variables such as maintenance plans and weather delays.

RELIABILITY DATA

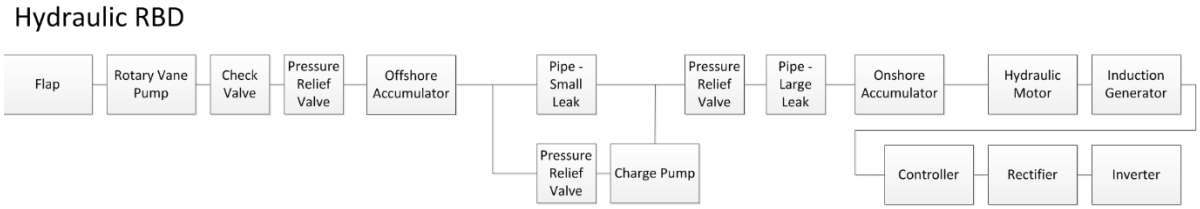

Figure 4: Hydraulic System Reliability Block Diagram

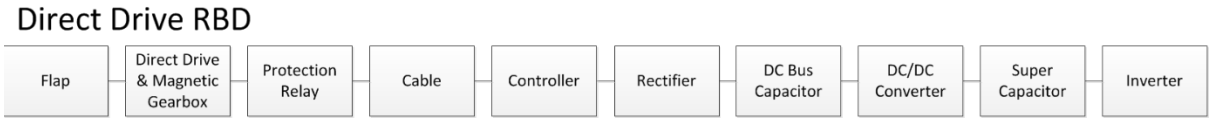

Figure 5: Direct Drive Electrical System Reliability Block Diagram

Figure 4 shows the RBD of the hydraulic system. It can be seen here that most of the equipment is in series, making each component essential for the proper operation of the wave generator. There is a limited degree of redundancy in the pipe, where the charge pump and pressure relief valve provide a way to compensate for small leaks in the pipe. The RBD of the direct drive electrical system in Figure 5, meanwhile, shows that all components are in series and are therefore critical to the operation of the system. These RBDs list all of the key components in each system. The reliability and availability of these components are given in Table 2 and Table 3.

Table 1: Hydraulic Wave Generator Reliability

Component	Nominal		Optimistic		Pessimistic	
	MTBF	MTTR	MTBF	MTTR	MTBF	MTTR
Rotary Vane Pump	60,000	68	9,090,900	34	17,300	136
Check Valve	1,886,800	33	2,564,200	16	531,900	66
Pipe (Small Leak)	1,098,900	48	1,531,000	24	234,700	72
Pipe (Large Leak)	653,600	79	918,100	39	124,500	158
Pressure Relief Valve	172,400	21	100,000,000	11	42,200	42
Charge Pump	17,600	36	200,000,000	18	3,800	72
Accumulator	3,571,400	25/49	50,000,000	13/25	1,315,800	50/98
Hydraulic Motor	8,000	40	27,000	20	4,000	80
Induction Generator	159,000	61	379,600	48	44,100	78
Rectifier	1,335,500	1	2,671,100	1	267,100	2
Inverter	1,335,500	1	2,671,100	1	267,100	2
Microcontroller	57,600	12	1,250,000	2	15,500	32

Table 2: Direct Drive Wave Generator Component Reliability

Component	Nominal		Optimistic		Pessimistic	
	MTBF	MTTR	MTBF	MTTR	MTBF	MTTR
Direct Drive & Magnetic Gearbox	33,700	199	44,300	99	12,500	371
Protection Relay	4,732,100	25	9,464,200	13	946,400	50
Cables	573,000	31	1,146,000	15	114,600	62
Rectifier	1,335,500	1	2,671,100	1	267,100	2
DC Bus Capacitor Bank	50,200	2	100,400	1	10,000	4
Inverter	1,335,500	1	2,671,100	1	267,100	2
Converter Control Board	57,600	12	1,250,000	2	15,500	32
DC/DC Converter	5,000,000	1	10,000,000	1	1,000,000	2
Super Capacitor	177,100	12	854,200	6	20,800	24

The reliability of each component is expressed in terms of Mean Time Between Failures (MTBF). The Meant Time To Repair (MTTR) is another important value needed to determine the availability of the component. This data is taken primarily from the IEEE Gold Book, which is a survey of U.S. power system equipment taken periodically between 1981 and 2007, and OREDA, a survey of offshore and onshore oil and gas equipment which corresponds with the marine environment experienced by wave energy conversion

equipment. This data is supplemented by surveys of wind farm equipment, a survey of rotating equipment used on military installations, datasheets, and other sources available in the literature.

This data includes the recorded hours of operation between failures and the working time to repair equipment when it fails. OREDA data does not include set up and take down time, so a scaling factor of 33% has been added to the OREDA repair time in order to account for set up and take down. Since most of the available reliability data is for land based systems, additional time has been added to the repair time of subsea equipment (12 hours for the optimistic case, 24 hours for the nominal case, and 48 hours for the pessimistic case) to reflect the difficulty of working in a subsea environment, such as travel time to and from the work site. This initial adjustment seems needs further refinement. This data also does not include routine maintenance, which is dependent on the maintenance strategy adopted at the site. This data also does not include inaccessibility due to weather. Weather and routine maintenance will be added for total downtime tabulated for the LCOE report.

RELIABILITY CALCULATION AND SIMULATION RESULTS

The reliability and availability of each of the two proposed PTO systems is calculated in the following sections. The reliability of each is first evaluated using the techniques from the IEEE Gold Book. A Monte Carlo simulation is then performed for each in BlockSim.

IEEE Gold Book Reliability Calculations

The hydraulic system is structured such that, for the most part, the components have series reliability. The one exception is the charge pump and the pipe (small leak) components, which are redundant. For simplicity, it will be assumed that these components have the ability to be repaired while the other component takes the load, and therefore the impact on reliability and availability can be neglected. These components are therefore neglected in this analysis, and the hydraulic wave generator simplifies to a set of components in series. The reliability of this system is therefore equal to the product of the reliabilities of each component, and similarly the availability of the system is equal to the product of the availabilities of each component. Using the data in Table 2, the equivalent MTBF and availability for the nominal, optimistic, and pessimistic case are calculated to be:

Table 3: Calculated Hydraulic System MTBF and Availability

Nominal		Optimistic		Pessimistic	
MTBF	**Availability**	**MTBF**	**Availability**	**MTBF**	**Availability**
5,900 Hr	99.31%	23,300 Hr	99.91%	2,400 Hr	96.76%

The RBD of the direct drive electrical system indicated that all of the components are series connected. The reliability of this system is therefore equal to the product of the reliabilities of each component, and similarly the availability of the system is equal to the product of the availabilities of each component. Using the data in Table 3, the equivalent MTBF and availability for the nominal, optimistic, and pessimistic case can be calculated to be:

Table 4: Calculated Direct Drive Electrical System MTBF and Availability

Nominal		Optimistic		Pessimistic	
MTBF	**Availability**	**MTBF**	**Availability**	**MTBF**	**Availability**
13,100 Hr	99.38%	27,500 Hr	99.77%	3,200 Hr	96.71%

BlockSim Monte Carlo Simulations

The two system concepts were simulated in the BlockSim reliability modeling software with a mission time of 20 years and 1000 Monte Carlo simulations to ensure the accuracy of the results. The results of these simulations, shown in Figure 6 and Figure 7, agree with the results of the calculations. The results show similar behavior for both systems. The MTBF in the nominal case indicates that the direct drive system may have a lower rate of failures, but this is within a margin of error. Inspecting the results more closely, the main contributors to system failure for the hydraulic and direct drive electrical systems have been listed in Table 5 and Table 6, respectively.

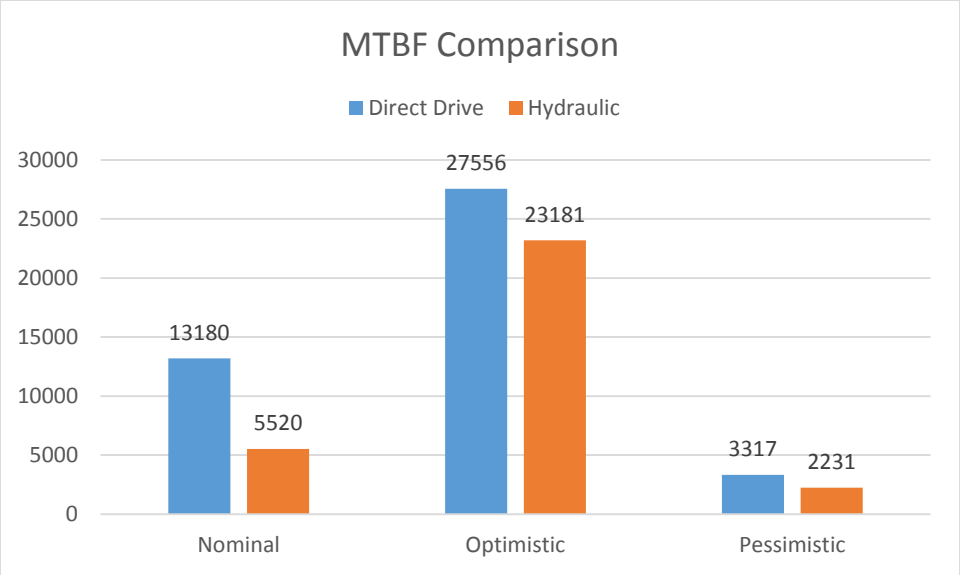

Figure 6: Wave Generator MTBF (hrs)

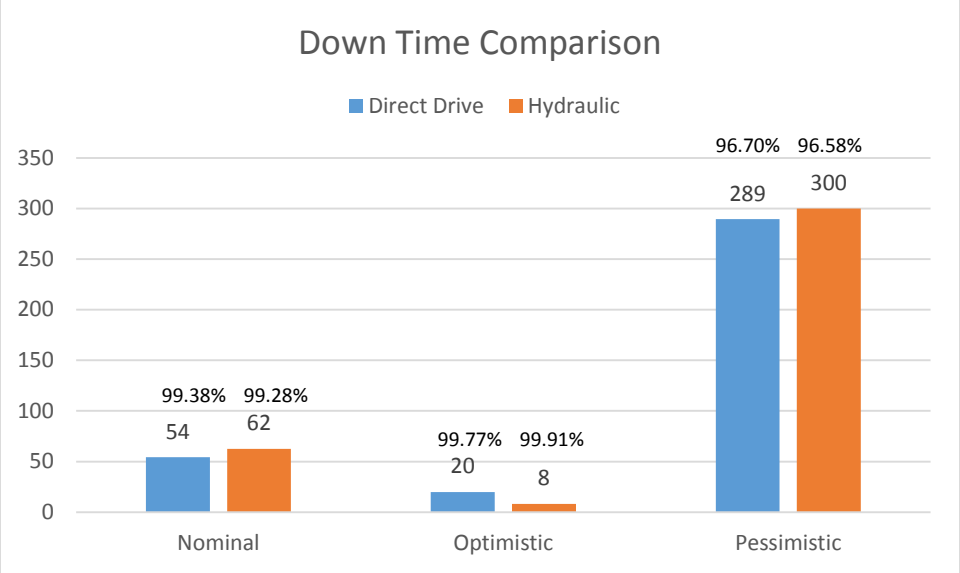

Figure 7: Wave Generator Downtime (hrs per year)

Table 5: Main Contributors to Hydraulic Wave Generator Failure

Scenario	Component	% of Total Failures	% of Downtime	# of Failures	MTTR (hr)
Nominal	Hydraulic Motor	68.71%	69.80%	21.809	40
	Rotary Vane Pump	9.28%	16.02%	2.944	68
	Control Board	9.44%	2.88%	2.996	12
Optimistic	Hydraulic Motor	87.01%	80.89%	6.576	20
	Induction Generator	6.75%	15.06%	0.51	48
Pessimistic	Hydraulic Motor	53.84%	56.39%	42.289	80
	Rotary Vane Pump	12.61%	22.44%	9.901	136
	Control Board	13.83%	5.80%	2.996	2

Table 6: Main Contributors to Direct Drive Wave Generator Failure

Scenario	Component	% of Total Failures	% of Downtime	# of Failures	MTTR (hr)
Nominal	Direct Drive & Magnetic Gear	38.51%	93.90%	5.119	199
	DC Bus Capacitor Bank	25.89%	0.63%	3.442	2
	Control Board	23.19%	3.41%	3.082	12
Optimistic	Direct Drive & Magnetic Gear	62.21%	98.52%	3.955	99
	DC Bus Capacitor Bank	27.12%	0.43%	1.724	1
Pessimistic	DC Bus Capacitor Bank	32.28%	1.18%	17.051	4
	Direct Drive & Magnetic Gear	25.92%	87.66%	13.693	371
	Control Board	20.86%	6.09%	11.018	32
	Super Capacitor	15.10%	3.31%	7.978	24

It can be seen from Table 5 that the main contributor to the failure of the hydraulic system is the hydraulic motor, with some contribution from the rotary vane pump, the converter control board, and the induction generator. This hydraulic motor is an off-the-shelf part from Danfoss with a long experience in the hydraulic actuator market. Danfoss recommends a stringent filtering system for the hydraulic fluid to remove salt and other contaminants in order to prolong the life of the equipment. Adding a filtration system could improve the performance of the hydraulic wave generator, moving it toward the optimistic performance trajectory. Such a system would have additional benefits for the other hydraulic equipment, particularly the rotary vane pump.

CONCLUSIONS

This report has considered the reliability and availability of the hydraulic and direct drive electrical wave energy conversion systems. From the system diagrams and list of components, the reliability and maintenance time information for each part were found from survey reports in the electrical power, oil and gas, military, hydraulic actuator, and wind generation fields. The reliability block diagram showed that there was little redundancy built into these systems.

The systems were found to have a failure rate between four times a year and once every four years. The availability was found to exceed 95% in all situations, though this does not account for delays due to weather or scheduled maintenance. Weather is a key factor in repairs for offshore devices, and has been seen to reduce availabilities of 97% down to 76% for offshore wind installations [1]. This factor, as well as scheduled maintenance, will be accounted for more fully in the LCOE calculations.

The hydraulic motor was found to be the main contributor to down time for the hydraulic system, while the magnetically geared generator was found to be the main contributor to system down time for the direct drive electrical system. A strong filtration system is expected to improve the performance of the hydraulic motor. Understanding the failure mechanisms of the prototype direct drive generator and minimizing their expected impact is critical for achieving the project availability and LCOE targets.

REFERENCES

[1] G.J.W. van Bussel, (1999) “The Development of an Expert System for the Determination of Availability and O&M Costs for Offshore Wind Farms.” [Online]. Available: http://www.lr.tudelft.nl/fileadmin/Faculteit/LR/Organisatie/Afdelingen_en_Leerstoelen/Afdeling_AEWE/Wind_Energy/Research/Publications/Publications_1999/doc/Bussel_eu99gvbnw.pdf. [Accessed December 16th, 2015].

[2] “IEEE 493 – Gold Book,” 2007.

[3] SINTEF and NTNU, “Offshore and Onshore Reliability Data Volume 1 – Topside Equipment,” 6th Edition, 2015.

[4] SINTEF and NTNU, “Offshore and Onshore Reliability Data Volume 2 – Subsea Equipment,” 6th Edition, 2015.

[5] P.J. Tavner, J.P. Hasson, “Predicting the Design Life of High Integrity Rotating Electrical Machines,” Ninth International Conference on Electrical Machines and Drives, 1999, pp. 286 – 290.

[6] ABB, PC6000 Datasheet, “MTBF_Calculation_PCS6000_Template,” 2011.

[7] “IEEE 493 – Gold Book,” 2007.

[8] F. Spinato, P.J. Tavner, G.J.W van Bussel, E. Koutoulakos, “Reliability of Wind Turbine Subassemblies,” IET Renewable Power Generation, Vol. 3, Issue 4, Sept. 2009, pp. 387 – 401.

[9] D.B. Murray, J.G. Hayes, M.G. Egan, D.L. O'Sullivan, "Supercapacitor Testing for Power Smoothing in a Variable Speed Offshore Wave Energy Converter," *Applied Power Electronics Conference and Exposition*, 2011, pp. 1933 – 1939.

[10] Danfoss. (2012, September). "Recommended Service Intervals for APP Pumps." [Online]. Available: http://www.danfoss.com/NR/rdonlyres/EAF2656C-E9A8-42E0-8F03-7C33680FEB13/0/180R9199_521B1135_DKCFNPI013C102_RecommendedserviceintervalsforAPPpumps_UK.pdf. [Accessed December 16th, 2015]

[11] Danfoss. (2015, 20 October). "Danfoss APP Pump Runs 27,000 Hours in Remote Island Location." [Online]. Available: http://high-pressurepumps.danfoss.com/technicalarticles/rc/danfoss-app-pump-runs-27,000-hours-in-remote-island-location/?ref=17179931651. [Accessed December 16th, 2015].

[12] Rima. "Rima Hydraulic Systems." [Online]. Available: http://www.rimagroup.com/pdf/hydraulics.pdf. [Accessed December 16th, 2015].